Dissertation

Characterization of Novel Non-Coding RNAs Potentially Involved in Breast Carcinogenesis

submitted by

Katharina JONAS, BSc. MSc.

for the Academic Degree of

Doctor of Philosophy (PhD)

at the

Medical University of Graz

Department of Internal Medicine, Division of Oncology

under the Supervision of

Assoc. Prof. Dr. Martin PICHLER

2024

Statutory Declaration

I hereby declare that this thesis is my own original work and that I have fully acknowledged by name all of those individuals and organizations that have contributed to the research for this thesis. Due acknowledgment has been made in the text to all other material used. Throughout this thesis and in all related publications I followed the “Guidelines of the Medical University of Graz on Good Scientific Practice”.

Date	Signature
26.01.2024	e.h. Katharina Jonas

Disclosures

Part of this thesis has been published in the following two publications:

1. Katharina Jonas [1,2], Felix Prinz [1,2], Manuela Ferracin [3], Katarina Krajina [4], Barbara Pasculli [5], Alexander Deutsch [6], Tobias Madl [7,8], Beate Rinner [9], Ondrej Slaby [10], Christiane Klec [1,2], and Martin Pichler [1,2,4]. MiR-4649-5p acts as a tumor-suppressive microRNA in triple negative breast cancer by direct interaction with PIP5K1C, thereby potentiating growth-inhibitory effects of the AKT inhibitor capivasertib. Breast Cancer Res. 2023;25:119.

   [1] Division of Oncology, Department of Internal Medicine, Medical University of Graz, Graz, Austria.
   [2] Research Unit for Non-Coding RNA and Genome Editing, Medical University of Graz, Graz, Austria.
   [3] Department of Medical and Surgical Sciences (DIMEC), University of Bologna, Bologna, Italy.
   [4] Translational Oncology, II. Med Clinics Hematology and Oncology, Augsburg, Germany.
   [5] Fondazione IRCCS Casa Sollievo della Sofferenza Laboratorio di Oncologia, San Giovanni Rotondo, FG, Italy.
   [6] Division of Hematology, Department of Internal Medicine, Medical University of Graz, Graz, Austria.
   [7] Division of Molecular Biology & Biochemistry, Gottfried Schatz Research Center for Cell Signaling, Metabolism and Aging, Medical University of Graz, Graz, Austria.
   [8] BioTechMed-Graz, Graz, Austria.
   [9] Department for Biomedical Research, Medical University of Graz, Graz, Austria.
   [10] Department of Biology, Faculty of Medicine and Central European Institute of Technology, Masaryk University, Brno, Czech Republic.

2. Katharina Jonas [1,2], Felix Prinz [1,2], Manuela Ferracin [3], Katarina Krajina [4], Alexander Deutsch [5], Tobias Madl [6,7], Beate Rinner [8], Ondrej Slaby [9], Christiane Klec [1,2], and Martin Pichler [1,2,4]. MiR-4646-5p Acts as a Tumor-Suppressive Factor in Triple Negative Breast Cancer and Targets the Cholesterol Transport Protein GRAMD1B. Non-Coding RNA. 2024;10(1):2.

   [1] Division of Oncology, Department of Internal Medicine, Medical University of Graz, Graz, Austria.
   [2] Research Unit for Non-Coding RNA and Genome Editing, Medical University of Graz, Graz, Austria.
   [3] Department of Medical and Surgical Sciences (DIMEC), University of Bologna, Bologna, Italy.
   [4] Translational Oncology, II. Med Clinics Hematology and Oncology, Augsburg, Germany.
   [5] Division of Hematology, Department of Internal Medicine, Medical University of Graz, Graz, Austria.

[6] Division of Molecular Biology & Biochemistry, Gottfried Schatz Research Center for Cell Signaling, Metabolism and Aging, Medical University of Graz, Graz, Austria.
[7] BioTechMed-Graz, Graz, Austria.
[8] Department for Biomedical Research, Medical University of Graz, Graz, Austria.
[9] Department of Biology, Faculty of Medicine and Central European Institute of Technology, Masaryk University, Brno, Czech Republic.

All co-authors have agreed to the use of their data in this thesis.

All contributions to the dissertation by others are specified in the Material & Methods section, as well as the respective Figure legends, and contributors are referenced by name and affiliation.

Acknowledgments

I am very grateful to the Doctoral College of Metabolic and Cardiovascular Disease (DK-MCD) of the Medical University of Graz for allowing me to perform my doctoral studies in such an outstanding scientific environment and for providing me with excellent multidisciplinary training.

I would also like to express my gratitude to the Österreichische Wissenschaftsfond (FWF) for funding my research (grant number DK-MCD 10.55776/W1226).

The completion of my dissertation would of course not have been possible without my supervisor Assoc. Prof. Dr. Martin Pichler, who supported and guided me greatly during my dissertation. He found the right measure between strong guidance and the freedom to allow me to develop into an independent researcher. Thanks should also go to my Thesis Committee members, Assoc. Prof. Dr. Beate Rinner and Prof. Dr. Tobias Madl, for giving me valuable input throughout my dissertation. I would also like to acknowledge Prof. Dr. Philipp Jost, head of the Division of Oncology, as he has strongly focused on expanding research, thus creating a stimulating scientific environment with close links to the clinics, which greatly favored my research experience.

I am deeply indebted to my parents, who have supported me in every way possible during my studies and have endowed me with love, strength, and their relentless belief in my abilities.

Last, but not least, I want to thank my friends and (former) colleagues, who have accompanied me through all the ups and downs of my dissertation and provided advice and encouragement when dearly needed.

Table of Contents

Abbreviations

27HC	27-hydroxycholesterol
ABHD16A	abhydrolase domain containing 16A, phospholipase
AEBP1	adipocyte enhancer-binding protein 1
Ago	Argonaute protein
AIM2	absent in melanoma 2
AKT	protein kinase B
ALDH1	aldehyde dehydrogenase 1
ANG	angiogenin
AP-1	activator protein 1
AR	androgen receptor
ARAP3	ArfGAP with RhoGAP domain, ankyrin repeat and PH domain 3
ARHGEF2	Rho/Rac guanine nucleotide exchange factor 2
BAD	BCL2 associated agonist of cell death
BAK	BCL2 homologous antagonist killer
BAX	BCL2 associated X, apoptosis regulator
BCL10	B-cell lymphoma/leukemia 10
BCL2	anti-apoptotic factor B cell lymphoma 2
BIK	BCL2 interacting killer
BL1	basal-like 1 subtype
BL2	basal-like 2 subtype
BRCA1	breast and ovarian cancer susceptibility protein 1
BRCA2	breast and ovarian cancer susceptibility protein 2
BSA	bovine serum albumin
CALD1	caldesmon 1
CARD19	caspase recruitment domain family member 19
CARD8	caspase recruitment domain family member 8
CASP3	caspase 3
CDKNA	cyclin-dependent kinase inhibitor 2A
CCL20	C-C motif chemokine ligand 20
CDK	cyclin-dependent kinase
CFH	complement factor H
CSC	cancer stem cell
CTLA-4	cytotoxic T-lymphocyte-associated protein-4

CXCL1	C-X-C motif chemokine ligand 1
DBP	D-box binding PAR BZIP transcription factor
ddPCR	digital droplet PCR
DEAB	N,N-diethylaminobenzaldehyde
DIABLO	Diablo IAP-binding mitochondrial protein
DMSO	dimethyl sulfoxide
EdU	5-ethynyl-2′-deoxyuridine
EGFR	epithelial growth factor receptor
EGR1	early growth response factor 1
EGR4	early growth response factor 4
ELISA	Enzyme-Linked Immunosorbent Assay
EMT	epithelial-to-mesenchymal transition
ER	endoplasmic reticulum
ER	estrogen receptor
ERK	extracellular signal-regulated kinase
ESR1	estrogen receptor 1
FACS	fluorescence-activated cell sorting
FADD	Fas-associated via death domain
FasL	Fas ligand
FBS	fetal bovine serum
FDA	Food and Drug Administration
FGF2	fibroblast growth factor 2
G-CSF	granulocyte colony-stimulating factor
GEFs	Rho guanine nucleotide-exchange factors
GEO	Gene Expression Omnibus
GO	Gene Ontology
GRAMD1B	GRAM domain-containing protein 1B
GSEA	gene set enrichment analysis
HDL	high-density lipoprotein
HDR	homology-directed repair
HER2	human epidermal growth factor receptor 2
HIF1A	hypoxia-inducible factor 1 subunit alpha
HR	hormone receptor
HUVEC	human umbilical vein endothelial cells
IFNγ	interferon-gamma

IL	interleukin
IM	immunomodulatory subtype
INPP4B	inositol polyphosphate 4-phosphatase type II
JAK	janus kinase
JNK	c-Jun N-terminal kinase
LAMA4	laminin subunit alpha 4
LAR	luminal androgen receptor subtype
LDL	low-density lipoprotein
LDLR	low-density lipoprotein receptor
lincRNA	long intergenic non-coding RNA
LNA	locked nucleic acid
lncRNA	long non-coding RNA
M	mesenchymal subtype
MAP3K1	mitogen-activated protein kinase kinase kinase 1
MAPK	mitogen-activated protein kinase
MED16	mediator complex subunit 16
miRNA	microRNA
MMP1	matrix metallopeptidase 1/collagenase
MSL	mesenchymal stem-like subtype
MTA1	metastasis-associated 1 protein
MUC1	mucin 1
ncRNA	non-coding RNA
NF-κB	nuclear factor kappa-light-chain-enhancer of activated B cells
NID2	nidogen 2
NIH	National Institutes of Health
NOG mouse	NODShi.Cg-*Prkdc*^{scid} *Il2rg*^{tm1Sug} mouse
NOXA	phorbol-12-myristate-13-acetate-induced protein 1
NPC1	Niemann-Pick type C protein 1
NRP2	neuropilin 2
NSG mouse	NOD.Cg-*Prkdc*^{scid} *Il2rg*^{tm1Wjl}/SzJ mouse
nt	nucleotide
NTC	no-template control
OCDO	6-oxo-cholestan-3β,5α-diol
PACS1	phosphofurin acidic cluster sorting protein 1
PACT	protein kinase R-activating protein

PARP	poly ADP ribose polymerase
PBS	phosphate-buffered saline
PD-1	programmed cell death protein-1
PDGFRA	platelet-derived growth factor receptor A
PDK1	phosphoinositide-dependent protein kinase 1
PD-L1	programmed cell death ligand-1
PEI	polyethyleneimine
pen/strep	penicillin/streptomycin
PHD3	prolyl-4-hydroxylase domain 3
PI3K	phosphatidylinositol 3-kinase
PIK3CA	phosphatidylinositol 4,5-bisphosphate 3-kinase catalytic subunit alpha
PIP_2	phosphatidylinositol 4,5-bisphosphate
PIP_3	phosphatidylinositol 3,4,5-trisphosphate
PIP5K1C	phosphatidylinositol-4-phosphate 5-kinase type 1 gamma
piRNA	piwi-interacting RNA
PLAGL2	PLAG1 like zinc finger 2
PLEKHG4	pleckstrin homology and RhoGEF domain containing G4
PM	plasma membrane
PR	progesterone receptor
pre-miRNA	precursor microRNA
pri-miRNA	primary microRNA
PTEN	phosphatase and tensin homolog
PUMA	p53 upregulated modulator of apoptosis
qPCR	quantitative PCR
RFU	relative fluorescent units
RIPA	radioimmunoprecipitation assay
RISC	RNA-induced silencing complex
RNA pol II	RNA polymerase II
SD	standard deviation
SDS-PAGE	sodium dodecyl sulfate-polyacrylamide gel electrophoresis
SEMA3A	semaphorin 3A
SERD	selective estrogen receptor downregulator
SERM	selective estrogen receptor modulator
siRNA	short-interfering RNA
sncRNA	small non-coding RNA

SOCS1	suppressor of cytokine signaling 1
SPRED3	sprouty related EVH1 domain containing 3
SR-B1	scavenger receptor class B, type I
SREBP-2	sterol regulatory element-binding protein 2
STAT	signal transducers and activators of transcription
SYNPO	synaptopodin
TAM	tumor-associated macrophage
TBS	Tris-buffered saline
TBS-T	Tris-buffered saline-Tween 20
TCGA	the Cancer Genome Atlas Project
TGFB	transforming growth factor beta
TIMP3	metalloproteinase inhibitor 3
TME	tumor microenvironment
TMEM120B	transmembrane protein 120B
TNBC	triple negative breast cancer
TNF	tumor necrosis factor
TP53	tumor protein P53
TRADD	TNFRSF1A associated via death domain
TRAIL	tumor necrosis factor-related apoptosis inducing ligand
TRBP	TAR RNA binding protein
Treg	regulatory T cell
TROP2	trophoblast cell-surface antigen 2
UTR	untranslated region
VEGF-A	vascular endothelial growth factor
ZEB1	zinc finger E-box binding homeobox 1
ZEB2	zinc finger E-box binding homeobox 2

Abstract (German)

Brustkrebs ist die häufigste Krebsart bei Frauen, wobei Tripel-negativer Brustkrebs (TNBC) besonders aggressiv und schwierig zu behandeln ist, weshalb dieser Subtyp Fokus der Dissertation war. Bei dem Ziel, ein besseres Verständnis über die Entstehung von TNBC zu erlangen, was die Entwicklung effizienterer Behandlungsstrategien ermöglichen könnte, liegt großes Potential in nicht-kodierenden RNAs (ncRNAs). Vor allem eine Klasse an kurzen ncRNAs, genannt microRNAs (miRNAs), ist häufig in vielen Krebsarten dereguliert und trägt so zu verschiedenen malignen Merkmalen bei. Ziel dieser Dissertation war daher, neue miRNAs mit einer Rolle in TNBC zu identifizieren, deren molekulare Mechanismen zu charakterisieren, und einen möglichen therapeutischen Nutzen zu untersuchen. Basierend auf einem miRNA Expressionsscreening von 3D Brustkrebs Sphären haben wir zwei miRNAs ausgewählt, deren Funktion in Brustkrebs zuvor nicht untersucht worden war. Diese zwei miRNAs waren miR-4646-5p (MIMAT0019707) und miR-4649-5p (MIMAT0019711).

Wir haben den Einfluss der beiden miRNAs auf verschiedene phänotypische Eigenschaften von TNBC-Zelllinien untersucht, mit Hilfe von synthetischen mimics zur Erzeugung einer Überexpression, sowie eines antisense Inhibitors im Fall von miR-4646-5p. Die phänotypischen Assays zeigten, dass miR-4646-5p Überexpression das Wachstum und die Migration von TNBC-Zellen verringert, während die Inhibierung den gegenteiligen Effekt hatte. Wir konnten außerdem feststellen, dass die Überexpression von miR-4646-5p zu einer TNBC zelllinienabhängige Induktion von Apoptose führte, sowie zu einer verringerten Bildung von kapillarähnlichen Strukturen von Endothelzellen, was auf anti-angiogenetische Eigenschaften hinweisen könnte. Überexpression von miR-4649-5p hatte ebenfalls verringertes Wachstum und Migration zur Folge, jedoch keinen Einfluss auf Apoptose oder Kapillarbildung. Eine Transkriptomanalyse zeigte vielfältige zugrundeliegende Genexpressionsänderungen. MiR-4646-5p verursachte zum Beispiel eine Herunterregulierung von pro-tumorigenen Zytokinen. Wir konnten auch je ein direktes Target der miRNAs identifizieren, welches zu deren tumor-suppressiven Eigenschaften beiträgt, nämlich das Cholesteroltransferprotein GRAMD1B im Fall von miR-4646-5p und die Phosphatidylinositol Kinase PIP5K1C im Fall von miR-4649-5p. PIP5K1C ist beispielsweise bekannt dafür, Migration und Wachstum zu fördern, letzteres durch Downstream Effekte auf den PI3K/AKT Signalweg. Eine Kombination des miR-4649-5p mimic mit pharmakologischer Inhibierung von PIP5K1C oder AKT zeigte additive wachstumsverringernden Effekte. Die tumor-suppressiven Effekte der beiden miRNAs müssen jedoch noch durch *in vivo* Experimente bestätigt werden. Im Hinblick auf therapeutischen Nutzen scheinen Kombinationen vielversprechender als mimics allein. Für miR-4646-5p wären Kombinationen mit Immuncheckpoint-Inhibitoren möglicherweise von Vorteil, wohingegen miR-4649-5p den Effekt von PI3K oder AKT-Inhibitoren wie Capivasertib verstärken könnte.

Abstract (English)

Breast cancer is the most common type of cancer in women, with the subtype of triple negative breast cancer (TNBC) standing out as particularly aggressive and difficult to treat, which is why it was the focus of this dissertation. In the aim of gaining a better understanding of the carcinogenesis of TNBC, ultimately allowing the development of more efficient treatment strategies, the realm of non-coding RNAs (ncRNAs) holds large potential. Especially a sub-class of short ncRNAs called microRNAs (miRNAs) is frequently deregulated in many cancer types and contributes to cancer hallmarks. The goal of this dissertation was thus to identify novel miRNAs with a role in TNBC, to characterize their molecular mechanisms, and to explore a potential therapeutic utility. Based on a previous miRNA expression screen of 3D breast cancer spheres, two miRNAs were selected that had not been studied in breast cancer prior. These two miRNAs were miR-4646-5p (MIMAT0019707) and miR-4649-5p (MIMAT0019711). We investigated the impact of the miRNAs on several important phenotypic characteristics of TNBC cells by employing synthetic mimics to induce ectopic overexpression, as well as an antisense inhibitor in case of miR-4646-5p. The phenotypic assays revealed that miR-4646-5p overexpression reduced the growth and migration of TNBC cell lines, while inhibition had corresponding opposite effects. Interestingly, we also observed a cell-line-specific induction of apoptosis upon miR-4646-5p overexpression in TNBC cells, and reduced tube formation of endothelial cells, which suggests anti-angiogenic properties of miR-4646-5p. Overexpression of miR-4649-5p reduced the growth, proliferation, and migration of TNBC cells, but had no impact on apoptosis or tube formation. Whole transcriptome analysis revealed diverse underlying mechanisms for the phenotypic effects we observed. For example, miR-4646-5p caused a broad downregulation of tumor-promoting cytokines. Ultimately, we also identify one direct target for each miRNA, the cholesterol transfer protein GRAMD1B for miR-4646-5p and the phosphatidylinositol kinase PIP5K1C for miR-4649-5p, both of which may contribute to the tumor-suppressive properties of the miRNAs. PIP5K1C, for example, is known to promote migration and cell growth, the latter due to downstream effects on PI3K/AKT signaling, which is frequently overactivated in TNBC. Thus, a combination of the miR-4649-5p mimic and pharmacologic PIP5K1C or AKT inhibition showed additive growth-reducing effects. The broad *in vitro* tumor-suppressive effects of the miRNAs remain to be confirmed *in vivo* as technical and biological challenges prevented us from doing so within this dissertation. Regarding therapeutic utility, combinatorial approaches may hold more potential than miRNA mimics alone. As miR-4646-5p may modulate the tumor microenvironment through its impact on cytokines, combinations with immune checkpoint inhibitors could be beneficial, whereas for miR-4649-5p *in vivo* combinations with PI3K or AKT inhibitors like capivasertib are evident.

1. Introduction

1.1. Breast cancer – Statistics

In 2020, more than 2.2 million new breast cancer cases were diagnosed in women, according to the World Health Organization (1). This makes breast cancer the worldwide leading type of malignancy in women, with an incidence rate of 24.5% of all new cancer cases among women (1). Moreover, breast cancer accounts for the highest number of cancer-related deaths in women, making up 15.5% (1). Incidence rates and mortality of breast cancer vary between countries though, owing to various reasons like screening and treatment availability, risk factor prevalence, and ethnic differences in susceptibility (2). But overall, breast cancer presents a major global burden. In the United States, for example, 239,612 new breast cancer cases and 42,273 breast cancer deaths were recorded in women in 2020 by the Centers for Disease Control and Prevention. In Austria, Statistik Austria reported that in 2020 breast cancer was responsible for 27.7% of all new cancer cases in women, with 5 443 cases, and for 17% of all cancer-related deaths (3). Thus, even though the 5-year survival rate for breast cancer patients in Austria is relatively high with 87% (3), the mortality rate of breast cancer is still substantial.

1.2. Breast cancer – Biology, subtypes, and origins of heterogeneity

Carcinogenesis of the breast originates in the epithelial layer of the mammary glands, which is composed of outer basal myoepithelial cells and inner luminal epithelial cells (2,4) (Figure 1). From a histological point of view, a basic classification is made based on whether the neoplastic lesion is located in a ductal or lobular region of the tree-like branches of the glands and whether it is still preinvasive (carcinoma *in situ*) or invasive (2). More relevant for treatment and prognosis is the histopathological determination of the tumor grade, or for example the Nottingham Prognostic Index, which takes into account tumor size, grade, and lymph node status (5). The most critical distinction regarding treatment choice is based on the immunohistochemical determination of the expression status of two hormone receptors (HR), the estrogen receptor (ER) and progesterone receptor (PR), and the human epidermal growth factor receptor 2 (HER2 or ERBB2) (6). This allows subgrouping into four major pathological subtypes: an HR+/HER2- subtype, an HR+/HER2+ subtype, an HR-/HER2+ subtype, and the triple negative breast cancer (TNBC) subtype, which lacks expression of all three receptors (2,6). For each of these subtypes, different treatment regimens and targeted therapies, for example against the respective receptors, are available (2,6), which will be detailed in a section further below.

Even though TNBC only accounts for 15-20% of all breast cancer cases, as the majority is HR-positive, this subtype stands out as particularly challenging due to its aggressiveness and difficulty to treat because of the lack of classic treatment targets (7,8). In particular, TNBC typically exhibits a high proliferative index, high rate of metastasis formation, and rapid emergence of resistance to chemotherapeutic treatment, traits that are responsible for a high risk of recurrence and a significantly lower 5-year survival rate than other subtypes (6–9). Due to these problematic characteristics and the clinical need to develop new and improved treatment approaches for TNBC, this particular subtype has been selected as the cancer type of interest in this dissertation.

The classification into subtypes based on HR and HER2 expression starts to paint a rough picture of the heterogeneity of breast cancer. Nevertheless, these classifications are only the very beginning of the immense biological and molecular complexity of this malignancy. Gene expression profiling studies of breast cancer, as for example conducted by Perou *et al.* (10) and Sørlie *et al.* (11), have revealed more complex and diverse intrinsic molecular subtypes which overlap with the pathological subtypes (Figure 1). Surrogate definitions of these molecular subtypes were first officially adopted by clinical experts at the St Gallen International Expert Consensus 2013, and include luminal A, luminal B, HER-2 enriched, and basal-like (12). The two luminal subtypes generally exhibit expression of ER and ER-related genes, together with or without PR, and high levels of keratin 8 and 18 (4,8). While luminal A shows higher expression of proliferation and cell cycle-related genes, luminal B expresses more luminal genes, like PR (13). As the name implies, the HER2-enriched subtype is particularly characterized by the expression of HER2 and associated genes (4). The basal-like subtype, which is the most distinct from the other subtypes, overexpresses keratin 5, 14, and 17, as well as epithelial growth factor receptor (EGFR)-related genes and proliferation-related genes (4,8,13). Most basal-like tumors lack expression of HR and HER2, and 80% of TNBCs in fact fall into this intrinsic molecular subtype (4,8). Further characterizations of the molecular landscape of breast tumors have revealed a fifth intrinsic subtype, referred to as claudin-low (14). Tumors belonging to this subtype show a low expression of genes relevant for cell adhesion and the formation of tight junctions, like claudins, occludin, and E-cadherin, while being enriched with genes that are associated with epithelial-to-mesenchymal transition (EMT), a process that enhances the motility and invasiveness of tumor cells and helps to facilitate their metastatic dissemination (14–16). The majority of claudin-low tumors also fall within the TNBC subgroup (15).

The molecular classifications of breast tumors by microarray or RNA-seq-based expression analysis are able to give valuable information regarding prognosis and treatment choice

(11,13,17,18). For this reason, panels of gene signatures have been developed, for example, the PAM50 gene signature, which relies on a 50-gene panel, in order to allow the implementation of these intrinsic subtypes into the clinical routine (17). Another well-studied panel in clinical use is the 21-gene panel Oncotype DX®, which is able to predict the risk of disease recurrence and can aid in the decision of whether HR+/HER2- patients with early breast cancer would benefit from neoadjuvant chemotherapy (19,20).

Molecular subtyping has also allowed to further divide the heterogenous TNBC subtype into six distinct transcriptome-defined groups, namely a basal-like 1 (BL1) and 2 (BL2), an immunomodulatory (IM), a mesenchymal (M), a mesenchymal stem–like (MSL), and a luminal androgen receptor (LAR) group (21). The value of this refined classification, referred to as Lehman's classification, lies in its ability to guide the development of novel molecular therapies, which are still urgently needed in case of TNBC, as well as to help predict which patients can benefit most from standard chemotherapy (21–24). For example, based on the distinct expression profiles of the subgroups, Burstein *et al.* have been able to identify potential subtype-specific treatment targets, like the platelet-derived growth factor receptor A (PDGFRA) in the mesenchymal group, and the cell surface protein mucin 1 (MUC1) and the androgen receptor (AR) in the luminal androgen receptor group (22). Others found that the basal-like 1 TNBC subtype shows the best response to neoadjuvant chemotherapy using carboplatin and docetaxel, whereas luminal androgen receptor type TNBC tumors exhibit the worst response rate (24). Nevertheless, despite the potential utility of TNBC transcriptome-based subtyping, no standard assays have been established yet for routine clinical use (2).

The above-discussed diversity of molecular breast cancer subtypes very well highlights the immense intertumoral heterogeneity of the disease. In addition, breast tumors also harbor substantial intratumoral heterogeneity, meaning that even within the same tumor, cancer cells exhibiting different molecular subtypes can be present which is also highly influenced by the diversity and heterogeneity of the tumor microenvironment (TME) (25). Nowadays, this intratumoral heterogeneity of breast cancer can be well dissected by the use of single-cell RNA-seq, which allows to profile and discern the molecular state of cancer cells as well as of non-cancerous cells present in the tumor, like immune cells (26,27). To help gain an understanding of how both inter- and intratumoral heterogeneity develop, two theories have been established (28,29): The theory of clonal evolution (30) and the cancer stem cell (CSC) theory. The CSC theory follows a "cell of origin" concept, meaning that breast cancer heterogeneity and subtypes arise because each tumor originates from a different cell type found in the mammary epithelium (31) (Figure 1). These cells of origin can be different stem and progenitor cells in various states of differentiation that have acquired mutational hits (4,32).

In analogy to normal stem cells, CSCs are defined as cells with a capability of unlimited self-renewal and the potential to give rise to heterogenous differentiated cancer cells, thereby being able to initiate the formation of a heterogenous tumor containing cell populations in various differentiation states starting from, in theory, a single CSC (29). The existence of CSCs in breast cancer has, for the first time, been indicated by an influential study by Al-Hajj *et al.* in 2003, which showed that a small subpopulation of human breast cancer cells, defined by a high expression of the surface marker CD44 and low/negative CD24 expression, can efficiently initiate tumor growth in immunodeficient mice, whereas the remaining breast cancer cell population failed to show tumorigenicity (33). These cancer-initiating breast CSCs have since been characterized further. For example, another breast CSC marker now commonly used for the isolation of breast CSCs has been identified, namely aldehyde dehydrogenase 1 (ALDH1) activity (34). CSCs with a high enzymatic ALDH1 activity were associated with increased occurrence of metastasis and poor prognosis of breast cancer patients (35). Another peculiar characteristic of CSCs is that they exhibit metabolic plasticity, meaning they can adapt more easily to changing conditions in the TME (36,37). In the presence of glucose or under hypoxia, a lack of oxygen, CSCs are preferentially in a more proliferative state where they primarily rely on aerobic glycolysis, whereas under glucose-deprivation they shift their metabolism towards oxidative phosphorylation and change into a quiescent state (36,37). In general, CSCs are proliferating less than the bulk of cancer cells and they have a highly effective drug efflux, all of which makes them incredibly hard to target with standard cancer therapy (36,38). Due to this, CSCs are associated with chemoresistance, relapse, and metastasis (36,38). As the percentage of CSCs in TNBC is higher than in other breast cancer subtypes, this may also be a factor contributing to the aggressive characteristics of this subtype (39,40).

As stated before, the CSCs model explains the existence of the different intrinsic molecular subtypes of breast cancer, in other words, the intertumoral heterogeneity, with the fact that each subtype originates from a different cell of origin with a different state of differentiation or degree of stemness (4,32) (Figure 1). For example, the claudin-low subtype is thought to originate from the most undifferentiated multipotent mammary stem cells (32) (Figure 1). Basal-like tumors arise from intermediate luminal progenitor cells, whereas luminal A and B tumors originate from more differentiated luminal cells (32) (Figure 1). The clonal evolution theory, on the other hand, postulates that different breast cancer subtypes can have the same cells of origin that have however acquired different genetic and epigenetic alterations (28). These cells, moreover, undergo successive clonal selection following a process of evolution shaped by the TME, which results in the simultaneous existence of genetically and epigenetically diverse cancer sub-clones that carry different selective advantages, thus explaining intratumoral

heterogeneity (29,41). The two models are not mutually exclusive. In fact, a combination of both probably comes closest to reality. For a stem cell to become a cancerous cell of origin, mutational changes have to occur that are also subjected to clonal selection, likely creating genetically diverse cancer-initiating CSCs (41).

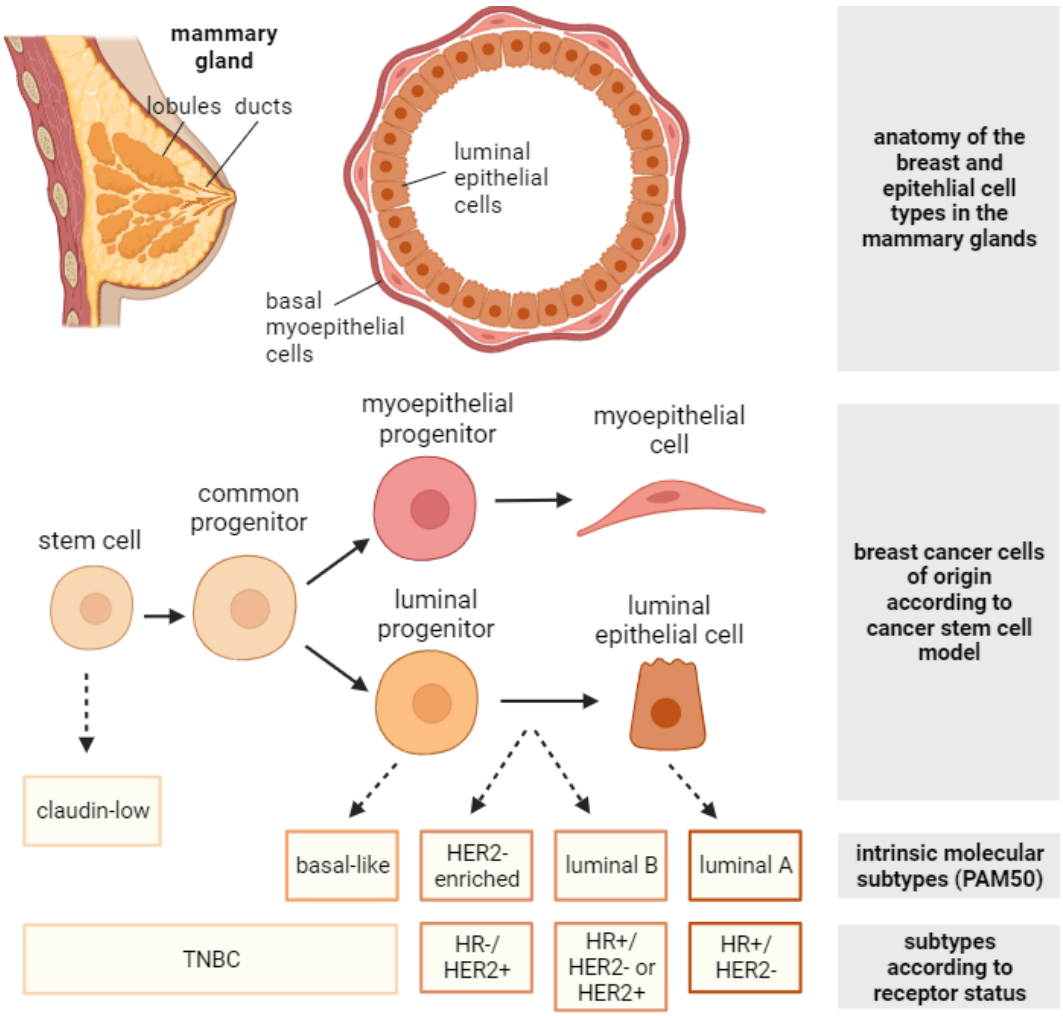

Figure 1: Breast cancer origins according to cancer stem cell model and breast cancer subtypes. *Breast cancer originates in the lobules or ducts of the mammary glands, which are formed by two types of epithelial cells, inner luminal epithelial cells and basal myoepithelial cells. According to the cancer stem cell theory, breast cancer heterogeneity arises due to different cells of origin along different stages of differentiation. Based on gene expression profiling (for example using the PAM50 gene panel), breast cancer can be classified into five intrinsic molecular subtypes. These subtypes also differ in their expression of hormone receptors (HRs) and the human epidermal growth factor receptor 2 (HER2). The triple negative breast cancer (TNBC) subtype, which is the most aggressive subtype, lacks expression of HRs and HER2. Most basal-like and claudin-low tumors fall into the TNBC category (Figure created with BioRender).*

1.3. Breast cancer – Characteristic genetic alterations

In order to facilitate the development of targeted treatments, it is essential to pin down mutational drivers of breast cancer initiation, progression, and relapse (28). There are a few known germline mutations with a high penetrance, meaning that if these genes are mutated, patients are very likely to develop breast cancer within their lifetime (42,43). These genes include breast and ovarian cancer susceptibility proteins 1 and 2 (*BRCA1* and *BRCA2*), tumor protein P53 (*TP53*), and phosphatase and tensin homolog (*PTEN)* (28,42,43). *BRCA1*, or rather its chromosomal location on 17q21, was first linked to familial breast cancer susceptibility in a genetic analysis of 23 extended families with 146 breast cancer cases that was published in 1990 by Hall *et al.* (44). In 1994, the gene was identified by positional cloning in a study by Miki *et al.* (45). In the same year, *BRCA2* on chromosome 13q12-13 was also found to be associated with inherited breast cancer (46). Both *BRCA1* and *BRCA2* function as tumor suppressor genes through their role in homology-directed repair (HDR) of DNA double-strand breaks (47). HDR presents the most precise way of repairing double-strand breaks. Thus, if this repair pathway is defective, as is the case when *BRCA1* or *BRCA2* are mutated, it can result in genomic instability, chromosomal rearrangements, mutations, and ultimately greatly increases the risk of developing certain cancers like breast but also ovarian cancer (43,47). The lifetime risk of a female patient with an inherited *BRCA1* and/or *BRCA2* mutation to develop breast cancer is up to 85% (48). According to the ClinVar database of the National Institutes of Health (NIH), oncogenic mutations of *BRCA1* and *BRCA2* are diverse and spread throughout the entire length of the genes, meaning there are no clear mutational hotspots, but most of them result in truncated and dysfunctional versions of the proteins (49). Another cause for elevated inherited breast cancer susceptibility are mutations in the *TP53* gene, which codes for the tumor suppressor protein p53 (50). P53 plays a central role as cellular gatekeeper in response to DNA damage or stress, by halting cell cycle progression, promoting DNA repair, or initiating apoptosis (51). Germline mutations in the *TP53* gene have a high penetrance and, according to a study by Mai *et al.*, cause a likelihood of 54% for women to develop breast cancer until the age of 70 (52). Despite being very rare, germline mutations of the tumor suppressor gene *PTEN,* which negatively regulates cell cycle progression, proliferation, and migration by inhibiting the phosphatidylinositol 3-kinase (PI3K)/ protein kinase B (AKT) signaling pathway, also cause increased breast cancer susceptibility with a lifetime risk of 85% (53,54). Overall, inherited mutations in high-penetrance genes only account for less than 25% of all breast cancer cases though (28,43). The majority is caused by a large variety of spontaneous somatic mutations in moderate and low-penetrance genes that confer an accumulated risk (2,28).

The frequency with which different mutations occur varies greatly between the different breast cancer subtypes (55,56). Luminal ER-positive tumors generally have the highest number of recurrent mutations (55,56). The most frequently mutated gene in luminal A tumors is *PIK3CA*, which was found to be mutated in 45% of breast cancers of this subtype analyzed by the Cancer Genome Atlas Network (55). Most somatic *PIK3CA* mutations occur in three hotspots of the gene and result in increased kinase activity of the protein product (57). The *PIK3CA* gene codes for the catalytic subunit p110α of the class IA PI3K family (57,58). Once activated through growth factor receptor tyrosine kinases, PI3Ks catalyze the phosphorylation of phosphatidylinositol 4,5-bisphosphate (PIP_2) to generate the lipid second messenger phosphatidylinositol 3,4,5-trisphosphate (PIP_3), a process that can be reversed by the phosphatase PTEN (57,58). PIP_3 then recruits, via their pleckstrin homology domains, AKT and phosphoinositide-dependent protein kinase 1 (PDK1) to the cell membrane, where AKT becomes phosphorylated consecutively by the mammalian target of rapamycin complex 2 (mTORC2) on Ser473 and by PDK1 on Thr308, causing its activation (58). AKT phosphorylates further downstream targets that ultimately promote cell growth and survival (58). In addition to *PIK3CA*, also other components of the PI3K/AKT signaling pathway are affected by somatic mutations in luminal A type breast cancer, in particular *PTEN* and the AKT isoform *AKT1* (59). Mutations of *PIK3CA* alone were not found to result in a consistent overactivation of AKT and downstream signaling processes, whereas a frequently concurrent loss of *PTEN* is strongly associated with overactivation of the pathway (59). Overall, despite having the highest mutational frequency of *PIK3CA,* ER-positive breast cancers show lower levels of PI3K/AKT pathway activation markers than HER2-positive or basal-like breast cancers (55). Other somatic gene alterations characteristic for ER-positive breast tumors include: inactivating mutations of the *MAP3K1* gene, coding for the mitogen-activated protein kinase kinase kinase 1, which lies upstream of various pathways including the c-Jun N-terminal kinase (JNK) signaling pathway, the extracellular signal-regulated kinase (ERK) pathway and the nuclear factor kappa-light-chain-enhancer of activated B cells (NF-κB) pathway, and is involved in maintaining a balance between cell survival and cell death (55,60); mutations of the *GATA3* gene, coding for the transcription factor GATA binding protein 3 which is required for the normal development of mammary glands and stimulates expression of the estrogen receptor 1 (*ESR1*) gene in a reciprocal manner (55,61); amplifications of the gene *CCND1* coding for cyclin D1, which promotes cell cycle progression and is capable of activating the ER pathway in a ligand-independent manner (55,62,63); and inactivating mutations of the previously discussed tumor suppressor gene *TP53*, whereby the frequency of these mutations was found to be higher in luminal B than in luminal A breast tumors, with 32 and 12% respectively (55).

A genetic alteration that particularly characterizes HER2-enriched tumors is the frequent amplification of the *HER2* gene locus on chromosome 17q12, resulting in the overexpression of the growth factor receptor and the activation of downstream pathways regulating proliferation and survival, such as the Ras pathway and PI3K/AKT pathway (2,55,64). Along with *HER2*, further genes like *TCAP*, *PNMT*, *PERLD1*, *GRB7*, and *TOP2A* can be co-amplified on chromosome 17q depending on the size of the amplicon (65). Other independent alterations found in HER2-positive breast cancers include mutations of *PIK3CA*, which occurred in 42% of cases in the Cancer Genome Atlas Project, and genomic losses of *PTEN* and *INPP4B*, which codes for inositol polyphosphate 4-phosphatase type II and inhibits PI3K/AKT signaling by dephosphorylating PIP_2 (55,66).

Basal-like or TNBC tumors, which will be discussed as alike for this section, are the main breast cancer subtype associated with germline and/or somatic *BRCA1* and *BRCA2* mutations, which were found in 20% of basal-like tumors in the Cancer Genome Atlas Network study cohort (55). Moreover, they harbor the highest frequency of *TP53* mutations with 80% of tumors being affected, resulting in an inactivation of the p53 pathway (55). Also *PIK3CA* mutations are found in basal-like tumors at a low (55) to medium frequency (67), depending on the study cohort. In addition to mutations of *PIK3CA*, also amplifications of the gene occur, and together with common losses of *PTEN* and *INPP4B*, this results in an overactivation of the PI3K/AKT pathway in basal-like cancers which is more pronounced than in any other breast cancer subtype (55). The overactivation of this pathway has been found to be associated with rapid cancer cell proliferation, aggressive tumor behavior, resistance to different types of therapy, and poor patient prognosis (68,69). Another pathway whose components are showing frequent alterations in TNBC is the Ras-Raf-MAPK pathway, where for example genes like *KRAS*, *BRAF,* and *HER1/EGFR* were found to be amplified (55). Other genomic alterations of TNBC show subgroup specificity, as for example the LAR subgroup shows a higher frequency of activating *HER2* mutations, as well as a higher number of PI3K pathway mutations, occurring at a frequency of 70%, as reported in a study by Jiang *et al.* on a cohort of 465 Chinese TNBC patients (67). The BL1 subtype, on the other hand, is characterized by high genomic instability, very frequent *TP53* mutations (with more than 90%), and frequent deletions of genes involved in DNA repair, like *BRCA2* and *TP53*, but also *PTEN* and the tumor suppressor *RB1* (70). In summary, the diverse genomic alterations found in breast cancer are, to a certain extent, also reflected in the intertumoral heterogeneity of the disease.

1.4. Breast cancer – Therapeutic options

On the one hand, the inter- and intratumoral heterogeneity of breast cancer does not allow for an effective uniform therapeutic approach. On the other hand, detailed molecular and genetic characterization of breast cancer heterogeneity has allowed to develop effective targeted treatments for certain breast cancer subtypes in the last 25 years, which are nowadays in use alongside systemic therapies like chemotherapy (2,6). In case of ER-positive/HER-negative breast cancer, endocrine therapy has remained a key therapeutic option (71). Endocrine therapy targets the strong dependence of this breast cancer subtype on the estrogen-responsive growth receptor pathway and either works by blocking the production of estrogen as is the case for aromatase inhibitors, by inhibiting the binding of estrogen to its receptor in a competitive manner as is the case for selective estrogen receptor modulators (SERMs) like tamoxifen, or by downregulating ER as is the case for selective estrogen receptor downregulators (SERDs) like fulvestran (71). For patients with early ER-positive breast cancer adjuvant endocrine treatment, meaning after surgery, for a minimum of 5 years, with or without chemotherapy, is standard of care (2). However, development of resistance to endocrine therapy, especially in the advanced and metastatic setting, is a frequent problem (71). Thus, in more recent years, another targeted treatment option has gained approval, namely cyclin-dependent kinase 4/6 (CDK4/6) inhibitors (62). CDK4 and CDK6 are serine/threonine-dependent kinases that are activated by D-type cyclins, like D1, D2, and D3, in response to mitogenic stimuli which in turn promote the progression of the cell cycle and thus cell growth (62). As stated in the previous section, the gene coding for cyclin D1 is found to be amplified particularly in ER-positive breast cancer (55). In addition, expression of the gene is directly upregulated via the ER-transcriptional pathway (62). Thus, targeting the CDK4/6-cyclin D signaling axis by use of CDK4/6 inhibitors has proven to be an effective treatment strategy for advanced ER-positive breast cancer (62).

Another example of the successful development of a targeted breast cancer treatment are antibodies against HER2, like trastuzumab and pertuzumab, which present the standard of care for the adjuvant therapy of HER2-positive breast cancer (6). Anti-HER2 antibodies function by binding to and downregulating HER2, thereby effectively impairing proliferation and survival of HER2-positive cancer cells (6). An even newer development are HER2 antibody-drug conjugates, like trastuzumab emtansine, which combines the HER2 antibody trastuzumab with a cytotoxic anti-mitotic agent called DM1 (6,72). This combination allows the targeted delivery of the cytotoxic agent to HER2-overexpressing cancer cells, where DM1, upon receptor-mediated endocytosis of the antibody-drug complex bound to HER2, is released from the complex in the lysosome and inhibits microtubule assembly, ultimately causing cell

death (72). HER2 antibody-drug conjugates are primarily in use for high-risk primary or relapsed/metastatic HER2-positive tumors (6). Another approach for the treatment of HER2-positive breast cancer are tyrosine kinase inhibitors like neratinib that target the catalytic activity of the receptor (6). Their utility is, however, secondary to that of anti-HER2 antibodies (6).

While for HR- and HER2-positive breast cancer, effective targeted treatments exist, overall treatment efficacy for TNBC is poor, and therapeutic options remain limited (73). The standard of care for TNBC is still chemotherapy, typically consisting of an anthracycline and a taxane (2). But, as stated previously, the response rate to standard chemotherapy is affected by the heterogeneity of TNBC and certain Lehman subtypes, like BL1 and MSN, respond better, whereas others, like the LAR and BL2 subtypes, show no sensitivity to these chemotherapeutics (7). Thus, new treatment approaches for TNBC are exigently needed. One important development in this regard has at least been made for TNBC patients with germline BRCA1 or BRCA2 mutations, namely poly ADP ribose polymerase (PARP) inhibitors like olaparib and talazoparib, which interfere with the repair of DNA single-strand breaks (74). When unrepaired, single-strand breaks eventually result in double-strand breaks (74). Thus, PARP inhibitors create a synthetic lethality in cancer cells that are HDR defective, as these cells do not have the means to repair the accumulating double-strand breaks (74). Due to this, PARP inhibitors can increase the sensitivity of the cells to DNA-damaging agents like chemotherapeutics (75). Nevertheless, TNBCs with *BRCA1/2* germline mutations that profit from this treatment approach only make up a minor percentage of cases (55). Another recent development in the treatment of TNBC are immune checkpoint inhibitors (76,77). In general, breast cancer patients do not show major benefits from immunotherapy, which aims to elicit an immune response against cancer cells (76). TNBC, however, exhibits certain characteristics that make it a better target for this type of treatment as it is generally more immunogenic than other subtypes due to genomic instability and a higher mutational burden, which causes an increased infiltration of lymphocytes including $CD8^+$ T cells, $CD4^+$ T cells, natural killer cells, macrophages and dendritic cells (8,73,76). But the tumor immune environment also comprises immunosuppressive components, like regulatory T cells (Tregs), tumor-associated macrophages (TAMs), and immune checkpoint molecules like programmed cell death protein-1 (PD-1) and cytotoxic T-lymphocyte-associated protein-4 (CTLA-4), co-inhibitory receptors that are expressed on immune cells and interfere with immune cell activity when they encounter their cognate ligands expressed on cancers cells (8,77,78). Thereby, immune checkpoints are a way for cancer cells to evade destruction by the immune system (78). The ligand for PD-1, PD-L1, is more frequently expressed in TNBC than in other breast cancer

subtypes and blocking the interaction between PD-1/PD-L1 with anti-PD-1 (e.g. pembrolizumab) or anti-PD-L1 antibodies (e.g. atezolizumab) can be effective in triggering an anti-tumor response in TNBC patients, especially in the early setting and in combinatorial treatments, for example with chemotherapy (76,77). But again, not all patients respond the same to immune checkpoint inhibitors, and better predictive markers are needed, aside from PD-L1 expression, the frequency of infiltrating lymphocytes and tumor mutational burden (8,76). While immune checkpoint inhibitors present the most advanced type of immunotherapy for TNBC up to now, further developments are still needed (76,77). The therapeutic approaches mentioned above, namely chemotherapy, PARP inhibitors, and immunotherapy, currently are the most relevant options for the treatment of TNBC, but other emerging developments are also promising (8). For example antibody-drug conjugates, like Sacituzumab govitecan, which is targeted against the trophoblast cell-surface antigen 2 (TROP2) that is highly expressed on cancer cells, and thereby delivers a chemotherapeutic agent called SN-38 to the cells (6,8). Sacituzumab govitecan was found to improve the survival of metastatic TNBC patients compared to single-agent chemotherapy and has also been approved by the Food and Drug Administration (FDA) in 2020 (79). As outlined previously, TNBC cells frequently harbor mutational changes in certain signaling pathways like the PI3K/AKT pathway (55), and efforts have been made to therapeutically target the resulting alterations in pathway activation (8). One approach in this regard are PI3K inhibitors, like alpelisib, an isoform-specific inhibitor against PI3Kα that is approved for use in HR-positive/HER2-negative metastatic breast cancer in combination with fulvestran and is also evaluated in TNBC patients in a phase III ongoing trial (80). Other approaches targeting the PI3K/AKT pathway also tested in patients with TNBC are AKT inhibitors, which have been evaluated in clinical trials together with chemotherapy alone or also together with anti-PD-L1 (81,82). The most promising example is capivasertib, an ATP-competitive pan-AKT inhibitor, which was shown to prolong both the overall survival and the progression-free survival of metastatic TNBC patients when combined with the chemotherapeutic paclitaxel versus paclitaxel alone in a phase II clinical trial (83). Overall though, despite certain improvements and emerging developments, the treatment of TNBC is still challenging due to the aggressiveness and the molecular heterogeneity of this breast cancer subtype, which requires the development and use of many different treatment approaches, ideally targeting multiple molecular components in combinatorial approaches (76). It is also essential to better understand the underlying reasons for TNBC carcinogenesis as well as intertumoral heterogeneity to allow for improved treatment strategies.

1.5. Non-coding RNA – History and general classification

While alterations in protein-coding genes and their contribution to the development of breast cancer have been discussed in the previous chapter, it is nowadays well known that also changes in the non-protein-coding genome play a significant role in cancer (84). A large part of the genome is, in fact, transcribed into various types of non-coding RNAs (ncRNAs), which fulfill diverse and crucial cellular functions (85–87). In 2002, the FANTOM Consortium and the RIKEN Genome Exploration Research Group published an analysis of the mouse transcriptome which, for the first time, showed that ncRNAs by far outnumbered protein-coding transcripts in mammalian cells (88). A central role of ncRNAs is to serve as a gene regulation network on various levels, thus likely contributing to developmental complexity and phenotypic variety in higher eukaryotes (89).

Regulatory ncRNAs can be roughly classified according to their length, with ncRNAs longer than 200 nucleotides (nt) being referred to as long non-coding RNAs (lncRNAs) and shorter ncRNAs being called small non-coding RNAs (sncRNAs) (90). LncRNAs are further distinguished for example based on their genomic origin, like long intergenic non-coding RNAs (lincRNAs) which are transcribed from regions in between protein-coding genes or antisense transcripts which originate from the antisense strands of introns or exons of coding genes (90–92). Not only are their origins diverse but also their functions, as they can interact with DNA, RNA, and protein, and regulate gene expression on the transcriptional, post-transcriptional, translational, as well as post-translational level (92). Regulatory sncRNAs comprise endogenous short-interfering RNAs (siRNAs), piwi-interacting RNAs (piRNAs), and microRNAs (miRNAs) (93). In the following sections, a focus will be put on miRNAs as they are the type of ncRNAs investigated in this dissertation.

The first microRNA, discovered in 1993, was *lin-4* in *Caenorhabditis elegans* as reported in a publication by Lee and colleagues, who cloned the *lin-4* gene locus (94). They identified the locus, which had previously been found to play an essential role in controlling developmental timing of *C. elegans* larvae, to code for a short non-protein coding RNA that targets the 3' untranslated region (UTR) of the lin-14 mRNA by complementary base-pairing (94). Thus, this finding also gave a first insight into the mechanism of action of miRNAs (94). In 2000, a second miRNA with a role in the development of *C. elegans* was discovered, termed let-7 (95). Reinhart *et al.* discovered in their study that the 21 nt-long RNA targets complementary sequences in several genes (95). A reporter gene carrying the target sequence from one of those genes was used to show that let-7 directly downregulates the reporter gene by binding to it, which could be abolished when the target sequence was deleted from the reporter (95).

This methodology of using reporter constructs has remained an important instrument for validating direct miRNA targets (96). Homologs of let-7 were subsequently discovered in a number of other species, including humans, where the miRNA exhibited a tissue-specific expression pattern (97). In general, miRNAs are well conserved across species (98), but show strong tissue-specific expression, indicating a role in cell-lineage development (99). In 2019, the miRbase database, the primary public repository for miRNA sequences and annotations, released its latest update containing 2654 mature annotated miRNA sequences in humans, highlighting the abundance of this small regulatory ncRNA species and the advances that have been made since the discovery of the first miRNA (100). A development that has particularly pushed forward the discovery of new miRNAs are small RNA deep sequencing methods (100).

1.6. MicroRNAs – Biogenesis and mechanisms of action

The biogenesis of miRNAs starts with their transcription by RNA polymerase II (RNA pol II) from introns of coding genes, sometimes also overlapping with exons, or from non-coding transcripts (101,102). MiRNAs are initially transcribed as long mono- or polycistronic primary miRNAs (pri-miRNAs) which undergo a first step of maturation in the nucleus by cleavage through the ribonuclease Drosha in complex with the RNA-binding protein DGCR8 (101–104). The resulting stem-loop precursor-miRNAs (pre-miRNA) with a length of around 70 nt are then exported into the cytoplasm by interacting with exportin-5 and Ran-GTP (101,102,105). Here, pre-miRNAs are further processed by a second RNase III enzyme called Dicer, which cuts close to the base of the stem-loop and thereby generates a double-stranded miRNA duplex of its final length of 18 to 22 nt (101,102,106). One strand of the duplex, either the 5p or 3p strand, depending on sequence and structural characteristics, is incorporated into the RNA-induced silencing complex (RISC) by directly interacting with a member of the Argonaute (Ago) protein family, accompanied by the recruitment of the double-stranded RNA-binding proteins TAR RNA binding protein (TRBP) and protein kinase R-activating protein (PACT) (101,102,107,108). Subsequently, the mature miRNA recognizes mRNA targets, a process that primarily relies on Watson-Crick base pairing between a so-called seed region in the 5’ region of the miRNA, more precisely nt 2-7/8, and a complementary sequence in the 3’ UTR of the mRNA target (109,110). However, functional miRNA target sites can also be located in the 5’ UTR or even the coding region of mRNAs (111,112), and in addition to canonical 8mer or 7mer complementary pairings of the seed region with a target site, supplementary or compensatory binding of the 3’ region of the miRNA to the mRNA can influence miRNA-target interaction and compensate for mismatches within the seed (110). It has also been observed that an adenosine in the mRNA sequence opposite the first miRNA nt strongly enhances miRNA

function, not particularly by enhancing the binding between mRNA target and miRNA but by providing anchorage for Ago2, a central component of RISC (113). Another aspect influencing miRNA target recognition is UTR context dependence, meaning the sequence surrounding the binding site in the UTR of a mRNA target and its proximity to, for example, the stop codon (110). Nevertheless, due to the shortness of the essential seed region, one miRNA can potentially target up to hundreds of different mRNAs (84,114,115).

Upon binding to a mRNA target, the miRNA-RISC initiates downregulation of the target by different means. For example, Ago2 as a component of RISC, is capable of cleaving target mRNA, thereby initiating its degradation (116,117). However, this form of target repression requires strong binding between miRNA and mRNA target, which is often not the case (117). Other mechanisms are less stringent and mediate translational inhibition (117). RISC can, for example, interfere with the initiation of translation by blocking the recruitment of the 60S ribosomal subunit, or impede elongation, as is the case for lin-4 and its mRNA target lin-14 (117,118). The repression of mRNA translation by miRNA-RISC appears to be more efficient when target binding sites are located in the 3' UTR of the mRNA as opposed to its coding region, which may provide an evolutionary explanation for why most miRNA target sites are found within 3' UTRs (102,119). Another function exerted by miRNA-RISC is to expedite mRNA deadenylation which causes its destabilization and accelerates degradation (120). Moreover, miRNA-RISC can favor the localization of mRNA to cytoplasmic P-bodies, where, on the one hand, mRNA decay can be promoted, and on the other hand, mRNA can be stored or sequestered from translation (114). How a miRNA mediates target downregulation may not exclusively rely on a single mode of action but may possibly be a dynamic interplay of several mechanisms (114).

The above-described maturation of miRNAs represents the canonical biogenesis pathway (Figure 2). There is, however, also a non-canonical pathway which is independent of Drosha (101,121). MiRNAs that bypass processing by Drosha are called mirtrons as they originate from short introns that, after splicing and debranching, have a structure similar to that of stem-loop pre-miRNAs and are thus directly exported and cleaved by Dicer, while skipping the first maturation step normally executed by Drosha (101,121).

While miRNAs are generally considered to exert their function in the cytoplasm of a cell, it is important to note that miRNAs can also be secreted from cells by being sorted into a type of extracellular vesicles called exosomes (122). Exosomes are formed as luminal multivesicular endosomes that are eventually released into the extracellular space or the circulation after fusion with the plasma membrane (123). Thereby, they function as mediators of intercellular

communication as they can be taken up by other cells, where their contained cargo, lipids, proteins, mRNA, and miRNAs, affects the recipient cell (123). The cargo of an exosome can be specific for the cell type it is released from and can also be impacted by disease conditions, which is why exosomal miRNAs have gained attention as potential disease biomarkers, in particular for cancer (122,124).

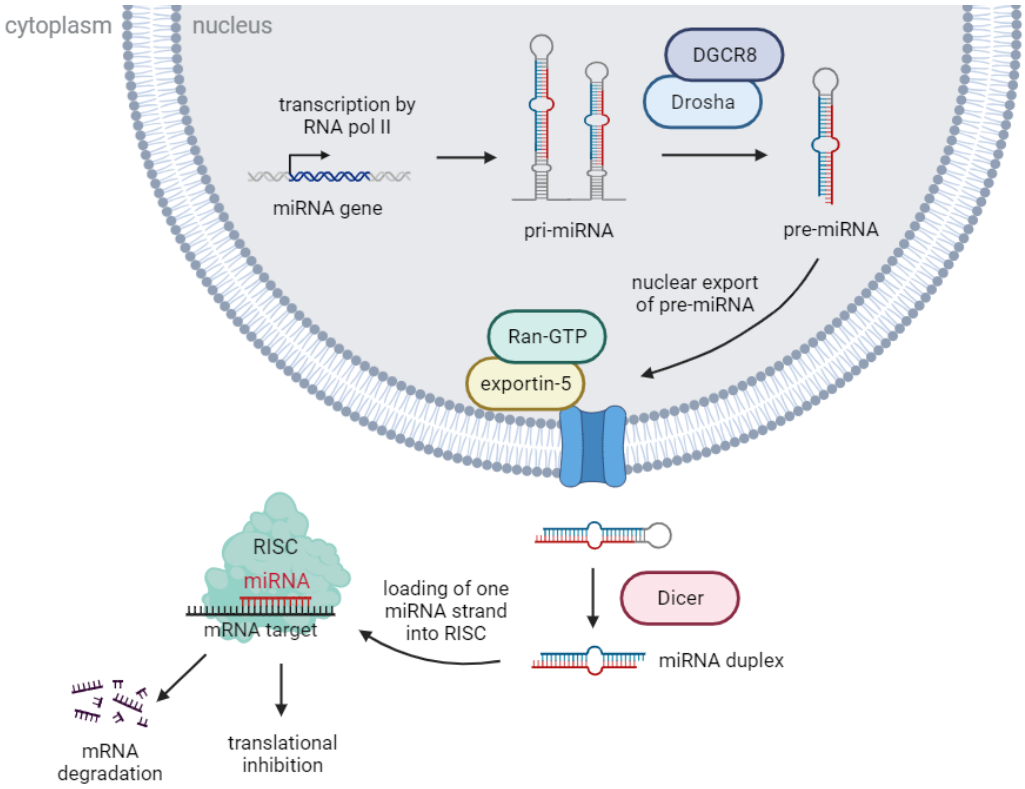

Figure 2: Canonical microRNA (miRNA) biogenesis. *MiRNAs are transcribed by RNA polymerase II into mono- or polycistronic primary miRNA (pri-miRNA) transcripts, which are cleaved by the ribonuclease Drosha in complex with the RNA-binding protein DGCR8 to form stem-loop precursor-miRNAs (pre-miRNA). The pre-miRNA is exported from the nucleus by interacting with exportin-5 and Ran-GTP. In the cytoplasm, the pre-miRNA is cleaved by the ribonuclease Dicer into a short miRNA duplex, from which one strand is incorporated into the RNA-induced silencing complex (RISC). The mature miRNA then recognizes a mRNA target by complementary base-pairing. This can result in the degradation of the mRNA, initiated by deadenylation or by cleavage through a component of RISC, or translational inhibition through blocking ribosome recruitment or translational elongation, or sequestration away from the ribosomal machinery (Figure created with BioRender).*

1.7. MicroRNAs – Role in cancer and breast cancer

It has been discovered that miRNA expression is frequently altered in different cancer types, which, due to the extensive number of miRNA targets, has a profound cellular impact and ties

miRNAs to the initiation, progression, and recurrence of tumors (125,115). The deregulation of miRNAs in cancer can be caused in different ways. For example, the two key enzymes in the biogenesis of miRNAs, Drosha and Dicer, are generally downregulated in various cancer types, including breast cancer, resulting in a global downregulation of mature miRNAs (125). Also other factors involved in the maturation process of miRNAs may be affected by cancer, as for example the DEAD-box RNA helicase p68, whose assembly with Drosha is impeded by oncogenic mutants of p53 (126). Other factors causing the deregulation of miRNAs in cancer occur on the genetic level, like translocations, deletions, or point mutations (117,127). In fact, Calin *et al.* have discovered that miRNAs are frequently located in cancer-associated genomic regions or fragile sites (128). While miRNAs are often downregulated, also upregulation is possible, which can be mediated via oncogenic transcription factor regulation or due to genomic amplifications (117,125). As an example, miR-10b was found to be highly expressed in metastatic breast cancer due to direct transcriptional activation by the EMT-associated transcription factor Twist (129). MiR-10b targets, amongst others, the tumor-suppressor HOXD10, which results in upregulation of members of the Rho GTPase, crucial regulators of cell adhesion and actin remodeling (129–131). Thereby, miR-10b promotes the invasiveness and metastatic dissemination of breast cancer cells (129,130).

Functionally, the deregulation of miRNAs can have either oncogenic or tumor-suppressive effects, depending on their mRNA targets and the cellular context (132). Oncogenic miRNAs, like miR-10b mentioned above, are generally overexpressed in cancer and primarily target tumor suppressor genes, thereby promoting tumorigenesis (132) (Figure 3). Conversely, tumor-suppressive miRNAs show a low expression and have mainly oncogenes as targets, meaning that their lack of expression favors tumorigenesis (132) (Figure 3). In case of breast cancer, a multitude of tumor-suppressive and oncogenic miRNAs have already been discovered that, owing to their diverse targets, are involved in many of the hallmarks of cancer, including sustained growth and proliferation, replicative immortality, invasion and metastasis, apoptotic resistance, angiogenesis, reprogrammed metabolic activity, and evasion of immune cell destruction (132,133) (Figure 3). In the following, some well-characterized miRNAs with a role in breast cancer will be described in order to highlight and exemplify the multifarious functions of miRNAs.

A miRNA that has already been discovered early on and has been studied extensively since is miR-21 (134). The miR-21 gene is located in a common fragile site that is frequently amplified in breast cancer (135). Its expression was thus found to be elevated in breast tumors and to have an oncogenic effect on proliferation, migration, invasion, and apoptosis by targeting various genes such as the tumor suppressor PTEN, metalloproteinase inhibitor 3 (TIMP3), and

the anti-apoptotic factor B cell lymphoma 2 (BCL2), highlighting the broad range of cancer hallmarks a single miRNA can influence (134,136,137). Efforts have also been made to use miR-21 expression levels as a circulating prognostic biomarker in breast cancer (135).

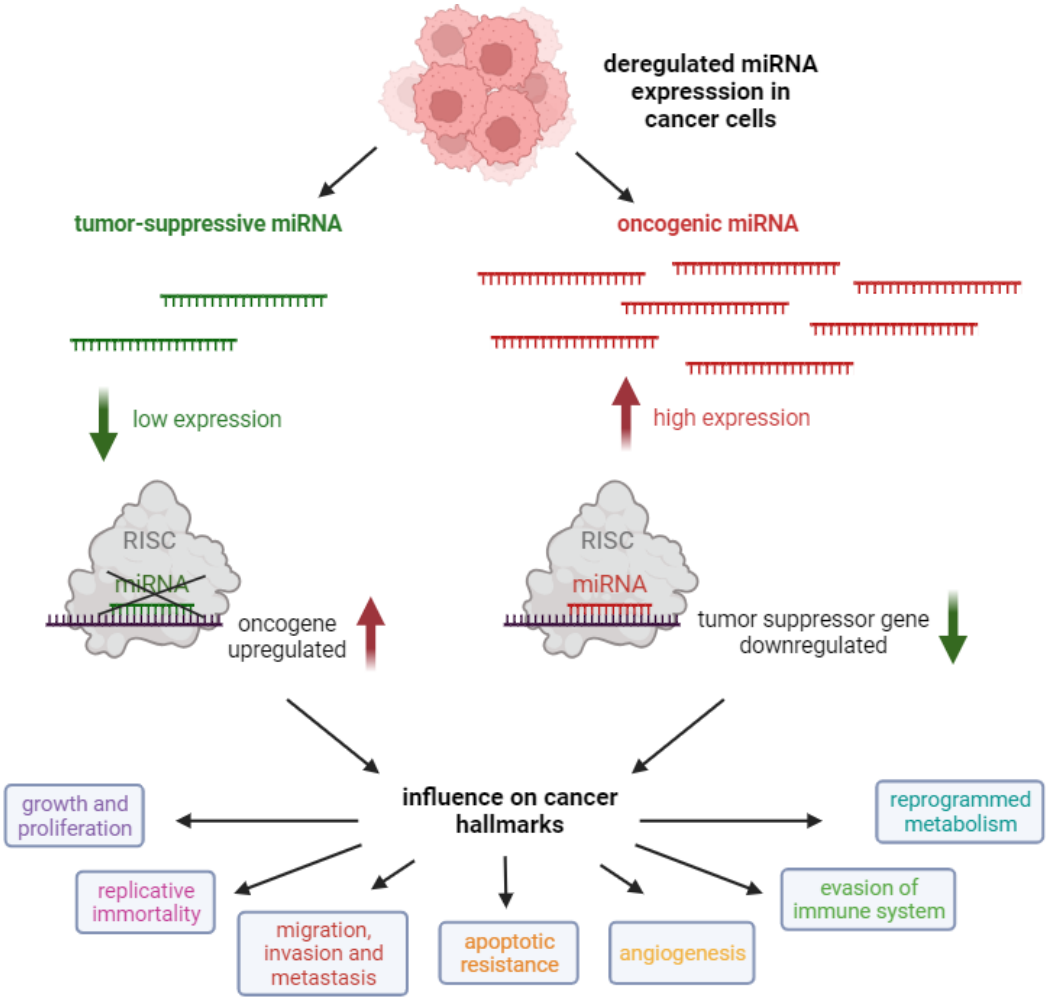

Figure 3: The role of tumor-suppressive and oncogenic microRNAs (miRNAs) in cancer cells. *Cancer cells frequently show deregulated expression of miRNAs, namely low expression of tumor-suppressive miRNAs and high expression of oncogenic miRNAs. Tumor-suppressive miRNAs generally target oncogenes, meaning the lack of tumor-suppressive miRNAs results in an upregulation of oncogenes. Oncogenic miRNAs, on the other hand, mostly target tumor suppressor genes so that their high expression in cancer cells causes a downregulation of tumor suppressor genes. Thereby, the deregulation of miRNAs affects several cancer hallmarks (Figure created with BioRender).*

One of the best known families of miRNAs is the miR-200 family, which is located on two different chromosomes and includes five miRNAs (miR-200b, miR-200a, miR-429, miR-200c, and miR-141) whose seed sequences are either identical or differ only by one nt (138). The miR-200 family is particularly known for its role in EMT and its expression is regulated by EMT-

associated transcription factors such as zinc finger E-box binding homeobox 1 and 2 (ZEB1 and ZEB2), which repress their transcription (138). The miR-200 family plays a relevant role in both the physiologic development and branching morphogenesis of the mammary glands, as well as the progression of breast cancer (138). Low expression of the miR-200 family results in high expression of its targets that include mesenchymal markers, thus promoting EMT and an invasive and aggressive breast cancer phenotype (138,139). The miR-200 family members also affect other aspects of cancer biology. They were, for example, found to directly target the pro-angiogenic cytokines interleukin-8 (IL-8) and C-X-C motif chemokine ligand 1 (CXCL1), thereby reducing *in vitro* tube formation of vascular endothelial cells and tumor angiogenesis *in vivo* (140). In addition, basal-like breast tumors were found to have a lower expression of the miR-200 members than luminal tumors and in turn exhibit higher IL-8 and CXCL1 expression as well as more strongly pronounced mesenchymal features that may contribute to the aggressiveness of the subtype (139–141). Substituting the low miR-200 family expression in a basal-like breast cancer mouse model through therapeutic delivery of miR-141 nanoliposomes was shown to reduce primary tumor growth and lung metastasis formation (140).

The fact that the miR-200 family affects endothelial cells and angiogenesis, amongst others by reducing the production and secretion of cytokines, highlights the importance of miRNAs not only for cancer cells directly but also in regard to the TME (142). MiR-155 gives another good example of how a miRNA can alter the TME. Overexpression of miR-155 in breast cancer cells directly targets the suppressor of cytokine signaling 1 (SOCS1), which results in the increased secretion of chemokines that recruit T cells, thereby promoting an anti-tumor immune response and sensitizing tumors to immune checkpoint inhibitors (143). MiR-155 is also known to regulate the function of various immune cells directly (142). For example, its expression in dendritic cells enhances their migration and maturation in the breast TME, thereby driving their activation of T cells and boosting anti-tumor immunity (144,145). In summary, two ways how miRNAs can affect cells in the TME are by modulating the secretion of cytokines and other signaling molecules from breast cancer cells, thereby having an indirect impact on cells like endothelial cells and immune cells, and by exerting direct regulatory roles in cells of the TME (142). Another mechanism of how miRNAs are involved in the communication of breast cancer cells with the TME is, as mentioned previously, by being released into exosomes (125,142). The recipient cells do not only have to be other cell types in the TME, like endothelial cells, but can also be other breast cancer cell subpopulations (146). For example, miR-155 was found to be enriched in exosomes from breast CSC and cells resistant to chemotherapy and to be

transferred to other breast cancer cells where it also induced chemoresistance and EMT characteristics (146).

The distinction of whether a miRNA acts as a tumor suppressor or an oncogene is not always so clear and easy to define due to the fact that a single miRNA can target a plethora of different genes, both tumor suppressors and oncogenes simultaneously, and the resulting net effect depends on the balance and expression of these targets which may differ in different cellular contexts (147). The already discussed miR-155 provides a good example of the complexity and sometimes even contradictory role a miRNA can have. Several studies, as detailed above, reported the tumor-suppressive effects of miR-155 on immune cells in the breast TME (143–145). Originally though, miR-155 was described to solely function as an oncogenic miRNA (148). More than 100 direct targets of miR-155 have been confirmed experimentally that are involved in regulating proliferation, EMT, angiogenesis, differentiation, and apoptosis (148). For example, by targeting and downregulating SOCS1, miR-155 enhances janus kinase (JAK)/signal transducers and activators of transcription (STAT) signaling, a pathway activated by growth factors and cytokines, which ultimately favors proliferation and breast tumor growth (149,150). On the other hand, this also causes increased secretion of anti-tumor immunity-promoting cytokines, thus having tumor-suppressive effects (143).

1.8. MicroRNAs – Role as diagnostic, prognostic, and therapeutic candidates in breast cancer

The critical involvement of miRNAs in many cancer hallmarks, as exemplified for breast cancer above, has initiated efforts to explore miRNAs for diagnostic, prognostic, and therapeutic purposes (151,152). As miRNAs can be found in the circulation and levels of certain miRNAs vary with disease conditions, they present promising candidates as minimally invasive biomarkers for the diagnosis and prognosis of cancer (152). For example, a study by Kahraman *et al.* showed that the expression of a panel of seven miRNAs measured from blood allowed for early diagnosis of TNBC (153). Moreover, they found that changes in the miRNA levels during neoadjuvant chemotherapy could also give predictive information about treatment response (153). Gasparini *et al.* have identified a four-miRNA panel, miR-155, miR-493, miR-30e, and miR-27a, that allowed them to subclassify TNBC cases and to predict high-risk patients (154). However, despite the diagnostic and prognostic power of such miRNA panels, none have been implemented in the clinics yet for the use in breast cancer, as verification, clinical validation, and standardization of miRNA level measurements pose some challenges (152).

In addition to diagnostic and prognostic purposes, miRNAs have also been extensively studied as potential therapeutic applications for the treatment of various types of cancer (151). Two approaches are to be discerned, the inhibition of oncogenic miRNAs by using complementary locked nucleic acid (LNA) antisense oligonucleotides and the upregulation/overexpression of tumor-suppressive miRNAs by using synthetic miRNA duplexes, so-called mimics, that consist of a guide strand with the miRNA sequence-of-interest and a complementary passenger strand that is rapidly degraded (151). Despite being promising candidates for cancer therapy due to their far-reaching impact on many aspects of carcinogenesis, miRNAs as therapeutics are facing some critical challenges (155). These challenges include rapid degradation of the naked miRNA in the circulation, as well as intracellular degradation in lysosomes after endosomal entrapment, insufficient penetration into tumors, immune- and neurotoxicity, and the need for cell-type specific delivery (155). Due to these points, multiple miRNA-based therapeutics have entered clinical trials but none have reached phase III so far (155). The first-in-human clinical trial of a miRNA therapeutic was based on the liposomal delivery of a miR-34a mimic, called MRX34 (156,157). The clinical trial was performed on different types of advanced solid tumors, including liver cancer, small-cell lung cancer and non-small cell lung cancer, lymphoma, melanoma, multiple myeloma, and renal cell carcinoma, and could show successful delivery of the miRNA to the tumors (156,157). However, the study had to be terminated early due to severe immune-related adverse events that led to the death of four patients (157). The systemic delivery of miRNAs can trigger an inflammatory type I interferon response by activating Toll-like receptors that can sense double-stranded RNA in endosomal and lysosomal compartments (158). Numerous new developments have been made to overcome the challenges that miRNA therapeutics are facing. For example, chemical modifications have been introduced that reduce the immunostimulatory properties of miRNA mimics, enhance their stability, and increase target binding affinity (152). Other improvements have been made in regard to delivery strategies. Different nanocarrier materials have been used, such as lipids, polymers like for example polyethyleneimine (PEI), inorganic materials like iron oxide and gold, and also exosomes (151,155,158). These nanoparticles allow protection of the miRNA payload in the circulation, targeted delivery through, for example, conjugation with cancer cell-targeting ligands, and also improved cellular uptake (151,155,158). To give an example of these developments regarding miRNA delivery strategies, a study by Sharma *et al.* has reported the successful use of hybrid lipo-polymeric nanoparticles for the co-delivery of a miR-34a mimic and a chemotherapeutic agent that were targeted to folate receptor-overexpressing breast cancer cells by being conjugated with folate (159). The approach has also allowed evasion of endo-lysosomal entrapment (159). Others have reported similar approaches, like the use of

PEI-poly-lactide-co-glycolide nanoparticles carrying the tumor-suppressive miR-542-3p combined with doxorubicin (160). The particles were specifically targeted to CD44, a cell adhesion glycoprotein that is overexpressed on cancer cells such as TNBC cells, by being coated with hyaluronic acid (160). More general targeting approaches include pH-sensitive nanocarriers that specifically release their cargo in the more acidic TME (158).

With many ongoing and upcoming developments in the pre-clinical field, there are currently also two clinical trials ongoing/planned that use miRNAs as therapeutic approaches in breast cancer. First, the INT-1B3 trial, which includes TNBC patients in a currently recruiting phase 1 clinical trial of a lipid nanoparticle-encapsulated miR-193a-3p mimic (161,162). And second, the TTX-MC138 trial is set to test first clinical pharmacodynamic properties of a dextran-coated iron oxide nanoparticle carrying an antisense oligonucleotide against miR-10b, including patients with metastatic breast cancer (162).

1.9. Rationale and aims of the dissertation

The aggressive breast cancer subtype TNBC still poses a therapeutic challenge and the development of more efficient therapies requires further elucidation of mechanisms of TNBC tumorigenesis and the identification of new therapeutic targets. As outlined above, miRNAs are known to be important contributors to virtually all hallmarks of breast cancer, including TNBC, and show strong therapeutic potential. They are thus also interesting players in TNBC that could not only serve as direct therapeutic targets but that might also reveal new oncogenic pathways and vulnerabilities of this particular breast cancer subtype.

The primary aim of this dissertation was to identify and extensively characterize new miRNAs with a potential role in TNBC. In order to characterize their function and to determine whether the identified miRNA candidates play a tumor-suppressive or oncogenic role in TNBC, the aim was to perform phenotypic *in vitro* assays investigating various important cancer cell characteristics commonly affected by miRNAs, like proliferation, migration, apoptosis, and angiogenesis, by means of two previously described approaches, namely ectopic miRNA upregulation by using mimics and miRNA inhibition by using antisense inhibitors. In addition to phenotypic characterization, a second aim was the characterization of pathways being affected by the deregulation of the miRNA candidates and the identification of direct targets that could help to explain phenotypic effects. Lastly, we aimed to explore the potential therapeutic utility of the miRNA candidates as well as of associated targets and pathways. To fully test a potential therapeutic utility, but also to confirm our *in vitro* findings, we aimed to conduct *in vivo* experiments.

For the initial selection of novel miRNA candidates with a potential role in TNBC, we made use of the results of a previous study. In this study, a so-called mammosphere model was applied to screen for miRNAs that were differentially expressed between 3D tumor spheres of breast cancer cells lines, referred to as mammospheres, and normal adherently growing breast cancer cell lines using a miRNA microarray (163). Three different breast cancer cell lines were used for this model, the two ER-positive cell lines MCF-7 and BT-474, and the TNBC cell line SUM159, that were cultured either in ultra-low attachment plates to form mammospheres or in conventional 2D cell culture dishes as controls (163). The mammosphere assay is a relevant model because it entails the enrichment of stem-cell-like breast cancer cells (164). As discussed in a previous chapter, breast CSC, whose percentage is higher in TNBC than in less aggressive subtypes, are cells with a tumor-initiating capability that exhibit metabolic plasticity and are associated with chemoresistance, metastasis and relapse, attributes also characteristic of TNBC (29,33,36,37,39,40,165). The mammosphere assay is thus a good model system for the identification of miRNAs with a role in TNBC carcinogenesis. In the study by Schwarzenbacher *et al.*, several up- and downregulated miRNAs were identified in the mammospheres, some of which were already known to play a role in breast cancer (163). For example, the top-most upregulated miRNA, miR-664, had been found to have a tumor-suppressive effect in breast cancer by targeting insulin receptor substrate 1 (IRS1), thereby reducing proliferation and invasion (166). Its expression had also been reported to be regulated by BRCA1 (167). As the aim of this dissertation was to identify and characterize new miRNAs with a potential role in breast cancer, we focused on deregulated candidates with a, at that point in time, still unknown function. For this reason, we selected the second and third most upregulated miRNA, miR-4649-5p and miR-4646-5p, both of which had not been studied or linked to cancer previously. Due to their significant deregulation in the stem cell-enriched mammospheres, alongside other miRNAs with an already proven function in breast cancer, it appeared rather likely that these two new miRNAs also play a role in breast cancer. The question to be answered was whether this is the case, particularly in TNBC, whether it is a tumor-suppressive or oncogenic role and what are the mechanisms behind it. By answering these questions, the knowledge generated in this dissertation could help to identify novel therapeutic vulnerabilities that might be of benefit in the treatment of TNBC.

2. Material and Methods

2.1. *In silico* analysis of patient data

To assess the prognostic relevance of the two miRNA candidates miR-4646-5p and miR-4649-5p, their host genes abhydrolase domain containing 16A, phospholipase (ABHD16A) and adipocyte enhancer-binding protein 1 (AEBP1), and their targets GRAM domain-containing protein 1B (GRAMD1B) and phosphatidylinositol-4-phosphate 5-kinase type 1 gamma (PIP5K1C), survival analyses were performed using an online Kaplan-Meier analysis platform, that offers different tools for the analysis of the prognostic significance of the expression of miRNAs, mRNAs, and protein levels. The tools used were: for miR-4646 and miR-4649 expression https://kmplot.com/analysis/index.php?p=service&cancer=breast_mirna (168), for ABHD16A, AEBP1, GRAMD1B and PIP5K1C mRNA expression https://kmplot.com/analysis/index.php?p=service&cancer=breast (169), and for PIP5K1C on the protein level https://kmplot.com/analysis/index.php?p=service&cancer=breast_protein (170). For miR-4646 and miR-4649, the overall survival of 97 patients with TNBC was analyzed based on RNA-seq data from the Cancer Genome Atlas Project (TCGA) (168). For ABHD16A, the overall survival of 144 TNBC patients and 296 patients with basal breast cancer (PAM50 classification) was analyzed based on Gene Expression Omnibus (GEO) microarray data (169). For AEBP1, the overall survival of 153 TNBC patients and 431 patients with basal breast cancer (PAM50 classification) was analyzed based on GEO microarray data (169). For GRAMD1B, the overall survival of 153 TNBC patients, the relapse-free survival of 392 TNBC patients, and the distant metastasis-free survival of 306 TNBC patients were analyzed based on GEO microarray data (169). For PIP5K1C, the overall survival of 153 TNBC patients, and the relapse-free survival of 392 TNBC patients were analyzed based on GEO microarray data (169), as well as the overall survival of 65 breast cancer patients (without subtype discrimination due to a small cohort size) based on proteomics data (170). For all analyses, patients were separated into groups of low and high-expression based on an optimal auto-selected cutoff and the groups were compared by log-rank test. The follow-up was limited to 60 months.

The online tool TNMplot (171) was used to analyze the expression of ABHD16A, AEBP1, GRAMD1B, and PIP5K1C in invasive breast tumors compared to healthy adjacent tissue based on RNA-seq TCGA data. For ABHD16A, AEBP1, and PIP5K1C, data from 112 samples per group was analyzed, for GRAMD1B from 70 samples. Statistical analysis was performed by Mann-Whitney-U tests.

2.2. Cell lines and cell culture conditions

For the purpose of this dissertation, the following human breast cancer (BC) cell lines were used: The non-malignant mammary epithelial cell line MCF-12A. The estrogen receptor positive BC cell lines MCF-7, T47D, and BT-474. The HER2-positive BC cell lines HCC1419 and SKBR3. The triple negative breast cancer cell lines HCC1937, BT-549, MDA-MB-468, MDA-MB-231, SUM159, and BT-20. MCF-12A, MCF-7, T47D, BT-474, HCC1419, SKBR3, HCC1937, BT-549, BT-20, MDA-MB-468, and MDA-MB-231 cells were obtained from the American Type Culture Collection (ATCC; Manassas, CA, USA). SUM159 cells were purchased from Asterand (Detroit, MI, USA). In addition, HEK239 cells were acquired from ATCC, and single-donor human umbilical vein endothelial cells (HUVECs) from Lonza (Basel, Switzerland).

HCC1419, HCC1937, and BT-549 cells were maintained in RPMI 1640 with L-glutamine (Gibco, Darmstadt, Germany) supplemented with 10% fetal bovine serum (FBS) (Serana, Pessin, Germany) and 1% penicillin/streptomycin (pen/strep; final concentration penicillin: 100 units/ml; final concentration streptomycin: 100 µg/ml; Sigma-Aldrich, St. Louis, MO, USA). MDA-MB-231, MDA-MB-468, and HEK239 cells were cultured in high-glucose DMEM (4.5 g/L D-Glucose, L-Glutamine, 25 mM HEPES; Gibco, Thermo Fisher Scientific, Waltham, MA, USA), 10% FBS (Serana), and 1% pen/strep (Gibco). MCF-7 cells were grown in MEM with Earle's salts containing 2 mmol/L L-Glutamine (PAA, Pasching, Austria), 1% sodium pyruvate (Gibco), 1% pen/strep (Sigma-Aldrich), and 10% FBS (Serana). BT-474 were grown in RPMI 1640 (with L-Glutamine, Gibco), 20% FBS (Serana), 1% pen/strep (Gibco), and 10 µg/ml insulin (Sigma-Aldrich). SKBR3 were cultured in McCoy's 5A modified Medium (Gibco; w/o L-Glutamine, 2.2 g/L sodium bicarbonate), 1% pen/strep (Sigma-Aldrich), and 10% FBS (Serana). SUM159 cells were grown in HyClone™ Ham's Nutrient Mixture F12 with L-Glutamine (Cytiva, Marlborough, MA, USA) supplemented with 2 mmol/L HEPES buffer (Gibco), 5 µg/ml insulin (Sigma-Aldrich), 1 µg/ml hydrocortisone (Sigma-Aldrich), 1% pen/strep (Sigma-Aldrich), and 5% FBS (Serana). BT-20 were maintained in Minimum Essential Medium – Eagle with Earle's BSS and L-Glutamine (Lonza, Basel, Switzerland) supplemented with 10% FBS (Serana) and 1% pen/strep (Sigma-Aldrich). HUVECs were maintained in EBMTM-2 Basal Medium (Lonza) that was supplemented with EGMTM-2 SingleQuots™ Supplements (Lonza) according to the supplier's instructions.

All cell lines were cultured under standard conditions in a humidified incubator at 5% CO_2 and 37 °C. The two cell lines that were used most extensively, namely SUM159 and MDA-MB-231, underwent mycoplasma testing using the Venor® GeM Mycoplasma Detection Kit (Minerva

Biolabs, Berlin, Germany), which was conducted by the Core Facility for Alternative Biomodels & Preclinical Imaging of the Medical University of Graz, Austria.

2.3. Transient transfection of miR-4646-5p and miR-4649-5p mimic/inhibitor and transient knockdown of GRAMD1B and PIP5K1C

In order to generate transient overexpression or inhibition of miR-4646-5p and miR-4649-5p, cells were transfected with synthetic miRNA mimics or locked nucleic acid (LNA) antisense inhibitors. For these transfections, 10 nM mirVana™ hsa-miR-4646-5p or hsa-miR-4649-5p mimic and the mirVana™ mimic control (Thermo Fisher Scientific), or 50 nM hsa-miR-4646-5p miRCURY LNA miRNA Inhibitor and the miRCURY LNA miRNA Inhibitor Control A (Qiagen, Venlo, The Netherlands), were used.

To achieve a transient knockdown of the two miRNA targets GRAMD1B and PIP5K1C, cells were transfected with 40 nM GRAMD1B siRNA #3 (targeting sequence AGGAATCGCTATCATTGACAA; Qiagen) or 20 nM PIP5K1C siRNA #8 (targeting sequence: TTCCTGTACTGTAAAGACTAA; Qiagen), respectively, and the AllStars Negative Control siRNA (Qiagen) in equal concentrations. For the purpose of assessing apoptosis induction, the AllStars Hs Cell Death Control siRNA (Qiagen) was transfected at a concentration of 10 nM.

For standard transfections (exceptions will be detailed in the respective methods sections), cells were transfected using the HiPerFect Transfection Reagent (Qiagen), where different protocols of the manufacturer were applied depending on the cell culture format. To transfect cells in the format of 6-well plates or 6 cm dishes, the fast-forward transfection protocol was followed. In brief, this means cell suspensions were added to the culture plates before adding the transfection mixes dropwise while rotating the plates. For 96-well plates, the reverse transfection protocol was applied, where the transfection mix was added to the wells first, followed by the cell suspension. Transfection mixes were prepared according to Table 1, mixed by vortexing, and incubated at room temperature for 20 min before adding them to the cells.

Table 1: Preparation of transfection mixes using HiPerFect (Qiagen). *Volumes are indicated for three cell culture formats. RNA stocks of 20 µM were prepared in RNase-free water and added to reach the desired final concentration in the total volume of medium used in each cell culture format. Standard total medium volumes were 200 µl in 96-well plates, 2.5 ml in 6-well plates, and 4 ml in 6 cm dishes.*

	96-well plate	**6-well plate**	**6 cm dish**
HiPerFect	0.75 µl	10 µl	20 µl
RNA stock (20 µM)	To reach desired final concentration	To reach desired final concentration	To reach desired final concentration
Serum-free medium	To total volume	To total volume	To total volume
Total volume transfection mix per well/dish	25 µl	100 µl	100 µl

2.4. Generation of stable miR-4646-5p and miR-4649-5p cell lines by lentiviral transduction

In addition to transient transfections, a stable miR-4646-5p inhibitor and a stable miR-4649-5p mimic cell line were generated by lentiviral transduction. For this purpose, SUM159 cells were seeded in a 12-well plate with 1 × 10^5 cells/well and incubated overnight in complete growth medium. The following day, the medium was changed to complete growth medium supplemented with 10 µg/ml polybrene (Santa Cruz Biotechnology, Santa Cruz, CA, USA) and ViralPlus Transduction Enhancer (Applied Biological Materials, Richmond, BC, Canada) in a 1:200 dilution. To transduce cells, 20 µl lentivirus were added dropwise per well. The following lentiviruses were used: LentimiRa-Off-hsa-miR-4646-5p Virus (titer 1.49 × 10^8 IU/ml), LentimiRa-GFP-hsa-miR-4649-5p Virus (titer 2.04 × 10^8 IU/ml), and Lenti-III-mir-Off Control Virus (titer 3.85 × 10^8 IU/ml). Lentiviruses were purchased ready-to-use from Applied Biological Materials. 24 h after transduction, the medium was changed back to normal growth medium. 48 h after transduction, puromycin dihydrochloride (Gibco) was added to a final concentration of 1.5 µg/ml to select for positively transduced cells. The selection was continued for one week, during which time medium was changed every second day and fresh puromycin was added. As the transduced lentiviral vectors co-expressed GFP, cells were sorted by fluorescence-activated cell sorting (FACS) for high GFP intensity, which was performed by the Imaging Core Facility, Center for Medical Research (ZMF), Medical University of Graz, Austria.

2.5. RNA isolation and cDNA synthesis

For subsequent reverse transcription quantitative PCR (qPCR) or digital droplet PCR (ddPCR), RNA was isolated from cultured cells at a confluency of approximately 75 to 95 % in biological triplicates by using TRIzol™ Reagent (Thermo Fisher Scientific) following the protocol provided by the manufacturer. In brief, cell culture medium was removed, cells were washed once with phosphate-buffered saline (PBS), and Trizol was added (1 ml per well of a 6-well plate). Trizol lysates were either processed immediately or stored at -20 °C. Lysates were homogenized by being passed through a 22G syringe before adding 100 µl 1-bromo-3-chloropropane (Sigma-Aldrich) per 1 ml Trizol. Samples were mixed by vigorous inversion, incubated for ~3 min, and centrifuged at 13 000 rpm 4 °C for 20 min to facilitate phase separation. Upper aqueous phases were transferred to new 2 ml tubes containing 0.5 ml isopropanol (Sigma-Aldrich). Samples were mixed by shaking, incubated for ~10 min, and centrifuged at 13 000 rpm 4 °C for 20 min to pellet precipitated RNA. Supernatant was removed and RNA pellets were washed three times with 1 ml 75% ethanol and centrifuged at 13 000 rpm 4 °C for 5 min. RNA pellets were dried at 55 °C for 10 min to remove residual ethanol and resuspended in 20 µl RNase-free

water. RNA concentrations were measured using a NanoDrop™ 2000/2000c (Thermo Fisher Scientific). For reverse transcription into cDNA, 1 µg of total RNA was used per sample. Depending on whether only miRNAs were detected from samples, or whether both mRNA and miRNAs were detected from the same sample, the miScript II RT Kit combined with the miScript HiFlex Buffer (Qiagen) or the QuantiTect Reverse Transcription Kit (Qiagen), was used, respectively. Both kits were used according to the manufacturer`s protocols.

2.6. Quantitative PCR (qPCR)

Quantitative PCR was conducted in technical duplicates of biological triplicates using the QuantiTect SYBR Green PCR Kit (Qiagen) as detailed in the manufacturer's two-step RT-PCR protocol. In brief, per qPCR reaction (total volume of 10 µl) 1 ng of cDNA was used for the detection of miRNAs or 10 ng for the detection of mRNAs from coding genes, together with 5 µl QuantiTect SYBR Green Master Mix (Qiagen) and the respective primers. For the detection of mRNAs, forward and reverse primers were added in a final concentration of 10 µM. These primers were designed using the NIH Primer Blast Tool (https://www.ncbi. nlm.nih.gov/tools/ primer-blast/) and ordered from Eurofins Scientific SE (Luxembourg City, Luxembourg). A list of all primer sequences for the detection of coding genes, including the two housekeeper genes GAPDH and U6, is given in Table 2. For the detection of miRNAs, pre-designed primer assays were used: the Hs_miR-4646-5p_1 miScript Primer Assay and the Hs_miR-4649-5p_1 miScript Primer Assay (Qiagen), together with the miScript Universal Primer from the miScript SYBR Green PCR Kit (Qiagen) in a 1:10 dilution according to the manufacturer. MiR-4646-5p and miR-4649-5p expression were normalized to the small nucleolar RNAs SNORD61 and SNORD95, using the Hs_SNORD61_11 and Hs_SNORD95_11 miScript Primer Assay (Qiagen).

qPCR measurements were performed in LightCycler® 480 Multiwell Plates 384 (Roche, Basel, Switzerland) using a LightCycler® 480 Real-Time PCR System (Roche). Ct values were calculated based on second derivative max. testing by the LightCycler® 480 software (Roche). To normalize the Ct values to receive delta Ct (ΔCt) values, the respective arithmetic mean from the two housekeeper genes was subtracted from each raw Ct value. To calculate relative expression levels as described by the ΔΔCt method, the ΔCt value of the respective negative control was subtracted from each treated sample. Unless indicated otherwise, relative expression was plotted as $2^{-\Delta\Delta Ct}$.

The qPCR on the panel of apoptosis-associated genes (Figure 14) was performed by Felix Prinz, currently PhD student at the Department of Internal Medicine, Division of Oncology, Medical University of Graz, Austria.

Table 2: List of all primer sequences used for qPCR detection of coding genes.

Gene name	Primer Sequence (5'->3')
ANG	**Forward** TATTCATGGCAACAAGCGCA **Reverse** TAGCTTGCAAGTGGTGACCT
BAD	**Forward** TGT GGA CTC CTT TAA GAA GGG AC **Reverse** CAC CAG GAC TGG AAG ACT CG
BAK	**Forward** TGC CCT CTG CTT CTG AGG A **Reverse** TTC CTG CTG ATG GCG GTA AA
BAX	**Forward** AGG GTG GTT GGG GGC TG **Reverse** AAA GTA GGA GAG GAG GCC GT
BCL10	**Forward** GGTCTGGACACCCTTGTTGA **Reverse** ACTGCTACATTTTAGTCCTTTCAGA
BIK	**Forward** CATGGAGGGCAGTGACGCAT **Reverse** TGTCCTCAGTCTGGTCGTAGA
CALD1	**Forward** AGAGCAGTGTGTATTCGGCT **Reverse** TGTTCCAATGATACCTTGTAGTCT
CARD19	**Forward** TGCAGAACTCAGATTGCACAGA **Reverse** AGCTCATGGGTCCCCTGTT
CARD8	**Forward** CAGAGGGACAAGATTCAGGAGA **Reverse** TTCAGGCCCCAGAAACTGAC
CASP3	**Forward** GGCGCTCTGGTTTTCGTTAAT **Reverse** TCCAGAGTCCATTGATTCGCT
CDKNA1	**Forward** TGCCGAAGTCAGTTCCTTGT **Reverse** GTTCTGACATGGCGCCTCC
CFH	**Forward** AGGATATGTAACAGCAGATGGTGA **Reverse** GGGTTGAGCTGACCATCCAT
DBP	**Forward** ACCCTCTTGAGTTGCACGTT **Reverse** CCCTCCAGTATCCAGAACGC
DIABLO	**Forward** ATCTGACTTCTACTTCCAGGCTGT **Reverse** GCTCTGGCTCCTATGATCACC
EGR1	**Forward** ACCTGACCGCAGAGTCTTTT **Reverse** GAGTGGTTTGGCTGGGGTAA
FADD	**Forward** CCTGGGGAAGAAGACCTGTG **Reverse** AGACTTTGAGCTGACGAGCC
FasL	**Forward** ATGGTTCTGGTTGCCTTGGT **Reverse** GCATCTGGCTGGTAGACTCTC
FGF2	**Forward** GCTGTACTGCAAAAACGGGG **Reverse** TAGCTTGATGTGAGGGTCGC
FOS	**Forward** CAGACTACGAGGCGTCATCC **Reverse** CGTGGGAATGAAGTTGGCAC
GAPDH	**Forward** AAGGTCGGAGTCAACGGATTT **Reverse** ACCAGAGTTAAAAGCAGCCCTG
GCSF	**Forward** TTGAGCCAACTCCATAGCGG **Reverse** TCCCAGTTCTTCCATCTGCTG
GRAMD1B	**Forward** TCAAACATGTGGCAGGTTCC **Reverse** TAAGGATGACCAGCAGCACC
HIF1A	**Forward** GGATTACCACAGCTGACCAGTTA **Reverse** GCAGTAGGTTTCTGCTGCCTT
IL6	**Forward** ACCCCCAATAAATATAGGACTGGA **Reverse** GAGAAGGCAACTGGACCGAA
LAMA4	**Forward** TGGACTGCCCAACCATAAGC **Reverse** CCGGATTTGCCTTCCTCGAT

Table 2 *(continued)*

Gene name	Primer Sequence (5'->3')
MMP1	**Forward** CTTTTGTCAGGGGAGATCATCG **Reverse** TGGGAGAGTCCAAGAGAATGG
NID2	**Forward** CTGGAGGAGGGATGGTGTTG **Reverse** TGTTGGGCAGTAGGGGTAGA
NOXA	**Forward** GGA GAT GCC TGG GAA GAA GG **Reverse** CAC TCG ACT TCC AGC TCT GC
NRP2	**Forward** GTACCAGATTGTGTTCGAGGG **Reverse** TTCTCACCTGCAAAAGCCGA
PACS1	**Forward** TAACCTTCTCCCTTCAGTACCC **Reverse** CGCCTTCATTAGGATGCTGC
PIP5K1C	**Forward** CGAATCGGATGACACGATGGG **Reverse** AAGCGCTCGGCATAGAAGC
PLAGL2	**Forward** AATGCACCGCACAATGGC **Reverse** ATTGAGAAAGCCTCCCCATCC
PUMA	**Forward** TGA AAT TTG GCA TGG GGT CTG **Reverse** CTC CCT GGG GCC ACA AAT
SEMA3A	**Forward** AAAGCGTGTGCTGAGTGTTG **Reverse** TTGTCGTCTTGTGCGTCTCT
SPRED3	**Forward** TACGTCATCCACGGGGAACG **Reverse** CCAAACTTGCAGTCACCCAG
TGFB	**Forward** GGAAATTGAGGGCTTTCGCC **Reverse** AGTGAACCCGTTGATGTCCA
TMEM120B	**Forward** TTTCAAGAACTGCAGGAGACGC **Reverse** TTGATGTTCGCTGCCATCTGC
TRADD	**Forward** CCCTCTCTGTCGGAGGTGA **Reverse** CTCAGCGGCCGATTCACTAC
TRAIL	**Forward** TCGTGATCTTCACAGTGCTCC **Reverse** GTACTTGTCCTGCATCTGCTT
U6	**Forward** CTCGCTTCGGCAGCACA **Reverse** AACGCTTCACGAATTTGCGT
VEGF-A	**Forward** CTCAGGGTTTCGGGAACCAG **Reverse** GTCGATGGTGATGGTGTGGT

2.7. Digital droplet PCR (ddPCR)

The expression of miR-4649-5p was not only measured by qPCR but also by ddPCR. For this purpose, 10 ng of total RNA were reverse transcribed into cDNA using the TaqMan Advanced miRNA cDNA Synthesis Kit (Thermo Fisher Scientific). All steps of the kit (poly(A) tailing, adaptor ligation, reverse transcription, and miR-Amp reaction) were conducted following the manufacturer`s protocol. Subsequently, cDNA was diluted 1:100 in RNase-free water and 5 µl of this dilution were mixed with 10 µl ddPCR Supermix for Probes without dUTP (BioRad, Hercules, CA, USA) and 0.5 µl TaqMan Advanced miRNA Assay for miR-4649-5p (Thermo Fisher Scientific). Water was added to a final reaction volume of 20 µl. Reaction mixes were filled into DG8™ Cartridges for QX200™ (BioRad) together with Droplet Generation Oil for Probes (BioRad) according to the manufacturer`s instructions and droplets were generated using a QX200™ droplet generator (BioRad). From each sample, droplets were generated in duplicates and were then transferred to semi-skirted 96-well ddPCR plates (BioRad) that were heat-sealed before performing the PCR reaction on a T100 Thermal Cycler (BioRad) under

the following conditions: 95 °C 10 min; 95 °C 30 sec + 61 °C 1 min x39; 98 °C 10 min; ramping 2 °C/sec. Droplets were measured with a QX200™ droplet reader (BioRad). Data was analyzed with the QX Manager Software Version 1.2 (BioRad).

2.8. WST-1 cell growth assay

To investigate the impact of the two miRNA candidates and their respective targets GRAMD1B and PIP5K1C on cell growth, so-called WST-1 assays (Roche) were conducted. To this end, 3 × 10^3 SUM159, 5 × 10^3 MDA-MB-231, or 6 × 10^3 BT-20 cells were seeded in the wells of 96-well plates, with four plates per experiment, one for each time point (24 h, 48 h, 72 h, and 96 h). The cells were transiently transfected with the respective miRNA mimics, miRNA inhibitor, siRNAs, or controls in six replicates following the HiPerFect reverse transfection protocol (Qiagen) as described before. To test combinations of miR-4649-5p mimic and PIP5K1C or AKT inhibition, cells were first seeded and transfected with the mimic or control as per standard procedure. After ~4h, once cells had become adherent, 10 µM of the PIP5K1C inhibitor UNC3230 (MedChemExpress, Monmouth Junction, NJ, USA) or 0.5 µM of the AKT inhibitor capivasertib (MedChemExpress) were added. Equal volumes of dimethyl sulfoxide (DMSO) were applied as vehicle control. At the indicated time points, the WST-1 reagent (Roche) was added in a 1:10 ratio before incubating the plates at 37 °C. After 60 or 120 min (depending on the cell line and signal intensity at the first measurement time point), colorimetric changes at 450 nm were detected with a SPECTROstar Omega (BMG LabTech, Ortenberg, Germany) and normalized to the reference wavelength of 620 nm.

2.9. Colony formation assay

While WST-1 assays allowed us to observe cell growth up to 96 h, we also wanted to confirm effects on growth over an extended period by performing clonogenic assays. Cells were transiently transfected in 6-well plates using HiPerFect as detailed above. After 24 h, cells were trypsinized and re-seeded in 6-well plates with 200 SUM159 cells/well or 500 MDA-MB-231 cells/well. Cells were incubated at 37 °C and 5% CO_2 for 7 days in the case of SUM159 cells or 14 days in the case of MDA-MB-231 cells. Colonies were stained using 0.04% crystal violet (Sigma-Aldrich) in 20% methanol/PBS and counted macroscopically. Experiments were performed in triplicates or sextuplicates.

2.10. EdU proliferation assay

Cell proliferation was measured by a flow cytometric 5-ethynyl-2′-deoxyuridine (EdU)-based assay employing the Click-iT™ Plus EdU Pacific Blue™ Flow Cytometry Assay Kit (Thermo

Fisher Scientific). For the assay, cells were transfected in 6 cm dishes according to the HiPerFect (Qiagen) fast-forward protocol described before. In order to avoid a negative impact of high cell density on proliferation, cells were seeded at lower numbers and confluence was monitored closely. For SUM159 cells 6×10^4 cells were seeded, for MDA-MB-231 2×10^5, and for BT-20 3×10^5. 72 h after transfection, cells were incubated with 10 µM EdU (Thermo Fisher Scientific) in growth medium at 37 °C for 2 h before harvesting by trypsinization. Subsequent washing, fixing, permeabilization, and EdU labeling with Pacific Blue™ picolyl azide was performed following the Click-iT™ Plus EdU Pacific Blue™ Flow Cytometry Assay protocol (Thermo Fisher Scientific). Measurements were performed with a CytoFLEX SI (Beckman Coulter, Brea, CA, USA) at a low flow rate and 20,000 events were recorded (in R1) per sample. Samples were gated to exclude dead cells and cell debris (gate R1), and cell aggregates (gate R2).

2.11. Aldehyde Dehydrogenase (ALDH) activity assay

To assess the impact of the two miRNA candidates on breast cancer stem cell properties, the activity of the enzyme ALDH1 was measured using the ALDEFLUOR® fluorescent reagent kit (Stemcell Technologies, Vancouver, Canada). Cells were transfected in 6 cm dishes using HiPerFect (Qiagen), as described previously. Cells were harvested by trypsinization after 48 h and processed following the Stemcell Technologies technical bulletin “Identification of ALDH-Expressing Cancer Stem Cells” (172). Cell counts were performed on a TC20™ Automated Cell Counter (BioRad) using Trypan Blue (Sigma-Aldrich), and viability was determined to be above 90%. Cell concentrations were adjusted to equal the sample with the lowest cell concentration (between 1.5×10^5 to 3×10^5 cells/ml) in each experiment. 1 ml of each sample was mixed with 5 µl of the ALDEFLUOR® substrate (Stemcell Technologies) that had been activated according to the manufacturer`s instructions. Half of this suspension (0.5 ml) was then additionally substituted with 5 µl of the 1.5 mM N,N-diethylaminobenzaldehyde (DEAB) stock (Stemcell Technologies) to inhibit ALDH activity. Samples were incubated for 30 min at 37 °C, subsequently stored on ice, and measured with a CytoFLEX SI (Beckman Coulter), recording 30,000 events per sample (in gate R1). Cell populations were gated to exclude dead cells and cell debris (gate R1), and cell aggregates (gate R2). DEAB samples were used to set the threshold for ALDH positive/negative cells for each sample individually.

2.12. Caspase-3/7 and caspase-9 activity assay

To assess the induction of apoptosis in response to miRNA overexpression, luminogenic assays were performed to measure the activity of the two effector caspases caspase-3 and -

7, and the initiator caspase caspase-9. To do so, the Caspase-Glo® 3/7 assay (Promega, Madison, WI, USA) and the Caspase-Glo® 9 assay (Promega) were used following the protocol provided by the manufacturer. Cells were seeded (3 × 10^3 SUM159 cells/well, 5 × 10^3 MDA-MB-231 cells/well, and 7 × 10^3 BT20 cells/well) and transfected in 96-well plates following the HiPerFect (Qiagen) reverse-transfection protocol described before. After 48 or 72 h, the luminogenic substrates were prepared according to the manufacturer`s instructions (the optional MG-123 inhibitor (Promega) was added to the Caspase-Glo® 9 reagent (Promega)) and added to the wells. After 1 h of incubation in the dark, samples were transferred to white 96-well plates and signals were measured with a LUMIstar Omega (BMG LabTech).

2.13. Protein extraction and Western blotting

For subsequent Western blotting, protein extraction was performed with radioimmunoprecipitation assay (RIPA) buffer (Sigma-Aldrich) that was freshly supplemented with Protease Inhibitor Cocktail P8340 (Sigma-Aldrich) in a 1:50 ratio, and Phosphatase Inhibitor Cocktail 3 (Sigma-Aldrich) in a 1:200 ratio in case of the detection of phosphorylation signals. In brief, cells were washed once with cold PBS, cold lysis buffer was added, cells were scraped off, and lysates were incubated on ice for at least 20 min before being cleared by centrifugation at 13,000 rpm for 15 min at 4 °C. Protein concentrations were measured using the Pierce™ BCA Protein Assay (Thermo Fisher Scientific) according to the manufacturer`s instructions. Protein samples were diluted 1:5 with RIPA buffer of which 25 µl were supplemented with 200 µl of the working reagent (49 parts Reagent A + 1 part Reagent B, Thermo Fisher Scientific) in duplicates. Bovine serum albumin (BSA) Protein Assay Standards (Thermo Fisher Scientific) were used to generate a standard curve. Absorbance was measured at 562 nm on a SPECTROstar Omega (BMG LabTech) after 30 min incubation at 37 °C.
25 µg of protein from each sample were substituted with 4x Laemmli buffer (BioRad) and 10% β-mercaptoethanol (Sigma-Aldrich) before denaturation at 95 °C for 5 min. Samples were loaded into 4–15% Mini-PROTEAN® TGX™ Precast Protein Gels (BioRad) and separated by sodium dodecyl sulfate-polyacrylamide gel electrophoresis (SDS-PAGE) at 120 V. As protein ladder, the Precision Plus Protein™ Dual Color Standard (BioRad) was used. Proteins were then plotted on a 0.45 µm nitrocellulose membrane (BioRad) by wet transfer in Tris/Glycin buffer (BioRad) supplemented with 20% methanol at 400 mA for 1.5 to 2 h. The membranes were subsequently incubated in 5% non-fat milk/Tris-buffered saline (TBS; BioRad) containing 0.1% Tween-20 (Sigma-Aldrich) (TBS-T) for at least 1 h before primary antibodies, diluted in 5 % BSA (Sigma-Aldrich)/TBS-T, were added overnight at 4 °C. A list of all primary antibodies and their dilutions is given in Table 3. After incubation with the respective primary antibody,

membranes were washed three times for ~10 min each in TBS-T before incubation with the secondary antibody (horse radish peroxidase-conjugated anti-rabbit antibody, Santa Cruz Biotechnology, Dallas, TX, USA) diluted 1:5000 in 5% milk/TBS-T for 1 h. Membranes were washed again three times before signal detection using either SuperSignal™ West Pico Chemiluminescent Substrate (Thermo Fisher Scientific) or SuperSignal™ West Femto Maximum Sensitivity Substrate (Thermo Fisher Scientific) depending on the signal intensity. Chemiluminescent substrates were mixed according to the manufacturer`s instructions and membranes were incubated for 3 to 5 min before image acquisition on a ChemiDoc Touch device (BioRad). Signals were quantified with the volume tools function of the Image Lab Software version 6.1.0 build 7 (BioRad). In case membranes were re-probed with different antibodies, they were stripped for 1h in 10 % acetic acid before blocking.

Table 3: List of all primary antibodies used for Western blotting. *The companies they were supplied by and the final dilutions they were used in are stated.*

Antibody	Company	Dilution
Akt (#9272, rabbit)	Cell Signaling Technology, Danvers, MA, USA	1:1000
Cofilin (ab42824, rabbit)	Abcam, Cambridge, United Kingdom	1:10,000
GRAMD1B (rabbit)	Proteintech Europe, Manchester UK	1:1000
PARP (#9542, rabbit)	Cell Signaling Technology, Danvers, MA, USA	1:1000
Phospho-Akt Ser473 (D9E XP® Rabbit mAb, #4060)	Cell Signaling Technology, Danvers, MA, USA	1:2000
Phospho-STAT3 Tyr705 (D3A7 XP® Rabbit mAb, #9145)	Cell Signaling Technology, Danvers, MA, USA	1:1000
PIP5K1C (#3296, rabbit)	Cell Signaling Technology, Danvers, MA, USA	1:1000
STAT3 (79D7 Rabbit mAb, #4904)	Cell Signaling Technology, Danvers, MA, USA	1:5000

2.14. Scratch assay

To assess cell migration, two different types of assays were performed. The first were so-called scratch assays or wound healing assays. For these, SUM159 cells were seeded in 6-well plates at high density (5×10^5 cells/well) and transfected in four replicates. After 24 h, scratches were introduced into the confluent cell layers. Subsequently, cells were washed once to remove floating cells. The size of the scratches over time was documented by microscopic pictures and the area of the scratches was measured using the “MRI Wound Healing Tool” plugin for ImageJ (NIH, Bethesda, MD, USA). The remaining area measured at each time point was normalized to the 0 h time point and presented as percentage of wound healing.

2.15. Transwell migration assay

The second type of migration assays were transwell assays using permeable transwell inserts for 24-well plates with a pore size of 0.4 µm (Corning Incorporated, Corning, NY, USA). Cells

were first seeded and transfected in 6-well plates as described previously. 24 h after the transfection, the medium was replaced with FBS-free medium in order to starve cells for 24 h before seeding them on the transwell membranes using 1.5 × 10^4 SUM159 cells or 2.5 × 10^4 MDA-MB-231 cells per transwell. To prepare the transwell membranes before seeding of the cells, they were coated with gelatin using a solution of 0.1% gelatin (Sigma-Aldrich) and 0.02 M acetic acid. The gelatine-coated membranes were dried overnight before re-hydration in FBS-free medium for 1 h at 37 °C. Cells were seeded on the membranes in FBS-free medium while the lower wells were filled with full growth medium to stimulate migration through the membrane. Cells were cultivated for 48 h before fixing them with cold methanol and staining with a 0.2% crystal violet (Sigma-Aldrich)/2% ethanol solution. Transwells were washed subsequently and cells from the top of the membranes that had not migrated were removed. Microscopic pictures were taken of five representative areas from each transwell from which migrated cells were counted at 40x magnification.

The SUM159 transwell migration assay presented in Figure 16A was performed by Julia Teppan, currently PhD student at the Division of Pharmacology, Otto Loewi Research Center, Medical University of Graz, Austria.

2.16. Tube formation assay

As a way to assess angiogenesis *in vitro*, tube formation assays using human umbilical vein endothelial cells (HUVECs) were performed. To this end, HUVECs were seeded and transfected with the miRNA mimics and controls using HiPerFect (Qiagen) according to the previously described standard fast-forward transfection protocol. After 48 h, the cells were seeded into 96-well plates with 1.5 × 10^4 cells/well that had been coated with the ECM625 matrix (Merck, Darmstadt, Germany) as instructed by the manufacturer. 16 h later, microscopic pictures were taken and tube formation was quantified based on the number of nodes, junctions, meshes, and the total length of the branches using the ImageJ plugin “Angiogenesis Analyzer” (NIH), the principle of which is described by Carpentier *et al.* (173).

The tube formation assays presented in Figure 18B and Figure 32 were performed by Christiane Klec, Priv.-Doz. PhD, Department of Internal Medicine, Division of Oncology, Medical University of Graz, Austria.

2.17. Transcriptome analysis by RNA-seq and identification of potential miRNA targets

To investigate changes in gene expression upon overexpression of the miRNA candidates, RNA-seq analysis was performed on SUM159 cells transiently transfected with the miR-4646-5p mimic, miR-4649-5p mimic, or mimic control in triplicates. RNA was isolated from the cells

48 h after transfection with the RNeasy Mini Kit (Qiagen), including DNase treatment as described by the manufacturer`s protocol. The subsequent steps were performed by Karin Wagner and Martina Strempfl from the Core Facility Molecular Biology, Center for Medical Research (ZMF), Medical University of Graz, Austria. The quality of the isolated RNA was measured using the Agilent RNA 6000 Nano Kit with the Agilent 2100 BioAnalyzer system (Agilent Technologies, Santa Clara, CA, USA). RNA quantification was conducted with a NanoDrop 2000 (Thermo Fisher Scientific). Per sample, 250 ng of RNA were applied in the library preparation using the NEBNext® rRNA Depletion Kit v2 and the NEBNext® Ultra™ II Directional RNA Library Prep Kit for Illumina® (New England Biolabs GmbH, Frankfurt am Main, Germany) as detailed in the manufacturer`s protocol. The libraries were quality controlled using the Agilent 2100 DNA high-sensitivity kit (Agilent Technologies) and pooled. Sequencing was performed by the Vienna BioCenter Core Facilities GmbH (Vienna, Austria) using an Illumina NovaSeq SP flow cell (Illumina, Eindhoven, Netherlands) that was run in SR100 mode. Subsequent analysis of raw data was performed by Slave Trajanoski, Core Facility Computational Bioanalytics, Medical University of Graz, Austria.

For the identification of potential direct targets of miR-4646-5p and miR-4649-5p, genes that were significantly downregulated based on multiple testing-adjusted p-values were ranked based on their fold-change in expression. From this list, the top 20 downregulated annotated, protein-coding genes of both miR-4646-5p and miR-4649-5p were used for *in silico* target predictions using TargetScan (174), miRWalk2.0 (175), and miRDB (176).

2.18. Gene set enrichment analysis and overrepresentation analysis of RNA-seq data

All significantly deregulated genes determined by RNA-seq were applied for gene set enrichment analysis (GSEA) using the GSEA software (UC San Diego and Broad Institute, San Diego, CA, USA). GSEA analysis was performed by Manuela Ferracin, Department of Medical and Surgical Sciences (DIMEC), University of Bologna, Italy.

Significantly downregulated genes were additionally used in a Gene Ontology (GO) enrichment analysis using the PANTHER Overrepresentation Test (http://www.pantherdb.org/; GO Ontology database DOI: 10.5281/zenodo.6799722, released 2022-07-01, reference list Homo sapiens, annotation data set GO molecular function complete, Fisher´s Exact Test).

2.19. Dual luciferase reporter assay

In order to confirm that miR-4646-5p and miR-4649-5p downregulate their respective targets GRAMD1B and PIP5K1C by directly binding to them, we performed dual luciferase reporter assays using the reporter vector pEZX-MT06 (Genecopoeia, Rockville, MD, USA).

Downstream of the firefly luciferase coding sequence the predicted miRNA binding sequences from the 3`UTRs of GRAMD1B and PIP5K1C were inserted, both as wild type (wt) and in a mutated (mut) version. The inserted sequences are presented in Table 4. In addition to the reporter vectors, an empty vector (CmiT000001-MT06; Genecopoeia) served as control. For the assays, 60,000 HEK293 cells/well were seeded in 24-well plates, where they reached ~70-80 % confluence after 48 h. Medium was replaced with fresh medium and cells were co-transfected with 200 ng of the reporter vectors per well and 50 nM mirVana™ miR-4646-5p mimic, mirVana™ miR-4649-5p mimic, or mirVana™ mimic control (Thermo Fisher Scientific) using the Lipofectamine® 2000 Transfection Reagent (Thermo Fisher Scientific) together with Opti-MEM® Reduced Serum Medium (Thermo Fisher Scientific) as instructed by the manufacturer. In brief, lipofectamine and DNA/RNA were diluted separately in Opti-MEM® each to a total volume of 50 µl per well, with 2 µl lipofectamine per well. The DNA/RNA mix was added to the lipofectamine mix, mixed by pulse vortexing, and incubated at room temperature for 5 min, before adding the 100 µl mixture to the cells dropwise. To test the functionality of the miR-4646-5p inhibitor, also 50 nM of the hsa-miR-4646-5p miRCURY LNA miRNA Inhibitor and the miRCURY LNA miRNA Inhibitor Control A (Qiagen) were co-transfected with 200 ng of the GRAMD1B wt reporter vector and 50 nM mirVana™ miR-4646-5p mimic or mirVana™ mimic control (Thermo Fisher Scientific). 24 h after transfections, assays were performed using the Luc-Pair Luciferase Assay Kit 2.0 (Genecopoeia) according to the manufacturer's instructions, where cells were lysed, 20 µl of the lysates transferred to white 96-well plates and the FLuc and RLuc Assay Working Solution (Genecopoeia) added sequentially as instructed. First firefly, then renilla luciferase signals, were measured with a LUMIStar Omega (BMG LabTech), and the former were normalized by the latter.

Table 4: Sequences from the 3`UTR of the genes GRAMD1B and PIP5K1C that were inserted into a CmiT000001-MT06 dual luciferase reporter vector (Genecopoeia) to test for direct interaction with miR-4646-5p and miR-4649-5p, respectively. *The predicted miRNA binding sites are marked in gray. Both sequences were inserted either as wild type (wt) or mutated (mut), where the mutated nucleotides are indicated in red.*

	Sequence (5`- 3`)
GRAMD1B wt	GCACAGCCAGAAGCCAAAACTATTCCCAGAAAGTTTTGAATGCAAAACT
GRAMD1B mut	GCACAGCCAGAAGCCAAAACTATAGCTGGCAAGTTTTGAATGCAAAACT
PIP5K1C wt	CCCCAAACACTGGTTTGCATCCCAGGTTCCTCGCCCACCTACCCCCGCCACACCCCGTCT
PIP5K1C mut	CCCCAAACACTGGTTTGCATCGTAGGTTCCAGGTTCACCTACCCCCGCCACACCCCGTCT

2.20. G-CSF and IL6 ELISA

Enzyme-linked Immunosorbent Assays (ELISAs) were performed to investigate the effect of miR-4646-5p overexpression on the secretion of granulocyte colony-stimulating factor (G-CSF) and interleukin-6 (IL-6) from SUM159 and MDA-MB-231 cells. Cells were seeded (2 × 10^5 SUM159 cells/well, 4 × 10^5 MDA-MB-231 cells/well) and transfected in 6 well-plates using HiPerFect (Qiagen) according to the standard transfection conditions detailed before. 24 h later, the growth medium was replaced with FBS-free medium for 40 h before harvesting the supernatant and clearing it by centrifugation at 1500 rpm for 10 min. The Human G-CSF Instant ELISA™ Kit (Invitrogen, Thermo Fisher Scientific) and IL-6 Human Instant ELISA™ Kit (Invitrogen, Thermo Fisher Scientific) were performed according to the manufacturer`s instructions, however using 50 µl supernatant as input in both assays. Each sample was measured in technical duplicates, as well as the included standards and blank, as indicated by the manufacturer. Assay plates were incubated for 3 h, washed 6 times, and substrate solutions were added as instructed by the manufacturer. Absorbance was measured with a SPECTROstar Omega spectrophotometer (BMG LabTech) at 450 nM with 620 nM as a reference.

2.21. *In vivo* experiments - Orthotopic TNBC mouse model

The orthotopic TNBC mouse model was generated in collaboration with Assoc. Prof. Priv.-Doz. Mag. Dr. Beate Rinner and Ines Anders from the Core Facility Alternative Biomodels & Preclinical Imaging, Medical University of Graz, Austria. Experiments were performed in accordance with the regulations of the Institutional Animal Care and Use Committee at the Medical University of Graz, Austria, and approved by the Austrian Ministry for Science according to the Austrian Animal Testing Act 2012 (TVG 2012). Female athymic nude mice (Crl:NU(NCr)-*Foxn1*^{nu}) were obtained from Charles River (Wilmington, MA, USA). 5 × 10^5 stable SUM159 miR-4646-5p inhibitor cells or SUM159 control cells were injected into the mammary fat pads of the mice in a volume of 50 µl PBS. 8 mice were injected with the miR-4646-5p inhibitor cells on the right side and the control cells on the left. Tumor growth was monitored by ultrasound and tumor size was measured. The ethical endpoint was defined as severe weight loss, severe clinical observations, or tumor sizes > 1000 mm^3. The experiment was terminated after 75 days.

2.22. *In vivo* experiments – Metastatic TNBC mouse model

The metastatic TNBC mouse model was generated by the company Experimental Pharmacology & Oncology Berlin-Buch GmbH (EPO; Berlin-Buch, Germany) and experiments

were performed as approved by the local authorities and in accordance with the German Animal Welfare Act. NODShi.Cg-*Prkdc*^{scid} *Il2rg*^{tm1Sug} (NOG) mice (Janvier Labs, France) were intravenously injected via the tail vein with 5 × 10^5 MDA-MB-231 cells stably expressing luciferase (the cell line was provided by EPO). 6 days after cell injections, mice were randomized into three treatment groups with 7 mice per group and treated with mirVana™ hsa-miR-4646-5p mimic, mirVana™ hsa-miR-4649-5p mimic, or mirVana™ mimic control (Thermo Fisher Scientific). Per injection, 0.5 nmol miRNA were applied intravenously in complex with Polyplus in vivo-jetPEI® Transfection Reagent (Polyplus, Illkirch, France) at a ratio of 6.25 according to the manufacturer's instructions. Mice received mimic injections twice per week, in total 6 times. Luminescent *in vivo* imaging was performed at 5 time points and body weight was measured twice per week. The ethical endpoint was defined as > 20% body weight loss and/or severe clinical observations and was reached after 35 days.

2.23. Statistical analysis

The statistical analysis of *in vitro* experiments was performed with GraphPad Prism Version 5.01 (GraphPad Software, Inc., San Diego, CA, USA). To compare miRNA mimic/inhibitor transfected samples with their respective control, unpaired, two-tailed independent t-tests with a 95% confidence interval were performed. Where more than two groups were compared to each other, which is indicated in the respective cases, one-way ANOVA and Tukey`s multiple comparison tests with a 95% confidence interval were performed. Other statistical tests that were performed for the analysis of *in silico* data are indicated in the respective cases. Overall, results were considered statistically significant with a p-value below 0.05 (*$p \leq 0.05$, **$p \leq 0.01$, ***$p \leq 0.001$).

3. Results

3.1. MiR-4646-5p and miR-4649-5p host genes, expression and prognostic value for TNBC patients

To gain a better understanding of the two selected miRNA candidates, miR-4646-5p and miR-4649-5p, both of which had not been studied prior to this dissertation, we first determined their genomic localization using the online USCS Genome Browser (Human Assembly Dec. 2013 GRCh38/hg38) (177).

The *miR-4646* gene (accession number MI0017273) is located on chromosome 6 (chr6:31701029-31701091) at the beginning of intron 3 of the abhydrolase domain containing 16A, phospholipase (*ABHD16A*) gene, which will therefore be referred to as the miR-4646-5p host gene. *ABHD16A*, which codes for a serine metabolism enzyme, has not been associated with cancer previously but has been reported to play a role in the generation of immunomodulatory signaling lipids and to be connected to developmental and neurological diseases (178–180). Analysis of RNA-seq-based expression data using the online TNMplot tool (171), showed higher expression of *ABHD16A* in breast tumor tissue compared to healthy adjacent tissue (n = 112, Mann-Whitney-U test, p = 0.0000901) (Figure 4A). Survival analysis using an online Kaplan-Meier plotter tool based on microarray expression data from the Gene Expression Omnibus (GEO) database (169) showed that higher *ABHD16A* expression is associated with a non-significant trend towards better survival in a TNBC patient cohort (n = 144; log-rank test; p = 0.12; hazard ratio = 0.59; 95% confidence interval 0.3 – 1.15) and significantly better overall survival in a cohort of patients with basal-like breast cancer (PAM50 classification) (n = 296; log-rank test; p = 0.0042; hazard ratio = 0.48; 95% confidence interval 0.28 – 0.8) (Figure 4B and 4C).

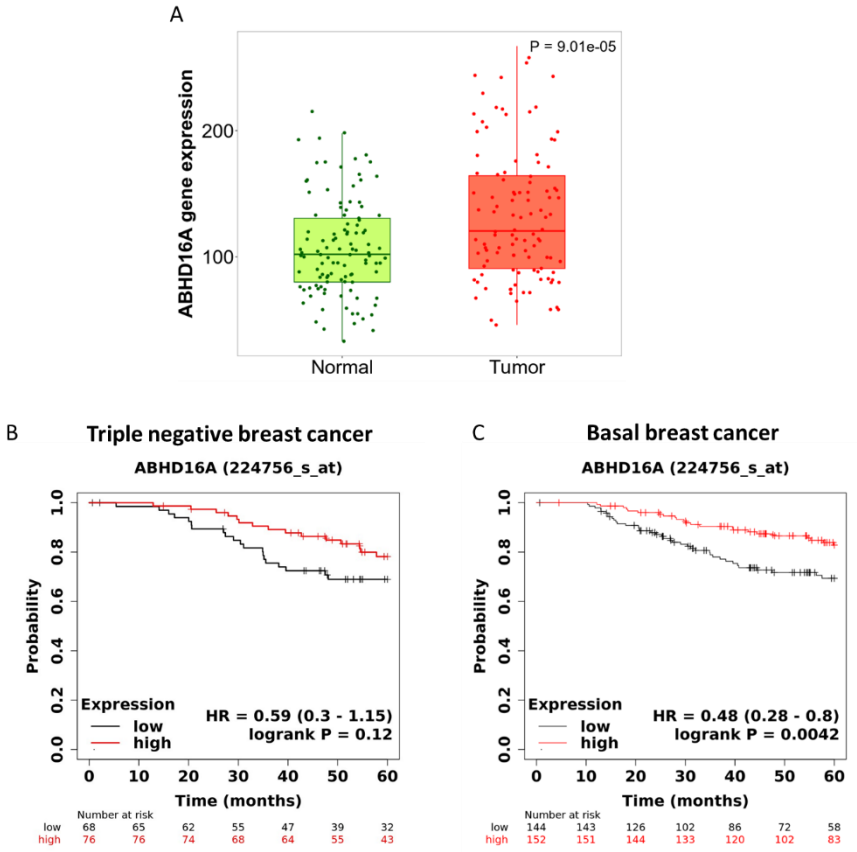

Figure 4: Expression and prognostic relevance of the miR-4646-5p host gene abhydrolase domain containing 16A, phospholipase (ABHD16A) in breast cancer. (A) *RNA-seq-based expression of ABHD16A in breast tumor tissue compared to healthy adjacent tissue (n = 112 per group; Mann-Whitney-U test; p = 0.0000901).* ***(B)*** *Overall survival of a triple negative breast cancer patient cohort split into an ABHD16A low (black; n = 68) and high (red; n = 76) expression group based on Gene Expression Omnibus (GEO) microarray data (log-rank test; p = 0.12; hazard ratio (HR) = 0.59; 95% confidence interval 0.3 – 1.15).* ***(C)*** *Overall survival of a patient cohort with basal breast cancer split into an ABHD16A low (black; n = 144) and high (red; n = 152) expression group based on GEO microarray data (log-rank test; p = 0.0042; hazard ratio (HR) = 0.48; 95% confidence interval 0.28 – 0.8).*

The region coding for the *miR-4649* stem-loop pre-miRNA (accession number MI0017276) is located on chromosome 7 (chr7:44110849-44110912) in intron 12 of the adipocyte enhancer-binding protein 1 (*AEBP1*) gene. RNA-seq-based expression data from TNMplot (171) showed higher expression of *AEBP1* in breast cancer compared to healthy tissue (n = 112, Mann-Whitney-U test, p = 0.0000000000156) (Figure 5A). Survival analysis based on GEO microarray data revealed higher expression of *AEBP1* to be associated with significantly worse overall survival of TNBC patients (n = 153; log-rank test; p = 0.00057; hazard ratio = 3.22; 95% confidence interval 1.59 – 6.52), and also a trend towards shorter survival in basal-like breast cancer patients (n = 431; log-rank test; p = 0.076; hazard ratio = 1.49; 95% confidence interval

0.96 – 2.34) (Figure 5B and 5C). In line with the association with worse patient survival, *AEBP1* has been described to play an oncogenic role, amongst others in breast cancer, where it promotes proliferation, migration, invasion, and cell survival (181,182).

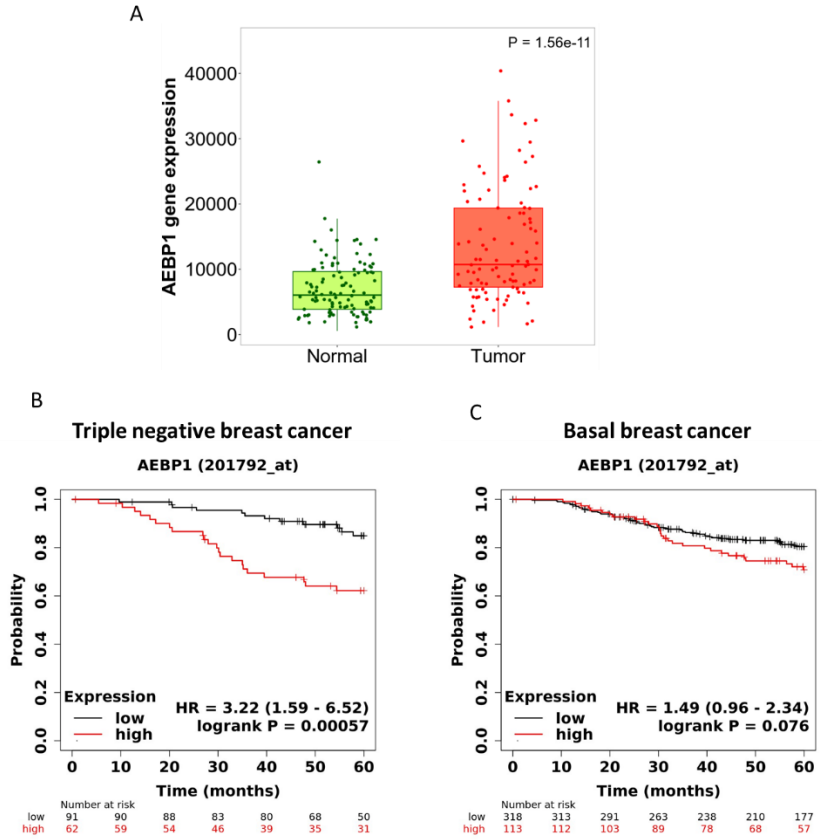

Figure 5: Expression and prognostic relevance of the miR-4649-5p host gene adipocyte enhancer-binding protein 1 (AEBP1) in breast cancer. (A) *RNA-seq-based expression of AEBP1 in breast tumor tissue compared to healthy adjacent tissue (n = 112 per group; Mann-Whitney-U test; p = 0.0000000000156).* ***(B)*** *Overall survival of a triple negative breast cancer patient cohort split into an AEBP1 low (black; n = 91) and high (red; n = 62) expression group based on Gene Expression Omnibus (GEO) microarray data (log-rank test; p = 0.00057; hazard ratio (HR) = 3.22; 95% confidence interval 1.59 – 6.52).* ***(C)*** *Overall survival of a patient cohort with basal breast cancer split into an AEBP1 low (black; n = 318) and high (red; n = 113) expression group based on GEO microarray data (log-rank test; p = 0.076; hazard ratio (HR) = 1.49; 95% confidence interval 0.96 – 2.34).*

The *miR-4646* gene and the *miR-4649* gene described above code for the full pre-miRNA stem-loop sequences and are 63 and 64 nt long, respectively. After being fully processed, the mature miR-4646-5p sequence (MIMAT0019707) is 22 nt, and the mature miR-4649-5p (MIMAT0019711) 24 nt long.

While the genomic location and the host genes of a miRNA can provide hints of the potential role of the miRNA in certain cases, the expression levels and functions of miRNAs and their

host genes are not always correlating (183). Thus, the next step was to use *in silico* data to analyze the expression of miR-4646-5p and miR-4649-5p themselves. However, using various *in silico* online tools, such as ENCORI (184) and miRCancer (185), we could not retrieve any breast cancer expression data of the two miRNAs.

Next, it was of interest to determine whether the two miRNA candidates have any clinical relevance for patients with TNBC. For this purpose, we used a Kaplan-Meier analysis tool specifically developed to determine the prognostic impact of miRNAs in breast cancer (168). The analysis, based on TCGA data from 97 TNBC patients, showed that higher expression of both *miR-4646* (log-rank test; p = 0.0018; hazard ratio = 0.21; 95% confidence interval 0.07 – 0.62) and *miR-4649* (log-rank test; p = 0.0079; hazard ratio = 0.26; 95% confidence interval 0.09 – 0.76) were associated with significantly better overall survival (Figure 6A and 6B). It must be kept in mind though that these results refer to the expression of the pre-miRNA genes and not the mature 5p sequences.

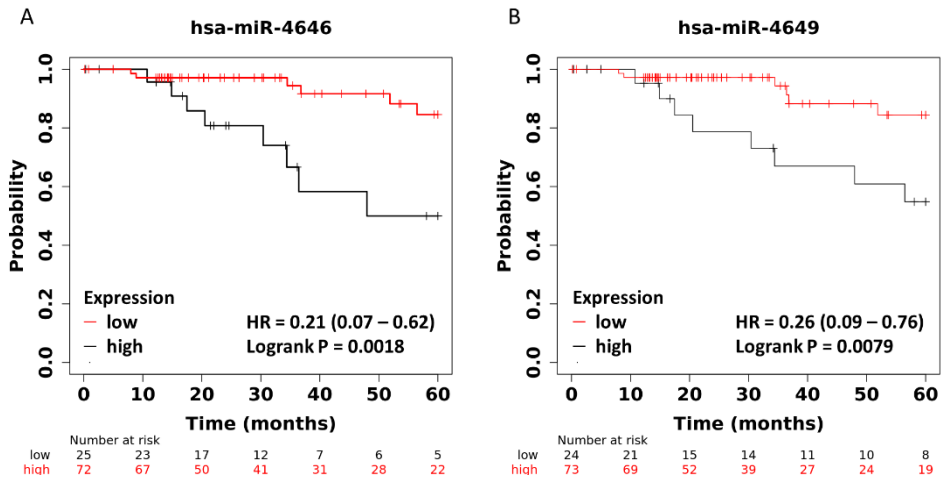

Figure 6: Impact of miR-4646 and miR-4649 expression on overall survival of patients with triple negative breast cancer. (A) *Overall survival of TNBC patients split into a miR-4646 low (black; n = 25) and high (red; n = 72) expression group based on TCGA data (log-rank test; p = 0.0018; hazard ratio (HR) = 0.21; 95% confidence interval 0.07 – 0.62).* ***(B)*** *Overall survival of TNBC patients split into a miR-4649 low (black; n = 24) and high (red; n = 73) expression group based on TCGA data (log-rank test; p = 0.0079; hazard ratio (HR) = 0.26; 95% confidence interval 0.09 – 0.76).*

3.2. Expression of miR-4646-5p in breast cancer cell lines and establishment of *in vitro* overexpression and inhibition systems

After investigating the expression and prognostic value of miR-4646-5p and miR-4649-5p in breast cancer tissue based on *in silico* data, we switched to readily available cell lines and screened the endogenous expression of the miRNAs in a panel of breast cancer cell lines from

different subtypes (luminal A, luminal B, HER2-positive, triple negative) and a healthy non-malignant control by quantitative PCR (qPCR). To do so, commercially available primer assays (Qiagen) were used that are designed to detect the mature miR-4646-5p and miR-4649-5p sequences. In parallel, we established overexpression and inhibition systems of the two miRNAs in TNBC cell lines by transient transfection of the cells with mimics (Thermo Fisher) and LNA antisense inhibitors (Qiagen) or the respective controls and confirmed the transfection efficiency by qPCR. The mimic overexpressions were used as positive controls to verify the specificity of the primer assays.

The endogenous expression level of miR-4646-5p in the breast cancer cell line panel was relatively uniform across the 12 cell lines, with two (one HER2-positive and one TNBC cell line) having a significantly higher expression and four (one luminal A, one luminal B, and two TNBC cell lines) having significantly lower levels than the non-malignant control cell line (Figure 7). Overall, to give a rough assessment of the abundance of miR-4646-5p in the cells, one can take a look at the raw Ct values, representing the PCR cycles at which the detection threshold was reached. For miR-4646-5p the Ct values were generally in the upper range around 28 (out of 35 cycles), which indicates a medium to low expression level of miR-4646-5p compared to the abundantly expressed housekeeper genes SNORD62 and SNORD95, whose Ct values lay between 15 to 20, depending on the cell line.

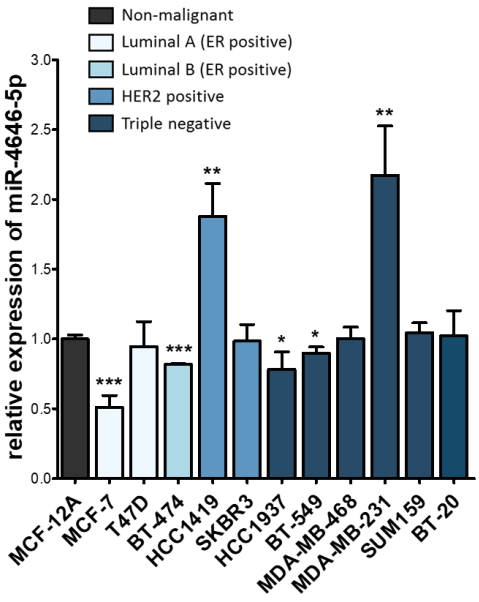

Figure 7: Expression of miR-4646-5p in a panel of breast cancer cell lines. *Expression was measured by qPCR and is depicted relative to a non-malignant control cell line. Breast cancer cell lines are grouped according to their molecular subtype (the estrogen receptor (ER) positive luminal A and luminal B subtypes, HER2 positive subtype, and triple negative subtype) (mean ± SD; n = 3; *p ≤ 0.05, **p ≤ 0.01, ***p ≤ 0.001).*

As the focus of the dissertation was TNBC, we selected three TNBC cell lines, SUM159, MDA-MB-231, and BT-20, for miR-4646-5p mimic and inhibitor transfections. PCR melting curves from the two TNBC cell lines SUM159 and MDA-MB-231 attested the specificity of the employed primer assay, as only one specific melting curve peak was detected at the same melting temperature for both the endogenous miR-4646-5p as well as the synthetic miR-4646-5p mimic (Figure 8A). The mimic transfections caused a strong overexpression of the miRNA seen by qPCR (Figure 8B). The inhibitor transfections, however, did not cause a reduction detectable by qPCR (Figure 8C). This does not mean though that the inhibitor did not perform its function, as LNA antisense inhibitors do not necessarily trigger degradation of the bound miRNA but primarily sequester it and block its interaction with mRNA targets (186). Thus, despite functional inhibition, the miRNA may still be detectable at unchanged levels (186). To really prove the inhibition of the miRNA, functional confirmation is required which is only possible when a specific target binding sequence of the miRNA is known. Once we had identified such a target sequence (which will be described in sections 3.5.1 and 3.5.2), we used this sequence in a dual luciferase reporter assay, where cells are transfected with a vector that expresses both a constitutive renilla luciferase and a firefly luciferase that is fused to the target sequence of interest (187,188). Upon co-transfection with the miRNA mimic, the miRNA will thus bind to the firefly reporter construct and cause RISC-induced degradation or translational inhibition of the reporter (187,188). Thereby, the firefly signal will be reduced relative to the renilla signal, which serves as a normalization control (187,188). If, in addition to the miRNA mimic, also the inhibitor is added, the inhibitor should bind to the mimic and block its function, thereby rescuing the luciferase signal. This is also what we observed upon co-transfection of the miR-4646-5p mimic and the miR-4646-5p inhibitor, but not a negative inhibitor control (Figure 8D), demonstrating the functionality of the miR-4646-5p inhibitor.

In addition to transient overexpression/inhibition of the miRNAs, we also aimed for the generation of stable cell lines by using lentiviruses. As we wanted to use constitutively expressed vectors and had discovered that overexpression of miR-4646-5p caused reduced growth and was also capable of inducing apoptosis (the results will be presented in sections 3.4.1 and 3.4.2, respectively), we chose the stable expression of an inhibitor in order to circumvent gradual loss of miR-4646-5p overexpressing cells. We transfected the SUM159 cell line with a commercial LentimiRa-Off-hsa-miR-4646-5p virus or Lenti-III-mir-Off Control virus. As both vectors co-expressed GFP, highly GFP-positive cells were enriched by FACS (Figure 8E).

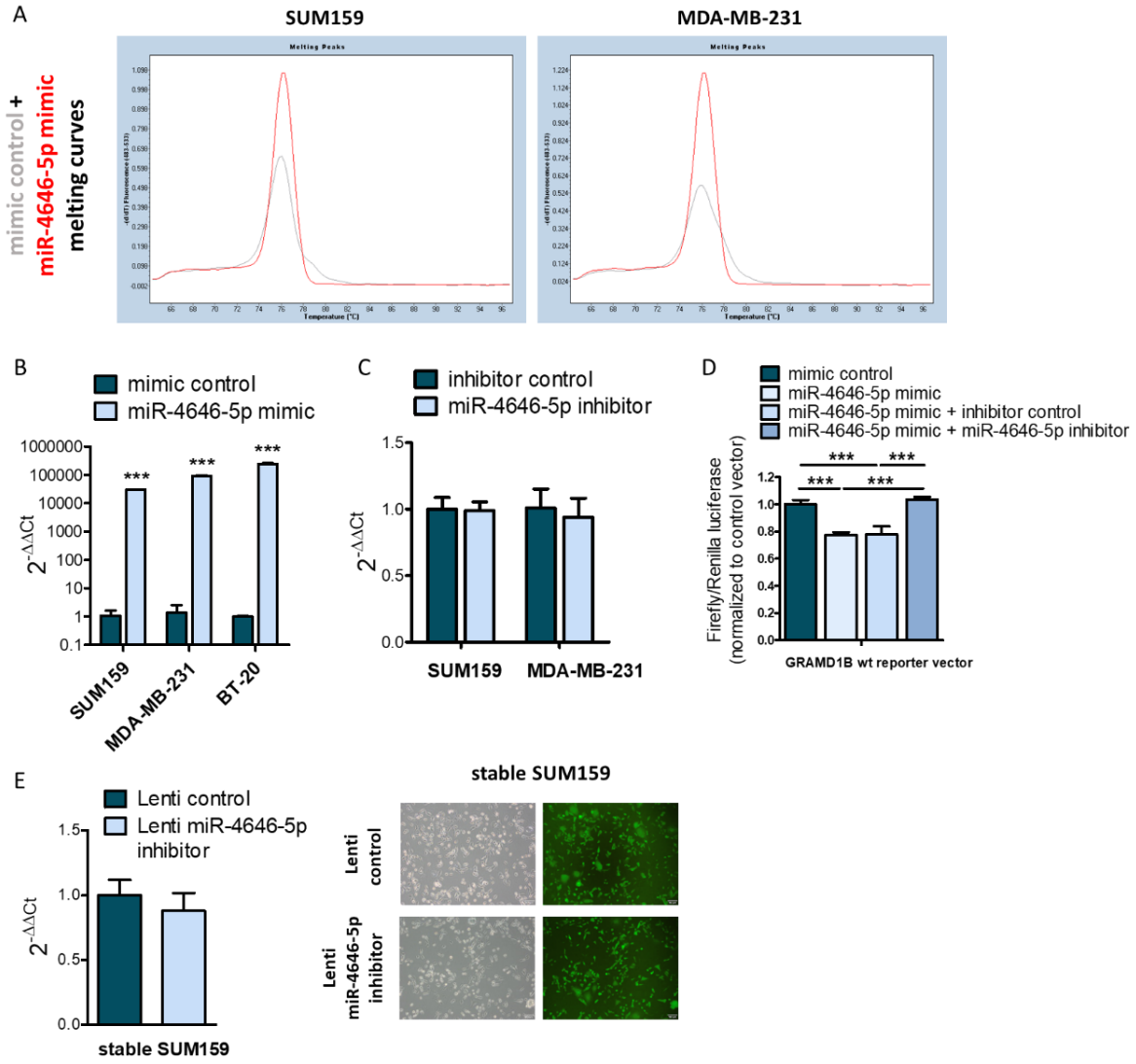

Figure 8: MiR-4646-5p overexpression and inhibition in triple negative breast cancer (TNBC) cell lines. ***(A)*** *Melting curve analysis of quantitative PCR (qPCR)-based detection of miR-4646-5p in SUM159 and MDA-MB-231 cells transfected with miR-4646-5p mimic (red) or mimic control (gray).* ***(B)*** *Transient overexpression of miR-4646-5p 48 h after mimic transfection of SUM159, MDA-MB-231, and BT-20 TNBC cells as determined by qPCR. Expression is depicted relative to the mimic controls (mean ± SD; n = 3; ***p ≤ 0.001).* ***(C)*** *Transient inhibition of miR-4646-5p 48 h after inhibitor transfection of SUM159, and MDA-MB-231 cells as measured by qPCR. Expression is depicted relative to the inhibitor controls (mean ± SD; n = 3).* ***(D)*** *Dual luciferase reporter assay in HEK293 cells with a reporter carrying the direct miR-4646-5p binding site located in the 3`UTR of the wildtype (wt) GRAM domain-containing protein 1B (GRAMD1B) gene. The reporter was co-transfected with combinations of the miR-4646-5p mimic and inhibitor or the respective controls. Luciferase signals were normalized to the respective signals from an empty control vector (n = 3; mean ± SD; ***p ≤ 0.001).* ***(E)*** *Stable lentiviral inhibition of miR-4646-5p in SUM159 cells as measured by qPCR, depicted relative to the control (mean ± SD; n = 3). Bright-field and fluorescent images of the GFP-sorted cell line are presented on the right.*

3.3. Expression of miR-4649-5p in breast cancer cell lines and establishment of *in vitro* overexpression systems

While for miR-4646-5p PCR melting curve analysis showed specific amplification of the endogenously expressed miRNA in TNBC cell lines, melting curves for the second miRNA candidate revealed a surprise. The miR-4649-5p primer assay facilitated specific amplification of the synthetic miR-4649-5p mimic, which served as a positive control (Figure 9A). However, the endogenous expression of miR-4649-5p in the three control transfected TNBC cell lines resulted in numerous unspecific peaks at higher melting temperatures and almost no detectable amplification with the specific melting temperature of around 76 °C (Figure 9A), which would indicate very low endogenous expression of the miRNA. We also generated a stable SUM159 miR-4649-5p overexpression cell line by transfection with a LentimiRa-GFP-hsa-miR-4649-5p virus followed by sorting for high GFP intensity. Here, we achieved a medium overexpression level (approx. 2-fold, Figure 9B) as opposed to the much higher transient mimic overexpression (approx. 15-fold, Figure 9B) and could still detect some unspecific melting temperature peaks (Figure 9A). Compared to the barely detectable endogenous miR-4649-5p levels though, the unspecific signals decreased and the specific signal increased with the stable overexpression (Figure 9A). Based on this, it seems that in the absence of miR-4649-5p, which is the case endogenously, the primer mostly picks up unspecific sequences, whereas the higher the level of the miRNA, the more the amplification of the specific product prevails.

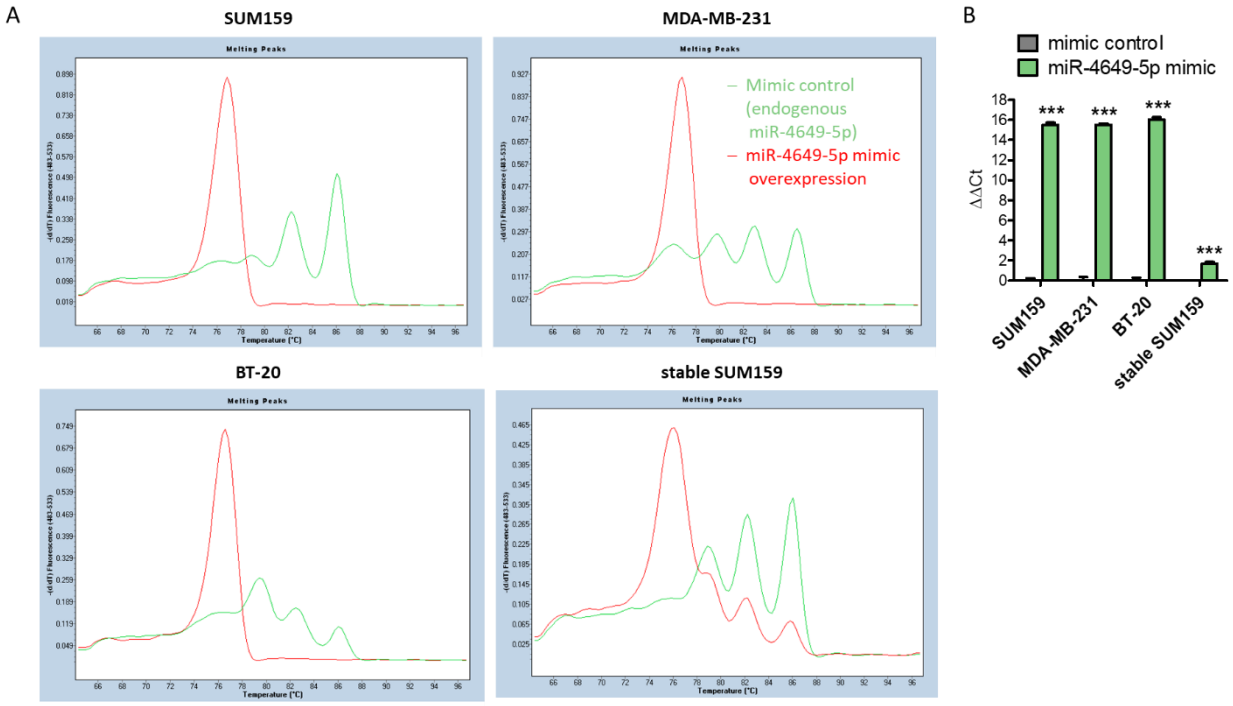

Figure 9: Expression of miR-4649-5p in triple negative breast cancer cell lines. (A) *Melting curves of the qPCR-based detection of the endogenous miR-4649-5p expression (green) in mimic control transfected cells and transient or stable miR-4649-5p mimic overexpression (red) as positive controls.* ***(B)*** *Transient (48 h) and stable miR-4649-5p mimic overexpression in TNBC cells as determined by qPCR. MiR-4649-5p expression is depicted relative to the mimic controls (mean ± SD; n = 3; ***p ≤ 0.001).*

In the next step, we sought to confirm the very low expression of miR-4649-5p in the TNBC cell lines by an independent approach using different primers. To this end, we performed digital droplet PCR (ddPCR), a PCR variant where the PCR reaction is partitioned into thousands of single droplets and the presence of the cDNA in the droplets is measured at the endpoint, giving either a positive or negative call for each droplet (189). This allows the absolute quantification of target molecules even when they are present at very low quantity (189). As previously for the qPCR, transient and stable miR-4649-5p overexpression served as positive controls. Transient overexpression in SUM159, MDA-MB-231, and BT-20 cells resulted in a strong increase of miR-4649-5p positive droplets, while stable overexpression in SUM159 caused a medium increase (Figure 10A and 10B), comparable to what had been seen by qPCR (Figure 9B). The endogenous levels of miR-4649-5p in the cell lines gave almost no positive droplets, similar to the no-template controls (Figure 10A and 10B). Thereby we confirmed the very low endogenous expression level of miR-4649-5p in the TNBC cell lines. Due to this virtually non-existent endogenous expression, we only generated gain-of-function systems,

meaning mimic overexpression, for this miRNA and did not include a miR-4649-5p inhibitor in the study.

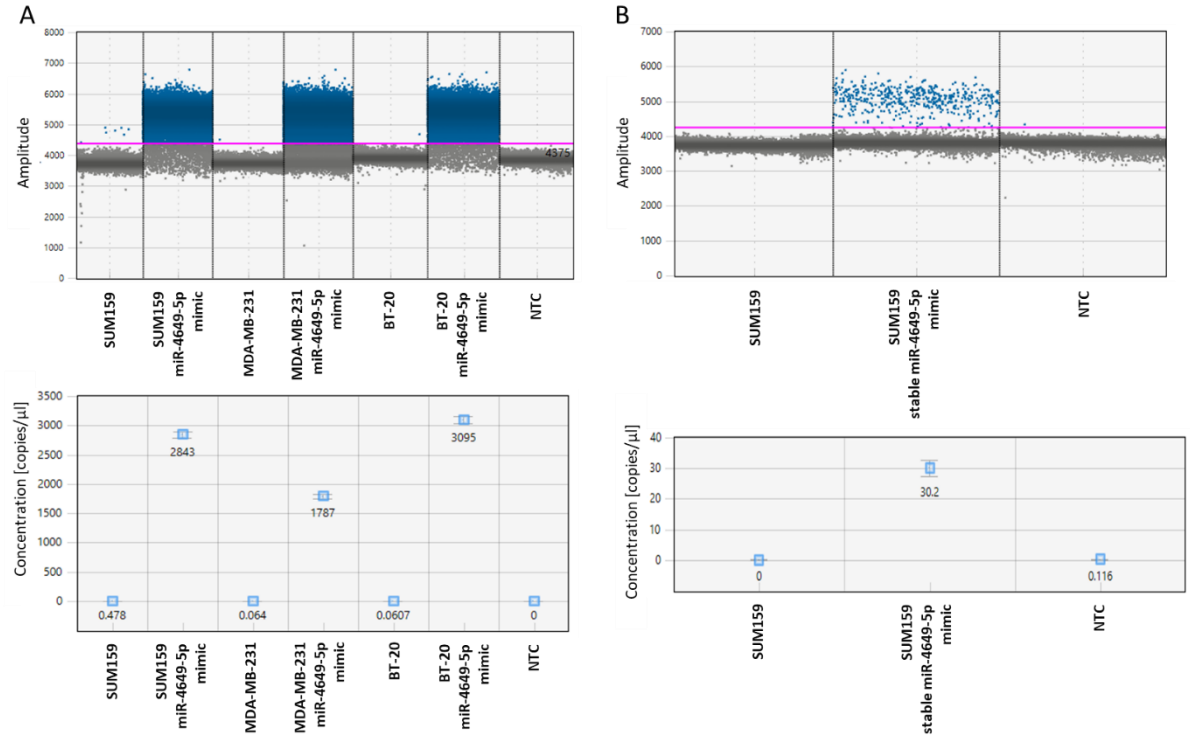

Figure 10: Digital droplet PCR (ddPCR) detecting miR-4649-5p expression in TNBC cells. (A) *Endogenous miR-4649-5p or transient miR-4649-5p mimic overexpression as a positive control in SUM159, MDA-MB-231, and BT-20 cells. Droplet distributions with the threshold for positive droplets (top) and quantifications of miR-4649-5p copies per µl (bottom) are presented (NTC = no-template control).* ***(B)*** *Endogenous miR-4649-5p or stable miR-4649-5p mimic overexpression as positive control in SUM159 cells. Droplet distributions with the threshold for positive droplets (top) and quantifications of miR-4649-5p copies per µl (bottom) are presented (NTC = no-template control).*

In the following sections, the results covering the first aim of the dissertation, the *in vitro* characterization, and the second aim, the analysis of affected pathways and targets, will be presented separately, first for miR-4646-5p, then for miR-4649-5p.

3.4. *In vitro* characterization of miR-4646-5p

3.4.1. Growth and proliferation

Once we had established gain- and loss-of-function systems of miR-4646-5p in our cell lines, we started to characterize the impact of the deregulation of the miRNA on various phenotypic cell properties in order to determine whether miR-4646-5p has a relevant biological role in TNBC cells and if so, whether it is tumor-suppressive or oncogenic. The first aspect we

investigated was cell growth by performing WST-1 assays with the three TNBC cell lines SUM159, MDA-MB-231, and BT-20. This type of assay allows to determine the presence of viable metabolically active cells by spectrophotometric measurement of the production of a formazan dye (190). Performing this assay over a time span of 96 h we could assess cell growth. We observed that miR-4646-5p mimic transfection caused a significant decrease in growth after 72 and 96 h compared to the mimic control, whereas inhibition had the opposite effect and resulted in increased cell numbers after 96 h (Figure 11A and 11B).

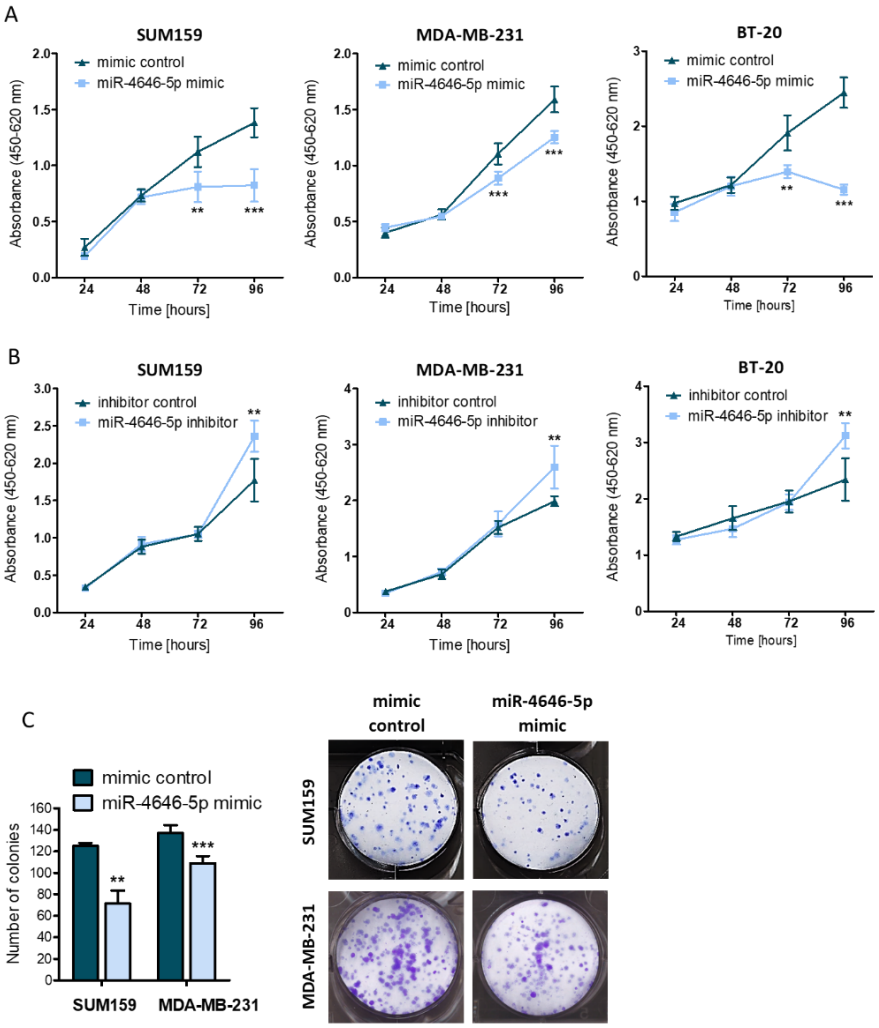

Figure 11: Impact of miR-4646-5p on the growth of TNBC cell lines. ***(A)*** *Impact of transient miR-4646-5p mimic transfection on cell growth as determined in WST-1 assays in SUM159, MDA-MB-231, and BT-20 cells (n = 6; mean ± SD; **p ≤ 0.01, ***p ≤ 0.001).* ***(B)*** *Impact of transient miR-4646-5p inhibitor transfection on cell growth as determined in WST-1 assays in SUM159, MDA-MB-231, and BT-20 cells (n = 6; mean ± SD; **p ≤ 0.01).* ***(C)*** *Colony formation of SUM159 and MDA-MB-231 cells transiently transfected with miR-4646-5p mimic or control. Colonies were counted after 7 days (SUM159) or 14 days (MDA-MB-231) (representative pictures on the right) and are presented in absolute numbers (mean ± SD; n = 3 for SUM159, n = 6 for MDA-MB-231; **p ≤ 0.01; ***p ≤ 0.001).*

As the effect of the mimic had been stronger than the effect of the inhibitor and as it had apparent tumor-suppressive properties, which were more of interest to us than the opposite caused by the inhibitor, we further focused on the mimic. We confirmed the growth-reducing effect of the miR-4646-5p mimic over an extended period by colony formation assays, for which cells were cultured for 7 (in case of SUM159) or 14 days (in case of MDA-MB-231) (BT-20 cells did not show colony formation under these conditions). Both cell lines showed a reduction in colony numbers upon miR-4646-5p mimic transfection (Figure 11C).

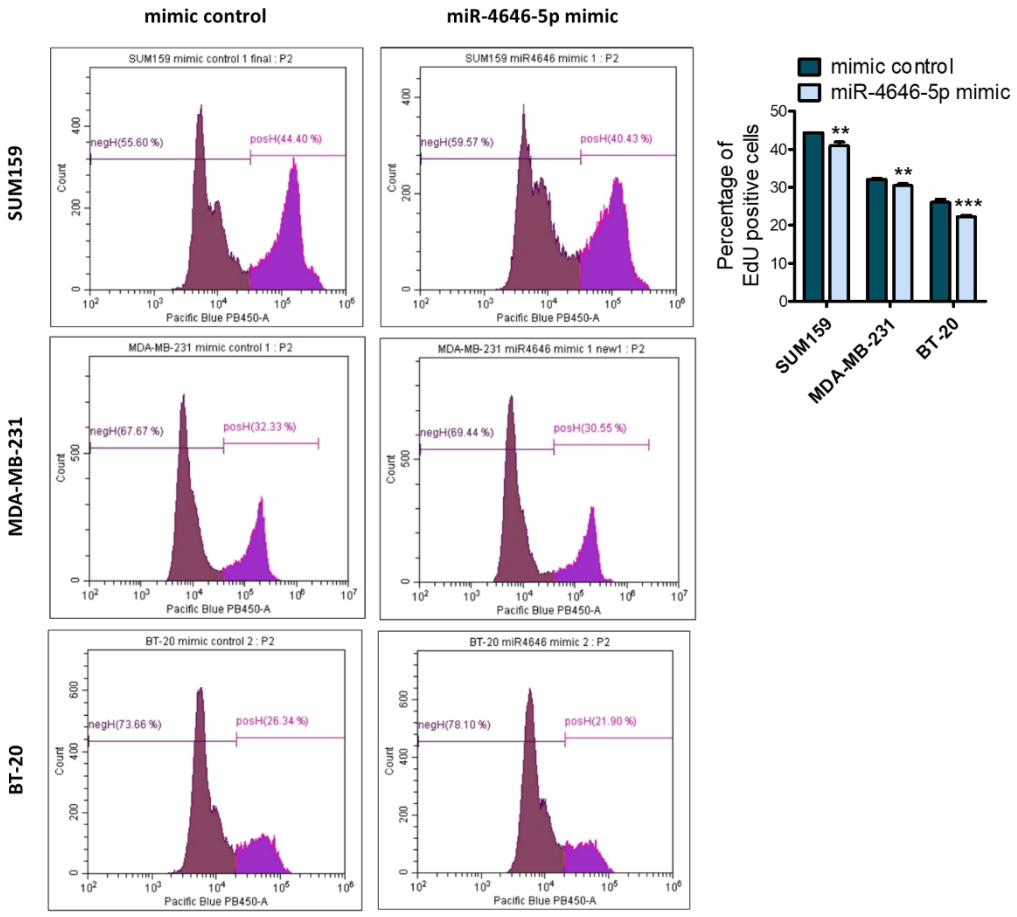

Figure 12: Impact of miR-4646-5p on the proliferation of TNBC cell lines. *Flow cytometric EdU assays were performed 72 h after transient miR-4646-5p mimic transfection of SUM159, MDA-MB-231, and BT-20 cells. Representative histograms are presented on the left, showing the distribution and gating of EdU negative and positive cells, and the quantification on the right (mean ± SD; n = 3, n = 2 for SUM159 mimic control; MDA-MB-231 results of miR-4646-5p mimic and mimic control cells were compared by t-test; SUM159 and BT-20 were tested by one-way ANOVA and Tukey`s multiple comparison test to correct for multiple testing, as the mimic control had also been compared to miR-4649-5p mimic transfected samples in the same experiment; **p ≤ 0.01, ***p ≤ 0.001).*

Finally, we wanted to understand the mechanisms behind the reduced cellular growth and reduced colony numbers we had observed. To this end, we assessed cell proliferation by performing flow cytometric EdU assays, where cells were incubated with the nucleoside analog EdU (5-ethynyl-2'-deoxyuridine) for 2 h, during which time it is incorporated into the newly synthesized DNA of proliferating cells. After labeling EdU with the fluorescent dye pacific blue (PB-450A), positive proliferating cells were counted by flow cytometry. We observed that 72 h after the transfection with the miR-4646-5p mimic the percentage of EdU-positive cells was reduced in all three cell lines compared to the mimic control (Figure 12). The effect was consistent and significant but not very strong. Nevertheless, as this was only a snapshot of a short time window of 2 h, these reductions in the numbers of proliferating cells might still contribute to the more substantial decrease in cell/colony numbers seen over a longer period of time.

3.4.2. Apoptosis

We had the hypothesis that, in addition to effects on proliferation, the growth-reducing properties of miR-4646-5p may also have been caused by another mechanism, namely by the induction of cell death via apoptosis. To investigate this, we performed caspase-3/7 activity assays. Caspase-3 and -7 are proteases that execute the cleavage of various substrates in the final stages of the apoptotic cascade, resulting in characteristic hallmarks of apoptotic cells like the exposure of phosphatidylserine on the cell surface, nuclear condensation, and the fragmentation of genomic DNA (191). A luminescent assay showed that 48 h after miR-4646-5p mimic transfection, there was a significant increase in caspase-3/7 activity in SUM159 and MDA-MB-231 cells, but not in BT-20 cells (Figure 13A). The increase was more pronounced in the SUM159 cell line though and after 72 h the effect in the MDA-MB-231 cells was not detectable anymore (Figure 13A). To further confirm the apparently cell-line-specific impact on apoptosis, we also measured the activity of caspase-9, an initiator caspase, which lies further upstream of caspase-3 and -7 (191), in SUM159 and MDA-MB-231 cells and received similar results. While in the SUM159 cells, the miR-4646-5p mimic significantly increased caspase-9 activity after 48 and 72 h, there was no effect in MDA-MB-231 cells (Figure 13B). Finally, we checked for cleavage of PARP, a substrate of caspase-7, by Western blotting which again indicated induction of apoptosis in the SUM159 cell line after miR-4646-5p overexpression but not in the MDA-MB-231 cell line (Figure 13C).

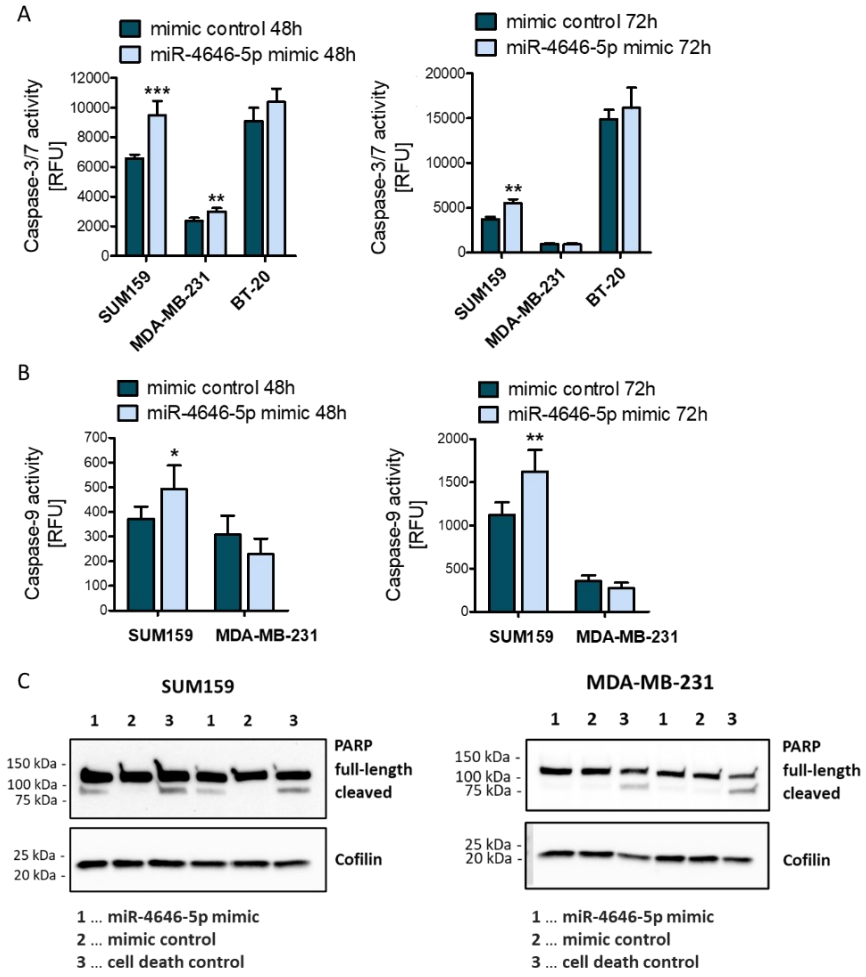

Figure 13: Impact of miR-4646-5p on the induction of apoptosis in TNBC cell lines. (A) *Caspase-3/7 activity was measured in a luminescent assay 48 or 72 h after miR-4646-5p mimic or control transfection of SUM159, MDA-MB-231, and BT-20 cells (n = 4 for 48 h; n = 6 for 72 h; mean ± SD; for the 48 h time points miR-4646-5p and the control samples were compared by one-way ANOVA and Tukey`s multiple comparison test as the control samples were also compared to miR-4649-5p mimic samples in the same experiment; **p ≤ 0.01, ***p ≤ 0.001; RFU = relative fluorescence units).* ***(B)*** *Caspase-9 activity was measured in a luminescent assay 48 or 72 h after miR-4646-5p mimic or control transfection of SUM159 and MDA-MB-231 cells (n = 6; mean ± SD; *p ≤ 0.05, **p ≤ 0.01; RFU = relative fluorescence units).* ***(C)*** *The cleavage of PARP 48 h after transient miR-4646-5p mimic, negative mimic control, or positive cell death control transfection of SUM159 and MDA-MB-231 cells was detected by Western blotting (n = 2).*

As previously addressed in the introduction, the net effects of miRNAs are frequently context-dependent due to their large number of indirect and direct targets which often show different expression patterns in different tissues or cell lines (147). Thus, the fact that only one of the tested cell lines exhibited signs of apoptosis in response to miR-4646-5p upregulation may be due to differences in the expression of certain apoptotic genes that are involved in mediating

this specific effect of the miRNA in the cell lines. To substantiate this, we screened the SUM159 and MDA-MB-231 cell lines, transfected with the miR-4646-5p mimic or mimic control, for their expression of a panel of apoptosis-related genes. Indeed, we discovered that the two cell lines, one of which did show induction of apoptosis in response to miR-4646-5p and one did not, differed in their expression of certain apoptosis marker genes (Figure 14). SUM159 cells did not express the pro-apoptotic genes *BAK* and *NOXA*, whereas MDA-MB-231 cells did (Figure 14). In addition, the miR-4646-5p mimic caused a significant increase in the pro-apoptotic genes *BAD*, *BAX*, *BCL10*, and *TRADD* in SUM159 cells, whereas MDA-MB-231 cells only showed an increase in *TRADD* (Figure 14).

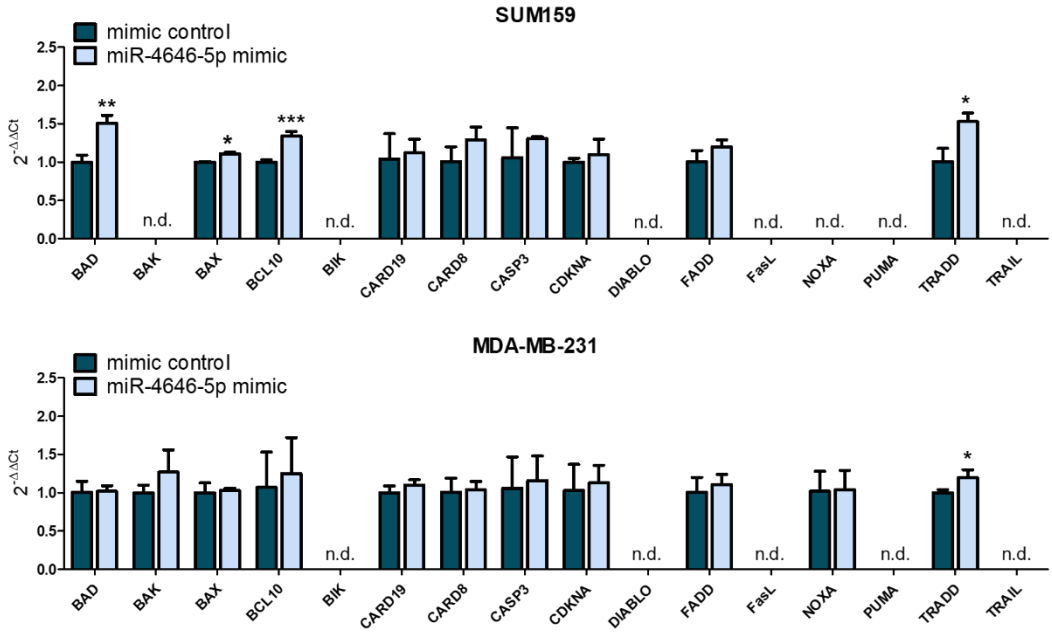

Figure 14: Expression of pro-apoptotic genes in TNBC cell lines in response to miR-4646-5p overexpression. *Expression was measured by qPCR 48 h after miR-4646-5p mimic or control transfection of SUM159 and MDA-MB-231 cells (n = 3; mean ± SD; *p ≤ 0.05, **p ≤ 0.01, ***p ≤ 0.001; n.d. = not detected). BAD…BCL2 associated agonist of cell death, BAK…BCL2 homologous antagonist killer, BAX…BCL2 associated X, apoptosis regulator, BCL10…B-cell lymphoma/leukemia 10, BIK… BCL2 interacting killer, CARD19…caspase recruitment domain family member 19, CARD8…caspase recruitment domain family member 8, CASP3…caspase 3, CDKNA…cyclin dependent kinase inhibitor 2A, DIABLO… Diablo IAP-binding mitochondrial protein, FADD…Fas-associated via death domain, FasL…Fas ligand, NOXA…phorbol-12-myristate-13-acetate-induced protein 1, PUMA…p53 upregulated modulator of apoptosis, TRADD…TNFRSF1A associated via death domain, TRAIL…tumor necrosis factor-related apoptosis inducing ligand. (The qPCR presented here was performed by Felix Prinz, PhD student at the Department of Internal Medicine, Division of Oncology, Medical University of Graz, Austria.)*

3.4.3. Migration

Another cancer cell characteristic we investigated was migration as the migratory behavior of cancer cells, which is closely connected to EMT, presents an essential requirement for the spreading and dissemination of cancer, ultimately enabling the formation of distant metastases (192). It is also a hallmark frequently influenced by the deregulation of miRNAs (132). To study the potential impact of miR-4646-5p on the migration of TNBC cells *in vitro*, we first performed so-called scratch or wound healing assays, where a scratch is introduced into a confluent cell layer and the closure of the scratch over time is monitored microscopically. For this particular assay, we could only use the SUM159 cell line, as the MDA-MB-231 cells tended to detach very easily, resulting in their re-seeding in the scratched area, thereby interfering with effects that were mediated by migration. The SUM159 cell line showed that miR-4646-5p upregulation by mimic transfection resulted in a delayed closure of the scratch, whereas miR-4646-5p inhibition promoted spreading of the cells to close the scratch (Figure 15A and 15B). We also employed the stable miR-4646-5p inhibitor cell line for this assay and could confirm the increased wound healing we had observed after transient inhibition (Figure 15C).

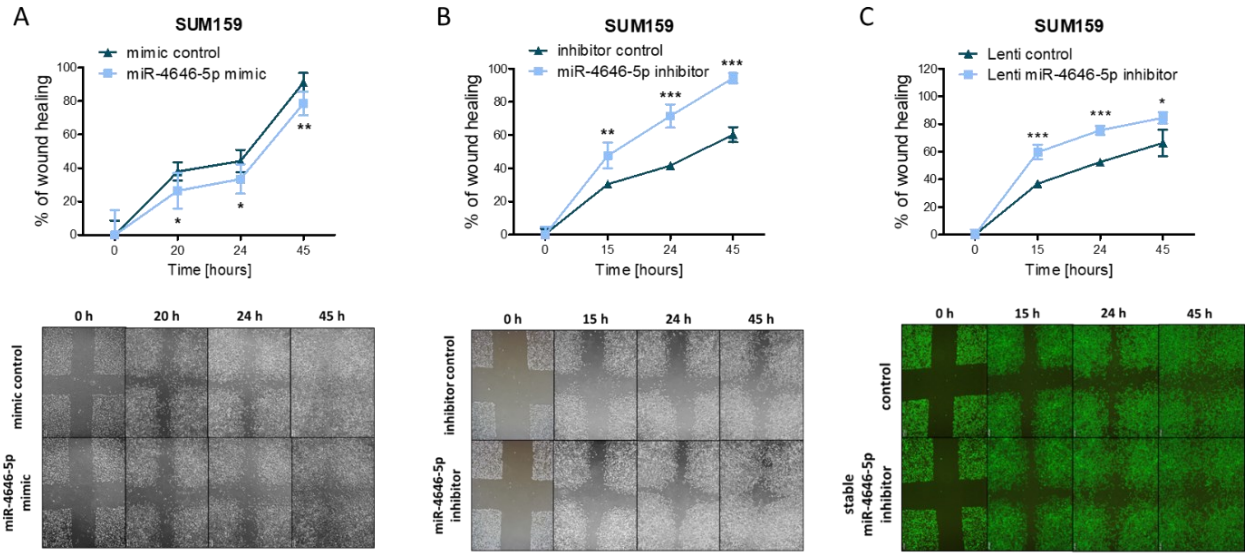

Figure 15: Impact of miR-4646-5p on the migration of TNBC cells. *The impact of* ***(A)*** *transient miR-4646-5p mimic,* ***(B)*** *transient miR-4646-5p inhibitor, and* ***(C)*** *stable lentiviral miR-4646-5p inhibition was assessed with SUM159 cells in scratch assays. For each time point, the percentage of scratch closure relative to the first time point (0 h) was calculated (representative pictures at the bottom) (mean ± SD; n = 4;* ***(A)*** *n = 8; *p ≤ 0.05, **p ≤ 0.01, ***p ≤ 0.001).*

The closure of the scratch in a wound healing assay is, however, not only facilitated by cell migration but is also influenced by cell growth, a characteristic that we had already discovered to be altered by miR-4646-5p deregulation. Due to this, we then performed transwell migration

assays to confirm our initial findings. For these transwell assays, cells were seeded on top of a permeable membrane, and the number of cells migrating through the membrane toward FBS as an attractant was quantified. Both SUM159 and MDA-MB-231 cells showed that miR-4646-5p overexpression decreased cell migration through the membrane, while miR-4646-5p inhibition increased it (Figure 16A and 16B). In summary, miR-4646-5p was able to reduce TNBC cell migration *in vitro*.

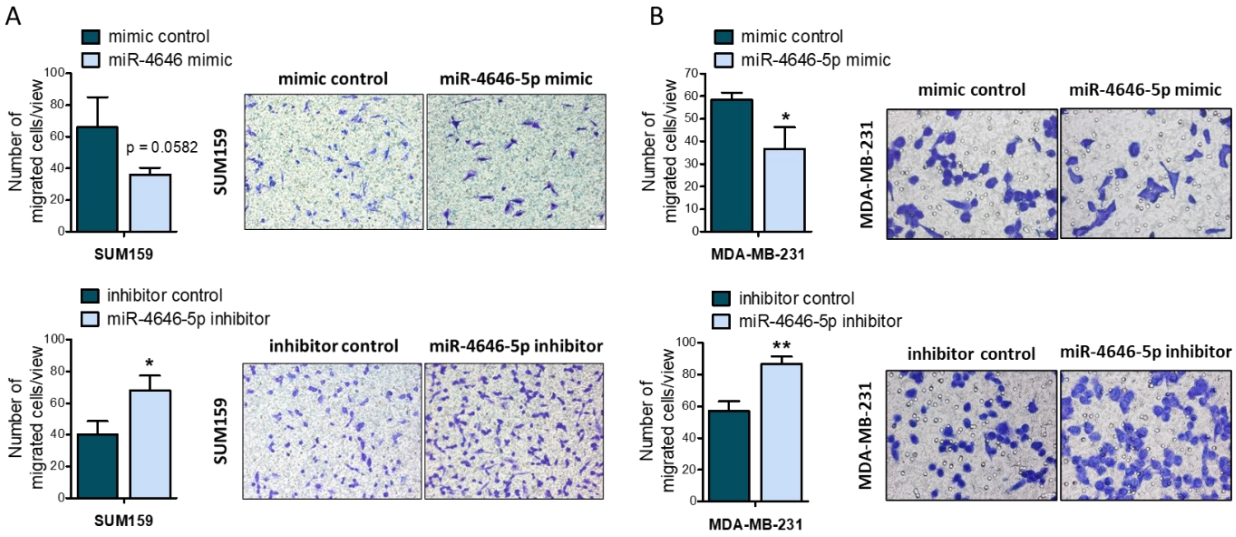

Figure 16: Impact of miR-4646-5p on the migration of TNBC cells. *The effects of the miR-4646-5p mimic and miR-4646-5p inhibitor on cell migration were determined in transwell migration assays with* ***(A)*** *SUM159 and* ***(B)*** *MDA-MB-231 cells. From each transwell, migrated cells were counted in five representative fields of view at 40x magnification (representative images in* ***(A)*** *are 20x magnification, in* ***(B)*** *40x magnification) and are presented in absolute numbers (n = 3; mean ± SD; *p ≤ 0.05, **p ≤ 0.01) (The transwell assays presented in* ***(A)*** *were performed by Julia Teppan, PhD student at the Division of Pharmacology, Otto Loewi Research Center, Medical University of Graz, Austria).*

3.4.4. Stemness

As the two miRNA candidates that were characterized in the dissertation had originally been selected due to their deregulation in cancer stem cell-enriched mammospheres (163,164), we were interested in determining whether they had an impact on properties of stemness. To this end, we measure the enzymatic activity of ALDH1, a common marker used to discern breast cancer stem cells (193), in a flow cytometric assay. In SUM159 cells, the transfection with the miR-4646-5p mimic caused a significant decrease in ALDH1-positive cells (Figure 17). In the MDA-MB-231 and the BT-20 cell line though, no effect could be detected (Figure 17).

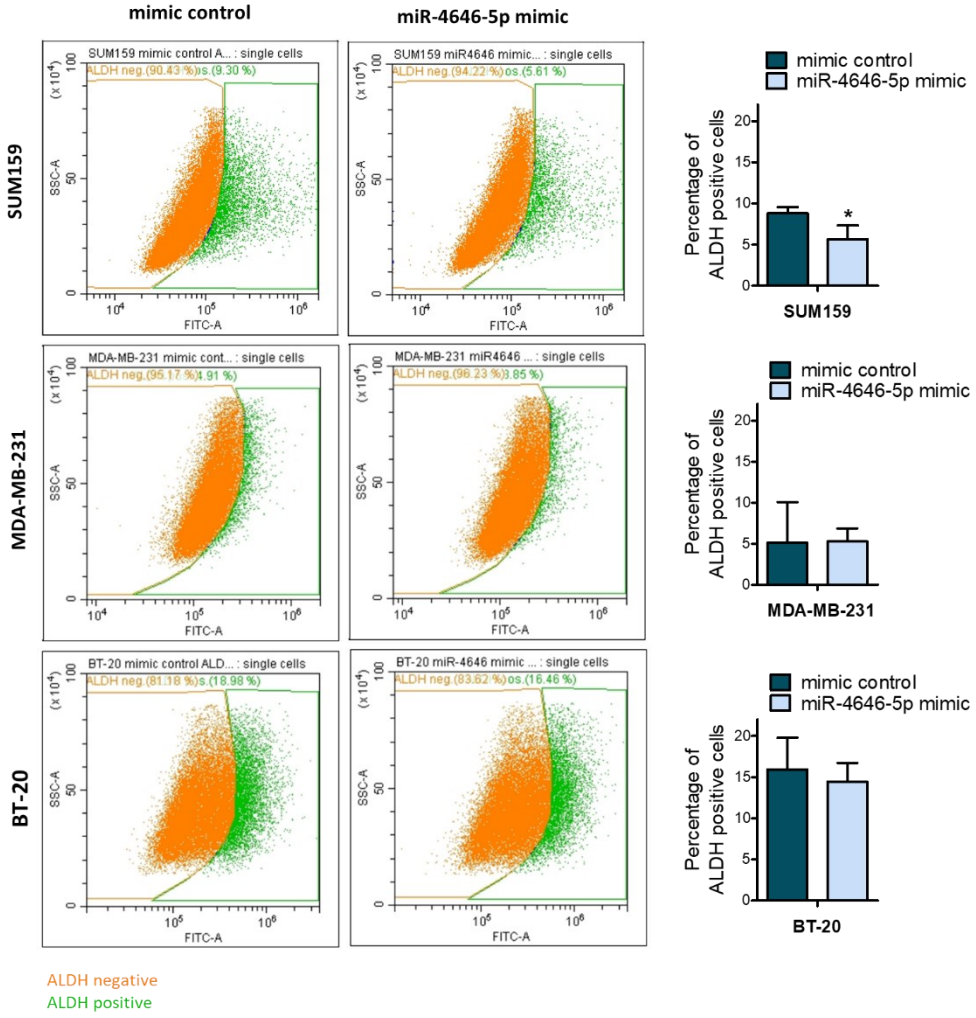

Figure 17: Impact of miR-4646-5p on aldehyde dehydrogenase (ALDH) activity in TNBC cells. *ALDH-positive cells were measured in a flow cytometric assay 48 h after miR-4646-5p mimic or control transfection of SUM159, MDA-MB-231, and BT-20 cells. Representative scatter plots are shown on the left, illustrating the gating for ALDH negative and positive cells set according to ALDH-inhibitor-treated negative controls for each sample (n = 4; mean ± SD; *p ≤ 0.05).*

3.4.5. Angiogenesis

As discussed in the introduction, miRNAs frequently have an impact on the TME and can influence immune cell activity and the formation of new blood vessels by endothelial cells by various means (142). Therefore, we investigated whether miR-4646-5p affects angiogenesis. As a way to assess angiogenesis *in vitro*, we performed tube formation assays where endothelial cells, in this case human umbilical vein endothelial cells (HUVECs), are seeded on a basement membrane matrix that typically contains, amongst others, laminin, collagen, entactins, heparan sulfate proteoglycans, matrix metalloproteinases, and various growth factors, and that supports the rapid formation of branched capillary-like tubes by the endothelial

cells (194). These pseudo-capillary structures are then quantified by image analysis tools (195). We observed that HUVECs that were transiently transfected with the miR-4646-5p mimic showed a reduced ability to form tubes (Figure 18A and 18B). This was visible microscopically as well as by the quantification of nodes, meshes, junctions, and the total tube length, all of which were significantly decreased by the miR-4646-5p mimic (Figure 18B).

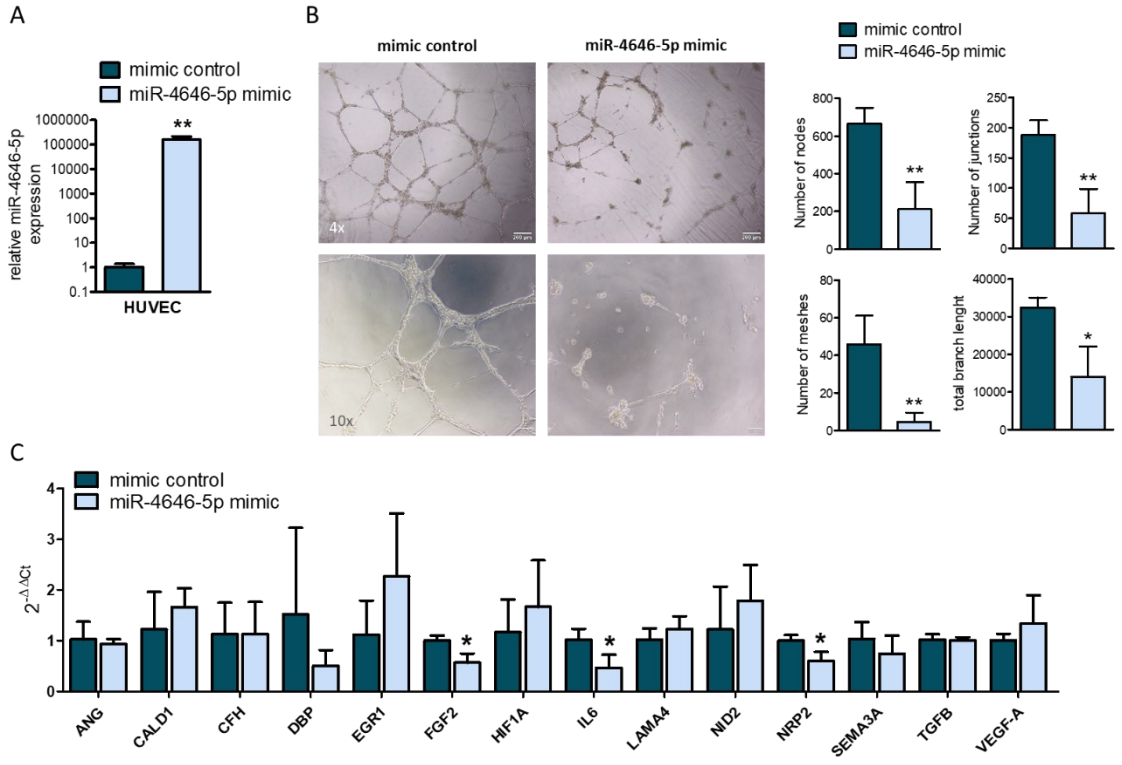

Figure 18: Impact of miR-4646-5p on the in vitro tube formation of endothelial cells. (A) *Transfection efficiency of human umbilical vein endothelial cells (HUVECs) 48 h after transfection with the miR-4646-5p mimic determined by qPCR (n = 3; mean ± SD; **p ≤ 0.01).* ***(B)*** *In vitro tube formation assay of HUVECs transfected with the miR-4646-5p mimic or control. Representative pictures on the left (4x and 10x magnification), and quantifications of the number of nodes, junctions, meshes, and the total length of the branches on the right (n = 3; mean ± SD; compared by one-way ANOVA and Tukey`s multiple comparison test, as the mimic control was compared to miR-4649-5p mimic samples in the same experiment; *p ≤ 0.05, **p ≤ 0.01) (The assay was performed by Christiane Klec, Priv.-Doz. PhD, Department of Internal Medicine, Division of Oncology, Medical University of Graz, Austria).* ***(C)*** *Expression of angiogenesis-associated genes as measured by qPCR 48 h after miR-4646-5p mimic or control transfection of HUVECs (n = 3; mean ± SD; *p ≤ 0.05). ANG…angiogenin, CALD1…caldesmon, CFH…complement factor H, DBP…D-box binding PAR BZIP transcription factor, EGR1…early growth response factor 1, FGF2…fibroblast growth factor 2, HIF1A…hypoxia-inducible factor 1 subunit alpha, IL-6…interleukin 6, LAMA4…laminin subunit alpha 4, NID2…nidogen 2, NRP2…neuropilin 2, SEMA3A…semaphorin 3A, TGFB…transforming growth factor beta, VEGF-A…vascular endothelial growth factor.*

To gain further insight into the mechanisms behind the effect on tube formation, we investigated the expression of a panel of angiogenesis-associated genes by qPCR and discovered that three of these genes were downregulated in the HUVECs upon miR-4646-5p mimic transfection, namely fibroblast growth factor 2 (FGF2), interleukin 6 (IL6), and neuropilin-2 (NRP2) (Figure 18C). All three of these genes have been reported to promote the migration, proliferation, and vascularization of endothelial cells (196–198) and their downregulation in the HUVECs could thus provide an explanation for the reduced *in vitro* tube formation caused by miR-4646-5p.

3.5. Identification of miR-4646-5p targets and affected pathways

3.5.1. Transcriptome analysis and identification of potential targets

In the previous chapters, the results covering the first aim of the dissertation have been presented, which showed that miR-4646-5p overexpression was able to reduce the growth, proliferation, and migration of TNBC, to induce apoptosis in TNBC cells in a cell-line-specific context, and to reduce the tube formation of endothelial cells. In summary, the *in vitro* characterization indicated a tumor-suppressive role of miR-4646-5p in TNBC. In order to understand the mechanisms behind these effects we continued with the second aim which was to elucidate the molecular pathways and targets that are altered by the miRNA. To get an overview of the molecular changes caused by miR-4646-5p we performed a whole transcriptome analysis by RNA-seq of SUM159 cells that were transfected with the miR-4646-5p mimic. In total, 605 genes were significantly differentially expressed compared to control transfected cells. 277 of those genes were upregulated and 328 were downregulated (Figure 19A). As described in the introduction, miRNAs generally cause posttranscriptional downregulation of their direct targets. Therefore, as we were interested in identifying direct targets, we focused on downregulated genes, the top 20 of which, sorted according to fold-change, are presented in Figure 19B. The majority of the top downregulated genes had previously been reported to have oncogenic functions, as will be detailed in the discussion. Their downregulation by miR-4646-5p thus supports the tumor-suppressive properties of the miRNA that we had observed *in vitro*.

A

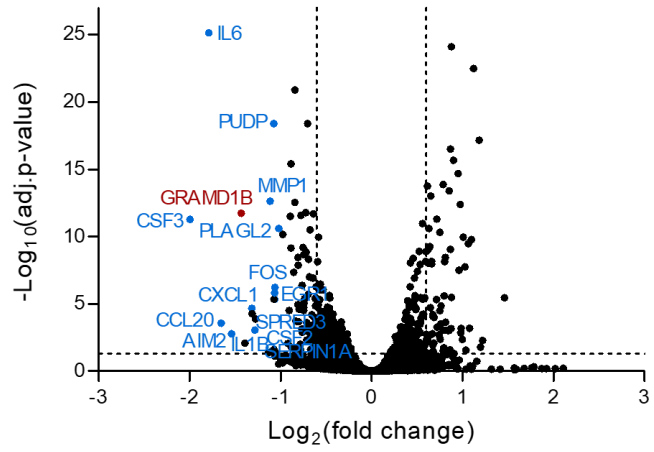

B

Gene Name	Fold-change	adj. p-value
CSF3	- 3,98	5.285e-12
IL6	- 3,45	7.017e-26
CCL20	- 3,14	0.000274
AIM2	- 2,90	0.001698
GRAMD1B	- 2,70	1.808e-12
CXCL1	- 2,49	2.192e-05
SPRED3	- 2,43	0.0009108
MMP1	- 2,17	2.307e-13
IL1B	- 2,13	0.0303237
PUDP	- 2,11	4.005e-19
CSF2	- 2,10	4.520e-06
SERPINA1	- 2,10	0.0243591
FOS	- 2,09	1.498e-06
EGR1	- 2,09	4.520e-06
TFPI2	- 1,96	6.773e-11
BCL9	- 1,87	3.031e-05
CXCL8	- 1,85	3.034e-12
ETV4	- 1,85	4.047e-16
CXCL3	- 1,85	7.016e-10
NPAS2	-1,84	0.01685

Figure 19: RNA-seq results of SUM159 cells transfected with the miR-4646-5p mimic. (A) *Volcano plot illustrating the miR-4646-5p mimic vs. mimic control RNA-seq results. Dashed lines indicate the adjusted p-value cut-off (0.05) that was used to determine significantly deregulated genes, and the 1.5-fold-change thresholds. Top-downregulated genes are highlighted in color and labeled.* ***(B)*** *List of the top 20 annotated significantly downregulated genes, sorted according to fold-change in expression. Genes with previously reported oncogenic functions are highlighted in blue.*

In order to further narrow down the RNA-seq results and to eventually identify direct targets of miR-4646-5p (the steps taken to do so are illustrated in Figure 20A), we used the top 20 downregulated genes and performed *in silico* target predictions using three online tools: TargetScan (174), miRWalk2.0 (175), and miRDB (176). These online tools employ different algorithms to identify potential binding sites for a given miRNA within a potential target gene based on canonical complementary sites, but also considering the context and surrounding sequence of the site, structural accessibility, and supplementary pairings (174). For four of the top downregulated genes at least one of the prediction tools predicted potential binding sites for miR-4646-5p. These four genes were GRAM domain containing 1B (*GRAMD1B*), sprouty related EVH1 domain containing 3 (*SPRED3*), matrix metallopeptidase 1 (*MMP1*), and Fos proto-oncogene (*FOS*). We then continued by confirming the downregulation of these four genes in SUM159 and MDA-MB-231 cells by qPCR. Out of the four candidates, only GRAMD1B and FOS were expressed in all three cell lines (Figure 20B). While FOS was only significantly downregulated in one of the three cell lines, GRAMD1B was significantly reduced in two cell lines (Figure 20B). Moreover, GRAMD1B had the highest number of predicted binding sites within its 3`UTR (Table 5). Based on this, we selected GRAMD1B and continued with our efforts to confirm it as a direct target of miR-4646-5p.

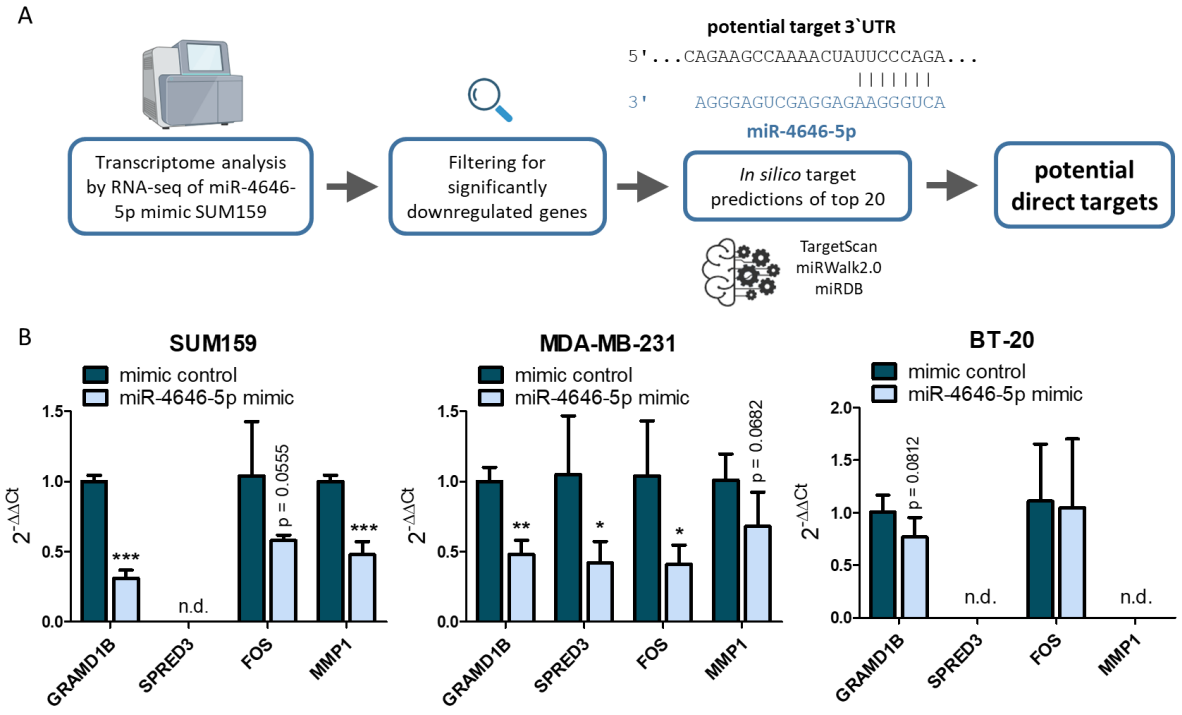

Figure 20: Identification of potential miR-4646-5p target genes. (A) *Scheme illustrating the process of identifying potential direct targets of miR-4646-5p from RNA-seq data.* ***(B)*** *Expression of four selected potential targets of miR-4646-5p measured by qPCR 48 h after transfection of SUM159, MDA-MB-231, and BT-20 cells with the miR-4646-5p mimic or control (n = 3; mean ± SD; *p ≤ 0.05, **p ≤ 0.01, ***p ≤ 0.001; n.d. = not detected). GRAMD1B…GRAM domain containing 1B, SPRED3…sprouty related EVH1 domain containing 3, MMP1…matrix metallopeptidase 1, FOS…Fos proto-oncogene.*

Table 5: Potential binding sites between miR-4646-5p and the 3`untranslated region (UTR) of the GRAM domain-containing protein 1B (GRAMD1B) gene as predicted by TargetScan *(7mer-A1…exact match of target to positions 2-7 of the miRNA (seed) followed by an 'A'; 7mer-m8…exact match of target to positions 2-8 of the mature miRNA; 8mer…exact match of target to positions 2-8 of the mature miRNA followed by an 'A').*

Site number	Target position	Predicted consequential pairing of target region (top) and miR-4646-5p (bottom)	Site type	Context score percentile
1	Position 1623-1629 of *GRAMD1B* 3' UTR	5' ...AAGAAACCCCAGAUGUCCCAGAU... 3' AGGGAGUCGAGGAGAAGGGUCA	7mer-A1	84
2	Position 1632-1638 of *GRAMD1B* 3' UTR	5' ...CAGAUGUCCCAGAUGUCCCAGAA... 3' AGGGAGUCGAGGAGAAGGGUCA	7mer-A1	86
3	Position 2097-2104 of *GRAMD1B* 3' UTR	5' ...CAGAAGCCAAAACUAUUCCCAGA... 3' AGGGAGUCGAGGAGAAGGGUCA	8mer	97
4	Position 2299-2305 of *GRAMD1B* 3' UTR	5' ...UACCUCUCAGGACCA-UUCCCAGG... 3' AGGGAGUCGAGGAGAAGGGUCA	7mer-m8	33

***Table 5** (continued)*

Site number	Target position	Predicted consequential pairing of target region (top) and miR-4646-5p (bottom)	Site type	Context score percentile
5	Position 3234-3240 of *GRAMD1B* 3' UTR	5' ...CCCAGAGGCUGAAGCUUCCCAGU... 3' AGGGAGUCGAGGAG-AAGGGUCA	7mer-m8	33
6	Position 3272-3278 of *GRAMD1B* 3' UTR	5' ...AGGGCAGUGUCUGCAUUCCCAGG... 3' AGGGAGUCGAGGAGAAGGGUCA	7mer-m8	33
7	Position 3878-3884 of *GRAMD1B* 3' UTR	5' ...UCUGGAUGCUUGUGGUCCCAGAA... 3' AGGGAGUCGAGGAGAAGGGUCA	7mer-A1	78

3.5.2. Confirmation of GRAMD1B as a direct target of miR-4646-5p

GRAMD1B was the fifth most downregulated gene in the RNA-seq analysis of miR-4646-5p mimic transfected cells with a 2.7-fold downregulation and showed 7 predicted miR-4646-5p binding sites according to the TargetScan algorithm. We could furthermore confirm the downregulation of GRAMD1B in SUM159 and MDA-MB-231 cells by qPCR. The next step was to determine whether GRAMD1B is also reduced on the protein level when miR-4646-5p is overexpressed. By Western blotting, changes in the protein level are hard to detect by eye, but after background subtraction and normalization to a housekeeper (Cofilin), densitometric quantification showed a consistent reduction of GRAMD1B protein levels in both SUM159 and MDA-MB-231 cells (Figure 21A). To ascertain whether the downregulation of GRAMD1B by miR-4646-5p is mediated via a direct interaction between the two, we performed dual luciferase reporter assays using the predicted binding site of the GRAMD1B 3`UTR with the highest score according to TargetScan (binding site 3 in Table 5). The 7 nt long seed binding site complementary to miR-4646-5p plus the flanking region 22 and 19 nt up- and downstream, respectively, were inserted into the reporter vector. In addition, a reporter was generated where the binding site was mutated by exchanging 5 nt within the seed target site. Co-transfection of HEK293 cells with the wild type (wt) reporter and the miR-4646-5p mimic resulted in a significant reduction of the luciferase reporter signal compared to the mimic control, whereas this effect was abrogated when the binding sequence was mutated (Figure 21B). These results confirmed the direct interaction between miR-4646-5p and GRAMD1B.

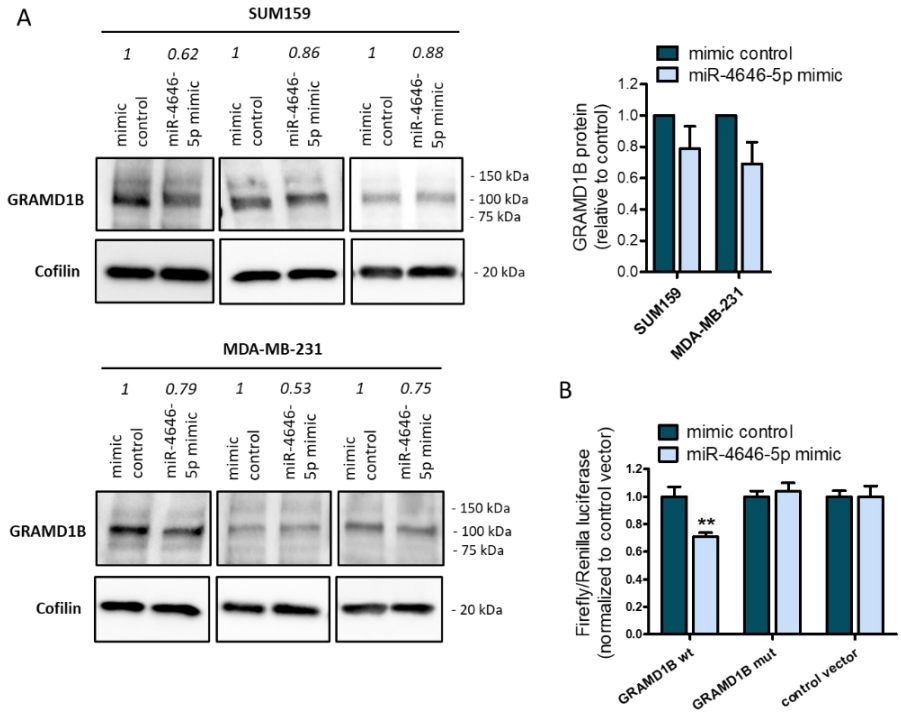

Figure 21: Impact of miR-4646-5p on the protein levels of its target GRAM domain containing 1B (GRAMD1B) and confirmation of direct interaction between miR-4646-5p and GRAMD1B by luciferase reporter assays. (A) *Western blots showing the effect of 48 h of miR-4646-5p mimic transfection in SUM159 and MDA-MB-231 cells on the protein level of GRAMD1B. Blots with the fold-change in GRAMD1B signal intensity (normalized to the housekeeper Cofilin) indicated on top, and the summarized fold changes on the right (n = 3; mean ± SD).* ***(B)*** *Dual luciferase reporter assay in HEK293 cells using a reporter with a wildtype (wt) or mutated (mut) miR-4646-5p binding sequence from the GRAMD1B 3' UTR. The reporter vectors were co-transfected with the miR-4646-5p mimic or mimic control. Luciferase signals were normalized to the respective signals of the control vector (n = 3; mean ± SD; **p ≤ 0.01).*

The next question to be answered was whether targeting GRAMD1B could also contribute to the tumor-suppressiveness of miR-4646-5p. GRAMD1B codes for a protein that sits in the membrane of the endoplasmic reticulum (ER) and that can, via its GRAM domain, sense free cholesterol in the plasma membrane (199,200). In response to an increase in free cholesterol, GRAMD1B transfers this excess to the ER, where a sensor for cholesterol regulates cholesterol *de novo* biosynthesis and cholesterol uptake (199,201,202). Thereby, GRAMD1B contributes to cholesterol homeostasis in the cell (199,202). The role of GRAMD1B in cancer, though, is not well studied yet and there are contradictory reports on whether it has a tumor-suppressive or oncogenic function (203–205). To assess the role of GRAMD1B in TNBC we thus studied the effect of a GRAMD1B knockdown, using an siRNA (Figure 22A), on cell growth. We observed that this knockdown significantly reduced the growth of SUM159 and

MDA-MB-231 cells in WST-1 assays, as well as their colony formation (Figure 22B and 22C). Importantly, this phenocopies the effect of the miR-4646-5p mimic, which provides further evidence that GRAMD1B is a target of miR-4646-5p and indicates that targeting and downregulating GRAMD1B may be a factor contributing to the tumor-suppressiveness of miR-4646-5p.

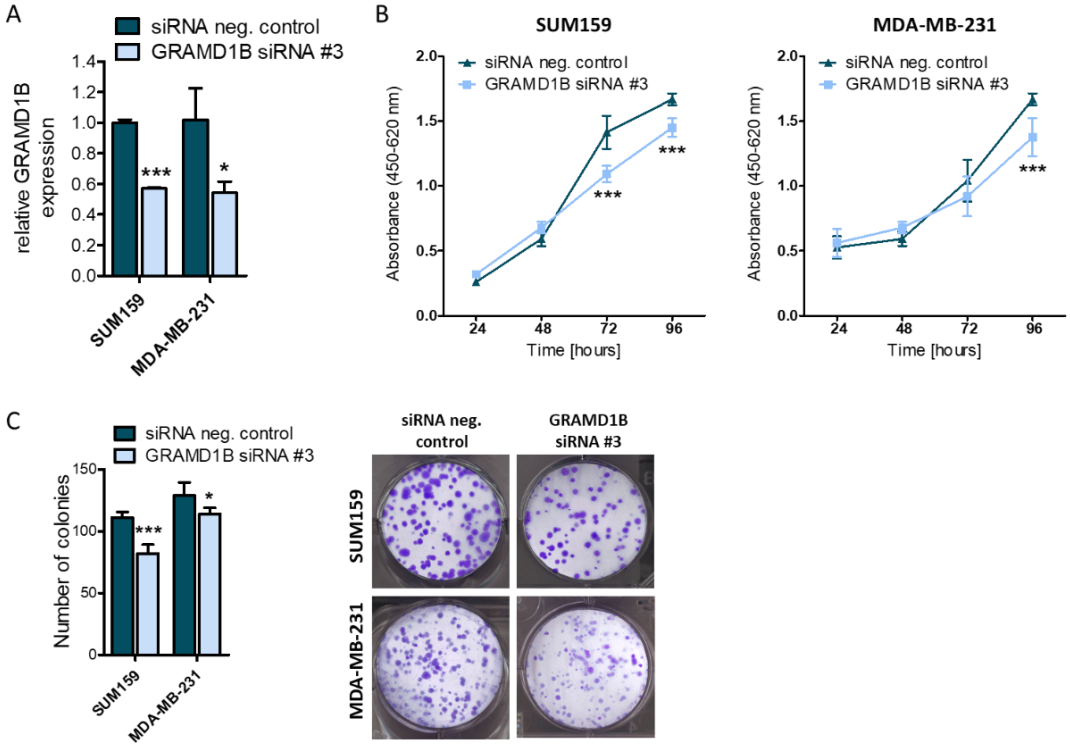

Figure 22: Impact of GRAMD1B knockdown on the growth of TNBC cells. (A) *Knockdown efficiency of GRAMD1B 48 h after siRNA transfection of SUM159 and MDA-MB-231 cells measured by qPCR (n = 3; mean ± SD; *p ≤ 0.05, ***p ≤ 0.001).* ***(B)*** *Impact of GRAMD1B knockdown on the growth of SUM159 and MDA-MB-231 cells as determined in WST-1 assays (n = 6; mean ± SD; ***p ≤ 0.001).* ***(C)*** *Impact of GRAMD1B knockdown on colony formation of SUM159 and MDA-MB-231 cells after 7 and 14 days, respectively. Colonies (representative pictures on the right) were counted and are shown in absolute numbers (n = 6; mean ± SD; **p ≤ 0.01; ***p ≤ 0.001).*

To gain further insight into whether GRAMD1B really acts as an oncogenic factor in TNBC, we looked at its expression in breast tissue using gene chip data from TNMplot (171). However, this did not indicate a difference in the expression between paired breast tumors and normal adjacent tissue (n = 70; Mann-Whitney-U test; p = 0.438; Figure 23A). We then assessed whether GRAMD1B has any prognostic relevance for TNBC. While the overall survival of TNBC patients was significantly better with higher expression of GRAMD1B (n = 153; log-rank test; p = 0.048; hazard ratio = 0.37; 95% confidence interval 0.13 – 1.04; Figure 23B), relapse-free survival (n = 392; log-rank test; p = 0.0031; hazard ratio = 1.75; 95% confidence interval

1.2 - 2.55; Figure 23C) and distant metastasis-free survival of TNBC patients (n = 306; log-rank test; p = 0.021; hazard ratio = 1.68; 95% confidence interval 1.08 - 2.64; Figure 23D) were significantly worse. It has to be considered that for the tumor expression analysis, as well as for the expression data used in the survival analysis, bulk RNA is used, not only originating from cancer cells but also from cells of the TME, like stromal cells and immune cells. This may have an impact on the results and different functions of GRAMD1B in different cell types may have contributed to these discrepancies as the cell types may also play different roles in regard to different clinical endpoints.

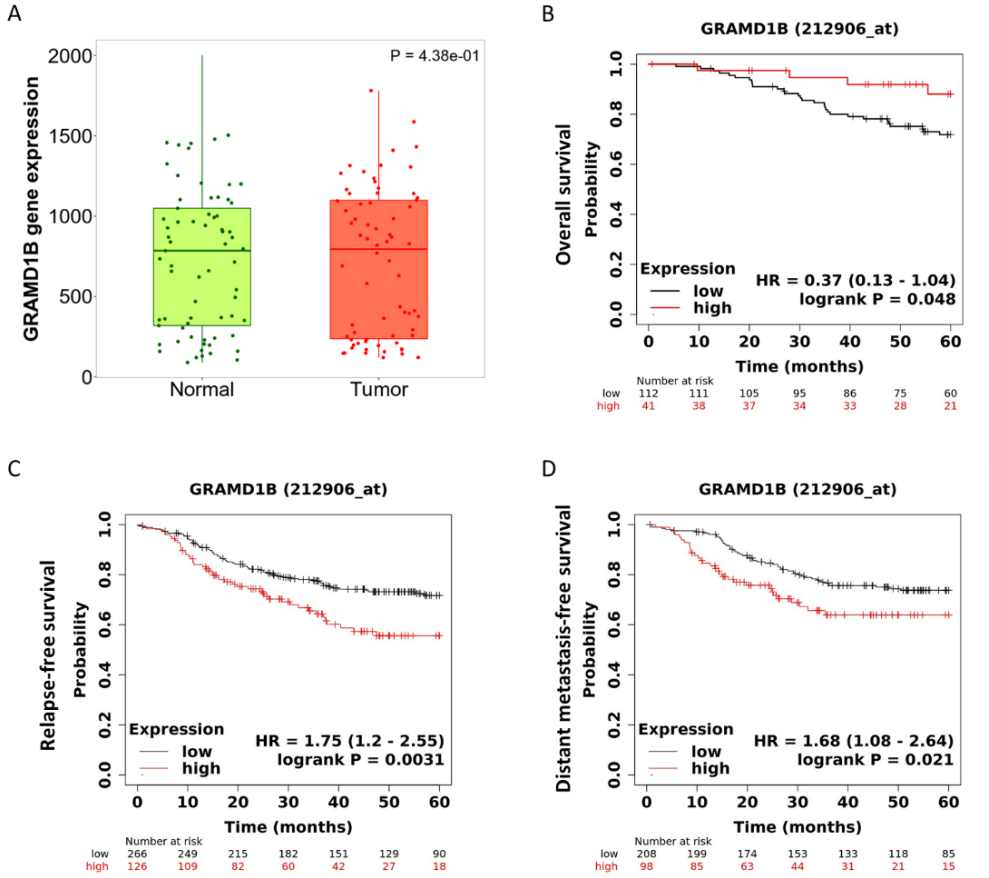

Figure 23: Expression of GRAMD1B in breast tumors and its prognostic relevance. (A) *RNA-seq-based expression of GRAMD1B in breast tumor tissue compared to healthy adjacent tissue (n = 70 per group; Mann-Whitney-U test; p = 0.438).* ***(B)*** *Overall survival of TNBC patients in a GRAMD1B high (n = 41, red) and low (n = 112, black) expression group based on microarray data (log-rank test; p = 0.048; hazard ratio (HR) = 0.37; 95% confidence interval 0.13 – 1.04.* ***(C)*** *Relapse-free survival of TNBC patients in a GRAMD1B high (n = 126, red) and low (n = 266, black) expression group based on microarray data (log-rank test; p = 0.0031; hazard ratio (HR) = 1.75; 95% confidence interval 1.2 - 2.55).* ***(D)*** *Distant metastasis-free survival of TNBC patients in a GRAMD1B high (n = 98, red) and low (n = 208, black) expression group based on microarray data (log-rank test; p = 0.021; hazard ratio (HR) = 1.68; 95% confidence interval 1.08 - 2.64).*

Two previous studies by Khanna and colleagues have investigated the role of GRAMD1B in gastric cancer and TNBC, more precisely in MDA-MB-231 cells, and reported opposing effects on JAK/STAT signaling in the two studies (204,205). In gastric cancer, the authors found GRAMD1B to have an oncogenic role and described a positive feedback loop between GRAMD1B and JAK/STAT signaling. Conversely, the knockdown of GRAMD1B decreased, by unknown mechanisms, the activation of STAT3 as seen in a reduction in the phosphorylation of tyrosine 705 (Y705), which resulted in increased cell death (204). In MDA-MB-231 cells, however, the same authors describe that GRAMD1B exerts a tumor-suppressive effect on cell migration (205). In this setting, knockdown of GRAMD1B increased the activation of JAK2/STAT3 and also AKT, which promoted cell migration (205). We investigated the impact of GRAMD1B knockdown on AKT and STAT3 phosphorylation in our two TNBC cell lines SUM159 and MDA-MB-231 by Western blotting. This, however, did not reveal any impact on AKT or STAT3 activation (Figure 24A and 24B).

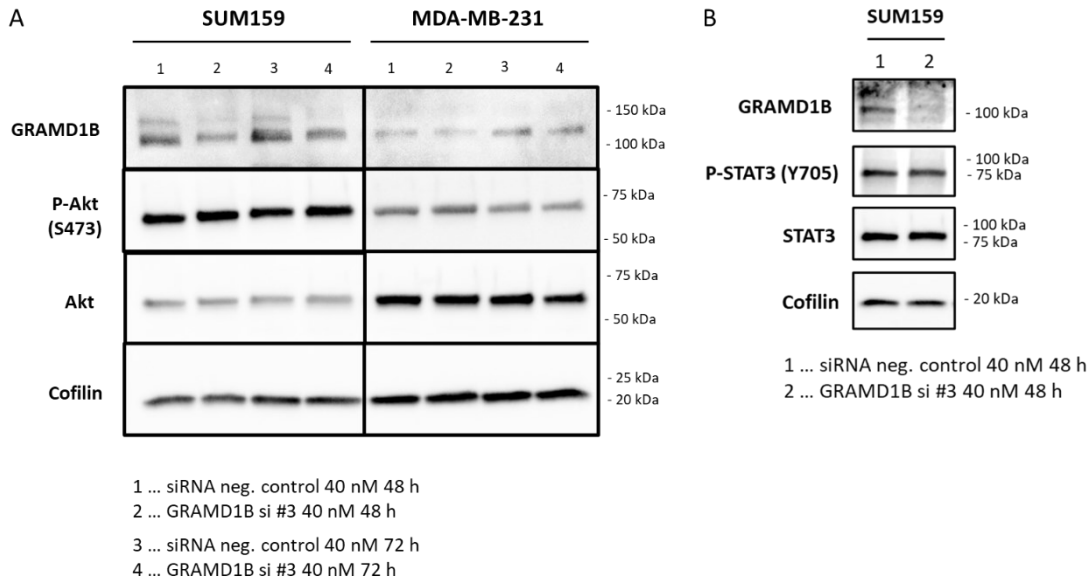

Figure 24: Impact of GRAMD1B on AKT and STAT3 activation. (A) *Western Blot of SUM159 and MDA-MB-231 cells transfected with GRAMD1B siRNA for 48 and 72 h determining the impact on the phosphorylation of AKT at serine 473 (P-AKT S473).* ***(B)*** *Western Blot of SUM159 cells transfected with GRAMD1B siRNA assessing the impact on STAT3 phosphorylation at tyrosine 705 (P-STAT3 Y705).*

3.5.3. Signaling pathways affected by miR-4646-5p

To be able to understand the cellular effects that a miRNA causes it is often not enough to just look at a single target, since miRNAs affect a plethora of direct and indirect targets, influencing entire signaling pathways, and the net phenotype is always a cumulative effect of diverse mechanisms (84,114,115,147). For this reason, we did not only aim to identify a direct target

of miR-4646-5p in this dissertation but to also look at the molecular impact of the miRNA on a broader scale. To fulfill this aim, we performed gene set enrichment analysis (GSEA) on the RNA-seq data. This revealed that the cholesterol biosynthesis pathway was enriched in upregulated genes (Figure 25A), which aligns with the role of the direct target GRAMD1B in cholesterol homeostasis. Moreover, we discovered an enrichment of genes that were downregulated within two cytokine signaling pathways, namely interleukin-10 (IL-10) signaling and tumor necrosis factor (TNF) target genes (Figure 25B and 25C). The downregulated genes in the IL-10 signaling pathway included cytokines like interleukin-1α (*IL1A*), interleukin-1β (*IL1B*), interleukin-6 (*IL6*), granulocyte colony-stimulating factor (*GCSF* or *CSF3*), C-C motif chemokine ligand 20 (*CCL20*), and C-X-C motif chemokine ligand 1 (*CXCL1*), all of which have been reported to have breast tumor-promoting functions (206–217). Downregulated TNF target genes also included *IL6*, *CCL20*, and *CXCL1*, but also other cytokines associated with oncogenic functions like granulocyte-macrophage colony-stimulating factor (*GMCSF* or *CSF2*) and CXC motif chemokine ligand 3 (*CXCL3*) (218–220), and the two transcription factors *FOS* proto-oncogene and early growth response factor 1 (*EGR1*). Fos and EGR1 are part of the mitogen-activated protein kinase (MAPK) pathway, a pathway that is stimulated by various cytokines and growth factors, and both play a role in regulating the proliferation, migration, invasion, and apoptosis of tumor cells (221,222). Fos is, moreover, a component of the activator protein 1 (AP-1) transcription factor complex that controls the expression of numerous cytokines, including IL-2, IL-4, IL-6, IL-8, interferon-gamma (IFNγ), and TNFα (223,224).

In addition to the GSEA analysis of the RNA-seq data, we also conducted a gene ontology (GO) overrepresentation analysis of the significantly downregulated genes. This highlighted that molecular functions like serine and threonine receptor kinase activity, growth factor receptor binding, and cytokine receptor binding were overrepresented amongst the genes downregulated by miR-4646-5p (Figure 25D). This is in accordance with the GSEA results showing a broad downregulation of cytokine signaling pathways and also fits the reduced growth that we observed in our *in vitro* characterization when overexpressing miR-4646-5p.

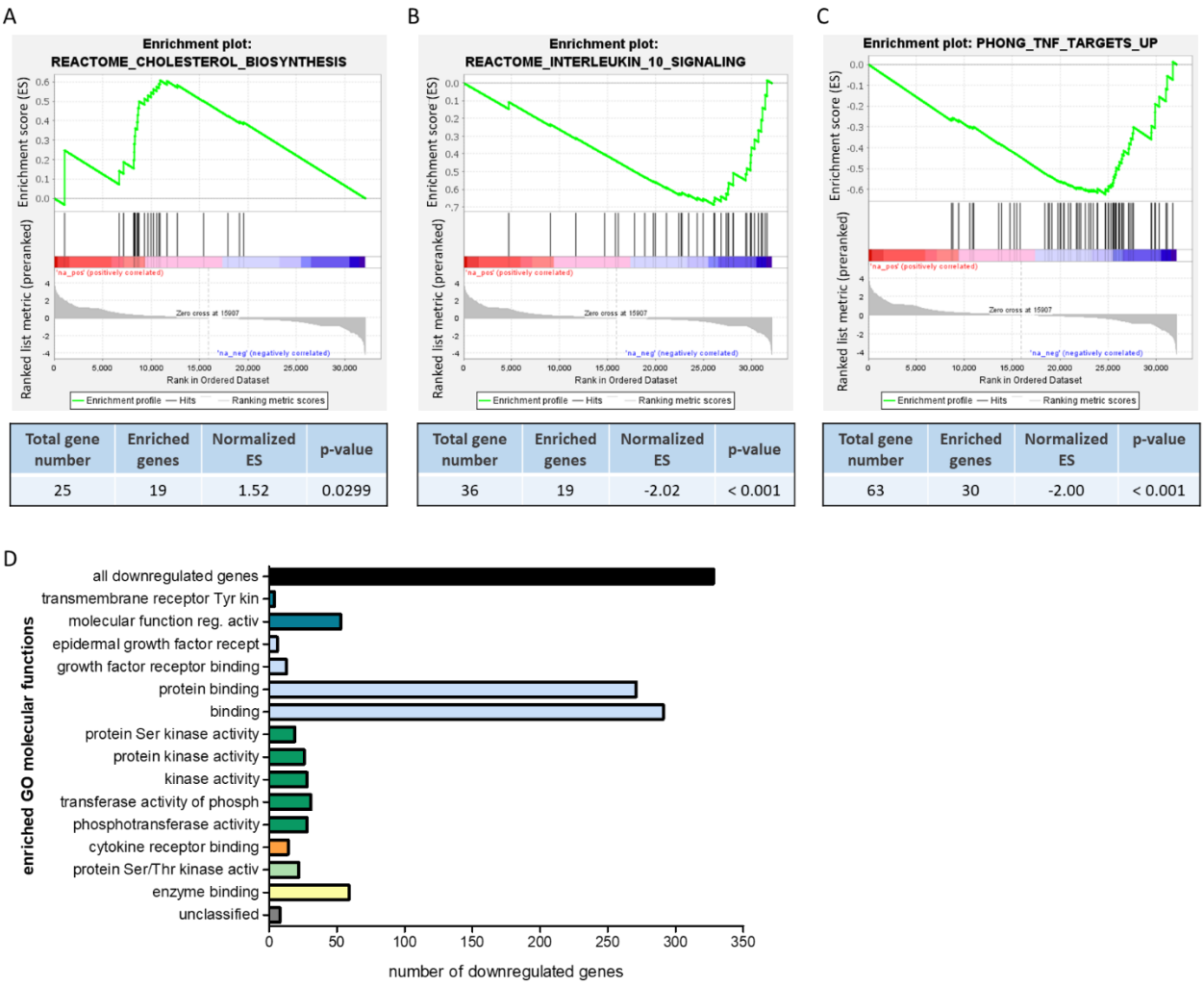

Total gene number	Enriched genes	Normalized ES	p-value
25	19	1.52	0.0299

Total gene number	Enriched genes	Normalized ES	p-value
36	19	-2.02	< 0.001

Total gene number	Enriched genes	Normalized ES	p-value
63	30	-2.00	< 0.001

Figure 25: Gene set enrichment analysis (GSEA) and gene ontology (GO) overrepresentation analysis of miR-4646-5p mimic SUM159 RNA-seq results. *GSEA showing enrichment of* ***(A)*** *upregulated genes in cholesterol biosynthesis (normalized enrichment score = 1.52; p = 0.0299),* ***(B)*** *downregulated genes in interleukin-10 signaling (normalized enrichment score = -2.02; p < 0.001), and* ***(C)*** *downregulated tumor necrosis factor (TNF) targets (normalized enrichment score = -2.00; p < 0.001). Total numbers of genes in each pathway and numbers of enriched genes are indicated (GSEA analysis was performed by Manuela Ferracin, Department of Medical and Surgical Sciences (DIMEC), University of Bologna, Bologna, Italy).* ***(D)*** *PANTHER GO overrepresentation test of genes significantly downregulated by miR-4646-5p. Depicted are the numbers of downregulated genes in all GO molecular functions with significant enrichments (false discovery rate p-value < 0.05, Fisher´s Exact test).*

3.5.4. Effect of miR-4646-5p on cytokine production and secretion

GSEA analysis and GO analysis of the RNA-seq data revealed that miR-4646-5p has broad effects on cytokine signaling in TNBC cells. This also becomes apparent when looking at the list of the top downregulated genes which contains numerous cytokines and chemokines

(Figure 19B). Even though none of the 8 cytokines amongst the top 20 downregulated genes showed any canonical miR-4646-5p binding sites, their apparently indirect downregulation is still of interest. Thus, to confirm the impact on cytokines, we selected the top two downregulated genes, which were G-CSF and IL-6, and validated their downregulation by the miR-4646-5p mimic in both SUM159 and MDA-MB-231 cells on the RNA level by qPCR. While G-CSF was substantially reduced in the SUM159 cell line, we could not detect any expression of the cytokine in the MDA-MB-231 cell line (Figure 26A). IL-6 was expressed in both cell lines and significantly reduced upon miR-4646-5p mimic transfection (Figure 26B).

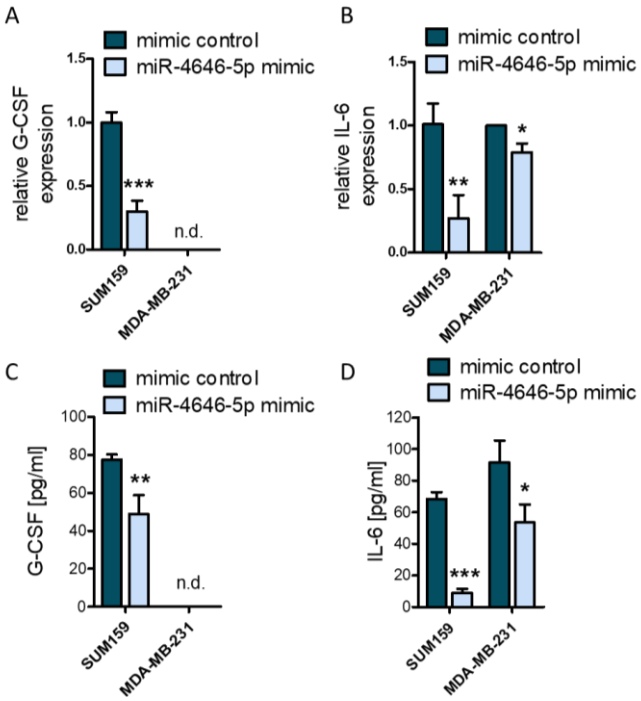

Figure 26: Impact of miR-4646-5p on expression and secretion of the two cytokines granulocyte colony-stimulating factor (G-CSF) and interleukin-6 (IL-6)*. Expression of* ***(A)*** *G-CSF and* ***(B)*** *IL-6 in SUM159 and MDA-MB-231 cells 48 h after miR-4646-5p mimic transfection as determined by qPCR (n = 3; mean ± SD; *p ≤ 0.05, **p ≤ 0.01, ***p ≤ 0.001; n.d. = not detected). ELISAs measuring the secretion of* ***(C)*** *G-CSF and* ***(D)*** *IL-6 from SUM159 and MDA-MB-231 cells after miR-4646-5p mimic or control transfection (n = 4; mean ± SD; *p ≤ 0.05, **p ≤ 0.01, ***p ≤ 0.001; n.d. = not detected).*

More important than the mRNA level though was whether the downregulation would also affect the level of cytokine secretion, thereby potentially impinging on autocrine and paracrine cytokine signaling in the TME. To investigate this, we performed ELISAs of the conditioned cell culture medium and found that the secretion of G-CSF by SUM159 was reduced, whereas MDA-MB-231 did not secrete any G-CSF, which was in line with it not being detectable by qPCR (Figure 26C). IL-6 secretion was significantly reduced in both SUM159 and MDA-MB-231 and also here, the degree of reduction on the level of secretion correlated with the degree

of reduction on the mRNA level, showing a stronger effect in the SUM159 than the MDA-MB-231 (Figure 26D). In summary, our findings showed that miR-4646-5p reduced the expression and secretion of breast cancer-promoting cytokines. The miRNA might thus also have an immunomodulatory effect in the TME.

3.6. *In vitro* characterization of miR-4649-5p

3.6.1. Growth and proliferation

As with the first miRNA candidate, we also went through all steps of the *in vitro* characterization with the second miRNA, miR-4649-5p, starting with investigating its impact on the growth of TNBC cell lines. As stated previously, for miR-4649-5p we only employed a mimic in the phenotypic assays and no inhibitor due to the already very low endogenous levels of the miRNA. WST-1 assays showed that miR-4649-5p upregulation reduced the growth of SUM159, MDA-MB-231, and BT-20 cells (Figure 27A). Moreover, colony formation was impeded in SUM159 and MDA-MB-231 (BT-20 cells did not show colony formation under these conditions) (Figure 27B).

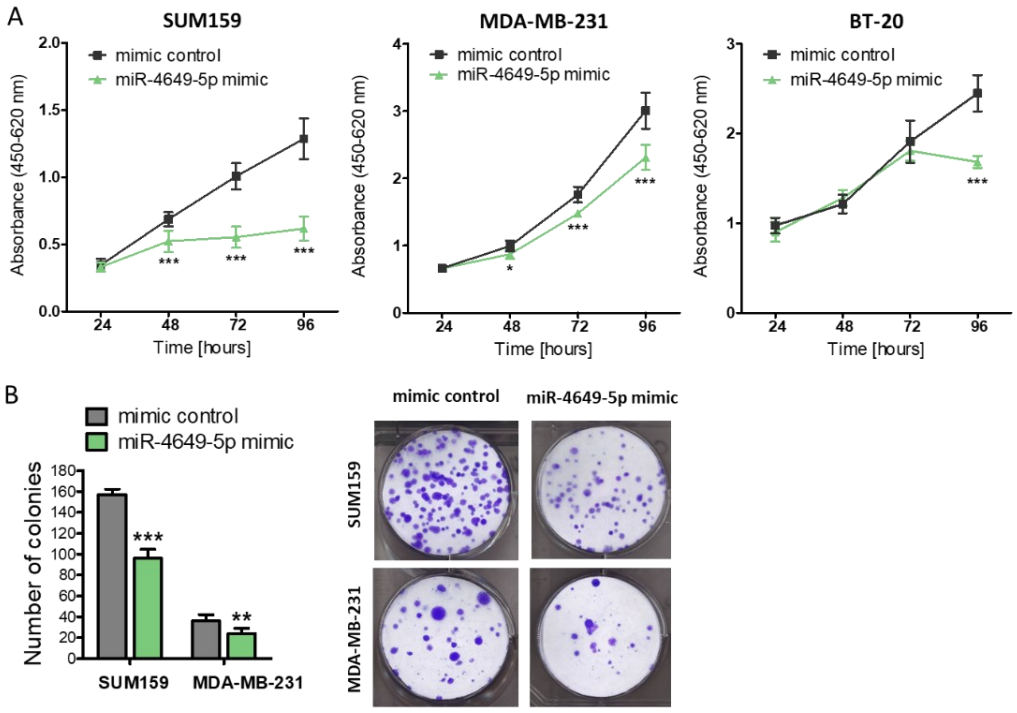

Figure 27: Impact of miR-4649-5p on the growth of TNBC cell lines. (A) *Impact of transient miR-4649-5p mimic transfection on cell growth as determined in WST-1 assays with SUM159, MDA-MB-231, and BT-20 cells (n = 6; mean ± SD; *p ≤ 0.05, ***p ≤ 0.001).* ***(B)*** *Colony formation of SUM159 and MDA-MB-231 cells transiently transfected with miR-4649-5p mimic or control after 7 and 14 days, respectively. Colonies (representative pictures on the right) were counted and are shown in absolute numbers (n = 6; mean ± SD; **p ≤ 0.01; ***p ≤ 0.001).*

Seeing that miR-4649-5p had an impact on cell growth we then continued to assess whether this is connected to an effect on proliferation. EdU assays showed a significant decrease in the percentage of proliferating cells upon miR-4649-5p mimic transfection in all three tested cell lines (Figure 28), which is in accordance with the reduced growth we observed.

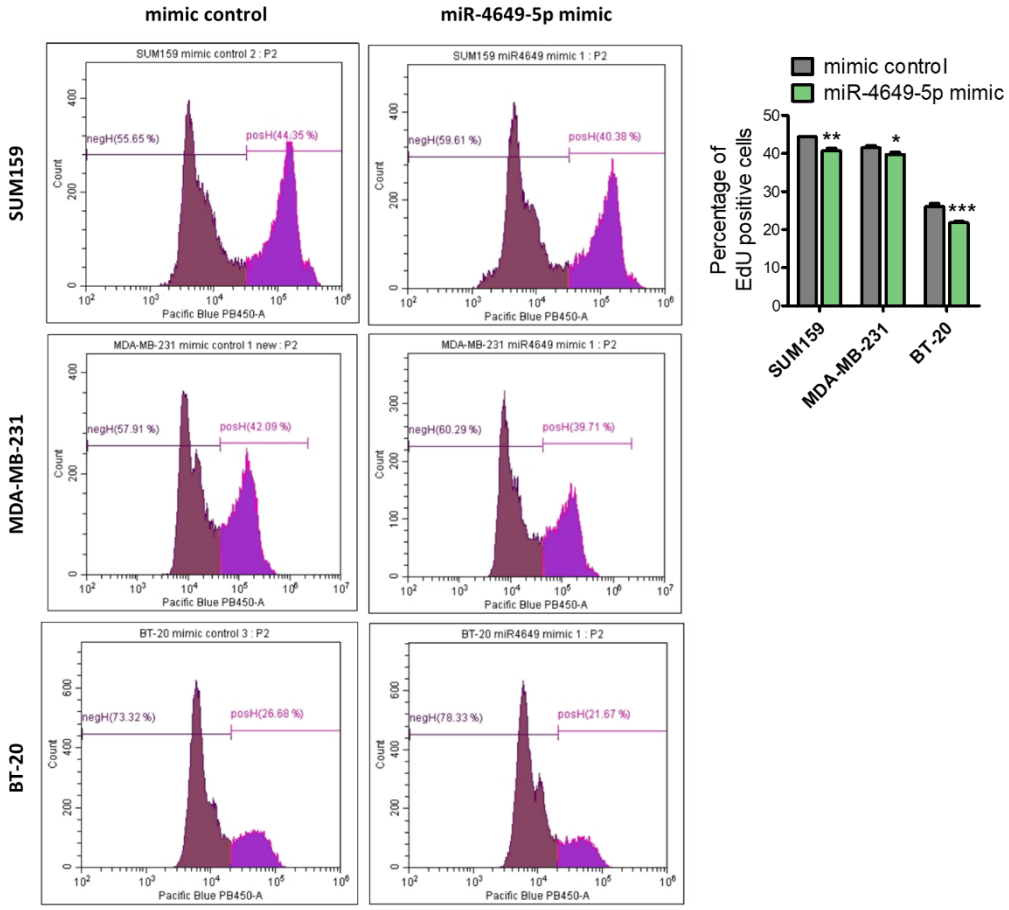

Figure 28: Impact of miR-4649-5p on the proliferation of TNBC cell lines. *Flow cytometric EdU assays were performed 72 h after transient miR-4649-5p mimic transfection of SUM159, MDA-MB-231, and BT-20 cells. Representative histograms are presented on the left, showing the distribution and gating of EdU negative and positive cells, and the quantification on the right (mean ± SD; n = 3, n = 2 for SUM159 mimic control; MDA-MB-231 results of miR-4649-5p mimic and mimic control cells were compared by t-test; SUM159 and BT-20 were tested by one-way ANOVA and Tukey`s multiple comparison test to correct for multiple testing, as the mimic control had also been compared to miR-4646-5p mimic transfected samples in the same experiment; *p ≤ 0.05, **p ≤ 0.01, ***p ≤ 0.001).*

3.6.2. Apoptosis

The next step in the *in vitro* characterization was to check whether miR-4649-5p has an effect on apoptosis, which we measured in a luminescent caspase-3/7 activity assay. While the first miRNA candidate, miR-4646-5p, had shown changes in caspase-3/7 activity 48 h after mimic

transfection in at least two of the three tested cell lines (Figure 13A), the miR-4649-5p mimic did not show any impact (Figure 29). Due to this finding, we did not continue with any other assays investigating apoptosis.

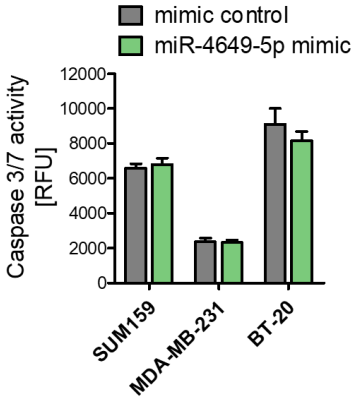

***Figure 29: Impact of miR-4649-5p on the induction of apoptosis in TNBC cell lines**, as determined by a caspase-3/7 activity assay 48 h after miR-4649-5p mimic or control transfection of SUM159, MDA-MB-231, and BT-20 cells (n = 4; miR-4649-5p and control samples were compared by one-way ANOVA and Tukey`s multiple comparison test as the controls were also compared to miR-4646-5p mimic samples in the same experiment; mean ± SD; RFU = relative fluorescence units).*

3.6.3. Migration

As previously described, we performed two different types of assays to study the impact of the miRNA candidates on migration *in vitro*. Scratch assays with SUM159 cells showed that transient overexpression of miR-4649-5p slowed down the closure of the scratch, indicating reduced cell migration (Figure 30A). We also employed the stable miR-4649-5p mimic cell line which could reproduce the delay in the closure of the scratch (Figure 30B). Moreover, transwell migration assays with SUM159 and MDA-MB-231 cells confirmed the migration-reducing effect of transient miR-4649-5p mimic transfection in an independent experimental approach (Figure 30C).

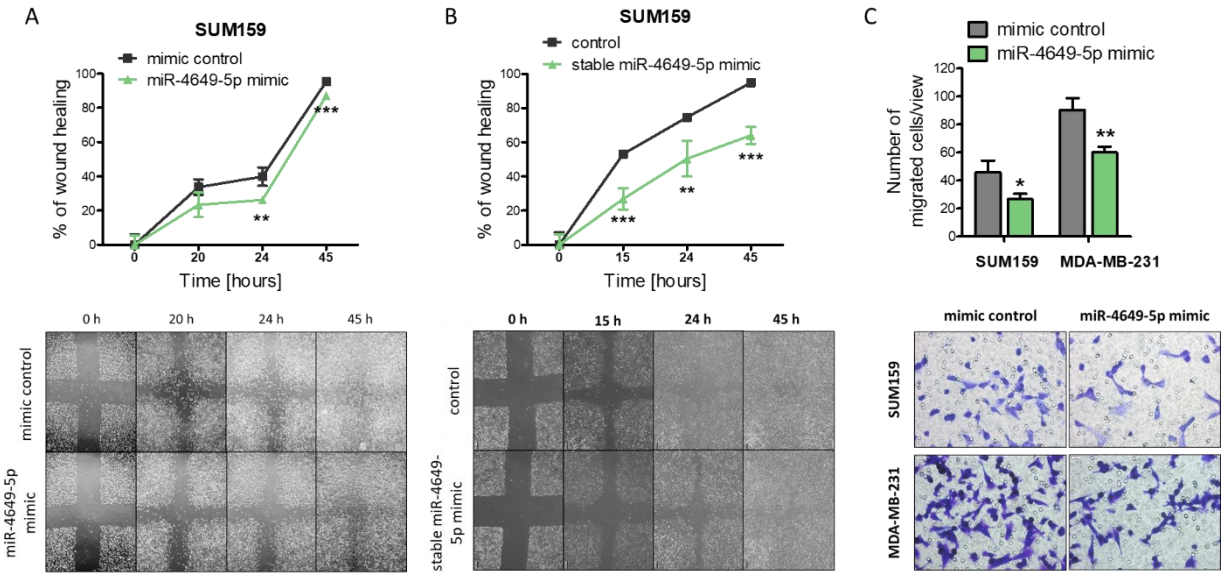

Figure 30: Impact of miR-4649-5p on the migration of TNBC cells. *The impact of* ***(A)*** *transient miR-4649-5p mimic, and* ***(B)*** *stable miR-4649-5p mimic overexpression on the migration of SUM159 cells was assessed in scratch assays. For each time point, the percentage of scratch closure relative to the first time point (0 h) was calculated (representative pictures at the bottom) (mean ± SD; n = 4; **p ≤ 0.01, ***p ≤ 0.001).* ***(C)*** *The effect of transient miR-4649-5p overexpression on the migration of SUM159 and MDA-MB-231 cells was assessed in transwell migration assays. Five representative fields of view were counted per transwell (representative pictures at 40x magnification are shown at the bottom) and are presented in absolute numbers (n = 3; mean ± SD; *p ≤ 0.05, **p ≤ 0.01).*

3.6.4. Stemness

To assess whether miR-4649-5p has an impact on stem cell properties of TNBC cells, we measured ALDH1 activity in SUM159 cells but did not observe any change upon miR-4649-5p mimic transfection (Figure 31). Based on this, it appears miR-4649-5p does not play a significant role in breast cancer stemness. However, we only performed the assay on the SUM159 cell line and not on any additional cell lines, which would have been essential to rule out cell line-specific differences. Moreover, investigating additional stem cell markers would have allowed a more unmitigated verdict.

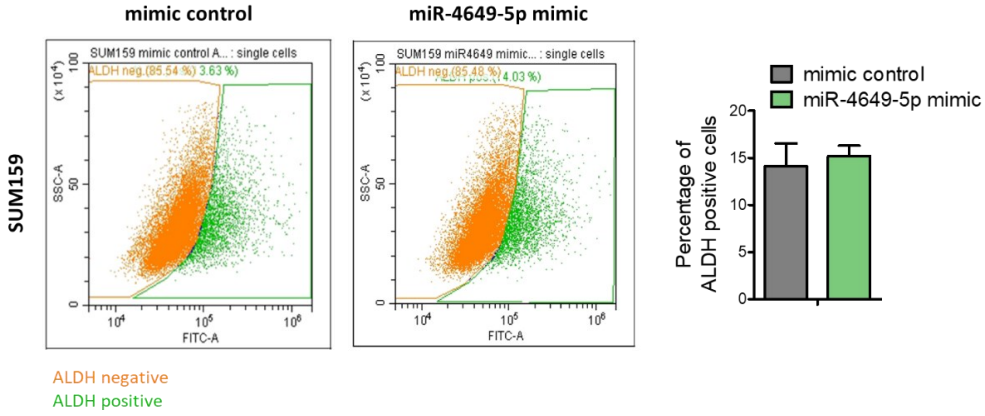

Figure 31: Impact of miR-4649-5p on aldehyde dehydrogenase (ALDH) activity in TNBC cells. *ALDH-positive cells were measured in a flow cytometric assay 48 h after miR-4649-5p mimic or control transfection of SUM159 cells. Representative scatter plots on the left illustrate the gating for ALDH negative and positive cells set according to ALDH-inhibitor-treated negative controls for each sample (n = 4; mean ± SD).*

3.6.5. Angiogenesis

For the first miRNA candidate, we had discovered that its overexpression is able to reduce the *in vitro* tube formation ability of endothelial cells substantially, indicating angiogenesis-inhibiting properties (Figure 18B). The same approach with miR-4649-5p showed that this miRNA does not affect tube formation of HUVECs, neither microscopically nor regarding the number of nodes, junctions, meshes, and total branch length (Figure 32).

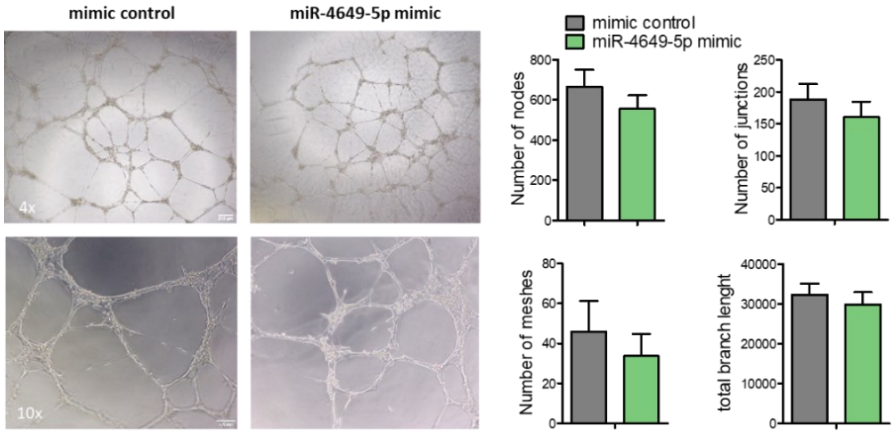

Figure 32: Impact of miR-4649-5p on the in vitro tube formation of endothelial cells. *Human umbilical vein endothelial cells (HUVECs) were transfected with the miR-4649-5p mimic or control. Representative pictures on the left (4x and 10x magnification), and quantifications of the number of nodes, junctions, meshes, and the total branch length (n = 3; mean ± SD; compared by one-way ANOVA and Tukey`s multiple comparison test, as the control was compared to miR-4646-5p mimic samples in the same experiment) (The assay was performed by Christiane Klec, Priv.-Doz. PhD, Department of Internal Medicine, Division of Oncology, Medical University of Graz, Austria).*

3.7. Identification of miR-4649-5p targets and affected pathways

3.7.1. Transcriptome analysis and identification of potential targets

The *in vitro* characterization of miR-4649-5p in TNBC cell lines showed that ectopic overexpression of the otherwise endogenously very low miRNA has tumor-suppressive effects in regard to growth, proliferation, and migration, while no distinct effects could be seen on apoptosis and ALDH activity of TNBC cells, as well as the tube formation ability of endothelial cells. To uncover the molecular background of these effects we conducted an RNA-seq analysis of SUM159 cells transiently transfected with the miR-4649-5p mimic and compared their transcriptome to mimic control transfected cells. This revealed 433 genes that were significantly differentially expressed in the miR-4649-5p mimic cells, 238 of which were upregulated and 195 were downregulated (Figure 33A).

A

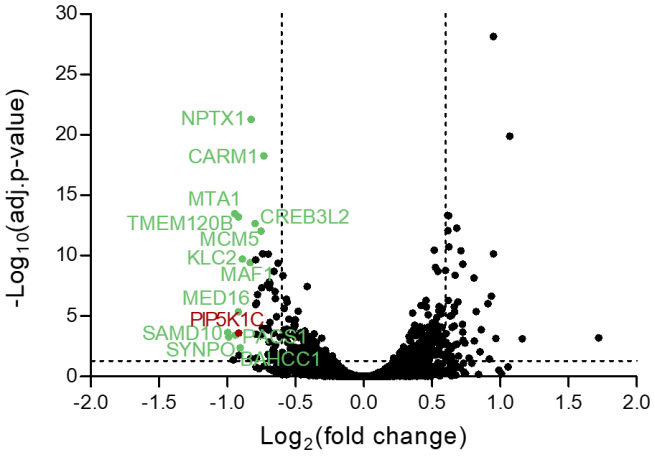

B

Gene Name	Fold-change	adj. p-value
SAMD10	- 0,996	0,00022
SYNPO	- 0,991	0,00053
MTA1	- 0,946	3,31E-14
PACS1	- 0,941	0,00036
MED16	- 0,920	4,31E-06
TMEM120B	- 0,918	5,99E-14
PIP5K1C	- 0,916	0,00024
BAHCC1	- 0,906	0,00398
KLC2	- 0,891	1,86E-10
MAF1	- 0,832	3,68E-10
ADAM19	- 0,830	0,03113
NPTX1	- 0,825	5,16E-22
CREB3L2	- 0,797	2,13E-13
PLAGL2	- 0,793	1,10E-06
R3HDM4	- 0,792	2,12E-10
MLLT1	- 0,787	0,00032
RIN3	- 0,787	0,02972
ATG4D	- 0,785	7,97E-07
PPARD	- 0,779	1,62E-07
ANKRD13B	- 0,757	0,00040

Figure 33: RNA-seq results of SUM159 cells transfected with the miR-4649-5p mimic. (A) *Volcano plot illustrating the miR-4649-5p mimic vs. mimic control RNA-seq results. Dashed lines indicate the adjusted p-value cut-off (0.05) that was used to determine significantly deregulated genes, and the 1.5-fold-change thresholds. Top-downregulated genes are highlighted in color and labeled.* ***(B)*** *List of the top 20 annotated significantly downregulated genes, sorted according to fold-change in expression. Genes with previously reported oncogenic functions are highlighted in green.*

As previously discussed, we then focused on the downregulated genes in order to look for potential direct targets of the miRNA and sorted them according to their fold-change in expression. The top 20 annotated downregulated genes (Figure 33B) were then screened for potential miR-4649-5p binding sites using the *in silico* tools TargetScan (174), miRWalk2.0 (175), and miRDB (176). Out of the 20 candidates, 16 were found to have at least one potential

binding site according to at least one of the prediction algorithms (the steps taken to identify potential direct targets are illustrated in Figure 34A). For further confirmations, we selected the top 4 candidates that had predicted binding sites according to more than just one of the algorithms and that had previously been connected to cancer and might thus provide an explanation for the tumor-suppressive properties of miR-4649-5p. These 4 candidates were phosphofurin acidic cluster sorting protein 1 (*PACS1*), transmembrane protein 120B (*TMEM120B*), phosphatidylinositol-4-phosphate 5-kinase type 1 gamma (*PIP5K1C*), and PLAG1 like zinc finger 2 (*PLAGL2).* We sought to confirm the RNA-seq results from the SUM159 cell line in all three TNBC cell lines by qPCR but discovered that PIP5K1C was the only candidate that was significantly downregulated by the miR-4649-5p mimic in all three cell lines (Figure 34B). PIP5K1C also appeared to be a promising candidate as it had two potential binding sites for miR-4649-5p (Table 6), as opposed to just one site in the other candidates.

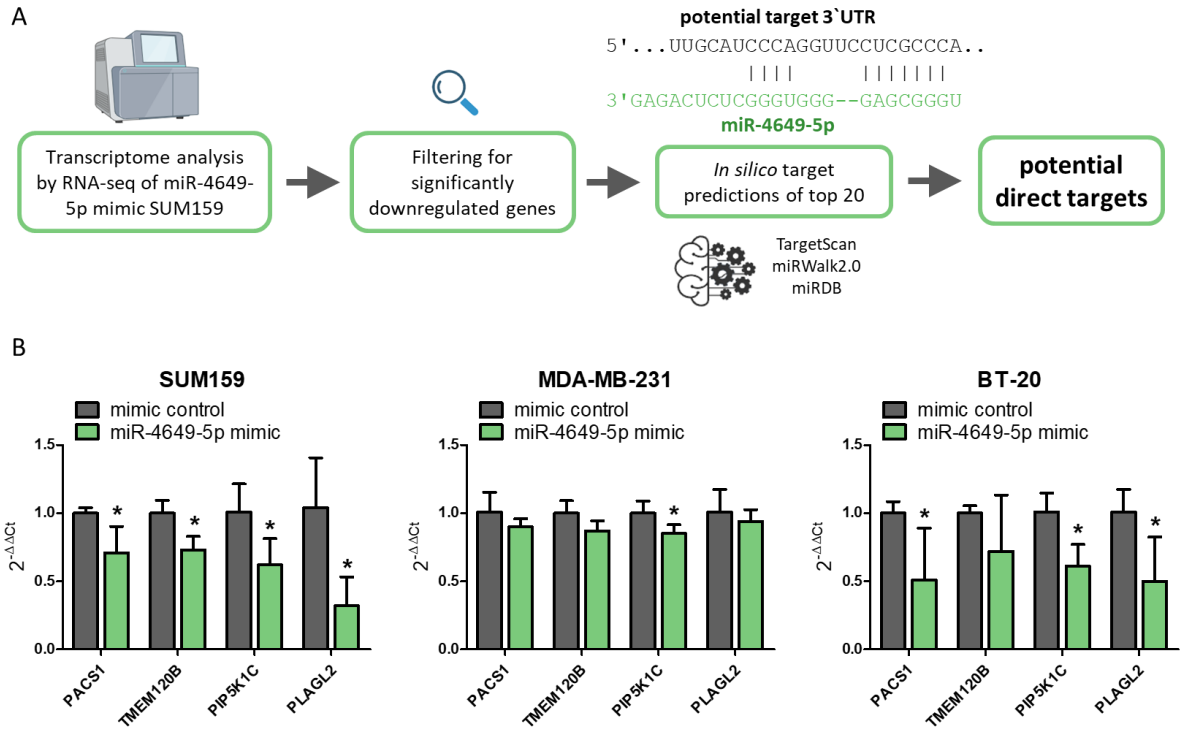

Figure 34: Identification of potential miR-4649-5p target genes. (A) *Scheme illustrating the process of identifying potential direct targets of miR-4649-5p from RNA-seq data.* ***(B)*** *Expression of four selected potential targets of miR-4649-5p measured by qPCR 48 h after transfection of SUM159, MDA-MB-231, and BT-20 cells with the miR-4649-5p mimic or control (n = 3; mean ± SD; *p ≤ 0.05). PACS1…phosphofurin acidic cluster sorting protein 1, TMEM120B…transmembrane protein 120B, PIP5K1C…phosphatidylinositol-4-phosphate 5-kinase type 1 gamma, and PLAGL2…PLAG1 like zinc finger 2.*

Table 6: Potential binding sites between miR-4649-5p and the 3`untranslated region (UTR) of the phosphatidylinositol-4-phosphate 5-kinase type 1 gamma (PIP5K1C) gene as predicted by TargetScan *(7mer-m8…exact match of target to positions 2-8 of the mature miRNA; 8mer…exact match of target to positions 2-8 of the mature miRNA followed by an 'A').*

Site number	Target position	Predicted consequential pairing of target region (top) and miR-4649-5p (bottom)	Site type	Context score percentile
1	Position 586-592 of *PIP5K1C* 3' UTR	5' ...ACUGUGGGGACAGCCCUCGCCCU... 3' GAGACUCUCGGGUGGGGAGCGGGU	7mer-m8	60
2	Position 2918-2925 of *PIP5K1C* 3' UTR	5' ...UUGCAUCCCAGGUUCCUCGCCCA... 3' GAGACUCUCGGGUGGG--GAGCGGGU	8mer	92

3.7.2. Confirmation of PIP5K1C as a direct target of miR-4649-5p

Based on RNA-seq data which we confirmed by qPCR together with *in silico* target prediction results, PIP5K1C appeared to be a likely direct target of miR-4649-5p. Therefore, we next aimed to confirm that miR-4649-5p upregulation results in the downregulation of PIP5K1C not only on the RNA level but also on the protein level. Western blotting showed that PIP5K1C signals were generally reduced upon miR-4649-5p mimic transfection (Figure 35A). The final confirmation of a direct interaction between miR-4649-5p and PIP5K1C came from a dual luciferase reporter assay. Of the two predicted binding sites, we selected the one with the higher prediction score according to the TargetScan algorithm (site number 2 in Table 6), which was a 7 nt long sequence complementary to the seed region of miR-4649-5p together with a 4 nt long supplementary site complementary to the 3' region of the miRNA. This region of the PIP5K1C 3`UTR, with an additional 20 and 24 nt upstream and downstream, respectively, was cloned into the luciferase reporter vector. Co-transfection of this wt reporter with the miR-4649-5p mimic significantly reduced the luciferase signal which was not the case with a vector where the sequence had been mutated by exchanging 4 nt in the seed binding region and 2 nt in the supplementary binding region (Figure 35B). These results indicate that the miRNA is able to directly bind to this region in the 3`UTR of PIP5K1C in a sequence-specific manner which results in the RISC-mediated downregulation of the target.

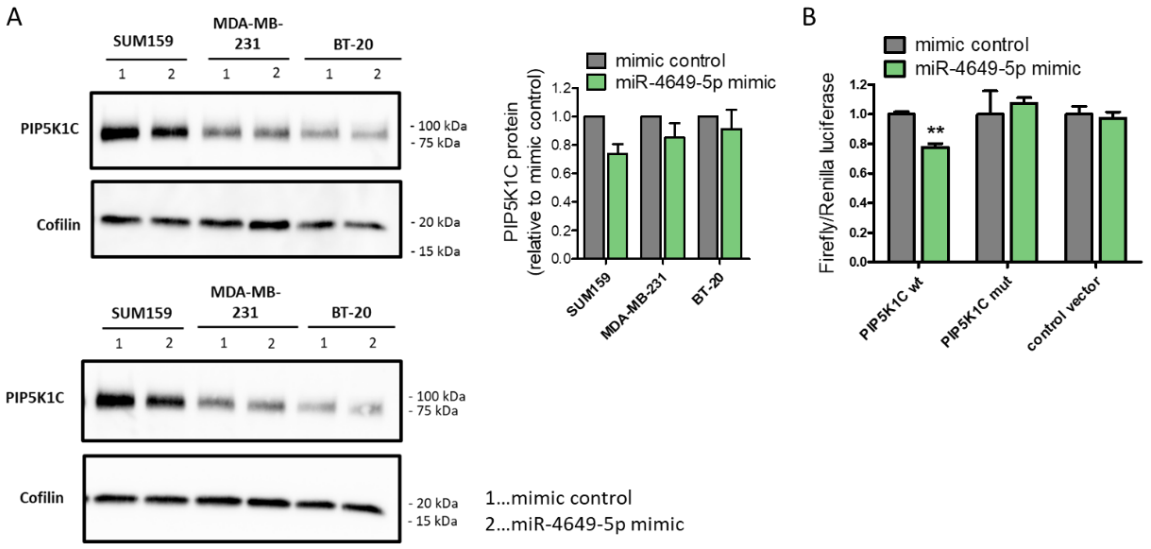

Figure 35: Impact of miR-4649-5p on the protein levels of its target phosphatidylinositol-4-phosphate 5-kinase type 1 gamma (PIP5K1C) and confirmation of direct interaction between miR-4649-5p and PIP5K1C by luciferase reporter assays. (A) *Western blots showing the effect of 48 h of miR-4649-5p mimic transfection in SUM159, MDA-MB-231, and BT-20 cells on the protein level of PIP5K1C. PIP5K1C signal intensities were normalized to the housekeeper Cofilin and are presented relative to the mimic controls as fold-change (on the right) (n = 2; mean ± SD for miR-4649-5p samples, mimic controls were set to 1).* ***(B)*** *Dual luciferase reporter assay in HEK293 cells using a reporter with a wildtype (wt) or mutated (mut) miR-4649-5p binding sequence from the PIP5K1C 3' UTR. The reporter vectors were co-transfected with the miR-4649-5p mimic or mimic control (n = 3; mean ± SD; **p ≤ 0.01).*

The *PIP5K1C* gene codes for a type I phosphatidylinositol 4-phosphate 5-kinase that catalyzes the formation of phosphatidylinositol 4,5-bisphosphate (PI4,5P_2 or PIP_2), a versatile lipid second messenger that plays a crucial role in actin dynamics, focal adhesion, cell motility, and migration (225–228). Moreover, PIP_2 is the precursor of other downstream lipid messengers that are affecting pathways involved in cell growth and survival (227,229). PIP5K1C has previously been described to promote migration, invasion, growth, and metastasis of different cancer types, including TNBC (230–232). According to this, targeting and downregulating PIP5K1C could also account for some of the tumor-suppressive effects of miR-4649-5p. To investigate this possibility, we examined the role of PIP5K1C in TNBC further. The knockdown of PIP5K1C by a commercial siRNA (Figure 36A and 36B) decreased the growth of SUM159 and MDA-MB-231 cells, as well as their colony formation (Figure 36C and 36D). This is in line with the effects of miR-4649-5p overexpression and suggests a contribution of PIP5K1C to the phenotype caused by miR-4649-5p.

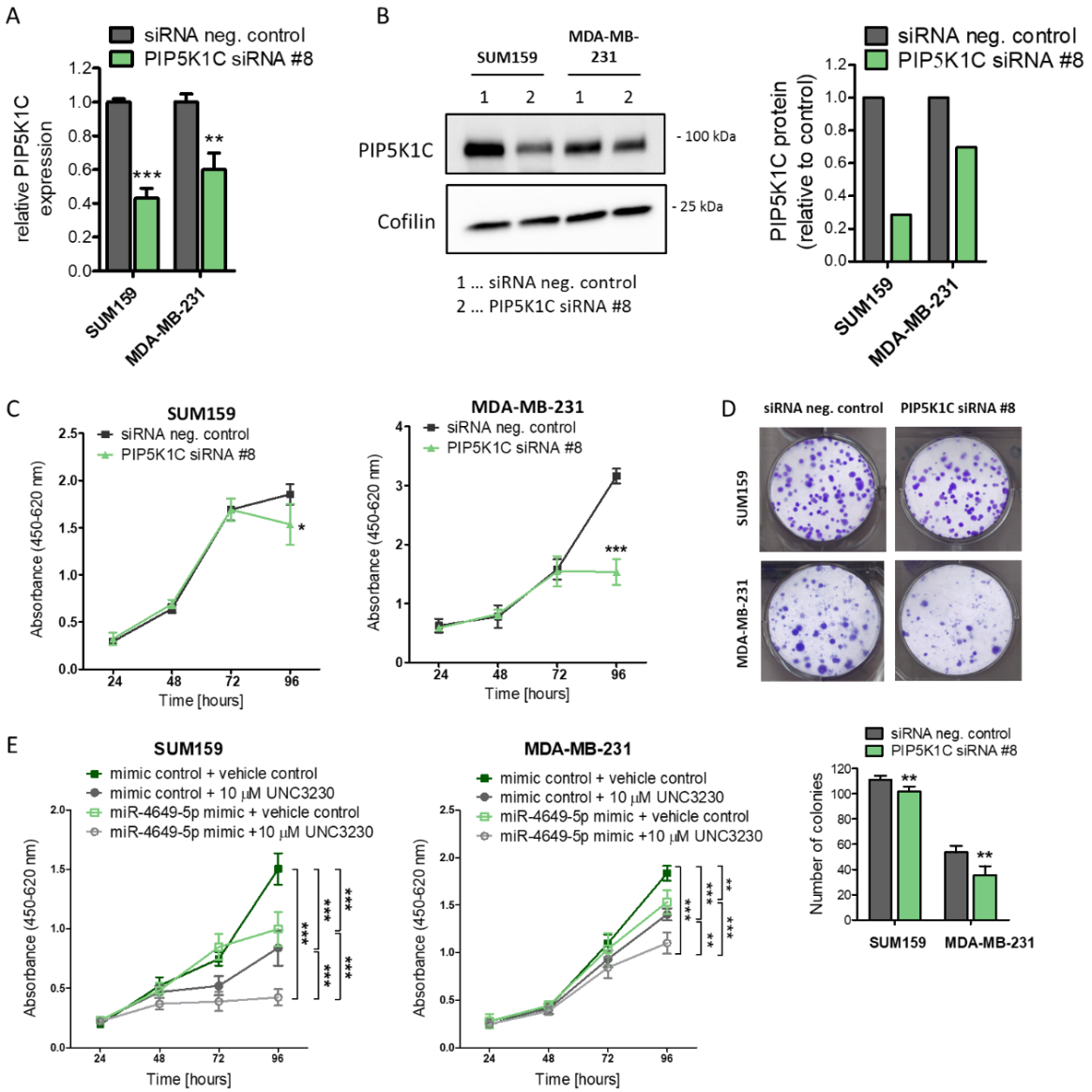

Figure 36: Impact of PIP5K1C knockdown or pharmacologic inhibition on the growth of TNBC cells. (A) *Knockdown efficiency of PIP5K1C 48 h after siRNA transfection of SUM159 and MDA-MB-231 cells measured by qPCR (n = 3; mean ± SD; **p ≤ 0.01, ***p ≤ 0.001).* ***(B)*** *Knockdown efficiency of PIP5K1C protein 48 h after siRNA transfection of SUM159 and MDA-MB-231 cells assessed by Western blotting. Representative blot on the left, quantification of PIP5K1C signals normalized to the housekeeper Cofilin on the right (n = 1).* ***(C)*** *Effect of PIP5K1C knockdown on cell growth as determined in WST-1 assays in SUM159 and MDA-MB-231 cells (n = 6; mean ± SD; *p ≤ 0.05, ***p ≤ 0.001).* ***(D)*** *Impact of PIP5K1C knockdown on colony formation of SUM159 and MDA-MB-231 cells. Colonies were counted after 7 and 14 days, respectively (representative pictures on top), and are presented in absolute numbers (n = 6; mean ± SD; **p ≤ 0.01).* ***(E)*** *Impact of miR-4649-5p mimic or mimic control combined with 10 µM of the PIP5K1C inhibitor UNC3230 or DMSO vehicle control on cell growth was determined in WST-1 assays with SUM159 and MDA-MB-231 cells (n = 6; means ± SD; **p ≤ 0.01, ***p ≤ 0.005, compared by one-way ANOVA and Tukey`s multiple comparison test).*

In addition to siRNA-mediated knockdown of PIP5K1C, we also made use of a selective pharmacologic PIP5K1C inhibitor called UNC3230 (233). MiRNAs do not function by switching the expression of a target off entirely but generally adjust gene expression in a nuanced manner. We therefore had the hypothesis that a combination of miR-4649-5p upregulation, which entails PIP5K1C downregulation, with additional pharmacologic inhibition of the remaining pool of PIP5K1C protein could have additive tumor-suppressive effects. In WST-1 assays, both the miR-4649-5p mimic and the treatment with UNC3230 separately had similar growth-reducing effects (Figure 36E). The combination of miR-4649-5p and UNC3230 significantly enhanced the growth reduction further (Figure 36E).

We wanted to assess the apparently oncogenic role of PIP5K1C in TNBC that we had observed *in vitro* in regard to cell growth, and that had been reported previously by other studies (231,232), further and examined the prognostic relevance of PIP5K1C. Kaplan-Meier survival analysis showed that higher protein levels of PIP5K1C are associated with significantly worse overall survival of breast cancer patients including all subtypes (the patient cohort was too small to restrict it to only TNBC or basal-like) (n = 65; log-rank test; p = 0.0097; hazard ratio = 3.72; 95% confidence interval 1.28 – 10.8; Figure 37A). Higher PIP5K1C expression levels, based on microarray data, showed a non-significant trend towards worse overall survival of a TNBC patient cohort (n = 154; log-rank test; p = 0.1; hazard ratio = 1.98; 95% confidence interval 0.86 – 4.54; Figure 37B), and a significant association with worse relapse-free survival of a larger TNBC cohort (n = 392; log-rank test; p = 0.0091; hazard ratio = 1.64; 95% confidence interval 1.13 – 2.38; Figure 37C). In addition, RNA-seq-based expression data from TNMplot (171) revealed significantly higher expression levels of PIP5K1C in invasive breast tumors compared to adjacent healthy breast tissue (n = 112 per group; p = 0.0258; Mann-Whitney-U test; Figure 37D). Together, this data outlines an oncogenic role of PIP5K1C in breast cancer.

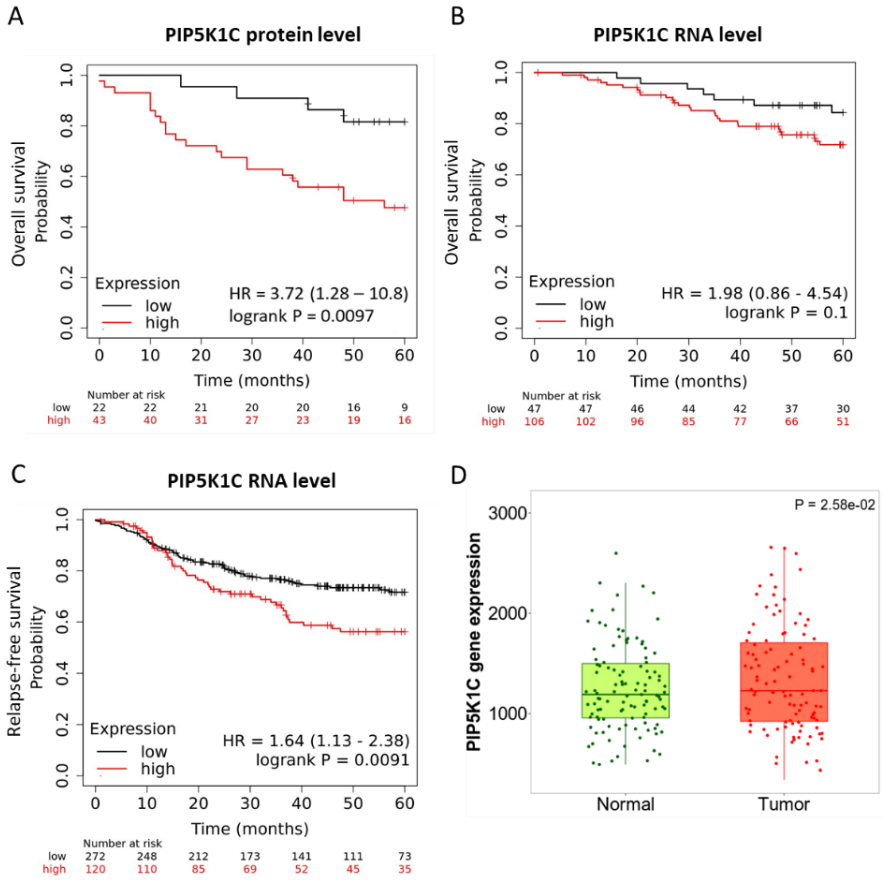

Figure 37: Prognostic relevance and expression of PIP5K1C in breast cancer. (A) *Overall survival of breast cancer patients in a group with high (n = 43, red) vs. low (n = 22, black) PIP5K1C protein levels based on proteomics data (log-rank test; p = 0.0097; hazard ratio (HR) = 3.72; 95% confidence interval 1.28 – 10.8).* ***(B)*** *Overall survival of TNBC patients in a PIP5K1C high (red; n = 106) vs. low (black; n = 47) expression group based on microarray data (log-rank test; p = 0.1; hazard ratio (HR) = 1.98; 95% confidence interval 0.86 – 4.54).* ***(C)*** *Relapse-free survival of TNBC patients in a PIP5K1C high (red; n = 120) vs. low (black; n = 272) expression group based on microarray data (log-rank test; p = 0.0091; hazard ratio (HR) = 1.64; 95% confidence interval 1.13 – 2.38).* ***(D)*** *RNA-seq-based expression of PIP5K1C in breast tumor tissue compared to healthy adjacent tissue (n = 112 per group; p = 0.0258; Mann-Whitney-U test).*

3.7.3. Signaling pathways affected by miR-4649-5p

To obtain a better overview of the molecular changes that occur when the otherwise low expression of miR-4649-5p is upregulated, we performed GSEA of the RNA-seq data and found that miR-4649-5p mimic transfection caused an enrichment of upregulated genes associated with oxidative phosphorylation and tight junctions (Figure 38A and 38B). While GSEA analysis did not provide significant pathway enrichments of downregulated genes, GO enrichment analysis revealed that the downregulated genes were enriched in ontologies like,

amongst others, epithelium and gland morphogenesis, metabolic processes, and transcription (Figure 38C).

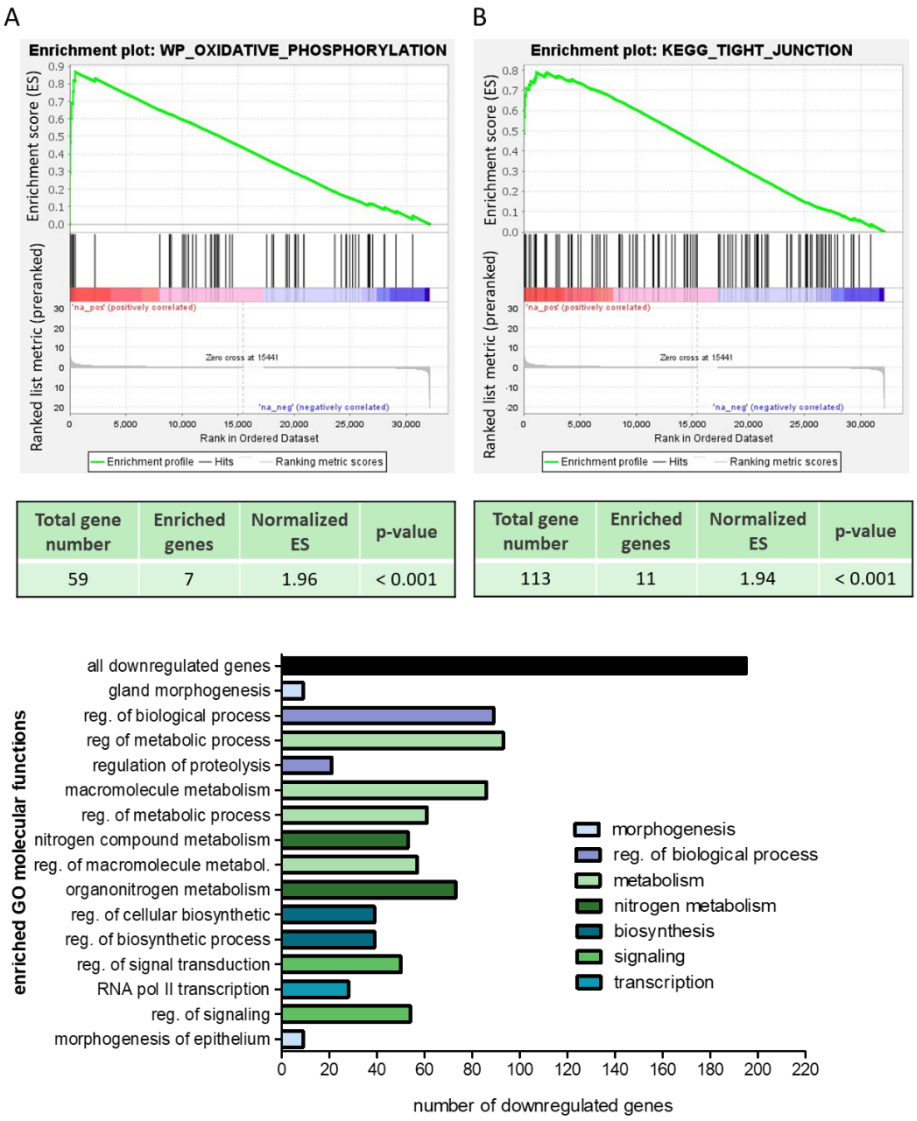

Figure 38: Gene set enrichment analysis (GSEA) and gene ontology (GO) overrepresentation analysis of miR-4649-5p mimic SUM159 RNA-seq results. *GSEA showing enrichment of upregulated genes in* ***(A)*** *oxidative phosphorylation (normalized enrichment score = 1.96; p < 0.001), and* ***(B)*** *tight junctions (normalized enrichment score = 1.94; p < 0.001). The total number of genes in each pathway and the number of enriched genes are indicated (GSEA analysis was performed by Manuela Ferracin, Department of Medical and Surgical Sciences (DIMEC), University of Bologna, Bologna, Italy).* ***(C)*** *PANTHER GO overrepresentation test of genes significantly downregulated by miR-4649-5p. Depicted are the numbers of downregulated genes in the top 15 GO molecular functions that showed significant enrichments of downregulated genes. The GO functions were sorted according to p-value, with the lowest p-value on top (all false discovery rate p-values < 0.05, Fisher´s Exact test).*

3.7.4. Influence of miR-4649-5p on AKT signaling

The miR-4649-5p target PIP5K1C plays a central role in cells by its production of PIP_2 which lies upstream of various signaling pathways (225–229). Pharmacologic inhibition of PIP5K1C and upregulation of miR-4649-5p showed additive anti-tumor effects *in vitro*, which could be promising regarding therapeutic approaches in TNBC. However, there is currently no clinically approved inhibitor of PIP5K1C available for the use in breast cancer. For this reason, we focused on pathways downstream of PIP5K1C to find an actionable target whose benefit could be boosted by combining it with the miR-4649-5p mimic. An interesting candidate for this intent was AKT, which is well known to promote cell survival, growth, and proliferation (229,234,235). To be activated, as described in the introduction, AKT is recruited to the cell membrane by interacting with phosphatidylinositol 3,4,5-trisphosphate ($PI3,4,5P_3$ or PIP_3), which is generated by PI3K by phosphorylation of PIP_2 (234). Therefore, the PI3K/AKT pathway, a frequently overactivated pathway in TNBC as discussed previously (55,235), lies downstream of PIP5K1C. This was confirmed by a Western Blot where the inhibition of PIP5K1C by UNC3230 caused a dose-dependent reduction in the phosphorylation of AKT (Figure 39A). This reduction in phosphorylation was further enhanced when combining UNC3230 with the miR-4649-5p mimic (Figure 39B), which is consistent with our finding of additive growth reductions (Figure 36E). Importantly, AKT can serve as a therapeutic target. Recent clinical trials of AKT inhibitors, like capivasertib, have shown promising results in patients with TNBC (81–83). We hypothesized that if upstream inhibition of PIP5K1C has additive effects together with miR-4649-5p upregulation, inhibition of AKT further downstream in the same pathway could exert similar effects. We could indeed show this in SUM59 cells using the pan-AKT inhibitor capivasertib, whose growth-reducing effect in WST-1 assays could be increased significantly by combination with the miR-4649-5p mimic (Figure 39C).

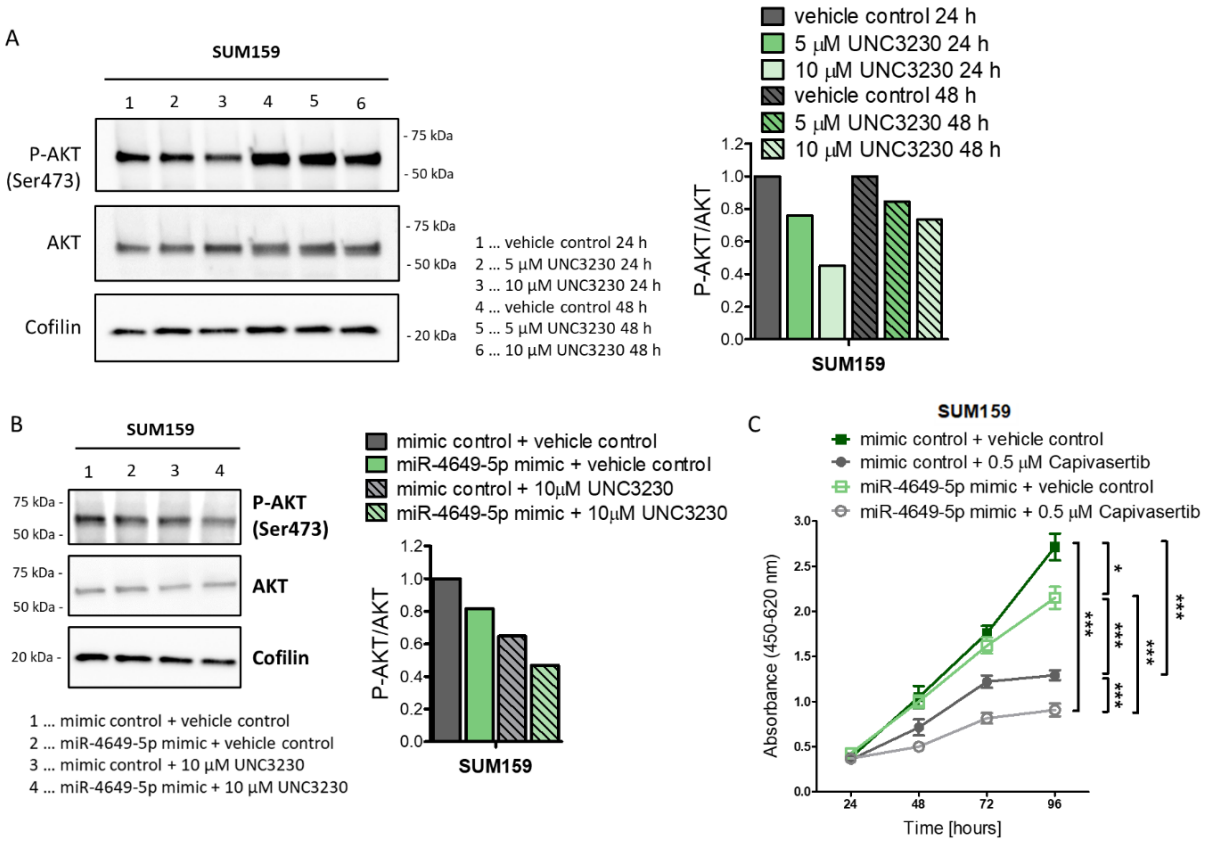

Figure 39: Impact of PIP5K1C and miR-4649-5p on AKT activation and additive effects of miR-4649-5p and AKT inhibition. (A) *Representative Western blot of SUM159 cells treated with two concentrations of the PIP5K1C inhibitor UNC3230 or vehicle control (DMSO) for 24 or 48 h (on the left), and the quantification of Pospho-AKT (Ser473) signals normalized to the housekeeper Cofilin and total AKT signals (on the right; n = 1).* ***(B)*** *Representative Western Blot of SUM159 cells treated with miR-4649-5p mimic or mimic control combined with 10 µM UNC3230 or vehicle control for 24 h (on the left), and the quantification of Pospho-AKT (Ser473) signals normalized to the housekeeper Cofilin and total AKT signals (on the right; n = 1).* ***(C)*** *The impact of transient miR-4649-5p mimic transfection in combination with 0.5 µM of the AKT inhibitor capivasertib or vehicle control (DMSO) on the growth of SUM159 was assessed in a WST-1 assay (n = 6; means ± SD; *p ≤ 0.05, ***p ≤ 0.001, compared by one-way ANOVA and Tukey´s multiple comparison test).*

In summary, the results emphasized the impact of miR-4649-5p on the PIP5K1C/PI3K/AKT signaling pathway (Figure 40), a clinically actionable pathway frequently overactivated in TNBC, which suggests a potential therapeutic utility of miR-4649-5p upregulation by potentiating the response to, for example, AKT inhibitors like capivasertib. With this finding, we were able to fulfill the third objective, namely to determine potential therapeutic utility, for the second miRNA at least *in vitro*.

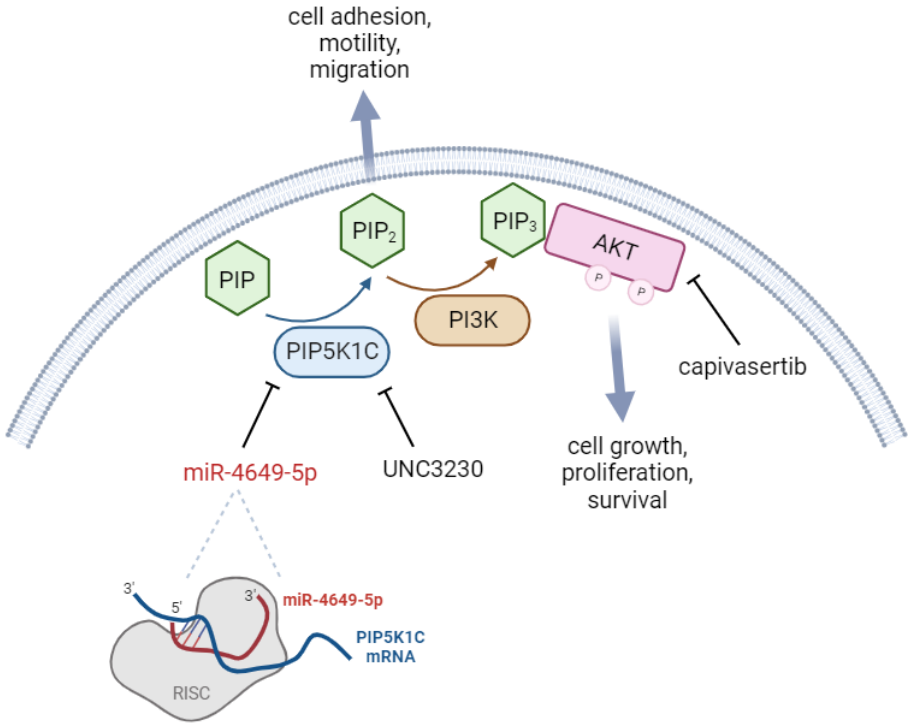

Figure 40: Scheme summarizing the involvement of miR-4649-5p in the PIP5K1C/PI3K/AKT signaling pathway. *MiR-4649-5p targets the PIP5K1C mRNA and thereby induces downregulation of PIP5K1C via the RNA-induced silencing complex (RISC). This affects the downstream production of the lipid second messengers PIP_2 and PIP_3 by PIP5K1C and PI3K, respectively. PIP_3 recruits AKT to the cell membrane where it becomes activated by phosphorylation. Once activated, AKT promotes cell growth, proliferation, and survival by phosphorylating downstream targets. Combinations of ectopic miR-4649-5p overexpression and the pharmacologic PIP5K1C inhibitor UNC3230 or the AKT inhibitor capivasertib thus have additive growth-reducing effects (Figure created with BioRender).*

3.8. *In vivo* experiments

3.8.1. Orthotopic mammary fat pad injection of stable miR-4646-5p inhibitor cells

We had achieved the primary aim of the dissertation and had characterized the role of both miRNA candidates in TNBC cell lines *in vitro* in regard to growth, proliferation, apoptosis, migration, stemness, and angiogenesis, which revealed tumor-suppressive effects of both miR-4646-5p and miR-4649-5p. Moreover, we had identified a direct target for each miRNA as well as affected pathways that corroborated and helped to explain the observed tumor-suppressive phenotypes. Once we had gathered this evidence we proceeded and sought to confirm our *in vitro* findings also *in vivo*. To this end, we wanted to make use of the stable SUM159 miR-4646-5p inhibitor and SUM159 miR-4649-5p mimic cell lines generated and

described previously. However, as we were not satisfied with the level of overexpression in the stable miR-4649-5p mimic cell line (Figure 9B), we only performed the experiment with the stable SUM159 miR-4646-5p inhibitor cell line. 5 × 10^5 cells in a volume of 50 µl PBS were injected into the mammary fat pads of 8 athymic nude mice, with the stable miR-4646-5p inhibitor cells on the right side and the control cell line on the left side of each mouse. We expected the mice to develop tumors within around 4 weeks. However, after almost 11 weeks most of the mice still had not developed tumors larger than 10 mm^3 (Figure 41A, 41B, and 41C). One of the control tumors had reached more than 1000 mm^3 though (the ethical endpoint) and a second control tumor as well as a miR-4649-5p inhibitor tumor were around 500 mm^3 (Figure 41A, 41B, and 41C). We terminated the experiment after 75 days but could not retrieve conclusive results due to the extreme variations in tumor growth.

A

Mouse ID	Tumor volume [mm^3] SUM159 control (left)	Tumor volume [mm^3] SUM159 miR-4646-5p inhibitor (right)	Comment
308	235.59	588.98	
310	-	-	Terminated early due to anal prolaps
312	463.68	1.46	
314	187.84	2.79	
316	0.87	2.42	
318	1048.94	7.80	Onset of cachexia
320	2.37	1.32	
322	3.41	13.62	

B

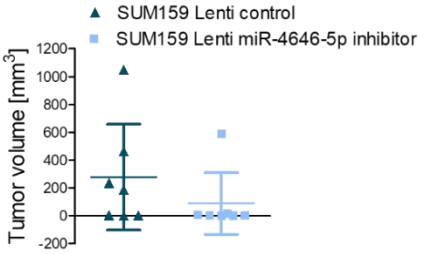

C

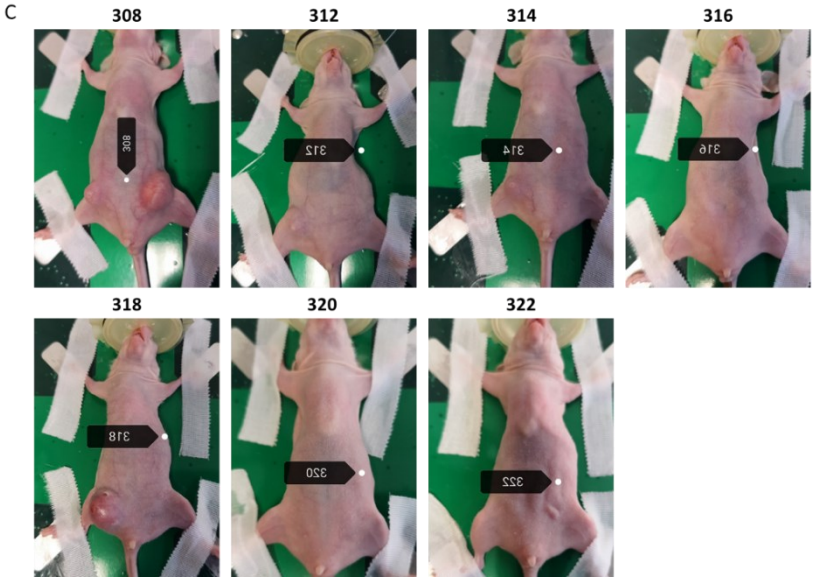

Figure 41: Mammary fat pad injection of stable SUM159 miR-4646-5p inhibitor cells into athymic nude mice. (A)(B) *Tumor volumes 70 days after injection of 5 × 10^5 SUM159 control (left side) or SUM159 stable lentiviral miR-4646-5p inhibitor cells (right side).* ***(C)*** *Images of all mice showing tumor growth 70 days after cell injections (The experiment was performed in collaboration with the Core Facility Alternative Biomodels & Preclinical Imaging, Medical University of Graz, Austria).*

3.8.2. Metastatic breast cancer model with systemic application of miRNA mimics

Due to the problems that we encountered in the first *in vivo* trial, we switched to a different model which would also allow us to better assess the therapeutic utility of the miRNAs. Instead of an orthotopic mammary tumor model, we decided to establish a metastatic TNBC model together with the company Experimental Pharmacology & Oncology Berlin-Buch (EPO) by tail vein injection of a luciferase-labeled SUM159 cell line into immunodeficient NMRI nude mice and to apply the miRNAs in a therapeutic approach by tail vein injection of PEI-complexed miRNA mimics. This form of application closely resembles the use of tumor-suppressor miRNA therapeutics in clinical trials (155,158,162) and has been tested in various mouse studies (236–238). To allow *in vivo* imaging of metastasis formation, we generated a stable mCherry-luciferase expressing SUM159 cell line. Despite FACS enrichment of highly positive cells, the luciferase activity of the cell line was eventually not high enough for *in vivo* imaging. We therefore switched to a mCherry-luciferase-expressing MDA-MB-231 cell line provided by EPO. Appropriate cell numbers for injection were determined in a pilot experiment, where 5×10^5 cells resulted in substantial growth and clear development of metastases in the lungs of the mice visible by bioluminescent imaging after 17 days. In an experiment with 7 mice per group injecting 5×10^5 cells per mouse, applying the miRNA mimics (miR-4646-5p mimic, miR-4649-5p mimic, and mimic control) twice per week with 2 nmol per injection, no luciferase signals could be detected in any of the groups even after 28 days (as opposed to 17 days in the pilot experiment). The reasons for this lack of tumor growth are not clear, but in an attempt to solve the problem, we switched from NMRI nude mice to NODShi.Cg-*Prkdc*^{scid} *Il2rg*^{tm1Sug} (NOG) mice, which are known to show improved tumor engraftment (239). In addition, we reduced the amount of miRNA mimics from 2 to 0.5 nmol per injection, applied twice per week, with the first treatment 6 days after injection of the cells (Figure 42A). In total, the mice received 6 miRNA mimic injections. Metastasis formation, which was primarily localized to the lungs, was monitored by bioluminescent imaging at 5 time points, starting one day before the first miRNA mimic application (Figure 42A and 42B). The experiment was ended 35 days after the cell injection (29 days after the first miRNA injection) due to mice reaching the ethical endpoint. The luminescent signals, which were normalized for each mouse to the first imaging time point (one day before the first miRNA mimic treatment and 5 days after the MDA-MB-231 cell injection), showed large variations within the treatment groups and did not reveal significant differences in tumor growth between the groups (Figure 42C). Due to this, we did not perform any further histological examinations of the tumors.

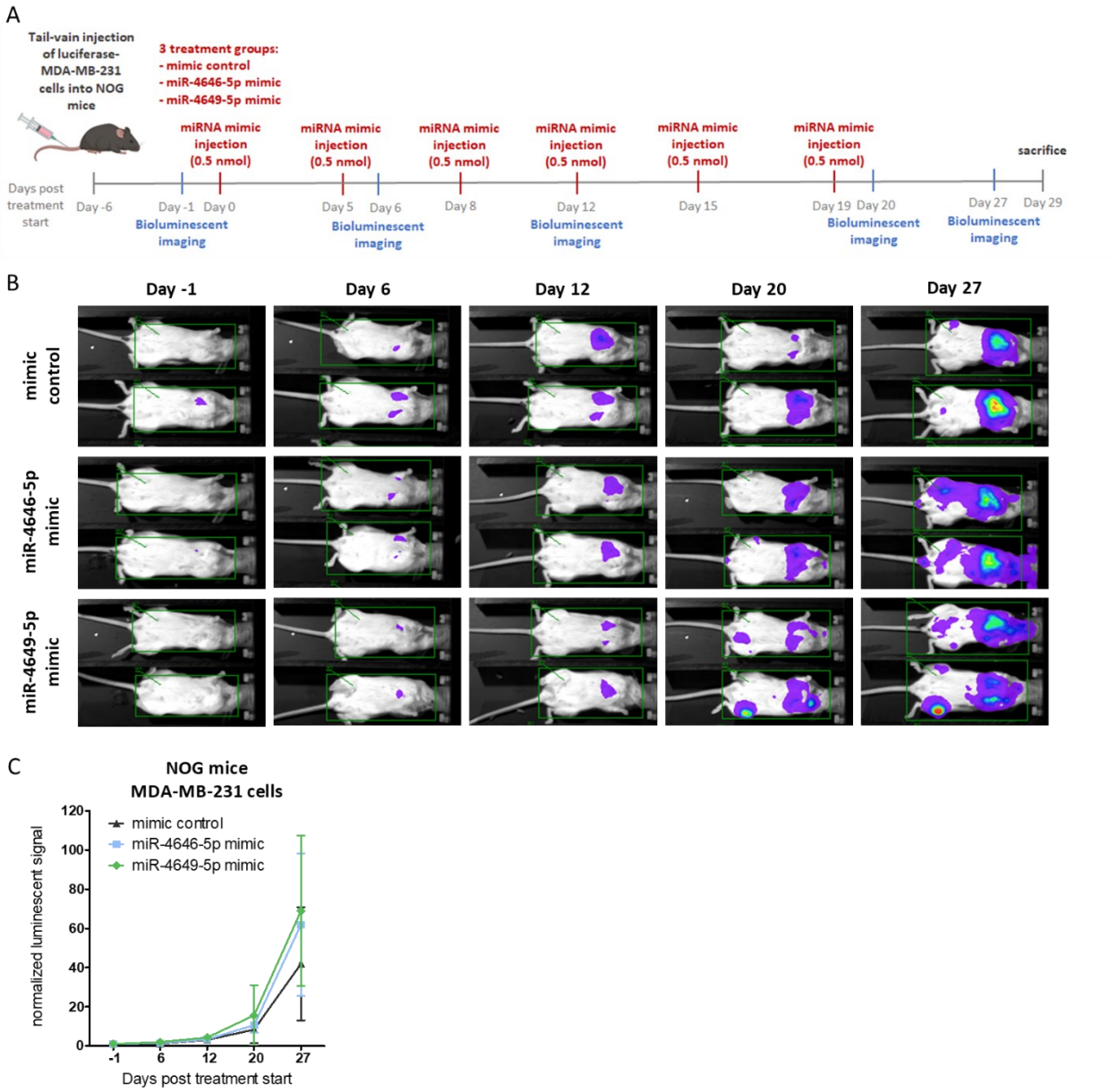

Figure 42: Metastatic TNBC mouse model testing the therapeutic potential of polymer-complexed miR-4646-5p and miR-4649-5p mimic injections. (A) *Scheme illustrating the timeline of the injection of luciferase-expressing MDA-MB-231 cells into NODShi.Cg-Prkdc^{scid} Il2rg^{tm1Sug} (NOG) mice, the injection of the miR-4646-5p mimic, miR-4649-5p mimic, and mimic control (where mice received a dose of 0.5 nmol per injection), and the time points where metastasis formation was measured by bioluminescent imaging.* ***(B)*** *Bioluminescent images of two representative mice per treatment group of the experiment described in (A). The indicated imaging days are counted as days post miRNA mimic treatment start.* ***(C)*** *Quantification of metastasis formation of the experiment described in (A). Luminescent signals (counts per second) were normalized for each mouse to the signals at the first imaging time point taken one day before the miRNA mimic treatment start (day -1) (n = 7; mean ± SD) (The experiment was performed by Experimental Pharmacology & Oncology Berlin-Buch GmbH (EPO), Berlin-Buch, Germany).*

4. Discussion

The primary aim of the dissertation was to identify and characterize novel miRNAs with a role in TNBC, the most aggressive subtype of breast cancer that also poses a therapeutic challenge. MiRNAs are of interest as it is well known by now that by their post-transcriptional downregulation of a wide range of genes, including tumor suppressors and oncogenes, they have a detrimental impact on the initiation, progression, and recurrence of different types of cancer, including breast cancer. Thus, identifying miRNAs with a function in TNBC could help to better understand the pathology of TNBC, to find new vulnerabilities of this breast cancer subtype, and to ultimately develop better treatment strategies.

In order to select miRNA candidates for this purpose, we made use of previously published data from a microarray-based screen of 3D breast cancer spheres called mammospheres (163), a model system that allows for the enrichment of cancer cells with stem cell characteristics (164). We selected the second and third most upregulated miRNAs in the mammospheres compared to 2D adherent breast cancer cells, as these two miRNAs had not yet been characterized in breast cancer. These miRNAs were miR-4649-5p and miR-4646-5p. Based on the fact that other miRNAs from this list of top deregulated miRNAs had previously been reported to play a role in breast cancer and TNBC (163,166), we formed the hypothesis that miR-4649-5p and miR-4646-5p might also be involved in TNBC carcinogenesis.

In the following, our findings from the characterization of miR-4646-5p will be discussed first. The results of miR-4649-5p will be addressed in the next chapter.

4.1. MiR-4646-5p

4.1.1. Low expression and association with patient survival as first indications for tumor-suppressive function of miR-4646-5p in TNBC

As a first step, we made use of *in silico* data to determine whether and to which extent miR-4646-5p is expressed in breast cancer and whether its expression has prognostic relevance for breast cancer patients. While the host gene of miR-4646-5p, abhydrolase domain containing 16A, phospholipase (*ABHD16A*), was found to show higher expression in breast tumors than healthy tissue and to be linked to worse survival, we could not retrieve expression data for miR-4646-5p from online databases. This may be linked to the fact that the miRNA had not been studied previously or that its expression levels are very low. Indeed, survival analysis using TCGA data from an online tool revealed a very low overall expression of miR-4646 in TNBC and indicated significantly better overall survival of TNBC patients with higher miR-4646 expression. For the analysis we used an auto cut-off for the separation of high and low expression and due to the fact that the analysis tool issued a warning about low median

expression, it is questionable what the auto cut-off algorithm has defined as “high expression”. Thus, the validity of the survival analysis may be limited. Nevertheless, the information that miR-4646-5p showed a low expression, which could also provide an explanation for the lack of available expression data in other *in silico* online tools, together with the ostensibly favorable impact on TNBC patient survival, was a first hint at a potentially tumor-suppressive role of the miRNA. Tumor-suppressive miRNAs generally show a low expression in cancer (132). We also checked the expression of miR-4646-5p in a panel of breast cancer cell lines from different subtypes and a non-malignant control. Here we could detect the miRNA but could not see a distinctly lower expression in the cancer cell lines than in the non-malignant cells and no distinct pattern within the subtypes. Overall, though, the expression levels of miR-4646-5p, compared to the expression levels of small nucleolar RNAs used as housekeeper controls, were in the medium to low range.

4.1.2. MiR-4646-5p reduces growth of TNBC cells and can induce apoptosis in a cell-line-dependent context

Based on our first findings, we continued and wanted to test our hypothesis, about the involvement of miR-4646-5p in TNBC, *in vitro* by applying a synthetic mimic for the overexpression of miR-4646-5p as well as an antisense inhibitor to block the function of the miRNA. Using these overexpression and inhibition systems we investigated the impact of the deregulation of the miRNA on several important characteristics of cancer cells, which are known to be frequently affected by miRNAs, including growth, proliferation, apoptosis, migration, stemness, and angiogenesis.

We started with cell growth and observed that the mimic overexpression of miR-4646-5p caused reduced growth of three TNBC cell lines, while inhibition of miR-4646-5p had the corresponding opposite effect. In accordance with the growth reduction in assays lasting up to 96 h, we also saw that the mimic reduced colony formation over a longer time.

The impact of the miR-4646-5p inhibitor was less pronounced than the effect of the mimic in the growth assays. This might be due to the already rather low endogenous levels of miR-4646-5p, limiting the impact of inhibition. A problematic aspect of the inhibitor was also that we did not have the means to confirm the functionality of the inhibitor at first. As stated before, LNA miRNA inhibitors, such as the one used here, do not necessarily cause degradation of the miRNA that would become visible in a reduction detectable by qPCR (186). Only later on, after identifying a target binding sequence for miR-4646-5p, we could confirm that the inhibitor was able to bind to and block the function of miR-4646-5p. Due to this, for many of the phenotypic assays, which we performed before having definite proof for the function of the

inhibitor, we mostly focused on the mimic, also because the tumor suppressive effects we observed with the mimic were more of interest to us in regard to therapeutic utility than the growth-promoting effect of the inhibitor.

To understand the mechanisms behind the growth reductions, we investigated cell proliferation and saw that miR-4646-5p reduced the number of proliferating cells. The effects were not very strong though, and it was unclear whether this alone could account for the reductions in growth that we had observed. Most likely, the effects on growth were caused by a combination of different mechanisms, amongst others including reduced proliferation. We suspected the induction of cell death to be another contributing factor and discovered that miR-4646-5p overexpression induced apoptosis in a cell-line-dependent context. This was a surprising finding at first but context dependence of miRNAs is seen rather frequently and can be explained based on the fact that these effects are cumulative and are influenced by the large number of direct as well as indirect targets that a miRNA has (147). The target interactions of a miRNA can differ, not only between different types of cancer and different types of tissue but also between different cell lines of the same tissue or cancer type, which can be caused by polymorphisms and mutations in target binding sites, by differential interactions with RNA binding proteins, as well as by differences in the overall expression of the target genes (147,240). This means that when the set of genes that a miRNA targets differs depending on these contexts, the resulting net outcome may also differ. Even though the cell lines we applied for the study were all TNBC cell lines, they of course show inherent differences as TNBC generally exhibits a high degree of heterogeneity and can even be further subdivided based on gene expression profiling, as stated in the introduction (21). We could show that the two TNBC cell lines SUM159 and MDA-MB-231 differed in their expression of certain pro-apoptotic genes, both inherently as well as in response to miR-4646-5p overexpression. In addition, it has previously been reported that the two cell lines show differences in their mutational profiles, as SUM159 cells for example exhibit a *PIK3CA* and *HRAS* mutation whereas MDA-MB-231 cells harbor a *BRAF* and *KRAS* mutation (241). Together, these differences in the cell lines may contribute to the differential effect that miR-4646-5p showed in them regarding apoptosis.

4.1.3. MiR-4646-5p reduces migration of TNBC cells

The next phenotypic aspect we characterized was cell migration and we observed that overexpression of miR-4646-5p caused decreased migration, while miR-4646-5p inhibition resulted in increased migration of TNBC cell lines. We sought possible molecular contributors to this impact on migration from our RNA-seq data of SUM159 cells transfected with the miR-4646-5p mimic and found that three genes coding for Rho guanine nucleotide-exchange

factors (GEFs) were significantly downregulated. These genes were ArfGAP with RhoGAP domain, ankyrin repeat and PH domain 3 (ARAP3) (1.4-fold downregulation), Rho/Rac guanine nucleotide exchange factor 2 (ARHGEF2) (1.3-fold downregulation), and pleckstrin homology and RhoGEF domain containing G4 (PLEKHG4) (1.3-fold downregulation). Their downregulation by miR-4646-5p was of interest because GEFs facilitate the activation of Rho GTPase family members, which are key players in regulating focal cell adhesion and cytoskeleton remodeling, thereby controlling processes like cell migration (242,243). A bioinformatics analysis by Han and colleagues has identified ARAP3 expression to be associated with ER-negative breast cancer metastasis (244), and Wang *et al.* identified oncogenic functions of ARAP3 in papillary thyroid carcinoma, where downregulation of the protein caused reduced proliferation, migration, and invasion (245). ARHGEF2, also referred to as GEF-H1, was discovered to increase motility, invasion, and metastasis of colon cancer cells (246) and to be associated with metastatic behavior and poor prognosis in pancreatic cancer (247,248). PLEKHG4 has not been associated with cancer yet. However, its function in the activation of small GTPases and actin cytoskeleton rearrangement (249) suggests a similar role in cancer as for ARAP3 and ARHGEF2. In summary, the fact that the expression of these three genes, that are associated with promoting migration and metastasis, was downregulated by miR-4646-5p could have contributed to the reductions in migration that we saw in TNBC cells upon miR-4646-5p overexpression. While ARAP3 and ARHGEF2 were not found to contain potential binding sites for miR-4646-5p, likely making them indirect targets, the miRWalk2.0 algorithm (175) predicted a miR-4646-5p binding sequence in the 3' UTR of PLEKHG4. We did, however, not confirm direct interaction of the miRNA with this predicted site.

The processes regulated by Rho GTPases, namely the remodeling of the actin cytoskeleton and the formation of cell protrusions to initiate focal adhesion, only present the first steps a cell needs to undertake in order to migrate (192). Next, the cell has to degrade the extracellular matrix which is facilitated by proteases like matrix metalloproteinases (MMPs) (192). Among the downregulated genes in the RNA-seq data, MMP1 (collagenase) was the 8th most downregulated annotated gene (with a 2.2-fold change). MMP1 has previously been discovered to show high expression in TNBC, which was linked to increased invasion, migration, and metastasis formation (250,251). According to TargetScan (174), MMP1 carries one potential binding site for miR-4646-5p but we did not confirm whether miR-4646-5p really interacts with this site.

4.1.4. MiR-4646-5p has no conclusive effect on TNBC stemness

As miR-4646-5p had been found to be deregulated in cancer stem cell-enriched mammospheres (163), we were interested to see whether the miRNA is involved in regulating stemness, a characteristic that is more pronounced in TNBC than in other breast cancer subtypes and that plays a part in the aggressive traits of TNBC like increased resistance to chemotherapy, metastasis, and relapse (7,27,39,40). To this end, we measured the activity of ALDH1, an enzyme whose function is known to be linked to the aggressiveness of breast cancer stem cells and which is commonly used as a breast cancer stem cell marker (34,35,38,252,253). In a flow cytometric analysis, we found that miR-4646-5p overexpression significantly reduced ALDH1 activity in SUM159 cells but not in MDA-MB231 and BT-20 cells. Even though the reduction in the SUM159 cells could be interpreted as a hint for a cell-line-specific impact on stemness, further assays, for example looking at the two breast cancer stem cell markers CD24 and CD44 (33), would be required to draw a clear conclusion about a role of miR-4646-5p in TNBC stemness. Also, in our RNA-seq data of miR-4646-5p mimic transfected SUM59 cells we could not see a significant downregulation of ALDH1 on the RNA level, indicating that the effect of the miRNA on the activity of ALDH1 in SUM159 cells was mediated by indirect mechanisms, for example by targeting genes that are involved in regulating post-translational modifications of ALDH1, like acetylation, which affects its enzymatic activity (254).

4.1.5. MiR-4646-5p reduces tube formation of endothelial cells indicating potential anti-angiogenic properties

A previously discussed characteristic of cancer cells that we discovered to be influenced by miR-4646-5p was cell migration. A migratory phenotype is not the only prerequisite for a tumor to be able to metastasize. This process also requires angiogenesis, which describes the formation of new blood vessels in a tumor that facilitate the uptake of oxygen and nutrients, and allows dissemination of tumor cells to more distant sites of the body (255,256). We discovered that miR-4646-5p reduces the branching and *in vitro* tube formation of endothelial cells. This indicates that miR-4646-5p could potentially function as an angiogenesis-inhibiting miRNA. We also observed that miR-4646-5p overexpression caused a reduction of FGF2, IL6, and NRP2, three factors that are associated with the vascularization of endothelial cells (196–198). The downregulation of the three was apparently indirect, as none of them had conventional miR-4646-5p binding sites. The finding that miR-4646-5p might have anti-angiogenic properties was a very interesting finding because it showed that miR-4646-5p does not only have a tumor-suppressive effect on cancer cells but also plays a role in the tumor

microenvironment, which would support a therapeutic application of miR-4646-5p, since the miRNA would directly act on the tumor cells as well as suppress angiogenesis of endothelial cells. Nevertheless, these findings were only *in vitro*. Further confirmations would be needed to really substantiate the anti-angiogenic properties of miR-4646-5p also *in vivo*. Other assays, closer to the *in vivo* scenario, could have been conducted in addition, like the chick chorioallantoic membrane assay which better represents the complex cellular interactions and processes of tissue remodeling occurring during angiogenesis (257,258).

4.1.6. GRAMD1B is a direct target of miR-4646-5p and may contribute to the tumor-suppressiveness of the miRNA

In addition to the phenotypic characterization of the miRNA´s role in TNBC, another aim of the dissertation was the identification of a direct target of miR-4646-5p. To do so, we made use of the RNA-seq results and screened the top-downregulated genes for potential miR-4646-5p binding sites. While the first four downregulated genes (GCSF, IL6, CCL20, and AIM2) did not have any canonical binding sites for miR-4646-5p, the fifth most downregulated candidate in the list, GRAMD1B, was predicted to carry seven miR-4646-5p binding sites, one of which we were able to confirm experimentally by luciferase reporter assays. In addition, we found that the direct siRNA-mediated knockdown of GRAMD1B caused reduced growth and colony formation of TNBC cells which phenocopied the outcome of miR-4646-5p overexpression. This suggests that the direct targeting and downregulation of GRAMD1B may account, to some degree, for certain tumor-suppressive effects of miR-4646-5p.

To understand whether this could be the case, one needs to understand the role of GRAMD1B in the cell. GRAMD1B is one of three members of a highly conserved family of cholesterol transfer proteins (202). The three proteins belonging to this family, GRAMD1A, GRAMD1B, and GRAMD1C, are expressed in a tissue-specific manner, with GRAMD1A mostly being found in the brain, GRAMD1B showing the highest levels in steroidogenic organs like adrenal glands, and GRAMD1C being abundant in the liver and testes (202). Of note, GRAMD1B was 2.7-fold downregulated by miR-4646-5p in our RNA-seq data, whereas GRAMD1A was only (yet still significantly) 0.7-fold downregulated and GRAMD1C was not among the significantly downregulated genes, indicating that they are targeted differentially by miR-4646-5p. In fact, the TargetScan algorithm (174) could not identify any miR-4646-5p binding sites within the GRAMD1A and GRAMD1C gene. Despite this, all three GRAMD1 proteins are structurally and functionally very similar and are anchored in the endoplasmic reticulum (ER) via a transmembrane domain towards the C terminus (202). In addition, they carry an N-terminal GRAM domain and a central START-like or ASTER domain (202). The GRAMD1s, including

GRAMD1B, are recruited to contact sites formed between the ER and the plasma membrane (PM), where most of a cell`s cholesterol is stored, and detect accessible cholesterol in the PM together with anionic lipids via their GRAM domain (200–202). This recruitment to PM contact sites primarily occurs when there is an increase in the pool of accessible cholesterol in the PM, which results in the transfer of this excess of cholesterol to the ER via the START-like domain of the GRAMD1 proteins (200–202,259). Located in the membrane of the ER, there is a transcriptional master regulator for the uptake and de novo biosynthesis of cholesterol called sterol regulatory element-binding protein 2 (SREBP-2), whose activation by cleavage becomes blocked when cholesterol levels in the ER membrane are high, subsequently reducing the transcription of target genes required for the uptake and synthesis of cholesterol (260). Thus, the function of the GRAMD1s in transporting excessive cholesterol from the PM to the ER is essential in maintaining cellular cholesterol homeostasis (199,202,261).

In addition, GRAMD1B, in particular, plays an important role in the generation of steroid hormones, that are synthesized from cholesterol, as shown by Sandhu *et al.* who discovered that *GRAMD1B* knockout mice are deficient for steroidogenesis, have reduced storage of cholesteryl ester in lipid droplets, and higher expression of SREBP-2 target genes in the adrenal glands because of the disruption of cholesterol transport from the PM to the ER (202). Other publications further highlight the essential role of GRAMD1B. For example, Naito *et al.* showed that the triple knockout of all three *GRAMD1* genes in HeLa cells led to an increase of free cholesterol found in the PM and an impaired capacity of the cells to block the activation of SREBP-2 upon increases in free cholesterol (201). Similar findings were reported for macrophages from *GRAMD1B* knockout mice where the loss of GRAMD1B led to an accumulation of accessible cholesterol in the PM as well as increased expression of SREBP-2 transcriptional target genes that are associated with cholesterol synthesis and uptake (259). These reports align well with our observation that miR-4646-5p overexpression in SUM159 cells, which entails direct downregulation of GRAMD1B, caused an enrichment of upregulated genes in the cholesterol biosynthesis pathway.

The role of GRAMD1B in cancer has not been well studied yet. A first link between GRAMD1B and cancer was delivered by Wu and colleagues reporting a connection between GRAMD1B and chemoresistance in ovarian cancer, where a siRNA-mediated knockdown had synergistic anti-cancer effects together with paclitaxel in a mouse model (203). Khanna *et al.* then discovered an oncogenic role of GRAMD1B in gastric cancer cell lines where its knockdown caused a reduction in the phosphorylation/activation of STAT3 and in the expression of Bcl-xL, an anti-apoptotic factor, resulting in decreased growth and increased apoptosis (204). These findings are in accordance with what we observed in TNBC cells, namely that the

knockdown of GRAMD1B reduced cell growth. The same authors then published contradicting findings in MDA-MB-231 cells, where they reported an increase of STAT3 and AKT activation after the knockdown of GRAMD1B and that this caused increased migration of the cells (205). The authors did not address the opposing nature of their findings or try to elucidate the mechanism of how GRAMD1B is connected to STAT3 and AKT signaling. It also has to be considered that in the second paper, they only performed experiments in a single cell line. We tested whether knockdown of GRAMD1B influenced STAT3 and AKT activation in our TNBC cell lines, but could not find evidence for such a link. Unfortunately, we did not investigate the impact of GRAMD1B knockdown on cell migration as done in the publication by Khanna *et al.* but saw that miR-4646-5p overexpression reduced migration and that both miR-4646-5p overexpression as well as direct GRAMD1B knockdown reduced growth and colony formation of SUM159 and MDA-MB-231 cells. We also found that relapse-free survival and distant metastasis-free survival were significantly shorter in TNBC patients with higher expression of GRAMD1B, which would suggest an oncogenic role in TNBC, but the opposite was the case regarding overall survival. In summary, the role of GRAMD1B in cancer seems complex and by affecting the cholesterol household of cells it might have far-reaching effects on various other cellular processes and signaling pathways, which may also strongly depend on the cellular context and on whether and in which form cells are supplied with exogenous cholesterol.

Limiting the view on the function of GRAMD1B in cholesterol transport though, one could find an explanation for an oncogenic role of the protein. Cancer cells are in demand of higher levels of cholesterol due to their increased proliferation, as cholesterol serves as a building block in the formation of cell membranes as well as a precursor for the production of steroid hormones and various metabolites that have been shown to promote the proliferation and growth of breast cancer cells, as for example 6-oxo-cholestan-3β,5α-diol (OCDO) and 27-hydroxycholesterol (27HC) (262–264). Interestingly, endogenous 27HC, which is generated from cholesterol by oxidative processes, was found to increase STAT3 activation and vascular endothelial growth factor (VEGF) production in breast cancer cells, promoting EMT, invasion, migration, and angiogenesis (265,266).

To meet the high demand for cholesterol, cancer cells may prefer the uptake and use of exogenous cholesterol over the more time- and energy-consuming de novo biosynthesis, especially if high levels of cholesterol are present, which is usually the case in *in vitro* culture conditions or also *in vivo* owing to high-fat diets (262). For exogenous cholesterol to be used and metabolized in a cell it has to be transported between different cellular organelles mainly in a non-vesicular way, a process in which GRAMD1B plays a crucial role (201,202,259,267).

Exogenous cholesterol is generally taken up in two forms, as a component of high-density or low-density lipoproteins (HDL and LDL respectively), both of which follow different transport routes in the cell (202,267). GRAMD1B has been found to be involved in the transport of both HDL- and LDL-derived cholesterol (202,268). HDL-derived cholesterol is taken up into a cell`s PM upon interacting with the scavenger receptor class B, type I (SR-B1), and is then transferred from there to the ER by GRAMD1B (202). LDL-derived cholesterol enters a cell through the LDL receptor (LDLR), followed by endocytosis, and eventually ends up in lysosomes, from where it is transported to the PM or directly to the ER (267). GRAMD1B has been discovered to participate in this direct transfer between lysosomes and the ER by interaction with the lysosomal membrane protein Niemann-Pick type C protein 1 (NPC1) (268). Thus, we hypothesize that by transporting and thereby supporting the increased use of both HDL- and LDL-derived cholesterol, GRAMD1B could fulfill a beneficial role for breast cancer cells as both HDL- and LDL-derived cholesterol, as well as derived metabolites like OCDO and 27HC, have been described to have pro-tumorigenic effects in breast cancer. For example, in a breast cancer mouse model, tumor cells were shown to express higher levels of SR-B1, which was associated with higher uptake of HDL by the tumor cells, resulting in lower HDL serum levels and enhanced tumor growth and metastasis (269). Others have shown that HDL can promote the proliferation and migration of ER-positive as well as TNBC cells and that these effects are mitigated upon knockdown of SR-B1 (270). Similar findings were reported for LDL, for example, that in hyperlipidemic mice, breast cancer cells show higher LDLR expression, which promotes tumor growth (271), and that *in vitro*, LDL-derived cholesterol enhances proliferation, migration, and loss of adhesion of breast cancer cells (272). Moreover, the storage of excessive cholesterol in the form of cholesteryl ester in lipid droplets gives breast cancer cells an energetic advantage, for example, to fuel cell migration (262,273). Sandhu *et al.* showed that this storage of cholesteryl ester is significantly impaired in GRAMD1B knockout mice (202).

In summary, based on this evidence, we believe that GRAMD1B can have oncogenic functions in breast cancer by supporting the intracellular transport, storage, and use of exogenous cholesterol, which provides breast cancer cells with a source to fuel their increased demands for growth and migration. Hence, downregulation of GRAMD1B by miR-4646-5p, which would impede the use of exogenous cholesterol, could contribute to the tumor-suppressive effects of the miRNA. It is unclear though, whether or to what degree a lack of GRAMD1B in breast cancer could be substituted by the function of GRAMD1A or GRAMD1C, as there are no reports about their expression or function in breast cancer yet. Further research on the seemingly complex role of all three GRAMD1s in breast cancer is needed.

4.1.7. MiR-4646-5p broadly downregulates tumor-promoting cytokines

Limiting the view to single direct targets of a miRNA will not give a complete picture of the molecular mechanisms of the miRNA. We thus also aimed to decipher the effects of miR-4646-5p on a broader pathway-spanning scale by GSEA and GO enrichment analysis. In doing so, we discovered that miR-4646-5p overexpression caused a broad downregulation of cytokine signaling, for example, seen in an enrichment of downregulated genes involved in IL-10 signaling and TNF target genes, which included some of the top-downregulated tumor-promoting cytokines like G-CSF, IL-6, CCL20, CXCL1, and IL-1B. The chemokine CCL220, for example, has a well-described role in breast cancer where it promotes tumor growth, migration, invasion, chemoresistance, and angiogenesis via autocrine signaling as well as by suppressing anti-tumor immunity (215). Also for CXCL1, more and more evidence emerges showing its breast cancer-promoting properties, like its ability to stimulate migration and invasion of ER-negative breast cancer cells, to sustain breast CSCs self-renewal, and to maintain tumor immune evasion (216,217). Concerning IL-1B, another cytokine downregulated by miR-4646-5p on the mRNA level, it was discovered to promote migration, invasion, and bone metastasis of breast cancer (208). All three, CCL20, CXCL1, and IL-1B, were more than 2.2-fold downregulated by miR-4646-5p by apparently indirect mechanism as none of them were predicted to have miR-4646-5p binding sites. Along with these three, there were numerous other cytokines found to be downregulated. A possible explanation for this broad downregulation of tumor-promoting cytokines could be that miR-4646-5p affects transcription factors that regulate cytokine expression. A potential candidate contributing to this could be Fos, which was 2.1-fold downregulated by miR-4646-5p and which, as part of the AP-1 transcription factor complex, is known to control the expression of numerous cytokines (223,224).

The two most downregulated genes by miR-4646-5p in the RNA-seq data were also cytokines, namely G-CSF and IL-6. G-CSF has been found to support the proliferation and growth of breast cancer cells in various ways, on the one hand by autocrine signaling, on the other hand by triggering the recruitment of certain immune cells, for example, myeloid-derived suppressor cells, which facilitate tumor immune evasion by interfering with T cell activation (212–214). Of note, it was also discovered that, compared to breast cancer cells from ER-positive subtypes, TNBC cells have a higher expression of G-CSF which is connected to worse overall survival of patients with TNBC (214). Regarding IL-6, which activates the JAK/STAT3 pathway, autocrine signaling has also been reported to stimulate the proliferation, migration, invasion, and survival of breast cancer cells (209). Interestingly, high levels of IL-6 were also found to promote the expansion of breast CSCs, which in turn creates a positive feedback loop causing

a dramatic increase in the secretion of IL-6 from CSCs (210). Moreover, IL-6 supports tumor formation by inhibiting the activity of natural killer cells, dendritic cells, and effector T cells, thus making the tumor microenvironment immunosuppressive (145,211). Importantly, for G-CSF and IL-6 we were not only able to show their downregulation by miR-4646-5p on the RNA level but to also prove that the secretion of the cytokines by TNBC cells is reduced.

Overall, the broad downregulation of these cytokines by miR-4646-5p corroborates the tumor-suppressive properties of miR-4646-5p that we observed *in vitro*, as many of the cytokines are known to have autocrine oncogenic effects on breast cancer cells. Moreover, the altered secretion of these signaling molecules may also modulate the tumor microenvironment in an *in vivo* setting and favor anti-tumor immune responses. This is something that remains to be tested though. As immunotherapy, like immune checkpoint inhibitors, is becoming a viable treatment option for TNBC patients (76–78), miR-4646-5p mimics may be able to add a benefit in this setting and therapeutic combinations with anti-PD-L1 would be worth testing *in vivo*.

4.1.8. Opposing oncogenic role of miR-4646-5p in gastric cancer

Contrary to our findings in TNBC, a recent paper by Yang *et al.* described an oncogenic role of miR-4646-5p in gastric cancer, where they also discovered that miR-4646-5p is a mirtronic miRNA (274). They identified prolyl-4-hydroxylase domain 3 (PHD3) as a target of miR-4646-5p, which resulted in the stabilization of hypoxia-inducible factor 1-alpha (HIF1α), upregulation of RhoA, upregulation of the miR-4646-5p host gene ABHD16A via a positive feedback loop, accumulation of lysophosphatidylserines and ultimately increased invasion and metastasis *in vivo* (274). Our study did however not reveal PHD3 as a target of miR-4646-5p in TNBC cells as it was not found to be downregulated in our RNA-seq data set. And while they reported upregulation of RhoA (274) (which we did not observe in the RNA-seq analysis), we discovered downregulation of Rho-activating GEFs. They also ascribed part of the phenotype caused by miR-4646-5p to the positive feedback loop via HIF1α that entails upregulation of the miR-4646-5p host gene ABHD16A (274). However we did also not detect such an upregulation, and while they stated that high ABHD16A expression is associated with worse survival of gastric cancer patients (274), we discovered it to be associated with better overall survival in patients with TNBC and basal breast cancer. As discussed previously, miRNA effects can be context-dependent due to the plethora of genes they target, and whether a miRNA is oncogenic or tumor suppressive can vary between different types of cancer (147), as it seems to be the case for miR-4646-5p in TNBC and gastric cancer.

4.2. MiR-4649-5p

4.2.1. MiR-4649-5p shows very low expression in TNBC cells and its overexpression inhibits their growth and migration

What struck us as a surprising finding was that, while the other miRNA candidate showed low expression, the second candidate miR-4649-5p was almost completely undetectable in TNBC cell lines, both by qPCR and by ddPCR, a PCR variant that allows very sensitive measurements (189). Also *in silico* data used for a survival analysis indicated a very low overall expression of miR-4649-5p in TNBC patients. A shortcoming though is that we could not compare the expression of the miRNA in breast cancer to healthy tissue, as no data on this was available from databases. We also did not measure the expression in non-malignant cell lines to see if the expression might be higher than in TNBC cells. Interestingly, the miR-4649-5p host gene AEBP1 exhibited higher expression levels in breast cancer than in healthy tissue and was connected to worse overall survival in TNBC patients. This does not necessarily contradict the low expression of miR-4649-5p that we observed in TNBC cell lines. Others have reported discordant expression of host genes and intronic miRNAs due to independent transcriptional regulation (183).

The low expression of miR-4649-5p led us to build the hypothesis that upregulation of the miRNA could potentially exert tumor-suppressive effects in TNBC cells. Using a synthetic miR-4649-5p mimic to facilitate overexpression, we could observe a reduction in growth, colony formation, proliferation, and migration. We did not see an impact on apoptosis, ALDH activity, and tube formation of endothelial cells. Overall, the phenotype we observed for miR-4649-5p was tumor-suppressive, similar to but still distinct from our other studied miRNA.

4.2.2. MiR-4649-5p downregulates numerous oncogenic factors

To answer our research question of how miR-4649-5p facilitated its tumor-suppressive effects on a molecular level we performed whole transcriptome analysis followed by GSEA and GO enrichment analysis. In doing so, we observed that miR-4649-5p overexpression caused an enrichment of upregulated genes associated with oxidative phosphorylation and tight junctions. A hallmark of cancer cells is that they rely less on oxidative phosphorylation and instead undergo a metabolic switch towards aerobic glycolysis, which allows them to divert glycolytic intermediates into the biosynthesis of, for example, nucleotides, amino acids, and lipids, that are required to build biomass for rapidly dividing cancer cells (133,275). This suggests that an upregulation of oxidative phosphorylation as seen after miR-4649-5p overexpression, and thus switch away from aerobic glycolysis, might impair the proliferative capacity of the cancer cells.

Tight junctions are epithelial cell-cell contact sites that are important in maintaining epithelial tissue structure and integrity, and a loss or deregulation of components of tight junctions can be linked to breast cancer progression (276). It was thus interesting to see that miR-4649-5p affected genes involved in the formation of tight junctions.

Furthermore, GO enrichment analysis revealed that genes downregulated by miR-4649-5p were enriched in ontologies like epithelium and gland morphogenesis, metabolic processes, and transcription. Morphogenesis of glands and the epithelium is accompanied by increased plasticity and an invasive and migratory EMT phenotype, which are characteristics that are not only involved in gland development in the breast but are also closely connected to tumorigenesis in the breast (277). Increased metabolic processes as well as increased RNA transcription are also characteristics associated with cancer cells (275,278). Hence, the overall downregulation of these processes by miR-4649-5p aligns with and may contribute to the tumor-suppressive properties of the miRNA.

A look at the top downregulated genes by miR-4649-5p further corroborates the anti-tumorigenic capabilities of the miRNA. Of the top 10 downregulated genes, 8 have previously been reported to play an oncogenic role in various types of cancer. The second most downregulated gene, for example, was *SYNPO* (synaptopodin) which is a direct target of the transcription factor early growth response factor 4 (EGR4) and promotes the proliferation of small cell lung cancer cells (279). The third most downregulated gene, *MTA1* (metastasis-associated 1 protein), is linked to EMT, invasiveness, and metastasis of breast cancer (280,281). Among the top 10 was also *PACS1*, coding for phosphofurin acidic cluster sorting protein 1, which shows higher expression in cervical cancer than in healthy tissue and which promotes cancer cell proliferation (282). The next gene in the list, *MED16* (mediator complex subunit 16), has been discovered to favor the progression of ER-positive breast tumors (283). The 6th most downregulated gene was *TMEM120B*, which codes for a member of the transmembrane protein family, whose involvement in cancer is increasingly recognized (284). TMEM120B itself was identified to serve as a risk factor in osteosarcoma as part of a prognostic panel (284). Overall, the fact that all these genes that are associated with pro-tumorigenic functions were downregulated by miR-4649-5p corroborates the tumor-suppressiveness we observed for the miRNA in TNBC.

4.2.3. PIP5K1C is a direct target of miR-4649-5p that may explain the reduced migration caused by miR-4649-5p overexpression

After addressing the aim of phenotypic characterization of the role of miR-4649-5p in TNBC cells and the question of underlying molecular changes, we also wanted to pin down a direct

target of the miRNA. All of the downregulated genes mentioned above were predicted to have potential binding sites for miR-4649-5p, but we did not confirm whether they really interact with the miRNA. We decided to focus on the 7th most downregulated gene, *PIP5K1C*, because, first, its crucial and versatile role in cells made it an interesting candidate, and second, among four selected genes of the top downregulated candidates, it was the only one where we could show its downregulation by the miR-4649-5p mimic not only in the SUM159 cell line (as done by RNA-seq) but also in two other TNBC cell lines.

As previously mentioned, *PIP5K1C* codes for phosphatidylinositol 4-phosphate 5-kinase type 1 gamma and fulfills an important role in the cell by generating the lipid second messenger PIP_2 in a dynamic and spatially controlled manner (225,226). PIP_2 is able to interact with and activate numerous actin-binding proteins that subsequently trigger polymerization of actin filaments, whereby it regulates the dynamic rearrangement of the cytoskeleton (227). Moreover, PIP_2 connects the cytoskeleton to focal adhesion proteins and regulates the turnover of focal adhesion points (227,228). Due to these cellular functions, PIP_2, and ergo PIP5K1C, play a central role in promoting actin dynamics, focal adhesion, cell motility, and migration (226–228). In hepatocellular carcinoma, for example, it has been discovered that PIP5K1C is dynamically directed toward the leading edge of PM protrusions where it catalyzes an increase in PIP_2 that facilitates cell-matrix adhesion, increased migration and invasion, and ultimately metastasis (230). Li *et al.* reported that the stable knockdown of a specific splice variant of PIP5K1C called PIPKIγ90, which is recruited to focal adhesion points, caused a significant reduction in the migratory and invasive capabilities of MDA-MB-231 cells (231). A study by Sun and colleagues showed similar results, namely that a PIP5K1C knockdown reduced the migration, invasion, and proliferation of breast cancer cell lines *in vitro* (232). In addition, they reported a connection between higher PIP5K1C tissue staining and worse survival in a breast cancer patient cohort (232). PIP5K1C and PIP_2 were moreover found to play a role in endocytosis and intracellular protein trafficking, for example of E-cadherin (227,285,286). E-cadherin is a transmembrane glycoprotein and an essential component of adherence junctions, which connect epithelial cells with each other along the basolateral membrane (285). E-cadherin thereby helps to maintain epithelial integrity and cell polarity but is strongly downregulated when cells switch to a more mesenchymal migratory phenotype during EMT (287). PIP5K1C and PIP_2 were found to regulate the endocytosis of E-cadherin and to steer its path toward lysosomal degradation (286). Increased function of PIP5K1C could thus contribute to cancer progression by promoting EMT through increased degradation of E-cadherin (285,286).

In summary, these studies outline a clear oncogenic role of PIP5K1C in cancer by promoting a migratory and invasive phenotype. This is in accordance with what we observed, namely that PIP5K1C showed higher expression levels in breast tumor tissue than in healthy tissue and that higher expression is associated with shorter overall and relapse-free survival of TNBC patients. Importantly, the targeting and downregulation of PIP5K1C by miR-4649-5p might thus also account for the reduced migration that we observed upon miR-4649-5p overexpression.

4.2.4. MiR-4649-5p affects AKT signaling downstream of PIP5K1C which opens up therapeutic utility

Aside from an effect on migration, we also observed that miR-4649-5p overexpression, as well as the direct knockdown or pharmacologic inhibition of PIP5K1C, reduced the growth of TNBC cell lines. We could even achieve additive growth reductions by combining miR-4649-5p overexpression and PIP5K1C inhibition which we believe suggests that miR-4649-5p downregulates PIP5K1C to a certain degree and that thereby the kinase activity of the remaining protein pool can be targeted more efficiently by the inhibitor.

The effect of miR-4649-5p on the migration of TNBC cells might be explained by PIP5K1C and its direct product PIP_2, as discussed above. To explain the impact on cell growth, one may focus on pathways lying a bit further downstream, as for example the PI3K/AKT pathway. As previously described, PIP_2 serves as a precursor for PIP_3, which is generated by PI3K and mediates the recruitment of AKT to the cell membrane, where the kinase becomes activated by phosphorylation and subsequently promotes cell cycle progression, growth, and survival (58,229,234,235). We observed that miR-4649-5p overexpression and pharmacologic PIP5K1C inhibition reduced the phosphorylation of AKT in an additive manner. This finding highlights a pathway where miR-4649-5p directly targets and downregulates PIP5K1C on a post-transcriptional level, resulting in reduced production of PIP_2 and consequently PIP_3, and ultimately decreased recruitment and activation of AKT. This pathway could help to explain the effects we observed on growth, as both miR-4649-5p overexpression and PIP5K1C knockdown or inhibition reduced TNBC cell growth. This theory is strengthened by the fact that a combination of miR-4649-5p overexpression and PIP5K1C inhibition further enhanced the growth reduction, as this is in line with the additive reduction of AKT phosphorylation.

The PI3K/AKT pathway is frequently overactivated in TNBC and has thus been subjected to therapeutic targeting strategies (8,55,235). We could show in SUM159 cells, which harbor an activating mutation in the *PIK3CA* gene that codes for a catalytic subunit of PI3K (58,241), that miR-4649-5p overexpression is able to enhance the growth-reducing effects of the AKT inhibitor capivasertib. This finding opens up a potential therapeutic utility of the miR-4649-5p

mimic in making TNBC cells more vulnerable to capivasertib, which is already under clinical investigation for the treatment of TNBC (81–83). Higher levels of miR-4649-5p could also potentiate the effect of other currently tested clinical approaches to target the PI3K/AKT pathway in TNBC, like for example the PI3Kα inhibitor alpelisib (80). *In vivo,* treatment combinations of the miR-4649-5p mimic with capivasertib or alpelisib could thus be explored in the future. It remains to be tested though, whether TNBC cells that do not exhibit overactivation of PI3K/AKT signaling also benefit from the additive effects between miR-4649-5p mimic and pharmacologic AKT inhibition seen in SUM59 cells.

4.3. Challenging aspects of *in vivo* experiments

The final aim of the dissertation was to confirm the *in vitro* findings on the tumor-suppressive properties of both miRNAs in an *in vivo* setting and to also use *in vivo* experiments to ultimately test the therapeutic utility of the miRNA mimics. However, the *in vivo* experiments turned out to be challenging. In a first approach, we injected stable miR-4646-5p inhibitor or control TNBC cells into the mammary fat pads of nude mice, but tumor growth took much longer than anticipated and showed large variations within the groups. Many had not developed tumors after 70 days, while only very few started growing and reached the ethical endpoint. The injected cell number and application procedure were based on previous experiences and literature reports. For example, in a study by Tian *et al.,* 1×10^6 SUM159 cells were implanted in the mammary glands of NOD.Cg-*Prkdc*^{scid} *Il2rg*^{tm1Wjl}/SzJ (NSG) mice and tumors reached the endpoint of 700–1100 mm^3 after 45 days (288). However, the NSG mice used in this study are one of the most immunodeficient mouse strains, whereas the athymic nude mice that we used only lack T cells but still have high natural killer cell activity and intact humoral immunity, which may have affected the engraftment of the human SUM159 cell line (239). In addition, in this study, Tian *et al.* injected twice as many cells as we did. Also other studies applied much higher cell numbers in similar models, for example, Choi *et al.*, who injected 3×10^6 SUM159 cells into the mammary fat pads of athymic nude mice (289). Moreover, cells are often not only injected in PBS as done by us but mixed with matrigel to aid engraftment (290,291). Based on this, it may be concluded that the problems we observed with the tumor formation in our *in vivo* model were based on a combination of the mouse strain, a cell number that was too low, and the omission of matrigel for the cell injection.

In a second *in vivo* approach, we aimed for a therapeutic application of the miRNAs and generated a metastatic TNBC mouse model using luciferase-labeled MDA-MB-231 cells and treated the mice by injection of PEI-complexed miR-4646-5p and miR-4649-5p mimics. However, also this model turned out to be challenging. After multiple pilot experiments to

determine the right mouse strain, cell line, cell number, and miRNA mimic concentration, the final experiment showed large variations in the luminescent signals within the treatment groups. These variations already started to appear early on after cell injection and it is unclear what caused them. One reason could have been imprecise injection volumes resulting in differences in the number of injected cells. In addition to technical challenges, biological variations may have contributed to the disparate signals. Aside from these difficulties, the miRNA mimic treatments also did not show any impact on tumor growth. The applied concentration of 0.5 nmol per injection with a total of 6 injections should have been high enough to achieve an effect when compared to other studies. For example, Hsu *et al.* treated immuno-competent C57BL/6 mice with 5 µg (which corresponds to 0.35 nmol) of miR-92a mimic mixed with in vivo-JetPEI transfection reagent in a volume of 50 µl, which was delivered 9 times by retroorbital injection at 3-day intervals and caused increased liver metastasis of mouse Lewis lung carcinoma cells (237). Another study reported intravenous injection of 10 µg (which corresponds to 0.7 nmol) of jetPEI/miR-124 complexes into athymic tumor-bearing mice, which was able to reduce tumor growth of prostate cancer xenografts alone and in combination with enzalutamide (236). The delivery strategy we choose for the mimics, complexed with the polymer PEI, is well-tested and known to facilitate the uptake of encapsulated miRNAs by endocytosis as well as subsequent endosomal escape, and is furthermore close to the application form used for miRNA therapeutics in clinical trials (155,158,162,236–238). Nevertheless, we did not actually confirm whether the mimics were sufficiently taken up by the MDA-MB-231 cells in our *in vivo* model and we also did not check whether a downregulation of the miRNA targets occurred in the cells. It can therefore not be excluded that we did not see an effect of the mimics on metastasis formation of the MDA-MB-231 cells simply because the mimics did not reach the cells sufficiently. A more targeted delivery approach of the mimics might have achieved better results.

What may have also contributed to the lack of a therapeutic effect of the mimics was the mouse strain. While the used NOG strain is highly immuno-deficient as it lacks mature T, B, and natural killer cells, and also shows cytokine signaling defects, which supports human cell engraftment (239), this lack of a functioning immune system may have also factored into the deficiency of the miRNA mimics to show an effect. As discussed in the introduction, miRNAs are known to not only exert effects on cancer cells directly but to also modulate the functions of cells in the TME, like endothelial cells, and, importantly, immune cells, which can contribute strongly to their tumor-suppressive or oncogenic properties (142). In the case of miR-4646-5p, we showed that the miRNA alters the secretion of tumor-promoting cytokines. Thus, the lack of immune cells in the TME may have deprived the mimic of some of its tumor-suppressive effects.

Overall, the use of these highly immunodeficient mice presents a disadvantage in the sense that they cannot model the full complexity of the TME in humans. To test the full potential of the miRNA mimics, humanized mouse models engrafted with human immune cells would present an ideal model.

Finally, it has to be considered that most of the effects of both miRNAs were not very pronounced *in vitro* and thus might simply not have been strong enough to show an impact *in vivo*. Single treatments of only the miRNA mimics might not be efficient enough and it might be more interesting to test treatment combinations that could potentiate each other, for example, a combination of the miR-4646-5p mimic with immune checkpoint inhibitors and of the miR-4649-5p mimic with capivasertib or alpelisib.

5. Conclusions

It can be concluded that the primary aim of the dissertation, to identify and characterize novel miRNAs with a role in TNBC, was met. Our *in vitro* characterization of the two previously unexplored miRNAs miR-4646-5p and miR-4649-5p showed that both exerted similar yet distinct tumor-suppressive effects in TNBC cells. Ectopic upregulation of miR-4646-5p decreased growth, colony formation, proliferation, and migration of TNBC cells, and furthermore showed context-dependent effects on the induction of apoptosis. Interestingly, miR-4646-5p was also able to reduce the tube formation of endothelial cells *in vitro*, which suggests angiogenesis-inhibiting properties. MiR-4649-5p, on the other hand, did not have an impact on endothelial cells or the induction of apoptosis in TNBC cells, but overexpression of the otherwise very low expressed miRNA also reduced the growth, colony formation, proliferation, and migration of TNBC cells.

We also met the second aim of the dissertation and identified direct targets of both miRNAs, the cholesterol transfer protein GRAMD1B for miR-4646-5p, and the phosphatidylinositol kinase PIP5K1C for miR-4649-5p, both of which may help to explain the observed phenotypes. Moreover, RNA-seq analysis also allowed us to study the pathways affected by the two miRNAs on a broader level, which revealed that the underlying molecular mechanisms of both miRNAs are rather complex and diverse and involve the deregulation of a multitude of both direct as well as indirect targets. For example, we discovered that miR-4646-5p has a broad effect on tumor-promoting cytokines, resulting in their reduced expression and secretion. MiR-4649-5p was also able to downregulate many oncogenic factors and seems to broadly affect metabolic and migratory processes. Due to the downregulation of its direct target PIP5K1C, which is known to play a role in cell migration, it also affects downstream PI3K/AKT signaling and thereby cell growth and proliferation. Based on this we were able to show that miR-4649-

5p overexpression potentiates the growth-reducing effects of the clinical AKT inhibitor capivasertib.

While both miRNAs showed promising tumor-suppressive effects *in vitro*, many of the effects were not very strongly pronounced and a therapeutic utility of the miR-4646-5p and miR-4649-5p mimic remains to be confirmed *in vivo*, as the *in vivo* experiments intended to be conducted as the final aim of the dissertation proved to be challenging due to technical and biological reasons. Even though a different choice of the mouse model may have achieved better results, it can be concluded that combinatorial treatments hold more potential than the single use of the miRNA mimics. Based on the impact of miR-4646-5p on cytokine secretion, which may be able to modulate the tumor microenvironment to boost anti-tumor immunity, combinations of the mimic with immune checkpoint inhibitors like anti-PD-L1 should be tested. For the miR-4649-5p mimic, which we could show to render TNBC cells more vulnerable to capivasertib, combinations with inhibitors targeting the PI3K/AKT signaling pathway appear promising.

6. References

1. Sung H, Ferlay J, Siegel RL, Laversanne M, Soerjomataram I, Jemal A, et al. Global Cancer Statistics 2020: GLOBOCAN Estimates of Incidence and Mortality Worldwide for 36 Cancers in 185 Countries. CA A Cancer J Clin. 2021 May;71(3):209–49.
2. Harbeck N, Penault-Llorca F, Cortes J, Gnant M, Houssami N, Poortmans P, et al. Breast cancer. Nat Rev Dis Primers. 2019 Sep 23;5(1):66.
3. Krebsneudiagnosen 2020 trotz auffälligem Rückgang im Frühjahr auf dem Niveau der Vorjahre [Internet]. Statistik Austria; 2023 Feb [cited 2023 Jul 10] p. 4. Report No.: 12 993-021/23. Available from: https://www.statistik.at/fileadmin/announcement/2023/02/20230202Krebs2023.pdf
4. Sims AH, Howell A, Howell SJ, Clarke RB. Origins of breast cancer subtypes and therapeutic implications. Nat Rev Clin Oncol. 2007 Sep;4(9):516–25.
5. Haybittle JL, Blamey RW, Elston CW, Johnson J, Doyle PJ, Campbell FC, et al. A prognostic index in primary breast cancer. Br J Cancer. 1982 Mar;45(3):361–6.
6. Jacobs AT, Martinez Castaneda-Cruz D, Rose MM, Connelly L. Targeted therapy for breast cancer: An overview of drug classes and outcomes. Biochemical Pharmacology. 2022 Oct;204:115209.
7. Yin L, Duan JJ, Bian XW, Yu S cang. Triple-negative breast cancer molecular subtyping and treatment progress. Breast Cancer Res. 2020 Dec;22(1):61.
8. Zagami P, Carey LA. Triple negative breast cancer: Pitfalls and progress. npj Breast Cancer. 2022 Aug 20;8(1):95.
9. He L, Wick N, Germans SK, Peng Y. The Role of Breast Cancer Stem Cells in Chemoresistance and Metastasis in Triple-Negative Breast Cancer. Cancers. 2021 Dec 9;13(24):6209.
10. Perou CM, Sørlie T, Eisen MB, Van De Rijn M, Jeffrey SS, Rees CA, et al. Molecular portraits of human breast tumours. Nature. 2000 Aug 17;406(6797):747–52.
11. Sørlie T, Perou CM, Tibshirani R, Aas T, Geisler S, Johnsen H, et al. Gene expression patterns of breast carcinomas distinguish tumor subclasses with clinical implications. Proc Natl Acad Sci USA. 2001 Sep 11;98(19):10869–74.
12. Goldhirsch A, Winer EP, Coates AS, Gelber RD, Piccart-Gebhart M, Thürlimann B, et al. Personalizing the treatment of women with early breast cancer: highlights of the St Gallen International Expert Consensus on the Primary Therapy of Early Breast Cancer 2013. Annals of Oncology. 2013 Sep;24(9):2206–23.
13. Prat A, Pineda E, Adamo B, Galván P, Fernández A, Gaba L, et al. Clinical implications of the intrinsic molecular subtypes of breast cancer. The Breast. 2015 Nov;24:S26–35.
14. Herschkowitz JI, Simin K, Weigman VJ, Mikaelian I, Usary J, Hu Z, et al. Identification of conserved gene expression features between murine mammary carcinoma models and human breast tumors. Genome Biol. 2007;8(5):R76.

15. Prat A, Parker JS, Karginova O, Fan C, Livasy C, Herschkowitz JI, et al. Phenotypic and molecular characterization of the claudin-low intrinsic subtype of breast cancer. Breast Cancer Res. 2010 Oct;12(5):R68.

16. Zhang Y, Weinberg RA. Epithelial-to-mesenchymal transition in cancer: complexity and opportunities. Front Med. 2018 Aug;12(4):361–73.

17. Parker JS, Mullins M, Cheang MCU, Leung S, Voduc D, Vickery T, et al. Supervised Risk Predictor of Breast Cancer Based on Intrinsic Subtypes. JCO. 2009 Mar 10;27(8):1160–7.

18. Griguolo G, Bottosso M, Vernaci G, Miglietta F, Dieci MV, Guarneri V. Gene-expression signatures to inform neoadjuvant treatment decision in HR+/HER2− breast cancer: Available evidence and clinical implications. Cancer Treatment Reviews. 2022 Jan;102:102323.

19. Paik S, Shak S, Tang G, Kim C, Baker J, Cronin M, et al. A Multigene Assay to Predict Recurrence of Tamoxifen-Treated, Node-Negative Breast Cancer. N Engl J Med. 2004 Dec 30;351(27):2817–26.

20. Gianni L, Zambetti M, Clark K, Baker J, Cronin M, Wu J, et al. Gene Expression Profiles in Paraffin-Embedded Core Biopsy Tissue Predict Response to Chemotherapy in Women With Locally Advanced Breast Cancer. JCO. 2005 Oct 10;23(29):7265–77.

21. Lehmann BD, Bauer JA, Chen X, Sanders ME, Chakravarthy AB, Shyr Y, et al. Identification of human triple-negative breast cancer subtypes and preclinical models for selection of targeted therapies. J Clin Invest. 2011 Jul 1;121(7):2750–67.

22. Burstein MD, Tsimelzon A, Poage GM, Covington KR, Contreras A, Fuqua SAW, et al. Comprehensive Genomic Analysis Identifies Novel Subtypes and Targets of Triple-Negative Breast Cancer. Clinical Cancer Research. 2015 Apr 1;21(7):1688–98.

23. Lehmann BD, Jovanović B, Chen X, Estrada MV, Johnson KN, Shyr Y, et al. Refinement of Triple-Negative Breast Cancer Molecular Subtypes: Implications for Neoadjuvant Chemotherapy Selection. Sapino A, editor. PLoS ONE. 2016 Jun 16;11(6):e0157368.

24. Echavarria I, López-Tarruella S, Picornell A, García-Saenz JÁ, Jerez Y, Hoadley K, et al. Pathological Response in a Triple-Negative Breast Cancer Cohort Treated with Neoadjuvant Carboplatin and Docetaxel According to Lehmann's Refined Classification. Clinical Cancer Research. 2018 Apr 15;24(8):1845–52.

25. Turner KM, Yeo SK, Holm TM, Shaughnessy E, Guan JL. Heterogeneity within molecular subtypes of breast cancer. American Journal of Physiology-Cell Physiology. 2021 Aug 1;321(2):C343–54.

26. Chung W, Eum HH, Lee HO, Lee KM, Lee HB, Kim KT, et al. Single-cell RNA-seq enables comprehensive tumour and immune cell profiling in primary breast cancer. Nat Commun. 2017 May 5;8(1):15081.

27. Zhou J, Chen Q, Zou Y, Chen H, Qi L, Chen Y. Stem Cells and Cellular Origins of Breast Cancer: Updates in the Rationale, Controversies, and Therapeutic Implications. Front Oncol. 2019 Aug 28;9:820.

28. Polyak K. Breast cancer: origins and evolution. J Clin Invest. 2007 Nov 1;117(11):3155–63.

29. Zhou J, Chen Q, Zou Y, Chen H, Qi L, Chen Y. Stem Cells and Cellular Origins of Breast Cancer: Updates in the Rationale, Controversies, and Therapeutic Implications. Front Oncol. 2019 Aug 28;9:820.

30. Nowell PC. The Clonal Evolution of Tumor Cell Populations: Acquired genetic lability permits stepwise selection of variant sublines and underlies tumor progression. Science. 1976 Oct;194(4260):23–8.

31. Visvader JE. Cells of origin in cancer. Nature. 2011 Jan;469(7330):314–22.

32. Visvader JE. Keeping abreast of the mammary epithelial hierarchy and breast tumorigenesis. Genes Dev. 2009 Nov 15;23(22):2563–77.

33. Al-Hajj M, Wicha MS, Benito-Hernandez A, Morrison SJ, Clarke MF. Prospective identification of tumorigenic breast cancer cells. Proc Natl Acad Sci USA. 2003 Apr;100(7):3983–8.

34. Ginestier C, Hur MH, Charafe-Jauffret E, Monville F, Dutcher J, Brown M, et al. ALDH1 Is a Marker of Normal and Malignant Human Mammary Stem Cells and a Predictor of Poor Clinical Outcome. Cell Stem Cell. 2007 Nov;1(5):555–67.

35. Charafe-Jauffret E, Ginestier C, Iovino F, Tarpin C, Diebel M, Esterni B, et al. Aldehyde Dehydrogenase 1–Positive Cancer Stem Cells Mediate Metastasis and Poor Clinical Outcome in Inflammatory Breast Cancer. Clinical Cancer Research. 2010 Jan 1;16(1):45–55.

36. Chae YC, Kim JH. Cancer stem cell metabolism: target for cancer therapy. BMB Rep. 2018 Jul 31;51(7):319–26.

37. Walsh HR, Cruickshank BM, Brown JM, Marcato P. The Flick of a Switch: Conferring Survival Advantage to Breast Cancer Stem Cells Through Metabolic Plasticity. Front Oncol. 2019 Aug 20;9:753.

38. Zeng X, Liu C, Yao J, Wan H, Wan G, Li Y, et al. Breast cancer stem cells, heterogeneity, targeting therapies and therapeutic implications. Pharmacological Research. 2021 Jan;163:105320.

39. Li H, Ma F, Wang H, Lin C, Fan Y, Zhang X, et al. Stem Cell Marker Aldehyde Dehydrogenase 1 (ALDH1)-Expressing Cells are Enriched in Triple-Negative Breast Cancer. Int J Biol Markers. 2013 Oct;28(4):357–64.

40. O'Conor CJ, Chen T, González I, Cao D, Peng Y. Cancer stem cells in triple-negative breast cancer: a potential target and prognostic marker. Biomarkers in Medicine. 2018 Jul;12(7):813–20.

41. Greaves M, Maley CC. Clonal evolution in cancer. Nature. 2012 Jan;481(7381):306–13.

42. Stratton MR, Rahman N. The emerging landscape of breast cancer susceptibility. Nat Genet. 2008 Jan;40(1):17–22.

43. Shiovitz S, Korde LA. Genetics of breast cancer: a topic in evolution. Annals of Oncology. 2015 Jul;26(7):1291–9.

44. Hall JM, Lee MK, Newman B, Morrow JE, Anderson LA, Huey B, et al. Linkage of Early-Onset Familial Breast Cancer to Chromosome 17q21. Science. 1990 Dec 21;250(4988):1684–9.

45. Miki Y, Swensen J, Shattuck-Eidens D, Futreal PA, Harshman K, Tavtigian S, et al. A Strong Candidate for the Breast and Ovarian Cancer Susceptibility Gene *BRCA1*. Science. 1994 Oct 7;266(5182):66–71.

46. Wooster R, Neuhausen SL, Mangion J, Quirk Y, Ford D, Collins N, et al. Localization of a Breast Cancer Susceptibility Gene, *BRCA2* , to Chromosome 13q12-13. Science. 1994 Sep 30;265(5181):2088–90.

47. Chen CC, Feng W, Lim PX, Kass EM, Jasin M. Homology-Directed Repair and the Role of BRCA1, BRCA2, and Related Proteins in Genome Integrity and Cancer. Annu Rev Cancer Biol. 2018 Mar 4;2(1):313–36.

48. King MC, Marks JH, Mandell JB. Breast and Ovarian Cancer Risks Due to Inherited Mutations in *BRCA1* and *BRCA2*. Science. 2003 Oct 24;302(5645):643–6.

49. Van Der Groep P, Van Der Wall E, Van Diest PJ. Pathology of hereditary breast cancer. Cell Oncol. 2011 Apr;34(2):71–88.

50. Schon K, Tischkowitz M. Clinical implications of germline mutations in breast cancer: TP53. Breast Cancer Res Treat. 2018 Jan;167(2):417–23.

51. Vogelstein B, Lane D, Levine AJ. Surfing the p53 network. Nature. 2000 Nov;408(6810):307–10.

52. Mai PL, Best AF, Peters JA, DeCastro RM, Khincha PP, Loud JT, et al. Risks of first and subsequent cancers among *TP53* mutation carriers in the National Cancer Institute Li-Fraumeni syndrome cohort: Cancer Risk in *TP53* Mutation Carriers. Cancer. 2016 Dec 1;122(23):3673–81.

53. Chai C, Wu HH, Abuetabh Y, Sergi C, Leng R. Regulation of the tumor suppressor PTEN in triple-negative breast cancer. Cancer Letters. 2022 Feb;527:41–8.

54. Tan MH, Mester JL, Ngeow J, Rybicki LA, Orloff MS, Eng C. Lifetime Cancer Risks in Individuals with Germline *PTEN* Mutations. Clinical Cancer Research. 2012 Jan 15;18(2):400–7.

55. The Cancer Genome Atlas Network. Comprehensive molecular portraits of human breast tumours. Nature. 2012 Oct;490(7418):61–70.

56. Santarpia L, Bottai G, Kelly CM, Győrffy B, Székely B, Pusztai L. Deciphering and Targeting Oncogenic Mutations and Pathways in Breast Cancer. The Oncologist. 2016 Sep 1;21(9):1063–78.

57. Chalhoub N, Baker SJ. PTEN and the PI3-Kinase Pathway in Cancer. Annu Rev Pathol Mech Dis. 2009 Feb 1;4(1):127–50.

58. Miricescu D, Totan A, Stanescu-Spinu II, Badoiu SC, Stefani C, Greabu M. PI3K/AKT/mTOR Signaling Pathway in Breast Cancer: From Molecular Landscape to Clinical Aspects. IJMS. 2020 Dec 26;22(1):173.

59. Stemke-Hale K, Gonzalez-Angulo AM, Lluch A, Neve RM, Kuo WL, Davies M, et al. An Integrative Genomic and Proteomic Analysis of PIK3CA, PTEN, and AKT Mutations in Breast Cancer. Cancer Research. 2008 Aug 1;68(15):6084–91.

60. Pham TT, Angus SP, Johnson GL. MAP3K1: Genomic Alterations in Cancer and Function in Promoting Cell Survival or Apoptosis. Genes & Cancer. 2013 Nov 1;4(11–12):419–26.

61. Eeckhoute J, Keeton EK, Lupien M, Krum SA, Carroll JS, Brown M. Positive Cross-Regulatory Loop Ties GATA-3 to Estrogen Receptor α Expression in Breast Cancer. Cancer Research. 2007 Jul 1;67(13):6477–83.

62. Piezzo M, Cocco S, Caputo R, Cianniello D, Gioia GD, Lauro VD, et al. Targeting Cell Cycle in Breast Cancer: CDK4/6 Inhibitors. IJMS. 2020 Sep 4;21(18):6479.

63. Zwijsen RML, Wientjens E, Klompmaker R, Van Der Sman J, Bernards R, Michalides RJAM. CDK-Independent Activation of Estrogen Receptor by Cyclin D1. Cell. 1997 Feb;88(3):405–15.

64. Sircoulomb F, Bekhouche I, Finetti P, Adélaïde J, Hamida AB, Bonansea J, et al. Genome profiling of ERBB2-amplified breast cancers. BMC Cancer. 2010 Dec;10(1):539.

65. Staaf J, Jönsson G, Ringnér M, Vallon-Christersson J, Grabau D, Arason A, et al. High-resolution genomic and expression analyses of copy number alterations in HER2-amplified breast cancer. Breast Cancer Res. 2010 Jun;12(3):R25.

66. Rodgers SJ, Ooms LM, Oorschot VMJ, Schittenhelm RB, Nguyen EV, Hamila SA, et al. INPP4B promotes PI3Kα-dependent late endosome formation and Wnt/β-catenin signaling in breast cancer. Nat Commun. 2021 May 25;12(1):3140.

67. Jiang YZ, Ma D, Suo C, Shi J, Xue M, Hu X, et al. Genomic and Transcriptomic Landscape of Triple-Negative Breast Cancers: Subtypes and Treatment Strategies. Cancer Cell. 2019 Mar;35(3):428-440.e5.

68. Beg S, Siraj AK, Prabhakaran S, Jehan Z, Ajarim D, Al-Dayel F, et al. Loss of PTEN expression is associated with aggressive behavior and poor prognosis in Middle Eastern triple-negative breast cancer. Breast Cancer Res Treat. 2015 Jun;151(3):541–53.

69. Dong C, Wu J, Chen Y, Nie J, Chen C. Activation of PI3K/AKT/mTOR Pathway Causes Drug Resistance in Breast Cancer. Front Pharmacol. 2021 Mar 15;12:628690.

70. Bareche Y, Venet D, Ignatiadis M, Aftimos P, Piccart M, Rothe F, et al. Unravelling triple-negative breast cancer molecular heterogeneity using an integrative multiomic analysis. Annals of Oncology. 2018 Apr;29(4):895–902.

71. Hanker AB, Sudhan DR, Arteaga CL. Overcoming Endocrine Resistance in Breast Cancer. Cancer Cell. 2020 Apr;37(4):496–513.

72. Barok M, Joensuu H, Isola J. Trastuzumab emtansine: mechanisms of action and drug resistance. Breast Cancer Res. 2014 Apr;16(2):3378.

73. Yin L, Duan JJ, Bian XW, Yu S cang. Triple-negative breast cancer molecular subtyping and treatment progress. Breast Cancer Res. 2020 Dec;22(1):61.

74. Turk AA, Wisinski KB. PARP inhibitors in breast cancer: Bringing synthetic lethality to the bedside: PARP Inhibition in BRCA-Mutant Breast CA. Cancer. 2018 Jun 15;124(12):2498–506.

75. Rottenberg S, Jaspers JE, Kersbergen A, Van Der Burg E, Nygren AOH, Zander SAL, et al. High sensitivity of BRCA1-deficient mammary tumors to the PARP inhibitor AZD2281 alone and in combination with platinum drugs. Proc Natl Acad Sci USA. 2008 Nov 4;105(44):17079–84.

76. Luo C, Wang P, He S, Zhu J, Shi Y, Wang J. Progress and Prospect of Immunotherapy for Triple-Negative Breast Cancer. Front Oncol. 2022 Jun 20;12:919072.

77. Zhang X, Ge X, Jiang T, Yang R, Li S. Research progress on immunotherapy in triple-negative breast cancer (Review). Int J Oncol. 2022 Jun 28;61(2):95.

78. Cao Y, Chen C, Tao Y, Lin W, Wang P. Immunotherapy for Triple-Negative Breast Cancer. Pharmaceutics. 2021 Nov 25;13(12):2003.

79. Bardia A, Hurvitz SA, Tolaney SM, Loirat D, Punie K, Oliveira M, et al. Sacituzumab Govitecan in Metastatic Triple-Negative Breast Cancer. N Engl J Med. 2021 Apr 22;384(16):1529–41.

80. Fuso P, Muratore M, D'Angelo T, Paris I, Carbognin L, Tiberi G, et al. PI3K Inhibitors in Advanced Breast Cancer: The Past, The Present, New Challenges and Future Perspectives. Cancers. 2022 Apr 26;14(9):2161.

81. Martorana F, Motta G, Pavone G, Motta L, Stella S, Vitale SR, et al. AKT Inhibitors: New Weapons in the Fight Against Breast Cancer? Front Pharmacol. 2021 Apr 29;12:662232.

82. Andrikopoulou A, Chatzinikolaou S, Panourgias E, Kaparelou M, Liontos M, Dimopoulos MA, et al. "The emerging role of capivasertib in breast cancer." The Breast. 2022 Jun;63:157–67.

83. Schmid P, Abraham J, Chan S, Wheatley D, Brunt AM, Nemsadze G, et al. Capivasertib Plus Paclitaxel Versus Placebo Plus Paclitaxel As First-Line Therapy for Metastatic Triple-Negative Breast Cancer: The PAKT Trial. JCO. 2020 Feb 10;38(5):423–33.

84. Anastasiadou E, Jacob LS, Slack FJ. Non-coding RNA networks in cancer. Nat Rev Cancer. 2018 Jan;18(1):5–18.

85. Johnson JM, Edwards S, Shoemaker D, Schadt EE. Dark matter in the genome: evidence of widespread transcription detected by microarray tiling experiments. Trends in Genetics. 2005 Feb;21(2):93–102.

86. Mattick JS, Makunin IV. Non-coding RNA. Human Molecular Genetics. 2006 Apr 15;15(suppl_1):R17–29.

87. Djebali S, Davis CA, Merkel A, Dobin A, Lassmann T, Mortazavi A, et al. Landscape of transcription in human cells. Nature. 2012 Sep;489(7414):101–8.

88. The FANTOM Consortium and the RIKEN Genome Exploration Research Group Phase I & II Team*. Analysis of the mouse transcriptome based on functional annotation of 60,770 full-length cDNAs. Nature. 2002 Dec;420(6915):563–73.

89. Mattick JS. Non-coding RNAs: the architects of eukaryotic complexity. EMBO Reports. 2001 Nov;2(11):986–91.

90. Ma L, Bajic VB, Zhang Z. On the classification of long non-coding RNAs. RNA Biology. 2013 Jun;10(6):924–33.

91. Derrien T, Johnson R, Bussotti G, Tanzer A, Djebali S, Tilgner H, et al. The GENCODE v7 catalog of human long noncoding RNAs: Analysis of their gene structure, evolution, and expression. Genome Res. 2012 Sep;22(9):1775–89.

92. Yao RW, Wang Y, Chen LL. Cellular functions of long noncoding RNAs. Nat Cell Biol. 2019 May;21(5):542–51.

93. Sandberg K, Samson WK, Ji H. Decoding Noncoding RNA: Da Vinci Redux? Circ Res. 2013 Jul 19;113(3):240–1.

94. Lee RC, Feinbaum RL, Ambros V. The C. elegans heterochronic gene lin-4 encodes small RNAs with antisense complementarity to lin-14. Cell. 1993 Dec;75(5):843–54.

95. Reinhart BJ, Slack FJ, Basson M, Pasquinelli AE, Bettinger JC, Rougvie AE, et al. The 21-nucleotide let-7 RNA regulates developmental timing in Caenorhabditis elegans. Nature. 2000 Feb;403(6772):901–6.

96. Ritchie W, Rasko JEJ, Flamant S. MicroRNA Target Prediction and Validation. In: Schmitz U, Wolkenhauer O, Vera J, editors. MicroRNA Cancer Regulation [Internet]. Dordrecht: Springer Netherlands; 2013 [cited 2023 Oct 20]. p. 39–53. (Advances in Experimental Medicine and Biology; vol. 774). Available from: https://link.springer.com/10.1007/978-94-007-5590-1_3

97. Pasquinelli AE, Reinhart BJ, Slack F, Martindale MQ, Kuroda MI, Maller B, et al. Conservation of the sequence and temporal expression of let-7 heterochronic regulatory RNA. Nature. 2000 Nov;408(6808):86–9.

98. Lagos-Quintana M, Rauhut R, Lendeckel W, Tuschl T. Identification of Novel Genes Coding for Small Expressed RNAs. Science. 2001 Oct 26;294(5543):853–8.

99. Lagos-Quintana M, Rauhut R, Yalcin A, Meyer J, Lendeckel W, Tuschl T. Identification of Tissue-Specific MicroRNAs from Mouse. Current Biology. 2002 Apr;12(9):735–9.

100. Kozomara A, Birgaoanu M, Griffiths-Jones S. miRBase: from microRNA sequences to function. Nucleic Acids Research. 2019 Jan 8;47(D1):D155–62.

101. Davis BN, Hata A. Regulation of MicroRNA Biogenesis: A miRiad of mechanisms. Cell Commun Signal. 2009 Dec;7(1):18.

102. Shang R, Lee S, Senavirathne G, Lai EC. microRNAs in action: biogenesis, function and regulation. Nat Rev Genet [Internet]. 2023 Jun 28 [cited 2023 Oct 16]; Available from: https://www.nature.com/articles/s41576-023-00611-y

103. Lee Y. MicroRNA maturation: stepwise processing and subcellular localization. The EMBO Journal. 2002 Sep 2;21(17):4663–70.

104. Lee Y, Ahn C, Han J, Choi H, Kim J, Yim J, et al. The nuclear RNase III Drosha initiates microRNA processing. Nature. 2003 Sep;425(6956):415–9.

105. Bohnsack MT, Czaplinski K, Görlich D. Exportin 5 is a RanGTP-dependent dsRNA-binding protein that mediates nuclear export of pre-miRNAs. RNA. 2004 Feb;10(2):185–91.

106. Hutvágner G, McLachlan J, Pasquinelli AE, Bálint É, Tuschl T, Zamore PD. A Cellular Function for the RNA-Interference Enzyme Dicer in the Maturation of the *let-7* Small Temporal RNA. Science. 2001 Aug 3;293(5531):834–8.

107. Treiber T, Treiber N, Meister G. Regulation of microRNA biogenesis and its crosstalk with other cellular pathways. Nat Rev Mol Cell Biol. 2019 Jan;20(1):5–20.

108. Gregory RI, Chendrimada TP, Cooch N, Shiekhattar R. Human RISC Couples MicroRNA Biogenesis and Posttranscriptional Gene Silencing. Cell. 2005 Nov;123(4):631–40.

109. Brodersen P, Voinnet O. Revisiting the principles of microRNA target recognition and mode of action. Nat Rev Mol Cell Biol. 2009 Feb;10(2):141–8.

110. Bartel DP. MicroRNAs: Target Recognition and Regulatory Functions. Cell. 2009 Jan;136(2):215–33.

111. Lytle JR, Yario TA, Steitz JA. Target mRNAs are repressed as efficiently by microRNA-binding sites in the 5′ UTR as in the 3′ UTR. Proc Natl Acad Sci USA. 2007 Jun 5;104(23):9667–72.

112. Forman JJ, Legesse-Miller A, Coller HA. A search for conserved sequences in coding regions reveals that the *let-7* microRNA targets Dicer within its coding sequence. Proc Natl Acad Sci USA. 2008 Sep 30;105(39):14879–84.

113. Schirle NT, Sheu-Gruttadauria J, Chandradoss SD, Joo C, MacRae IJ. Water-mediated recognition of t1-adenosine anchors Argonaute2 to microRNA targets. eLife. 2015 Sep 11;4:e07646.

114. Chu CY, Rana TM. Small RNAs: Regulators and guardians of the genome. J Cell Physiol. 2007 Nov;213(2):412–9.

115. Romano G, Veneziano D, Acunzo M, Croce CM. Small non-coding RNA and cancer. Carcinogenesis. 2017 May;38(5):485–91.

116. Meister G, Landthaler M, Patkaniowska A, Dorsett Y, Teng G, Tuschl T. Human Argonaute2 Mediates RNA Cleavage Targeted by miRNAs and siRNAs. Molecular Cell. 2004 Jul;15(2):185–97.

117. Kwak PB, Iwasaki S, Tomari Y. The microRNA pathway and cancer. Cancer Science. 2010 Nov;101(11):2309–15.

118. Olsen PH, Ambros V. The lin-4 Regulatory RNA Controls Developmental Timing in Caenorhabditis elegans by Blocking LIN-14 Protein Synthesis after the Initiation of Translation. Developmental Biology. 1999 Dec;216(2):671–80.

119. Gu S, Jin L, Zhang F, Sarnow P, Kay MA. Biological basis for restriction of microRNA targets to the 3′ untranslated region in mammalian mRNAs. Nat Struct Mol Biol. 2009 Feb;16(2):144–50.

120. Wu L, Fan J, Belasco JG. MicroRNAs direct rapid deadenylation of mRNA. Proc Natl Acad Sci USA. 2006 Mar 14;103(11):4034–9.

121. Ruby JG, Jan CH, Bartel DP. Intronic microRNA precursors that bypass Drosha processing. Nature. 2007 Jul;448(7149):83–6.

122. Zhang J, Li S, Li L, Li M, Guo C, Yao J, et al. Exosome and Exosomal MicroRNA: Trafficking, Sorting, and Function. Genomics, Proteomics & Bioinformatics. 2015 Feb;13(1):17–24.

123. Mathieu M, Martin-Jaular L, Lavieu G, Théry C. Specificities of secretion and uptake of exosomes and other extracellular vesicles for cell-to-cell communication. Nat Cell Biol. 2019 Jan;21(1):9–17.

124. Ingenito F, Roscigno G, Affinito A, Nuzzo S, Scognamiglio I, Quintavalle C, et al. The Role of Exo-miRNAs in Cancer: A Focus on Therapeutic and Diagnostic Applications. IJMS. 2019 Sep 21;20(19):4687.

125. Rupaimoole R, Calin GA, Lopez-Berestein G, Sood AK. miRNA Deregulation in Cancer Cells and the Tumor Microenvironment. Cancer Discovery. 2016 Mar 1;6(3):235–46.

126. Suzuki HI, Yamagata K, Sugimoto K, Iwamoto T, Kato S, Miyazono K. Modulation of microRNA processing by p53. Nature. 2009 Jul;460(7254):529–33.

127. Calin GA, Dumitru CD, Shimizu M, Bichi R, Zupo S, Noch E, et al. Frequent deletions and down-regulation of micro- RNA genes *miR15* and *miR16* at 13q14 in chronic lymphocytic leukemia. Proc Natl Acad Sci USA. 2002 Nov 26;99(24):15524–9.

128. Calin GA, Sevignani C, Dumitru CD, Hyslop T, Noch E, Yendamuri S, et al. Human microRNA genes are frequently located at fragile sites and genomic regions involved in cancers. Proc Natl Acad Sci USA. 2004 Mar 2;101(9):2999–3004.

129. Ma L, Teruya-Feldstein J, Weinberg RA. Tumour invasion and metastasis initiated by microRNA-10b in breast cancer. Nature. 2007 Oct 11;449(7163):682–8.

130. Ibrahim SA, Yip GW, Stock C, Pan J, Neubauer C, Poeter M, et al. Targeting of syndecan-1 by microRNA miR-10b promotes breast cancer cell motility and invasiveness *via* a Rho-GTPase- and E-cadherin-dependent mechanism. Intl Journal of Cancer [Internet]. 2012 Sep 15 [cited 2023 Oct 24];131(6). Available from: https://onlinelibrary.wiley.com/doi/10.1002/ijc.27629

131. Clayton NS, Ridley AJ. Targeting Rho GTPase Signaling Networks in Cancer. Front Cell Dev Biol. 2020 Apr 3;8:222.

132. Loh HY, Norman BP, Lai KS, Rahman NMANAbd, Alitheen NBM, Osman MA. The Regulatory Role of MicroRNAs in Breast Cancer. IJMS. 2019 Oct 6;20(19):4940.

133. Hanahan D, Weinberg RA. Hallmarks of Cancer: The Next Generation. Cell. 2011 Mar;144(5):646–74.

134. Bautista-Sánchez D, Arriaga-Canon C, Pedroza-Torres A, De La Rosa-Velázquez IA, González-Barrios R, Contreras-Espinosa L, et al. The Promising Role of miR-21 as a Cancer Biomarker and Its Importance in RNA-Based Therapeutics. Molecular Therapy - Nucleic Acids. 2020 Jun;20:409–20.

135. Chen J, Wang X. MicroRNA-21 in breast cancer: diagnostic and prognostic potential. Clin Transl Oncol. 2014 Mar;16(3):225–33.

136. Song B, Wang C, Liu J, Wang X, Lv L, Wei L, et al. MicroRNA-21 regulates breast cancer invasion partly by targeting tissue inhibitor of metalloproteinase 3 expression. J Exp Clin Cancer Res. 2010 Dec;29(1):29.

137. Fang H, Xie J, Zhang M, Zhao Z, Wan Y, Yao Y. miRNA-21 promotes proliferation and invasion of triple-negative breast cancer cells through targeting PTEN. Am J Transl Res. 2017;9(3):953–61.

138. Hilmarsdottir B, Briem E, Bergthorsson J, Magnusson M, Gudjonsson T. Functional Role of the microRNA-200 Family in Breast Morphogenesis and Neoplasia. Genes. 2014 Sep 11;5(3):804–20.

139. Castilla MÁ, Díaz-Martín J, Sarrió D, Romero-Pérez L, López-García MÁ, Vieites B, et al. MicroRNA-200 Family Modulation in Distinct Breast Cancer Phenotypes. Katz E, editor. PLoS ONE. 2012 Oct 24;7(10):e47709.

140. Pecot CV, Rupaimoole R, Yang D, Akbani R, Ivan C, Lu C, et al. Tumour angiogenesis regulation by the miR-200 family. Nat Commun. 2013 Sep 10;4(1):2427.

141. Sarrió D, Rodriguez-Pinilla SM, Hardisson D, Cano A, Moreno-Bueno G, Palacios J. Epithelial-Mesenchymal Transition in Breast Cancer Relates to the Basal-like Phenotype. Cancer Research. 2008 Feb 15;68(4):989–97.

142. Kohlhapp FJ, Mitra AK, Lengyel E, Peter ME. MicroRNAs as mediators and communicators between cancer cells and the tumor microenvironment. Oncogene. 2015 Nov;34(48):5857–68.

143. Wang J, Wang Q, Guan Y, Sun Y, Wang X, Lively K, et al. Breast cancer cell–derived microRNA-155 suppresses tumor progression via enhancing immune cell recruitment and antitumor function. Journal of Clinical Investigation. 2022 Oct 3;132(19):e157248.

144. Yang P, Cao X, Cai H, Chen X, Zhu Y, Yang Y, et al. Upregulation of microRNA-155 Enhanced Migration and Function of Dendritic Cells in Three-dimensional Breast Cancer Microenvironment. Immunological Investigations. 2021 Nov 17;50(8):1058–71.

145. Wang J, Iwanowycz S, Yu F, Jia X, Leng S, Wang Y, et al. microRNA-155 deficiency impairs dendritic cell function in breast cancer. OncoImmunology. 2016 Nov;5(11):e1232223.

146. Santos JC, Lima NDS, Sarian LO, Matheu A, Ribeiro ML, Derchain SFM. Exosome-mediated breast cancer chemoresistance via miR-155 transfer. Sci Rep. 2018 Jan 16;8(1):829.

147. Svoronos AA, Engelman DM, Slack FJ. OncomiR or Tumor Suppressor? The Duplicity of MicroRNAs in Cancer. Cancer Research. 2016 Jul 1;76(13):3666–70.

148. Mattiske S, Suetani RJ, Neilsen PM, Callen DF. The Oncogenic Role of miR-155 in Breast Cancer. Cancer Epidemiology, Biomarkers & Prevention. 2012 Aug 1;21(8):1236–43.

149. Wang J. Role of miR-155 in breast cancer. Front Biosci. 2012;17(7):2350.

150. Ma J hui, Qin L, Li X. Role of STAT3 signaling pathway in breast cancer. Cell Commun Signal. 2020 Dec;18(1):33.

151. Kara G, Arun B, Calin GA, Ozpolat B. miRacle of microRNA-Driven Cancer Nanotherapeutics. Cancers. 2022 Aug 6;14(15):3818.

152. Ho PTB, Clark IM, Le LTT. MicroRNA-Based Diagnosis and Therapy. IJMS. 2022 Jun 28;23(13):7167.

153. Kahraman M, Röske A, Laufer T, Fehlmann T, Backes C, Kern F, et al. MicroRNA in diagnosis and therapy monitoring of early-stage triple-negative breast cancer. Sci Rep. 2018 Aug 2;8(1):11584.

154. Gasparini P, Cascione L, Fassan M, Lovat F, Guler G, Balci S, et al. microRNA expression profiling identifies a four microRNA signature as a novel diagnostic and prognostic biomarker in triple negative breast cancers. Oncotarget. 2014 Mar 15;5(5):1174–84.

155. Holjencin C, Jakymiw A. MicroRNAs and Their Big Therapeutic Impacts: Delivery Strategies for Cancer Intervention. Cells. 2022 Jul 29;11(15):2332.

156. Beg MS, Brenner AJ, Sachdev J, Borad M, Kang YK, Stoudemire J, et al. Phase I study of MRX34, a liposomal miR-34a mimic, administered twice weekly in patients with advanced solid tumors. Invest New Drugs. 2017 Apr;35(2):180–8.

157. Hong DS, Kang YK, Borad M, Sachdev J, Ejadi S, Lim HY, et al. Phase 1 study of MRX34, a liposomal miR-34a mimic, in patients with advanced solid tumours. Br J Cancer. 2020 May 26;122(11):1630–7.

158. Chen Y, Gao DY, Huang L. In vivo delivery of miRNAs for cancer therapy: Challenges and strategies. Advanced Drug Delivery Reviews. 2015 Jan;81:128–41.

159. Sharma S, Pukale S, Sahel DK, Singh P, Mittal A, Chitkara D. Folate targeted hybrid lipo-polymeric nanoplexes containing docetaxel and miRNA-34a for breast cancer treatment. Materials Science and Engineering: C. 2021 Sep;128:112305.

160. Wang S, Zhang J, Wang Y, Chen M. Hyaluronic acid-coated PEI-PLGA nanoparticles mediated co-delivery of doxorubicin and miR-542-3p for triple negative breast cancer therapy. Nanomedicine: Nanotechnology, Biology and Medicine. 2016 Feb;12(2):411–20.

161. Kotecki N, Opdam F, Robbrecht D, Strijbos M, Kroon K, Janicot M, et al. Phase I/Ib study with INT-1B3, a novel LNP-formulated micro-RNA (miR-193a-3p mimic) therapeutic for patients with advanced solid cancer. JCO. 2021 May 20;39(15_suppl):TPS2666–TPS2666.

162. Kim T, Croce CM. MicroRNA: trends in clinical trials of cancer diagnosis and therapy strategies. Exp Mol Med. 2023 Jul 10;55(7):1314–21.

163. Schwarzenbacher D, Klec C, Pasculli B, Cerk S, Rinner B, Karbiener M, et al. MiR-1287-5p inhibits triple negative breast cancer growth by interaction with phosphoinositide 3-kinase CB, thereby sensitizing cells for PI3Kinase inhibitors. Breast Cancer Res. 2019 Dec;21(1):20.

164. Dontu G. In vitro propagation and transcriptional profiling of human mammary stem/progenitor cells. Genes & Development. 2003 May 15;17(10):1253–70.

165. Zeng X, Liu C, Yao J, Wan H, Wan G, Li Y, et al. Breast cancer stem cells, heterogeneity, targeting therapies and therapeutic implications. Pharmacological Research. 2021 Jan;163:105320.

166. Wu L, Li Y, Li J, Ma D. MicroRNA-664 Targets Insulin Receptor Substrate 1 to Suppress Cell Proliferation and Invasion in Breast Cancer. oncol res. 2019 Mar 29;27(4):459–67.

167. Milevskiy MJG, Sandhu GK, Wronski A, Korbie D, Brewster BL, Shewan A, et al. MiR-29b-1-5p is altered in BRCA1 mutant tumours and is a biomarker in basal-like breast cancer. Oncotarget. 2018 Sep 11;9(71):33577–88.

168. Lánczky A, Nagy Á, Bottai G, Munkácsy G, Szabó A, Santarpia L, et al. miRpower: a web-tool to validate survival-associated miRNAs utilizing expression data from 2178 breast cancer patients. Breast Cancer Res Treat. 2016 Dec;160(3):439–46.

169. Győrffy B. Survival analysis across the entire transcriptome identifies biomarkers with the highest prognostic power in breast cancer. Computational and Structural Biotechnology Journal. 2021;19:4101–9.

170. Ősz Á, Lánczky A, Győrffy B. Survival analysis in breast cancer using proteomic data from four independent datasets. Sci Rep. 2021 Aug 18;11(1):16787.

171. Bartha Á, Győrffy B. TNMplot.com: A Web Tool for the Comparison of Gene Expression in Normal, Tumor and Metastatic Tissues. IJMS. 2021 Mar 5;22(5):2622.

172. Tan, Poh, Lee, Tracey. Technical Bulletin - Idenitification of ALDH-Expressing Cancer Stem Cells [Internet]. STEMCELL Technologies; 2009. Available from: https://www.stemcell.com/identification-aldh-expressing-cancer-stem-cells-using-aldefluor-lp.html

173. Carpentier G, Berndt S, Ferratge S, Rasband W, Cuendet M, Uzan G, et al. Angiogenesis Analyzer for ImageJ — A comparative morphometric analysis of "Endothelial Tube Formation Assay" and "Fibrin Bead Assay." Sci Rep. 2020 Jul 14;10(1):11568.

174. Agarwal V, Bell GW, Nam JW, Bartel DP. Predicting effective microRNA target sites in mammalian mRNAs. eLife. 2015 Aug 12;4:e05005.

175. Dweep H, Gretz N. miRWalk2.0: a comprehensive atlas of microRNA-target interactions. Nat Methods. 2015 Aug;12(8):697–697.

176. Chen Y, Wang X. miRDB: an online database for prediction of functional microRNA targets. Nucleic Acids Research. 2020 Jan 8;48(D1):D127–31.

177. Kent WJ, Sugnet CW, Furey TS, Roskin KM, Pringle TH, Zahler AM, et al. The Human Genome Browser at UCSC. Genome Res. 2002 Jun 1;12(6):996–1006.

178. Xu J, Gu W, Ji K, Xu Z, Zhu H, Zheng W. Sequence analysis and structure prediction of ABHD16A and the roles of the ABHD family members in human disease. Open Biol. 2018 May;8(5):180017.

179. Yahia A, Elsayed LEO, Valter R, Hamed AAA, Mohammed IN, Elseed MA, et al. Pathogenic Variants in ABHD16A Cause a Novel Psychomotor Developmental Disorder With Spastic Paraplegia. Front Neurol. 2021 Aug 20;12:720201.

180. Kamat SS, Camara K, Parsons WH, Chen DH, Dix MM, Bird TD, et al. Immunomodulatory lysophosphatidylserines are regulated by ABHD16A and ABHD12 interplay. Nat Chem Biol. 2015 Feb;11(2):164–71.

181. Majdalawieh AF, Massri M, Ro HS. AEBP1 is a Novel Oncogene: Mechanisms of Action and Signaling Pathways. Journal of Oncology. 2020 May 27;2020:1–20.

182. Li J, Ruan Y, Zheng C, Pan Y, Lin B, Chen Q, et al. AEBP1 Contributes to Breast Cancer Progression by Facilitating Cell Proliferation, Migration, Invasion, and Blocking Apoptosis. Discovery Medicine. 2023;35(174):45.

183. Sun Y, Ji F, Kumar MR, Zheng X, Xiao Y, Liu N, et al. Transcriptome integration analysis in hepatocellular carcinoma reveals discordant intronic miRNA-host gene pairs in expression. Int J Biol Sci. 2017;13(11):1438–49.

184. Li JH, Liu S, Zhou H, Qu LH, Yang JH. starBase v2.0: decoding miRNA-ceRNA, miRNA-ncRNA and protein–RNA interaction networks from large-scale CLIP-Seq data. Nucl Acids Res. 2014 Jan;42(D1):D92–7.

185. Xie B, Ding Q, Han H, Wu D. miRCancer: a microRNA–cancer association database constructed by text mining on literature. Bioinformatics. 2013 Mar 1;29(5):638–44.

186. Torres AG, Fabani MM, Vigorito E, Gait MJ. MicroRNA fate upon targeting with anti-miRNA oligonucleotides as revealed by an improved Northern-blot-based method for miRNA detection. RNA. 2011 May;17(5):933–43.

187. Sherf, Bruce A., Navarro, Shauna L., Hannah, Rita R., Wood, Keith V. Dual-LuciferaseTM Reporter Assay: An Advanced Co-Reporter Technology Integrating Firefly and Renilla Luciferase Assays. Promega Notes. 1996;57:2–9.

188. Clément T, Salone V, Rederstorff M. Dual Luciferase Gene Reporter Assays to Study miRNA Function. In: Rederstorff M, editor. Small Non-Coding RNAs [Internet]. New York, NY: Springer New York; 2015 [cited 2023 Nov 3]. p. 187–98. (Methods in Molecular Biology; vol. 1296). Available from: https://link.springer.com/10.1007/978-1-4939-2547-6_17

189. Taylor SC, Laperriere G, Germain H. Droplet Digital PCR versus qPCR for gene expression analysis with low abundant targets: from variable nonsense to publication quality data. Sci Rep. 2017 May 25;7(1):2409.

190. Roche. Product Information Sheet Cell Proliferation Reagent WST-1. Sigma-Aldrich; 2021.

191. Lamkanfi M, Kanneganti TD. Caspase-7: A protease involved in apoptosis and inflammation. The International Journal of Biochemistry & Cell Biology. 2010 Jan;42(1):21–4.

192. Friedl P, Wolf K. Tumour-cell invasion and migration: diversity and escape mechanisms. Nat Rev Cancer. 2003 May;3(5):362–74.

193. Ginestier C, Hur MH, Charafe-Jauffret E, Monville F, Dutcher J, Brown M, et al. ALDH1 Is a Marker of Normal and Malignant Human Mammary Stem Cells and a Predictor of Poor Clinical Outcome. Cell Stem Cell. 2007 Nov;1(5):555–67.

194. Arnaoutova I, George J, Kleinman HK, Benton G. The endothelial cell tube formation assay on basement membrane turns 20: state of the science and the art. Angiogenesis. 2009 Sep;12(3):267–74.

195. Carpentier G, Berndt S, Ferratge S, Rasband W, Cuendet M, Uzan G, et al. Angiogenesis Analyzer for ImageJ — A comparative morphometric analysis of “Endothelial Tube Formation Assay” and “Fibrin Bead Assay.” Sci Rep. 2020 Jul 14;10(1):11568.

196. Presta M, Rusnati M, Dell’Era P, Tanghetti E, Urbinati C, Giuliani R, et al. Examining New Models for the Study of Autocrine and Paracrine Mechanisms of Angiogenesis Through FGF2-Transfected Endothelial and Tumour Cells. In: Maragoudakis ME, editor. Angiogenesis [Internet]. Boston, MA: Springer US; 2000 [cited 2023 Nov 7]. p. 7–34. (Advances in Experimental Medicine and Biology; vol. 476). Available from: http://link.springer.com/10.1007/978-1-4615-4221-6_2

197. Zegeye MM, Andersson B, Sirsjö A, Ljungberg LU. IL-6 trans-Signaling Impairs Sprouting Angiogenesis by Inhibiting Migration, Proliferation and Tube Formation of Human Endothelial Cells. Cells. 2020 Jun 5;9(6):1414.

198. Geretti E, Shimizu A, Klagsbrun M. Neuropilin structure governs VEGF and semaphorin binding and regulates angiogenesis. Angiogenesis. 2008 Mar;11(1):31–9.

199. Naito T, Saheki Y. GRAMD1-mediated accessible cholesterol sensing and transport. Biochimica et Biophysica Acta (BBA) - Molecular and Cell Biology of Lipids. 2021 Aug;1866(8):158957.

200. Ercan B, Naito T, Koh DHZ, Dharmawan D, Saheki Y. Molecular basis of accessible plasma membrane cholesterol recognition by the GRAM domain of GRAMD1b. The EMBO Journal. 2021 Mar 15;40(6):e106524.

201. Naito T, Ercan B, Krshnan L, Triebl A, Koh DHZ, Wei FY, et al. Movement of accessible plasma membrane cholesterol by the GRAMD1 lipid transfer protein complex. eLife. 2019 Nov 14;8:e51401.

202. Sandhu J, Li S, Fairall L, Pfisterer SG, Gurnett JE, Xiao X, et al. Aster Proteins Facilitate Nonvesicular Plasma Membrane to ER Cholesterol Transport in Mammalian Cells. Cell. 2018 Oct;175(2):514-529.e20.

203. Wu SY, Yang X, Gharpure KM, Hatakeyama H, Egli M, McGuire MH, et al. 2′-OMe-phosphorodithioate-modified siRNAs show increased loading into the RISC complex and enhanced anti-tumour activity. Nat Commun. 2014 Mar 12;5(1):3459.

204. Khanna P, Chua PJ, Wong BSE, Yin C, Thike AA, Wan WK, et al. GRAM domain-containing protein 1B (GRAMD1B), a novel component of the JAK/STAT signaling pathway, functions in gastric carcinogenesis. Oncotarget. 2017 Dec 29;8(70):115370–83.

205. Khanna P, Lee JS, Sereemaspun A, Lee H, Baeg GH. GRAMD1B regulates cell migration in breast cancer cells through JAK/STAT and Akt signaling. Sci Rep. 2018 Jun 22;8(1):9511.

206. Nozaki S, Sledge GW, Nakshatri H. Cancer Cell-Derived Interleukin 1α Contributes to Autocrine and Paracrine Induction of Pro-metastatic Genes in Breast Cancer. Biochemical and Biophysical Research Communications. 2000 Aug;275(1):60–2.

207. Hao M, Huang B, Wu R, Peng Z, Luo KQ. The Interaction between Macrophages and Triple-negative Breast Cancer Cells Induces ROS-Mediated Interleukin 1α Expression to Enhance Tumorigenesis and Metastasis. Advanced Science. 2023 Oct;10(29):2302857.

208. Tulotta C, Lefley DV, Freeman K, Gregory WM, Hanby AM, Heath PR, et al. Endogenous Production of IL1B by Breast Cancer Cells Drives Metastasis and Colonization of the Bone Microenvironment. Clinical Cancer Research. 2019 May 1;25(9):2769–82.

209. Masjedi A, Hashemi V, Hojjat-Farsangi M, Ghalamfarsa G, Azizi G, Yousefi M, et al. The significant role of interleukin-6 and its signaling pathway in the immunopathogenesis and treatment of breast cancer. Biomedicine & Pharmacotherapy. 2018 Dec;108:1415–24.

210. Korkaya H, Kim G il, Davis A, Malik F, Henry NL, Ithimakin S, et al. Activation of an IL6 Inflammatory Loop Mediates Trastuzumab Resistance in HER2+ Breast Cancer by Expanding the Cancer Stem Cell Population. Molecular Cell. 2012 Aug;47(4):570–84.

211. Johnson DE, O'Keefe RA, Grandis JR. Targeting the IL-6/JAK/STAT3 signalling axis in cancer. Nat Rev Clin Oncol. 2018 Apr;15(4):234–48.

212. Zhao CL, Zhang GP, Xiao ZZ, Ma ZK, Lei CP, Song SY, et al. Recombinant Human Granulocyte Colony-Stimulating Factor Promotes Preinvasive and Invasive Estrogen Receptor-Positive Tumor Development in MMTV-erbB2 Mice. J Breast Cancer. 2015;18(2):126.

213. Waight JD, Hu Q, Miller A, Liu S, Abrams SI. Tumor-Derived G-CSF Facilitates Neoplastic Growth through a Granulocytic Myeloid-Derived Suppressor Cell-Dependent Mechanism. Blagosklonny MV, editor. PLoS ONE. 2011 Nov 16;6(11):e27690.

214. Hollmén M, Karaman S, Schwager S, Lisibach A, Christiansen AJ, Maksimow M, et al. G-CSF regulates macrophage phenotype and associates with poor overall survival in human triple-negative breast cancer. OncoImmunology. 2016 Mar 3;5(3):e1115177.

215. Kwantwi LB, Wang S, Sheng Y, Wu Q. Multifaceted roles of CCL20 (C-C motif chemokine ligand 20): mechanisms and communication networks in breast cancer progression. Bioengineered. 2021 Jan 1;12(1):6923–34.

216. Yang C, Yu H, Chen R, Tao K, Jian L, Peng M, et al. CXCL1 stimulates migration and invasion in ER-negative breast cancer cells via activation of the ERK/MMP2/9 signaling axis. Int J Oncol [Internet]. 2019 Jul 15 [cited 2023 Nov 9]; Available from: http://www.spandidos-publications.com/10.3892/ijo.2019.4840

217. Ciummo SL, D'Antonio L, Sorrentino C, Fieni C, Lanuti P, Stassi G, et al. The C-X-C Motif Chemokine Ligand 1 Sustains Breast Cancer Stem Cell Self-Renewal and Promotes Tumor Progression and Immune Escape Programs. Front Cell Dev Biol. 2021 Jun 14;9:689286.

218. Su X, Xu Y, Fox GC, Xiang J, Kwakwa KA, Davis JL, et al. Breast cancer–derived GM-CSF regulates arginase 1 in myeloid cells to promote an immunosuppressive microenvironment. Journal of Clinical Investigation. 2021 Oct 15;131(20):e145296.

219. See A, Chong P, Lu SY, Lim Y. CXCL3 is a Potential Target for Breast Cancer Metastasis. CCDT. 2014 Apr 31;14(3):294–309.

220. He X, Wang L, Li H, Liu Y, Tong C, Xie C, et al. CSF2 upregulates CXCL3 expression in adipocytes to promote metastasis of breast cancer via the FAK signaling pathway. Journal of Molecular Cell Biology. 2023 Apr 18;mjad025.

221. Trop-Steinberg S, Azar Y. AP-1 Expression and its Clinical Relevance in Immune Disorders and Cancer. The American Journal of the Medical Sciences. 2017 May;353(5):474–83.

222. Wang B, Guo H, Yu H, Chen Y, Xu H, Zhao G. The Role of the Transcription Factor EGR1 in Cancer. Front Oncol. 2021 Mar 24;11:642547.

223. Macián F, López-Rodríguez C, Rao A. Partners in transcription: NFAT and AP-1. Oncogene. 2001 Apr 30;20(19):2476–89.

224. Xiao W, Hodge DR, Wang L, Yang X, Zhang X, Farrar WL. NF-kappaB activates IL-6 expression through cooperation with c-Jun and IL6-AP1 site, But is independent of its IL6-NFkappaB regulatory

site in autocrine human multiple myeloma cells. Cancer Biology & Therapy. 2004 Oct;3(10):1007–17.

225. Porciello N, Kunkl M, Viola A, Tuosto L. Phosphatidylinositol 4-Phosphate 5-Kinases in the Regulation of T Cell Activation. Front Immunol [Internet]. 2016 May 13 [cited 2023 Nov 16];7. Available from: http://journal.frontiersin.org/Article/10.3389/fimmu.2016.00186/abstract

226. Kanaho Y, Kobayashi-Nakano A, Yokozeki T. The Phosphoinositide Kinase PIP5K That Produces the Versatile Signaling Phospholipid PI4,5P2. Biological & Pharmaceutical Bulletin. 2007;30(9):1605–9.

227. Mandal K. Review of PIP2 in Cellular Signaling, Functions and Diseases. IJMS. 2020 Nov 6;21(21):8342.

228. Ling K, Schill NJ, Wagoner MP, Sun Y, Anderson RA. Movin' on up: the role of PtdIns(4,5)P2 in cell migration. Trends in Cell Biology. 2006 Jun;16(6):276–84.

229. Engelman JA, Luo J, Cantley LC. The evolution of phosphatidylinositol 3-kinases as regulators of growth and metabolism. Nat Rev Genet. 2006 Aug;7(8):606–19.

230. Peng JM, Lin SH, Yu MC, Hsieh SY. CLIC1 recruits PIP5K1A/C to induce cell-matrix adhesions for tumor metastasis. Journal of Clinical Investigation. 2021 Jan 4;131(1):e133525.

231. Li X, Zhou Q, Sunkara M, Kutys ML, Wu Z, Rychahou P, et al. Ubiquitination of PIPKIγ90 by HECTD1 regulates focal adhesion dynamics and cell migration. Journal of Cell Science. 2013 Jan 1;jcs.117044.

232. Sun Y, Turbin DA, Ling K, Thapa N, Leung S, Huntsman DG, et al. Type I gamma phosphatidylinositol phosphate kinase modulates invasion and proliferation and its expression correlates with poor prognosis in breast cancer. Breast Cancer Res. 2010 Feb;12(1):R6.

233. Wright BD, Loo L, Street SE, Ma A, Taylor-Blake B, Stashko MA, et al. The Lipid Kinase PIP5K1C Regulates Pain Signaling and Sensitization. Neuron. 2014 May;82(4):836–47.

234. Vara JÁF, Casado E, De Castro J, Cejas P, Belda-Iniesta C, González-Barón M. PI3K/Akt signalling pathway and cancer. Cancer Treatment Reviews. 2004 Apr;30(2):193–204.

235. Li H, Prever L, Hirsch E, Gulluni F. Targeting PI3K/AKT/mTOR Signaling Pathway in Breast Cancer. Cancers. 2021 Jul 14;13(14):3517.

236. Shi XB, Ma AH, Xue L, Li M, Nguyen HG, Yang JC, et al. miR-124 and Androgen Receptor Signaling Inhibitors Repress Prostate Cancer Growth by Downregulating Androgen Receptor Splice Variants, EZH2, and Src. Cancer Research. 2015 Dec 15;75(24):5309–17.

237. Hsu YL, Huang MS, Hung JY, Chang WA, Tsai YM, Pan YC, et al. Bone-marrow-derived cell-released extracellular vesicle miR-92a regulates hepatic pre-metastatic niche in lung cancer. Oncogene. 2020 Jan 23;39(4):739–53.

238. Zhao Y, Tu MJ, Wang WP, Qiu JX, Yu AX, Yu AM. Genetically engineered pre-microRNA-34a prodrug suppresses orthotopic osteosarcoma xenograft tumor growth via the induction of apoptosis and cell cycle arrest. Sci Rep. 2016 May 24;6(1):26611.

239. Shultz LD, Ishikawa F, Greiner DL. Humanized mice in translational biomedical research. Nat Rev Immunol. 2007 Feb;7(2):118–30.

240. Erhard F, Haas J, Lieber D, Malterer G, Jaskiewicz L, Zavolan M, et al. Widespread context dependency of microRNA-mediated regulation. Genome Res. 2014 Jun;24(6):906–19.

241. Hollestelle A, Nagel JHA, Smid M, Lam S, Elstrodt F, Wasielewski M, et al. Distinct gene mutation profiles among luminal-type and basal-type breast cancer cell lines. Breast Cancer Res Treat. 2010 May;121(1):53–64.

242. Hodge RG, Ridley AJ. Regulating Rho GTPases and their regulators. Nat Rev Mol Cell Biol. 2016 Aug;17(8):496–510.

243. Clayton NS, Ridley AJ. Targeting Rho GTPase Signaling Networks in Cancer. Front Cell Dev Biol. 2020 Apr 3;8:222.

244. Han, Jian-Jun, Du, Bo-Rong, Zhang, Cui-Huan. Bioinformatic analysis of prognostic value of ARAP3 in breast cancer and the associated signaling pathways. Eur Rev Med Pharmacol Sci. 2017;21(10):2405–12.

245. Wang QX, Chen ED, Cai YF, Zhou YL, Zheng ZC, Wang YH, et al. Next-generation sequence detects ARAP3 as a novel oncogene in papillary thyroid carcinoma. OTT. 2016 Nov;Volume 9:7161–7.

246. Cao J, Yang T, Tang D, Zhou F, Qian Y, Zou X. Increased expression of GEF-H1 promotes colon cancer progression by RhoA signaling. Pathology - Research and Practice. 2019 May;215(5):1012–9.

247. Kent OA, Sandí MJ, Burston HE, Brown KR, Rottapel R. An oncogenic KRAS transcription program activates the RHOGEF *ARHGEF2* to mediate transformed phenotypes in pancreatic cancer. Oncotarget. 2017 Jan 17;8(3):4484–500.

248. Nakao Y, Nakagawa S, Yamashita Y ichi, Umezaki N, Okamoto Y, Ogata Y, et al. High ARHGEF2 (GEF-H1) Expression is Associated with Poor Prognosis Via Cell Cycle Regulation in Patients with Pancreatic Cancer. Ann Surg Oncol. 2021 Aug;28(8):4733–43.

249. Gupta M, Kamynina E, Morley S, Chung S, Muakkassa N, Wang H, et al. Plekhg4 Is a Novel Dbl Family Guanine Nucleotide Exchange Factor Protein for Rho Family GTPases. Journal of Biological Chemistry. 2013 May;288(20):14522–30.

250. Wang Q, Lv L, Tang Y, Zhang L, Wang L. MMP-1 is overexpressed in triple-negative breast cancer tissues and the knockdown of MMP-1 expression inhibits tumor cell malignant behaviors in vitro. Oncol Lett [Internet]. 2018 Nov 30 [cited 2023 Dec 2]; Available from: http://www.spandidos-publications.com/10.3892/ol.2018.9779

251. Lim JP, Nair S, Shyamasundar S, Chua PJ, Muniasamy U, Matsumoto K, et al. Silencing Y-box binding protein-1 inhibits triple-negative breast cancer cell invasiveness via regulation of MMP1 and beta-catenin expression. Cancer Letters. 2019 Jun;452:119–31.

252. Marcato P, Dean CA, Pan D, Araslanova R, Gillis M, Joshi M, et al. Aldehyde Dehydrogenase Activity of Breast Cancer Stem Cells Is Primarily Due To Isoform ALDH1A3 and Its Expression Is Predictive of Metastasis. Stem Cells. 2011 Jan 1;29(1):32–45.

253. Raha D, Wilson TR, Peng J, Peterson D, Yue P, Evangelista M, et al. The Cancer Stem Cell Marker Aldehyde Dehydrogenase Is Required to Maintain a Drug-Tolerant Tumor Cell Subpopulation. Cancer Research. 2014 Jul 1;74(13):3579–90.

254. Zhao D, Mo Y, Li MT, Zou SW, Cheng ZL, Sun YP, et al. NOTCH-induced aldehyde dehydrogenase 1A1 deacetylation promotes breast cancer stem cells. J Clin Invest. 2014 Dec 1;124(12):5453–65.

255. Chambers AF, Groom AC, MacDonald IC. Dissemination and growth of cancer cells in metastatic sites. Nat Rev Cancer. 2002 Aug 1;2(8):563–72.

256. Banerjee S, Dowsett M, Ashworth A, Martin LA. Mechanisms of Disease: angiogenesis and the management of breast cancer. Nat Rev Clin Oncol. 2007 Sep;4(9):536–50.

257. Guerra A, Belinha J, Mangir N, MacNeil S, Natal Jorge R. Simulation of the process of angiogenesis: Quantification and assessment of vascular patterning in the chicken chorioallantoic membrane. Computers in Biology and Medicine. 2021 Sep;136:104647.

258. Staton CA, Reed MWR, Brown NJ. A critical analysis of current *in vitro* and *in vivo* angiogenesis assays. Int J Experimental Path. 2009 Jun;90(3):195–221.

259. Ferrari A, He C, Kennelly JP, Sandhu J, Xiao X, Chi X, et al. Aster Proteins Regulate the Accessible Cholesterol Pool in the Plasma Membrane. Molecular and Cellular Biology. 2020 Sep 14;40(19):e00255-20.

260. Eberlé D, Hegarty B, Bossard P, Ferré P, Foufelle F. SREBP transcription factors: master regulators of lipid homeostasis. Biochimie. 2004 Nov;86(11):839–48.

261. Infante RE, Radhakrishnan A. Continuous transport of a small fraction of plasma membrane cholesterol to endoplasmic reticulum regulates total cellular cholesterol. eLife. 2017 Apr 17;6:e25466.

262. Huang B, Song B liang, Xu C. Cholesterol metabolism in cancer: mechanisms and therapeutic opportunities. Nat Metab. 2020 Feb 10;2(2):132–41.

263. Voisin M, De Medina P, Mallinger A, Dalenc F, Huc-Claustre E, Leignadier J, et al. Identification of a tumor-promoter cholesterol metabolite in human breast cancers acting through the glucocorticoid receptor. Proc Natl Acad Sci USA [Internet]. 2017 Oct 31 [cited 2023 Dec 4];114(44). Available from: https://pnas.org/doi/full/10.1073/pnas.1707965114

264. Raza S, Ohm JE, Dhasarathy A, Schommer J, Roche C, Hammer KDP, et al. The cholesterol metabolite 27-hydroxycholesterol regulates p53 activity and increases cell proliferation via MDM2 in breast cancer cells. Mol Cell Biochem. 2015 Dec;410(1–2):187–95.

265. Shen Z, Zhu D, Liu J, Chen J, Liu Y, Hu C, et al. 27-Hydroxycholesterol induces invasion and migration of breast cancer cells by increasing MMP9 and generating EMT through activation of STAT-3. Environmental Toxicology and Pharmacology. 2017 Apr;51:1–8.

266. Zhu D, Shen Z, Liu J, Chen J, Liu Y, Hu C, et al. The ROS-mediated activation of STAT-3/VEGF signaling is involved in the 27-hydroxycholesterol-induced angiogenesis in human breast cancer cells. Toxicology Letters. 2016 Dec;264:79–86.

267. Luo J, Jiang LY, Yang H, Song BL. Intracellular Cholesterol Transport by Sterol Transfer Proteins at Membrane Contact Sites. Trends in Biochemical Sciences. 2019 Mar;44(3):273–92.

268. Höglinger D, Burgoyne T, Sanchez-Heras E, Hartwig P, Colaco A, Newton J, et al. NPC1 regulates ER contacts with endocytic organelles to mediate cholesterol egress. Nat Commun. 2019 Sep 19;10(1):4276.

269. Llaverias G, Danilo C, Mercier I, Daumer K, Capozza F, Williams TM, et al. Role of Cholesterol in the Development and Progression of Breast Cancer. The American Journal of Pathology. 2011 Jan;178(1):402–12.

270. Danilo C, Gutierrez-Pajares JL, Mainieri MA, Mercier I, Lisanti MP, Frank PG. Scavenger receptor class B type I regulates cellular cholesterol metabolism and cell signaling associated with breast cancer development. Breast Cancer Res. 2013 Oct;15(5):R87.

271. Gallagher EJ, Zelenko Z, Neel BA, Antoniou IM, Rajan L, Kase N, et al. Elevated tumor LDLR expression accelerates LDL cholesterol-mediated breast cancer growth in mouse models of hyperlipidemia. Oncogene. 2017 Nov 16;36(46):6462–71.

272. Rodrigues Dos Santos C, Domingues G, Matias I, Matos J, Fonseca I, De Almeida JM, et al. LDL-cholesterol signaling induces breast cancer proliferation and invasion. Lipids Health Dis. 2014 Dec;13(1):16.

273. Antalis CJ, Uchida A, Buhman KK, Siddiqui RA. Migration of MDA-MB-231 breast cancer cells depends on the availability of exogenous lipids and cholesterol esterification. Clin Exp Metastasis. 2011 Dec;28(8):733–41.

274. Yang L, Hou Y, Du Y e, Li Q, Zhou F, Li Y, et al. Mirtronic miR-4646-5p promotes gastric cancer metastasis by regulating ABHD16A and metabolite lysophosphatidylserines. Cell Death Differ. 2021 Sep;28(9):2708–27.

275. Vander Heiden MG, Cantley LC, Thompson CB. Understanding the Warburg Effect: The Metabolic Requirements of Cell Proliferation. Science. 2009 May 22;324(5930):1029–33.

276. Brennan K, Offiah G, McSherry EA, Hopkins AM. Tight Junctions: A Barrier to the Initiation and Progression of Breast Cancer? Journal of Biomedicine and Biotechnology. 2010;2010:1–16.

277. Ingthorsson S, Briem E, Bergthorsson JT, Gudjonsson T. Epithelial Plasticity During Human Breast Morphogenesis and Cancer Progression. J Mammary Gland Biol Neoplasia. 2016 Dec;21(3–4):139–48.

278. Zatzman M, Fuligni F, Ripsman R, Suwal T, Comitani F, Edward LM, et al. Widespread hypertranscription in aggressive human cancers. Sci Adv. 2022 Nov 25;8(47):eabn0238.

279. Matsuo T, Dat LT, Komatsu M, Yoshimaru T, Daizumoto K, Sone S, et al. Early Growth Response 4 Is Involved in Cell Proliferation of Small Cell Lung Cancer through Transcriptional Activation of Its Downstream Genes. Minna JD, editor. PLoS ONE. 2014 Nov 20;9(11):e113606.

280. Li L, Liu J, Xue H, Li C, Liu Q, Zhou Y, et al. A TGF-β-MTA1-SOX4-EZH2 signaling axis drives epithelial–mesenchymal transition in tumor metastasis. Oncogene. 2020 Mar 5;39(10):2125–39.

281. Liu C, Han J, Li X, Huang T, Gao Y, Wang B, et al. FOXP3 Inhibits the Metastasis of Breast Cancer by Downregulating the Expression of MTA1. Front Oncol. 2021 Jul 7;11:656190.

282. Veena MS, Raychaudhuri S, Basak SK, Venkatesan N, Kumar P, Biswas R, et al. Dysregulation of hsa-miR-34a and hsa-miR-449a leads to overexpression of PACS-1 and loss of DNA damage response (DDR) in cervical cancer. Journal of Biological Chemistry. 2020 Dec;295(50):17169–86.

283. Li H, Li K, Shu D, Shen M, Tan Z, Zhang W, et al. MED16 Promotes Tumour Progression and Tamoxifen Sensitivity by Modulating Autophagy through the mTOR Signalling Pathway in ER-Positive Breast Cancer. Life. 2022 Sep 20;12(10):1461.

284. Du Y, Zeng X, Yu W, Xie W. A transmembrane protein family gene signature for overall survival prediction in osteosarcoma. Front Genet. 2022 Aug 5;13:937300.

285. Schill NJ, Anderson RA. Out, in and back again: PtdIns(4,5) *P* 2 regulates cadherin trafficking in epithelial morphogenesis. Biochemical Journal. 2009 Mar 1;418(2):247–60.

286. Schill NJ, Hedman AC, Choi S, Anderson RA. PIPKIγi5 regulates the endosomal trafficking and degradation of E-cadherin. Journal of Cell Science. 2014 Jan 1;jcs.132423.

287. Loh CY, Chai J, Tang T, Wong W, Sethi G, Shanmugam M, et al. The E-Cadherin and N-Cadherin Switch in Epithelial-to-Mesenchymal Transition: Signaling, Therapeutic Implications, and Challenges. Cells. 2019 Sep 20;8(10):1118.

288. Tian J, Raffa FA, Dai M, Moamer A, Khadang B, Hachim IY, et al. Dasatinib sensitises triple negative breast cancer cells to chemotherapy by targeting breast cancer stem cells. Br J Cancer. 2018 Dec;119(12):1495–507.

289. Choi DS, Blanco E, Kim YS, Rodriguez AA, Zhao H, Huang THM, et al. Chloroquine Eliminates Cancer Stem Cells Through Deregulation of Jak2 and DNMT1. Stem Cells. 2014 Sep 1;32(9):2309–23.

290. Kim SH, Kaschula CH, Priedigkeit N, Lee AV, Singh SV. Forkhead Box Q1 Is a Novel Target of Breast Cancer Stem Cell Inhibition by Diallyl Trisulfide. Journal of Biological Chemistry. 2016 Jun;291(26):13495–508.

291. Teo WW, Merino VF, Cho S, Korangath P, Liang X, Wu R c, et al. HOXA5 determines cell fate transition and impedes tumor initiation and progression in breast cancer through regulation of E-cadherin and CD24. Oncogene. 2016 Oct 20;35(42):5539–51.